Norwegian Meteorological Institute
met.no

met.no report

Report no. 12/2011
Air Pollution
ISSN: 0332-9879
Oslo, December 16, 2011

Operational SNAP Model for Remote Applications From NRPA

Jerzy Bartnicki, Hilde Haakenstad and Øystein Hov

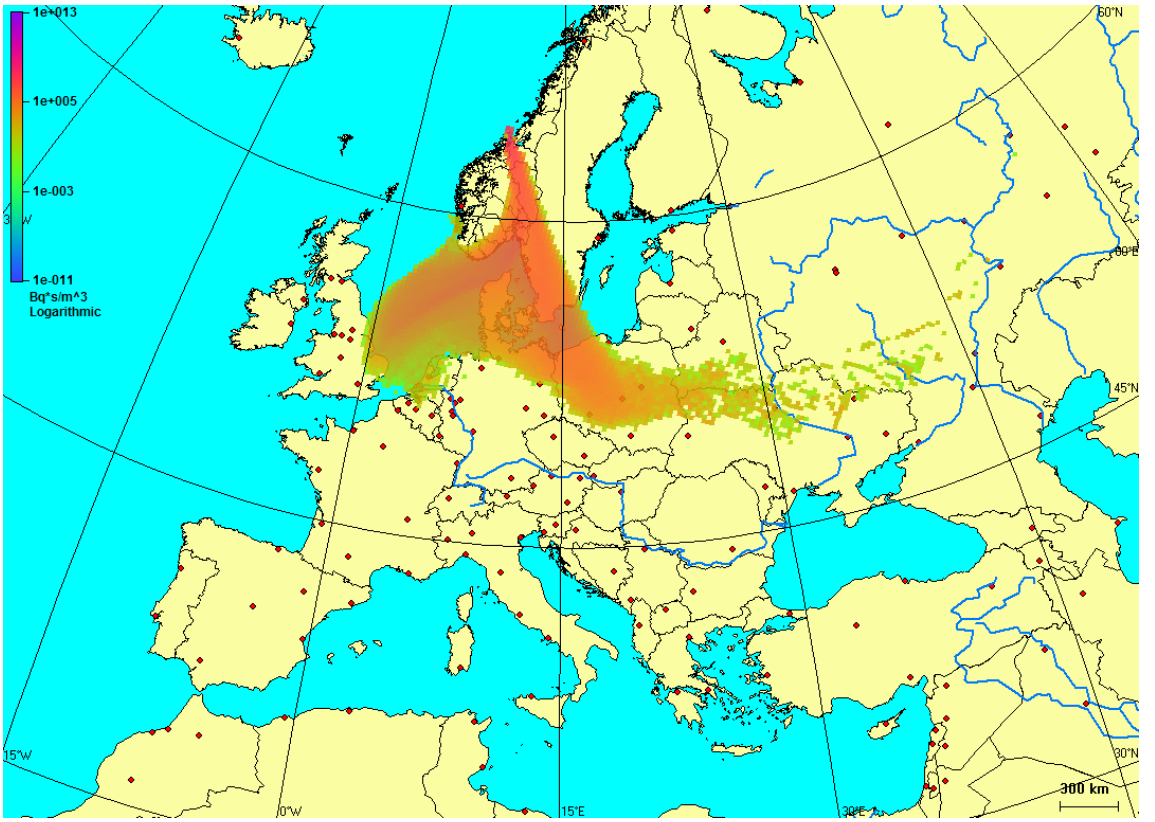

Norwegian Meteorological Institute
met.no

report

Number	Subject	Date	Classification	ISSN
12/2011	Air Pollution	December 16, 2011	☒ Open ☐ Restricted ☐ Confidential	0332-9879

Title

Operational SNAP Model for Remote Applications From NRPA

Authors

Jerzy Bartnicki, Hilde Haakenstad and Øystein Hov

Client(s)	Client reference
Norwegian Radiation Protection Authority	

Abstract

In the frame of collaboration with met.no the Norwegian Radiation Protection Authority (NRPA) has a possibility to run the SNAP model remotely in case of Nuclear Emergency. This sytem has been in operation for 10 years now and has functioned well, without any major problems. However, recently the model version available to NRPA has became a bit old compared to the operational SNAP version used at met.no. At the same time there has been a substantial change in the meteorological input to SNAP form app. 20 km horizontal resolution to app. 12 km resolution. In addition, the parameterizations of physical processes in SNAP have been improved. Therefore, there was a need for updating the SNAP version available to NRPA for remote runs, to make it the same as the operational version of SNAP used at met.no at present. In this report we describe the latest operational version of the SNAP model, as well as the remote SNAP applications from NRPA compatible with the ARGOS system. In addition to nuclear accident, these new applications include nuclear explosions and calculations of three-dimensional trajectories. We also report the results of the model sensitivity tests to major processes and the number of model particles used in the simulations.

Keywords

Nuclear accident, nuclear explosion, atmospheric dispersion, emergency, ARGOS

Disiplinary signature	Responsible signature
Hilde Fagerli	Øystein Hov

Postal address PO Box 43 Blindern N-0313 Oslo Norway
Office Niels Henrik Abels vei 40
Telephone +47 2296 3000
Telefax +47 2296 3050
e-mail: met.inst@met.no **Web:** met.no
Bank account 7695 05 00601
Swift code DNBANOKK

Contents

1. Introduction

In the frame of collaboration with met.no the Norwegian Radiation Protection Authority (NRPA) has a possibility to run the SNAP (Severe Nuclear Accident Program) model remotely in case of Nuclear Emergency. This option is very important for NRPA and especially for the Norwegian Crisis Committee in case of a real nuclear emergency, as well as for testing emergency preparedness. The system allows the experts located in NRPA to specify the source term for the nuclear accident and submit it to met.no where the SNAP model can be run at once. As soon, as the model run is finished the results are sent back to NRPA and are available for further processing within the ARGOS system. This process is relatively fast and can be repeated as many times as necessary with the updated source term. Such a system gives a lot of flexibility to the experts in NRPA and to the Crisis Committee as well.

This system for remote SNAP runs from NRPA has been in operation for 10 years now and has functioned well, without any major problems. However, recently the model version available to NRPA has become relatively old compared to the operational SNAP version used at met.no. At the same time there has been a substantial change in the meteorological input to SNAP form app. 20 km resolution to app. 12 km resolution. In addition, the parameterizations of physical processes in SNAP have been improved. Therefore, there was a need for updating the SNAP version available to NRPA, which was not exactly the same as the operational version of SNAP used by meteorologists at met.no. In this report we describe the latest operational version of the SNAP model, as well as the remote SNAP applications from NRPA in the frame of the ARGOS system. We also report the results of the model sensitivity tests to major processes and the number of model particles used in the simulations.

Many changes have been introduced into the latest version of the SNAP model. The most important of them follow the request from NRPA and are described below.

Meteorological data from the HIRLAM-12 Numerical Weather Prediction (NWP) model, operational at met.no at present (December 2011) are used as meteorological input for the latest version of the SNAP model. Compared to the old version, the computational domain of present version has been extended both in range and in number of nodes to 864×698. The number of vertical layers has been also increased from 40 to 60.

Since, the nuclear explosion option has been implemented in SNAP, correct parameterization of gravitational settling velocity for large particles become very important. In the new parameterization, large particles are can be faster deposited on the ground as it happens in reality.

Vertical diffusion process in the mixing layer was better parameterized by taking into account more accurate meteorological input data in the new version. The same applies to vertical diffusion above the mixing layer, however in this case sensitivity tests indicated that it should be kept at the minimum. Therefore, only the exchange mechanism between mixing layer and free atmosphere was improved.

The decay process for isotopes already deposited to the ground was introduced into new version. The decay constants are taken from the list of 382 isotopes provided by NRPA. Radioactive decay is applied to both, wet deposition matrix and dry deposition matrix.

In the new version of SNAP for remote applications from NRPA all the input information for SNAP runs is specified within the ARGOS framework. In this context, there are some specific

changes in the source term parameterization which can be sent from ARGOS to SNAP. In the new model version, a flexible vertical structure of initial release profile is possible, as well as a flexible time profile. For the nuclear explosion application, two initial shapes of the radioactive cloud are available in SNAP: the mushroom and the cylinder. However, as agreed with NRPA, only cylinder shape will be specified in the ARGOS files in the future. The choice of initial shape is not so important for this application, because as it was shown in [9], after long range transport of radioactive debris from the explosion, there is no significant difference in the model results for the mushroom and cylinder.

New results of SNAP have been made available to NRPA on automatic request. Now, both for accident and explosion application, the SNAP output for NRPA includes the following matrices with results: 1) wet deposition 2) dry deposition 3) total (wet+dry) deposition 4) instantaneous concentrations and 5) time integrated air concentrations. These fields are available for gases and particles.

In addition to nuclear accident option, two new applications were introduced into the present system: nuclear explosions and three-dimensional trajectories.

In the operational SNAP version available at met.no up to now, the source term for nuclear explosion included four classes of explosive yield: 1 kt, 10 kt, 100 kt and 1 Mt. To make SNAP source term compatible with the ARGOS source term, additional classes were introduced into the SNAP. So, at present eight classes of the explosive yield are available in SNAP, both for remote SNAP runs from NRPA and direct runs at met.no. These are the following: 1 kt, 3 kt, 10 kt, 30 kt, 100 kt, 300 kt, 1 Mt, 3 Mt. There are two options in SNAP for the initial shape of the radioactive cloud immediately after explosion: cylinder and a mushroom type. Both options were updated with parameters for the new classes, but only cylinder option will be used for the remote SNAP runs from NRPA.

Possibility of calculating three-dimensional trajectories is also included in the new version of SNAP for remote runs from NRPA. Only forward trajectories will be available initially for the remote runs, but the option for backward trajectories will be also implemented later in 2012.

Finally, a number of sensitivity tests and operational tests were performed with the latest SNAP version for remote applications from NRPA. This was an important part of the study indicating providing sensitivity ranking for simulations of nuclear accidents and explosions, and indicating the directions of future model improvements. The operational version of SNAP is ready at present at met.no, however, the operational testing of the model will require some more joint NRPA-met.no effort before the new version of SNAP will be fully operational for remote use from NRPA.

2. SNAP Model

The Severe Nuclear Accident Program (SNAP) is a Lagrangian particle model, which has been developed at met.no (former DNMI) for simulating atmospheric dispersion of radioactive debris, first from nuclear accidents and then from nuclear explosions. In addition to radioactive applications, SNAP was also used to simulate large fires in London and Russia and atmospheric dispersion of volcanic ash from Ejafjallajöokull eruption in 2010 [10].

The basic concept of a Lagrangian particle model is rather simple in principle. The emitted mass of radioactive debris or volcanic ash, as in this model version, is distributed among a large number of model particles. After the release, each model particle carries a given mass of selected pollutant which can be in the form of gas, noble gas or particulate matter. A model particle in this approach is given an abstract mathematical definition, rather than a physical air parcel containing a given pollutant. It is used in SNAP as a vehicle to carry the information about the pollutant emitted from the source. The model particle is not given a definite size and can be not subdivided or split into parts. On the other hand, the mass carried by the particle can be subdivided and partly removed during the transport.

As in case of many other models, the development of SNAP started after the Chernobyl accident which occurred in April 1986. The first, preliminary version of SNAP [31] was based on the early version of the NAME model [19]. This SNAP version became fully operational at DMNI in December 1995 [32], [30], [33] as a part of the major Management Project (MEMbrain), in the framework of EUREKA (EU-904) activity. This operational version of SNAP was tested against tracer measurements in the European Tracer Experiment (ETEX) [34], [35], [41] and then improved [3]. In 1996, SNAP was compared with two other models, one of Lagrangian type (NAME model from UK meteorological Office) and one Eulerian (EMEP model modified for radioactive pollution from the Norwegian Meteorological Institute) [20]. These three models produced similar results concerning the location of radioactive cloud, but the differences in concentrations were larger. The SNAP model was compared with many other models and tested on measurements available from the tracer releases not only in the frame of ETEX experiments, but also ATMES experiment [37].

In the frame of joint project between met.no and NRPA, SNAP was used in analysis of potential threat from hypothetical accident in Kola nuclear power plant [4], [7] [36], [38]. The results of SNAP calculations indicated that, in case of accident the radioactive cloud can reach Northern Norway already after six hours and Oslo after two days from the accident start.

In the early versions of the SNAP models only small (diameter below 1 μm) particles were taken into account in the model equations. Some measurements, performed by University of Life Sciences after Chernobyl accident, showed that in certain cases also much larger (of the order of 20 μm) particles, so called hot particles were transported for long distances reaching Norway. Therefore, parameterization of particles with arbitrary diameter and density was introduced into the SNAP model and this model version was applied to simulate the Chernobyl accident again [5], [6]. This version was also applied for simulating the potential release from Kola once again, this time focusing on radioactive particle of different size and density [8].

SNAP has been an active member of the ENSEMBLE group [15] and project for the last 10 years. There are at least three important advantages of ENSEMBLE on-going project: 1) possibility of comparing SNAP results with more than 20 other models in the same grid

system, 2) possibility for the backup in case of problems with SNAP, and 3) possibility of creating the ensemble forecast giving a hint on uncertainty of the results, very important for the decision makers [16], [17].

Introduction of particles with arbitrary size into the SNAP equations made it possible to create a model version for nuclear explosion [6], [9], [39], [40]. This model version was also used as a basis for developing the volcano eruption of SNAP, used to simulate atmospheric dispersion of volcanic ash from Ejafjallajökull eruption in 2010 [10].

2.1. Meteorological input and model domain

The SNAP model is flexible concerning, both model domain and meteorological data. The spatial and vertical structure of the SNAP model domain is in fact defined by the meteorological input. The Hi Resolution Limited Area Model (HIRLAM) model version 7.1.3 [45] is used as the meteorological input provider for SNAP at present. This Numerical Weather Prediction (NWP) model is currently operational at met.no and it is being run in different resolutions. Since, 2010, the HIRLAM-12 version with approximately 12 km spatial resolution and 66 hrs time horizon for the forecasts used for operational SNAP applications. The HIRLAM-12 is run 4 times a day, to produce 66 hour forecasts starting at 00, 06, 12 and 18 UTC. The main features of the HIRLAM-12 NWP model are summarized in Table 1 and the HIRLAM-12 model domain is shown in Fig. 1. The HIRLAM-12 domain shown in Fig. 1 is also a computational domain of the SNAP model for routine applications.

Table 1: Main features of the HIRLAM-12 NWP model.

Horizontal grid points (lon $\times$ lat)	864×698
Vertical levels	60
Mesh size (deg)	0.108×0.108
Analysis	3D-Var
Initialization	IDFI
Host model	ECMWF, IFS Cycle 36r, Richardson [26]
Boundary age	6
Boundary interval (h)	3
Forecast length (h)	66
Time step (min)	5
Condensation scheme	ISBA
Surface scheme	STRACO
Turbulence scheme	TKE-l
Radiation scheme	Savijärvi [42]

For historical reasons the FORTRAN code of SNAP has been developed for a single processor computer and was implemented on several platforms at met.no with the possibility of external use of the model by the Norwegian Radiation Authority (NRPA). This solution creates some backup and security for operational applications in nuclear emergency, but at the

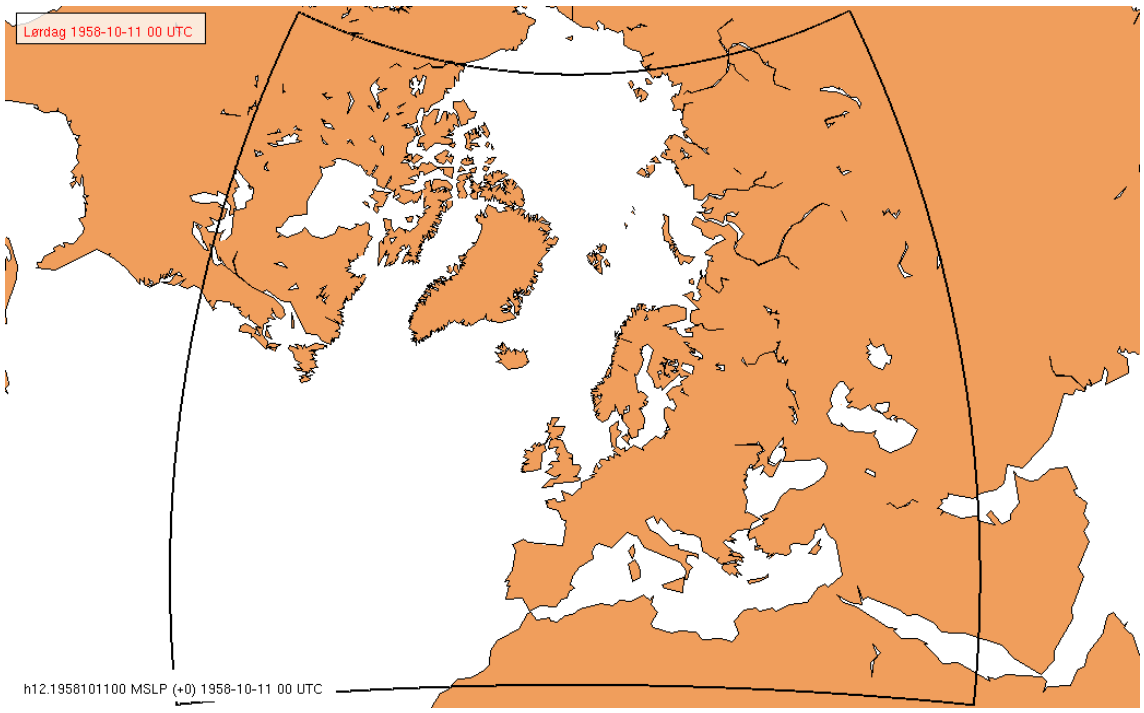

Figure 1: Computational domain of the operational HIRLAM-12 NWP model, used as meteorological input provider for SNAP and computational domain of the SNAP model.

same time it creates some limits for the operational model use in case of many different radionuclides and relatively long, over 10 days, release period. The main limits are: the available memory and the time of the computations. These limits of technical nature can be overcome in two ways: 1) by moving the model code and all computations to a massive parallel computer and 2) by installing a new dedicated server outside the fire wall at met.no, with large CPU memory and fast processors. In light of the latest development of heavy computing infrastructure available at met.no, the first option looks like a better solution. In this solution, NRPA can have a possibility to run the SNAP model on the parallel computer very quickly (several minutes) at any time of day and night, both in case of emergency and for the exercise.

2.2. Specification of SNAP run

All information necessary to run the SNAP model, both remotely from NRPA and directly at met.no, is included in the input file called ”snap.input”. The main parameters to be specified in the ”snap.input” file are the following:

1. Date and time of the accident start
2. Release position in geographical co-ordinates
3. Simulation period for the model run (maximum 66 hours with HIRLAM-12 as meteorological input)
4. Random walk procedure option (ON/OFF)
5. Time profile of source geometry
6. Time profile of release rate for each component
7. Maximum number of model particles per release
8. Specification of each component release (dry/wet deposition, radioactive decay, gravitational settling velocity, density and size for particles)
9. Relative mass/activity limit for model particle removal
10. Model time step
11. Type of model grid for meteorological input
12. Vertical layers used in the model run
13. Choice of input files with meteorological data
14. Specification of model output files

2.3. Source term

The source term is specified differently for each SNAP application. In the new version of the system, three applications of SNAP are possible for remote model runs from NRPA:

- Nuclear accident
- Nuclear detonation
- Trajectories

The source term for each of above listed application is described in more detail in the following sections.

2.3.1. Source term for nuclear accident

The source geometry is time dependent in the SNAP model and can be specified differently for each time segment of the release during the nuclear accident. However, the number of model particles released at each model time step is the same for the entire period of release. The source term can be also specified separately for each substance which is released into the atmosphere. Gases, noble gases, aerosols and large particles can be included for dispersion simulation in SNAP. In case of nuclear accident, the individual radionuclides are represented in the model by different model particles which can have different properties. The release rate is defined separately for each component released and can vary in time.

Source geometry As in the earlier versions of SNAP [40], [6], there are two options for parameterizing geometry of the source for nuclear accident and detonation: cylinder or two cylinders one above another (mushroom shape). The SNAP versions for remote applications

from NRPA assume that all model particles are uniformly mixed and distributed in the cylinder volume immediately after release. Different model particles are used for each substance - pollutant and therefore the trajectories of these model particles can also differ. The radius of the cylinder, as well as the bottom and top of the cylinder are specified in the input file for the model run. The definitions of the cylinder parameters in the "snap.input" file are the following:

```
RELEASE.RADIUS.M= 200
RELEASE.UPPER.M=  2000
RELEASE.LOWER.M=  0
```

According to the definition above, all model particles are uniformly distributed in the cylinder with 200 m radius, extending vertically from the ground to 2000 m. The parameters of cylinder can vary in time during the period of release and are specified in the "snap.input" file. The radius, base and top of each cylinder can change in different ways between the specified hours of the release. Three options - commands for this specification can be used in the SNAP input file: "BOMB", "STEPS" and "LINEAR". In the "BOMB" option all model particles are injected into cylinder only at time zero of the simulation. In the "STEPS" option emission rates are kept constant for each time sequence which is specified by the user. In the "LINEAR" option, there is a linear interpolation of the emission rates between each time step, which is specified by the user.

For example the statements in the "snap.input" file:

```
TIME.RELEASE.PROFILE.LINEAR
RELEASE.HOUR=       0,  24,  48,
RELEASE.RADIUS.M= 500, 400, 350,
RELEASE.UPPER.M=  300, 250, 200,
RELEASE.LOWER.M=   10,  10,  10
```

mean that all radioactive debris is uniformly released in the single cylinder in the period 0-48 hours. The base of the cylinder (10 m) remains unchanged in the entire period, whereas the release radius decreases linearly in time from initial 500 m to 400 m after 24 hours and 350 m after 48 hours. Also the top of the cylinder is getting lower linearly in time, from initial 300 m to 250 m after 24 hours and to 200 m after 48 hours.

Release rate The release rate can be specified individually for each component released and can change in time during the release period. As an example we show the time profile of release rates of three radionuclides I-131, Xe-133 and Cs-137 as specified in the "snap.input" file for 24 hours:

```
TIME.RELEASE.PROFILE.LINEAR
RELEASE.HOUR=       0,  12
RELEASE.BQ/SEC.COMP= 5.56e+08, 5.56e+08, 'I-131'
RELEASE.BQ/SEC.COMP= 1.11e+11, 1.11e+11, 'Xe-133'
RELEASE.BQ/SEC.COMP=  5.79e+10,  5.79e+10, 'Cs-137'
```

The above example was used as a source term in the MetNet exercise in February 2011. The release rate is defined separately for each component in Bq s^{-1}. SNAP simulation can be performed for many radionuclides in one model run, but the time profile of release is the same for all of them. This can be a certain limitation, but it can be overcome by running the model separately for each component with different time profile.

Components The radionuclides released during the nuclear accident and simulated by SNAP can be in the form of noble gases, gases and particles. In the previous SNAP version for remote application from NRPA, the list of possible radionuclides to be used included more than 300 positions. NRPA could simulate within the ARGOS system noble gases, aerosols and different isotopes of Iodine. In the present SNAP version for NRPA, the same options are possible and for Iodine three different forms are distinguished: aerosol, elemental and organic. There is also a table with the list of 382 isotopes which are included in ARGOS system and in SNAP. For each isotope on the list, the name of it, type (noble gas, aerosol and Iodine) and decay rate are specified.

Noble gas From the modelling point of view the most important features of noble gas is the lack of dry and wet deposition. This is reflected in the definition of Xe-133 component in the file "snap.input" shown below.

```
COMPONENT= 'Xe-133'
DRY.DEP.OFF
WET.DEP.OFF
RADIOACTIVE.DECAY.ON
HALF.LIFE.TIME.DAYS= 5.243
FIELD.IDENTIFICATION=1
```

The statement FIELD.IDENTIFICATION=1 assigns the output identifier for this component. Because of the lack of dry and wet deposition, noble gas can stay in the atmosphere for unlimited time. In SNAP runs, its presence in the air is mainly limited by the time necessary for noble gas to reach the lateral boundary of the model domain. The half-life time of Xe-133 used in the model calculations is slightly over 5 days. The following noble gases are taken into account in the SNAP runs for NRPA: Ar, Kr, Ra, Rn and Xe.

Aerosol Most of radionuclides included in SNAP are in the form of aerosol with particle size of the order of 1 μm. Therefore, gravitational settling velocity can be neglected for those component allowing shorter computational time. Aerosols are subject to dry and wet deposition during the transport, with wet deposition being more effective process than dry deposition. An example of aerosol specification in the "snap.input" file is given below for Cs-137:

```
COMPONENT= Cs-137
DRY.DEP.ON
WET.DEP.ON
RADIOACTIVE.DECAY.ON
HALF.LIFE.TIME.YEARS= 30.17
GRAVITY.OFF
RADIUS.MICROMETER= 0.5
```

2.3.2. Source term for nuclear detonation

The source term for nuclear detonation in SNAP is mainly determined by the explosive yield [40], [6]. In the previous, operational version of SNAP we considered four classes of the explosive yield: 1 kt, 10 kt, 100 kt and 1000 kt. In the present SNAP version for NRPA there are eight classes of explosive yield: 1 kt, 3 kt, 10 kt, 30 kt, 100 kt 300 kt, 1000 kt and 3000 kt.

Source geometry There are two options in SNAP for parameterizing geometry of the source for nuclear accident and detonation: cylinder and mushroom shape, but only cylinder option is used for remote applications from NRPA. Following Persson [22], parameters for the cylinder and activities, depending on eight explosive yield classes, are given in Table 2.

Table 2: Parameters for the cylinder, for the radioactive cloud shortly after the explosion and activities for explosive yield classes. Single cylinder cloud shape.

Explosive yield (kt)	Base of cylinder (km)	Top of cylinder (km)	Radius (km)	Activity (Bq)
1	0.50	1.50	0.6	2×10^{19}
3	1.40	3.10	1.0	6×10^{19}
10	2.25	4.75	1.4	2×10^{20}
30	4.10	8.40	2.3	6×10^{20}
100	5.95	12.05	3.2	2×10^{21}
300	8.00	18.50	5.8	6×10^{21}
1000	10.00	25.00	8.5	2×10^{22}
3000	12.00	32.00	11.1	6×10^{22}

An example of the source geometry and time profile for 10 particle classes in the detonation with explosive yield 10 kt, as specified in the file ”snap.input” is shown below.

```
TIME.RELEASE.PROFILE.BOMB
RELEASE.SECOND=    0
RELEASE.RADIUS.M=  1400.
RELEASE.LOWER.M= 2250.
RELEASE.UPPER.M= 4750.
RELEASE.BQ/STEP.COMP= 2.0e+20 'Aerosol_2.2mym'
RELEASE.BQ/STEP.COMP= 2.0e+20 'Aerosol_4.4mym'
RELEASE.BQ/STEP.COMP= 2.0e+20 'Aerosol_8.6mym'
RELEASE.BQ/STEP.COMP= 2.0e+20 'Aerosol_14.6mym'
RELEASE.BQ/STEP.COMP= 2.0e+20 'Aerosol_22.8mym'
RELEASE.BQ/STEP.COMP= 2.0e+20 'Aerosol_36.1mym'
RELEASE.BQ/STEP.COMP= 2.0e+20 'Aerosol_56.5mym'
RELEASE.BQ/STEP.COMP= 2.0e+20 'Aerosol_92.3mym'
RELEASE.BQ/STEP.COMP= 2.0e+20 'Aerosol_173.2mym'
RELEASE.BQ/STEP.COMP= 2.0e+20 'Aerosol_250mym'
```

There is large variation in the size of particles in the radioactive cloud after the explosion. In the SNAP model we assume that particle size spectrum is represented by 10 discrete classes. The total activity released during nuclear explosion is the sum of all ten classes. This is based on the assumption that the activity is uniformly distributed in the mass of the bomb material and that each particle size class gets an equal part of the original bomb material. This implies that a factor of 10 in difference in particle radius for two classes will result in a factor of 10^3 in the number of particles in two classes. In this way we attribute 10% of the original activity in each particle class.

Particle size classes and distribution of activity, in the SNAP model, are the same as in the MATCH model [22], [27] and are shown in Table 3 together with corresponding activity share, characteristic gravitational settling velocity and particle radius assumed to calculate this velocity. Density of the particles in Table 3 is assumed to be ca. 3 g cm^{-3}. In case of a detonation close to the ground, particles of soil origin will be excited and drown into the

updraft. This fraction of the material has lower density than the original ”bomb” material and also activity attached to this mass fraction will be quite different in composition. We are unsure how much of this extra activity is included in numbers presented in Table 3.

Table 3: Particle size classes and corresponding parameters used in the SNAP model calculations. Note: we have assumed an equal share of the activity to each size class.

Class No.	Range of particle radius (μm)	Activity share (%)	Gravitational settling velocity (cm/s)	Particle radius (μm) for the class
1	0 - 3	10	0.2	2.2
2	3 - 6.5	10	0.7	4.4
3	6.5 - 11.5	10	2.5	8.6
4	11.5 - 18.5	10	6.9	14.6
5	18.5 - 29	10	15.9	22.8
6	29 - 45	10	35.6	36.1
7	45 - 71	10	71.2	56.5
8	71 - 120	10	137.0	92.3
9	120 - 250	10	277.3	173.2
10	over 250	10	direct deposition	300.0

Ten particle classes with characteristic radius and gravitational settling velocity as specified in Table 3 are used for the fast operational SNAP run simulating the nuclear detonation. Specification of the component/classes in the file ”snap.input” is given below.

```
*
COMPONENT= Aerosol_2.2mym
DRY.DEP.ON
WET.DEP.ON
RADIOACTIVE.DECAY.OFF
RADIUS.MICROMETER= 2.2
GRAVITY.FIXED.CM/S= 0.2
FIELD.IDENTIFICATION=01
*
COMPONENT= Aerosol_4.4mym
DRY.DEP.ON
WET.DEP.ON
RADIOACTIVE.DECAY.OFF
RADIUS.MICROMETER= 4.4
GRAVITY.FIXED.CM/S= 0.7
FIELD.IDENTIFICATION=2
*
COMPONENT= Aerosol_8.6mym
DRY.DEP.ON
WET.DEP.ON
RADIOACTIVE.DECAY.OFF
RADIUS.MICROMETER= 8.6
GRAVITY.FIXED.CM/S= 2.5
FIELD.IDENTIFICATION=3
*
COMPONENT= Aerosol_14.6mym
DRY.DEP.ON
WET.DEP.ON
RADIOACTIVE.DECAY.OFF
RADIUS.MICROMETER= 14.6
GRAVITY.FIXED.CM/S= 6.9
FIELD.IDENTIFICATION=4
*
COMPONENT= Aerosol_22.8mym
DRY.DEP.ON
WET.DEP.ON
RADIOACTIVE.DECAY.OFF
RADIUS.MICROMETER= 22.8
GRAVITY.FIXED.CM/S= 15.9
FIELD.IDENTIFICATION=5
```

```
*
COMPONENT= Aerosol_36.1mym
DRY.DEP.ON
WET.DEP.ON
RADIOACTIVE.DECAY.OFF
RADIUS.MICROMETER= 36.1
GRAVITY.FIXED.CM/S= 35.6
FIELD.IDENTIFICATION=6
*
COMPONENT= Aerosol_56.5mym
DRY.DEP.ON
WET.DEP.ON
RADIOACTIVE.DECAY.OFF
RADIUS.MICROMETER= 56.5
GRAVITY.FIXED.CM/S= 71.2
FIELD.IDENTIFICATION=7
*
COMPONENT= Aerosol_92.3mym
DRY.DEP.ON
WET.DEP.ON
RADIOACTIVE.DECAY.OFF
RADIUS.MICROMETER= 92.3
GRAVITY.FIXED.CM/S= 137.0
FIELD.IDENTIFICATION=8
*
COMPONENT= Aerosol_173.2mym
DRY.DEP.ON
WET.DEP.ON
RADIOACTIVE.DECAY.OFF
RADIUS.MICROMETER=173.2
GRAVITY.FIXED.CM/S= 277.3
FIELD.IDENTIFICATION=9
*
COMPONENT= Aerosol_250mym
DRY.DEP.ON
WET.DEP.ON
RADIOACTIVE.DECAY.OFF
RADIUS.MICROMETER= 300.0
GRAVITY.FIXED.CM/S= 10000.0
FIELD.IDENTIFICATION=10
```

The statements: `DRY.DEP.ON` and `WEP.DEP.ON` mean that each component is a subject of dry and wet deposition during the atmospheric transport. The statement `RADIOACTIVE.DECAY.OFF` indicates that no radioactive decay is calculated during the model run. In this specification, ten particle classes with characteristic radius and constant gravitational settling velocity specified in Table 3 are used in the model run. An artificial, very large gravitational settling velocity was specified for class 10 with largest particles to simulate a direct deposition of these particles at the release location. It is also possible to run the model with the option of calculating gravitational deposition velocity for each model particle and at each model time step by including the statement, `DENSITY.G/CM3= ...` in the "snap.input" file. For example, `DENSITY.G/CM3=3` is the density of 3 gcm^{-3}. However, the execution time of the model with this option for the gravitational settling velocity can be up to 50% longer.

2.3.3. Source term for trajectories

Specification of the source term for three-dimensional trajectory calculations is relatively simple. Only forward trajectories are calculated which can start at arbitrary level within the vertical domain of the SNAP model. The specification necessary to start SNAP for trajectory calculations includes date and time of the start, geographical position, number of trajectories to be calculated in one SNAP run and start level in meters for each trajectory to be calculated.

2.4. Mixing height

As good as possible determination of the mixing height, which represents in the model the depth of atmospheric boundary layer (ABL), is very important for modelling atmospheric

transport and deposition of air pollution. The turbulent diffusion is significantly more intensive in the ABL and only pollution in the boundary layer is a subject of dry deposition.

The procedure to identify and calculate the mixing height h is based on critical Richardson Number formulation R_{iC}. The gradient Richardson Number, R_i, is calculated for a given model layer from

$$R_i = \frac{g\Delta\theta_i/\Delta z}{\bar{T}(\Delta\mathbf{u}/\Delta z)^2} \tag{1}$$

where $\Delta\theta_i/\Delta z$ and $\Delta\mathbf{u}/\Delta z$ are the gradients of potential temperature and wind speed, g is the acceleration due to gravity and $\bar{T}$ is the mean temperature of the layer. It is assumed that the mixing height can be determined from the meteorological input data at which a small positive number of R_i is reached, below which turbulent motion tends to persists and above which it is suppressed. The critical value R_{iC} is used to identify the top of the ABL that is, the mixing height h. The model gradients of potential temperature and wind, $\Delta\theta/\Delta z$ and $\Delta\mathbf{u}/\Delta z$, are used to search for R_{iC} layer by layer, starting from the surface and stepping upward trough the model layers. The value $R_{iC} = 1.8$ is used for determining the mixing height in the SNAP model.

2.5. Advection and diffusion

The advective displacement of each model particle is calculated at each model time step, Δt, which is equal to 5 minutes (300 s) in the present SNAP version. For this calculation, three-dimensional velocity is interpolated to particle position from the eight nearest nodes in the model grid. Bilinear interpolation in space is applied to horizontal components of the velocity field and linear interpolation for the vertical component. In addition, linear interpolation in time is applied between sequential meteorological input fields. The advective displacement of each particle in one model time step is calculated according to

$$\mathbf{x}'_{t+\Delta t} = \mathbf{x}_t + [\mathbf{u}(\mathbf{x}_t) + \mathbf{u}_g(\mathbf{x}_t)]\Delta t \tag{2}$$

where $\mathbf{x}_t = (x, y, \eta, t)$ is the position of particle, $\mathbf{u} = (x, y, \eta, t)$ is velocity from the numerical weather prediction model and $\mathbf{u}_g = \mathbf{u}_g(x, y, \eta, t)$ is the gravitational setting velocity for the given model particle, all at time t. The intermediate position of the particle after advection is denoted by the vector $\mathbf{x}'_{t+\Delta t}$.

The calculation of gravitational settling velocity included in Eq. 2 is described in the next Section. A relatively simple iterative procedure developed by Petersen [23] is used for numerical solution of Equation 2. We have found two iterations in this procedure to be entirely sufficient for calculating the new position of the model particle.

2.5.1. Gravitational settling velocity

For conditions when the Stokes law is valid, gravitational settling velocity with spherical shape of particles is a function of particle size, particle density and air density [43]:

$$v_g = \frac{d_p^2 g(\rho_p - \rho_a)C(d_p)}{18\nu} \tag{3}$$

where:
d_p is the particle diameter,
g is the acceleration due to gravity,
ρ_p is the particle density,
$\rho_a = \rho_a(p,T)$ is the density of the air at particle location,
$C(d_p)$ is Cunningham correction factor,
$\nu = \nu(T)$ is the dynamic molecular viscosity of the air at particle location.

The density of the air is calculated from the equation of state

$$\rho_a = \frac{p}{RT} \tag{4}$$

where
p is the atmospheric pressure,
T is the absolute temperature,
$R = 287.04$ is the gas constant for dry air ($Jkg^{-1}K^{-1}$)

Viscosity of the air is a function of temperature [24]:

$$\nu = 1.72 \times 10^{-5} \frac{393}{T+120} (\frac{T}{273})^{\frac{3}{2}} \tag{5}$$

and Cunningham correction factor for small particles [43] is calculated as:

$$C(d_p) = 1 + \frac{2\lambda}{d_p}(1.257 + 0.4e^{-0.55\frac{d_p}{2\lambda}}) \tag{6}$$

where $\lambda = 6.53 \times 10^{-8}$m is the mean free path of air molecules. Eq. 3 is not valid for particles with the radius larger than 10-15 μm. In case of the larger particle classes, correction to account for high Reynolds numbers is necessary. Such a correction was introduced in the SNAP model [6] leading to the following set of equations [43]:

$$\begin{array}{ll} v_g(1 + \frac{3}{16}Re + \frac{9}{160}Re^2 \ln 2Re) = \frac{d_p^2 g(\rho_p - \rho_a)C(d_p)}{18\nu} & 0.1 < Re \leq 2 \\ v_g(1 + 0.15Re^{0.578}) = \frac{d_p^2 g(\rho_p - \rho_a)C(d_p)}{18\nu} & 2 < Re \leq 500 \end{array} \tag{7}$$

where $Re = v_g d_p \rho_a / \nu$ is the Reynolds Number. Eq. 7 is non-linear and requires a numerical solution, which may significantly slow down the model performance, if it is applied to each individual particle at each model time step. In the present version of SNAP, there is an option for using the tabulated values of gravitational settling velocities for each of the selected particle class. This table is calculated only once at the beginning of each model run, so that application of these equations did not significantly reduced the model performance.

2.5.2. Random walk method

Random walk techniques giving effect to diffusion are described in detail in [28]. The Wiener-type of process used here is governed by a length scale, the sequence of steps following the

description by Mayron [19]. A slightly different parameterization is used for particles located within boundary layer and for those above, but can be described by the same equations. The new particle position is calculated as:

$$\begin{aligned} x'' &= x' + r_x l \\ y'' &= y' + r_y l \\ \eta'' &= \eta' + r_\eta l_\eta \end{aligned} \tag{8}$$

where $\mathbf{x''}_{t+\Delta t} = (x'', y'', \eta'')$ is the particle position vector at time $t + \Delta t$ after application of the diffusion algorithm; r_x,r_y,r_η are randomly sampled numbers from the range (-0.5,+0.5), generated from uniform distribution; l and l_η are the length scales from the horizontal and vertical turbulent motion. Horizontal diffusion above the ABL in SNAP is parameterized in the same way as for the particles below, but the value of the coefficient of proportionality is different for two regions. We assume horizontal length-scale for the turbulent motion, defining horizontal diffusion:

$$l = ax^b \tag{9}$$

where $x = |\mathbf{u}|\Delta t$, $|\mathbf{u}| = \sqrt{u^2 + v^2}$ is the wind speed in m/s, $b = 0.875$, $a = 0.5$ in ABL and $a = 0.25$ above.

The scale of vertical diffusion is $l_\eta = 0.08$ within ABL and $l_\eta = 0.001$ above the boundary layer. Parameterization of vertical diffusion in the volcano version of SNAP is relatively simple, probably too simple especially in the ABL. However, as seen from the aviation perspective, the most important for the model results is the diffusion above ABL. In most of the dispersion models, vertical diffusion is very week and in some models it is even neglected [27]. The advantage of the simplification related to vertical diffusion parameterization is a better performance of the model in relation to computational time.

2.5.3. Boundary conditions

When displaced, particles can reach the boundaries of the model domain. Since SNAP is a model of the Lagrangian type, formulation of boundary conditions is relatively simple.

For particles with larger diameter like 10 μm and above, the mechanism of gravitational settling can be effective in moving them quickly to the ground. If the position of model particle in the next time step is lower than the ground level $\eta > 1.0$, the entire particle is removed from the further computations and its entire mass is added to dry deposition matrix. In the random walk process, the model particles cannot penetrate the surface - the bottom boundary of the model domain. If the particle hits the ground in the random walk procedure, it is reflected back into the boundary layer.

A similar procedure is applied to the model particles reaching the upper boundary of the model domain. At the top of the model domain, there is no exchange of particles. This assumption implies the closed upper boundary conditions.

Particles can flow out of the lateral boundaries of the model domain, but none can enter the model domain from the outside. This implies open lateral boundary conditions.

2.6. Dry deposition

Many particles of different size are released into the atmosphere during nuclear accident and especially during nuclear explosion eruption. For the relatively large particles, the dry deposition process is dominated by the gravitational settling. However, for the relatively small particles with the diameter below 3 μm, other processes are dominating the removal of particles from the air. Therefore, not only gravitational settling, but also other surface related processes are included in the parameterization of dry deposition.

A key parameter in the dry deposition process is the dry deposition velocity v_d, which can be calculated based on the resistance analogy [43]. In this approach, dry deposition of gases is governed by steady-state mass conservation equation:

$$F = K(z)\frac{\partial c}{\partial z} \tag{10}$$

where $K(z)$ is the diffusion coefficient and c is the concentration. Integration of the Eq. 10 gives:

$$F = K(z)\frac{c(z)}{r(z)} \tag{11}$$

where $r(z) = \int_0^z \frac{dz}{K(z)}$ is the resistance to vertical transport. The Eq. 11 has the same form as equation for an electrical circuit with voltage corresponding to concentration, current to flux and electrical resistance to transport resistance.

The dry deposition velocity v_d is defined as an inverse of resistance, and the dry deposition flux can be calculated as:

$$F = v_d(z)c(z) \tag{12}$$

According to Seinfeld [43] Eq. 10 can be also applied for particles with the following formulation of dry deposition velocity:

$$v_d = \frac{1}{r_a + r_s + r_a r_s v_g} + v_g \tag{13}$$

In Equation 13, the aerodynamic resistance r_a accounts for turbulent diffusion from the free atmosphere to surface laminar sub-layer and it is a function of meteorological parameters such as wind speed, atmospheric stability and surface roughness. The surface layer resistance r_s is related to diffusion trough a laminar sub-layer and is more dependent on molecular than turbulent properties. For the latest version of SNAP, we have assumed the total resistance in Equation 13 to be 200 s m^{-1}. The gravitational settling velocity is dominating dry deposition process for large particles. For very large particles, emitted into the atmosphere during nuclear accident or explosion, this leads to the simplification $v_d \approx v_g$.

Venkatram and Pleim **??** pointed out that Eq. 13 is not strictly valid for particles because dry deposition flux associated with particles does not depend on the concentration gradient. Assuming that turbulent transport and particle settling can be added together, the vertical flux can be calculated as follows **??**:

$$F = K(z)\frac{c}{r} + v_g c = v_d c \tag{14}$$

The dry deposition velocity in Eq. 14 has the following form **??**:

$$v_d = \frac{v_g}{1 - e^{-rv_g}} \tag{15}$$

where r is the total resistance for particles. Since the differences between dry depositions calculated with Eq. 16 and Eq. 15 are small **??**, we still use Eq. 16 in operational version of SNAP

In our calculations, we assumed that the model particles located above the surface layer h are not affected by the dry deposition process. The height of the surface layer is defined as 10% of the mixing height. Reduction of the particle mass, m, due to dry deposition in one time step Δt, for each model particle located within the surface layer can be calculated as:

$$m(t + \Delta t) = m(t) exp(-\frac{v_d}{h_s}\Delta t) \tag{16}$$

where h_s is the height of the surface layer. In addition to mass reduction of the model particles in dry deposition process, the particles reaching the ground in due to gravitational settling are entirely eliminated from the model and their mass is added to dry deposition matrix.

The above parameterization of dry deposition is relatively simple, except gravitational settling velocity calculations. This simple approach can affect the deposition field and concentrations in the ABL. However, in SNAP applications for nuclear accidents and explosions, the uncertainty introduced by simplifications in dry deposition parameterization is much lower than the uncertainty due to unknown source term.

The present version of SNAP can be remotely applied from NRPA both for nuclear accidents and nuclear explosions. In case of nuclear explosion, relatively large particles, with diameter up to 300 μm are injected into the air. For these large particles, not dry deposition but gravitational settling is the most effective mechanism for removing them from the dry air. To take this fact into account, we first calculate vertical transport of model particles governed by the sum of large scale vertical velocity and gravitational settling velocity. If the model particle hits the ground, its activity is in 100% deposited to the surface and stored in the deposition matrix. In this way we can make consistent parameterization of dry deposition with calculation of gravitational settling and vertical transport.

2.7. Wet deposition

Wet deposition is the most effective process in removing soluble gases and particles of different size from the atmosphere. This process includes absorption of particles into the droplets in the clouds (rainout) and then droplet removal by precipitation (washout). Wet deposition process depends on many complicated factors, which are difficult to take into account, like for example occult deposition related to fog, scavenging by snow, effect of convective precipitation and orographic effects.

In the present version of the model, we have assumed that the mass of particle, m affected by precipitation is reduced during one model time step Δt in the following way:

$$m(t+\Delta t) = m(t)e^{-k_w \Delta t} \tag{17}$$

Following Baklanov and Sørensen [1], the coefficient of wet deposition k_w is a function of the particle radius r (in μm) and the precipitation intensity q (in mm per hour). For below cloud scavenging, the coefficient of wet deposition is calculated differently for three classes of particles:

$$k_w(r,q) = \begin{cases} a_0 q^{0.79} & r \leq 1.4 \\ (b_0 + b_1 r + b_2 r^2 + b_3 r^3) f(q) & 1.4 < r \leq 10.0 \\ f(q) & 10.0 < r \end{cases} \tag{18}$$

where
$f(q) = a_1 q + a_2 q^2$,
$a_0 = 8.4 \times 10^{-5}$, $a_1 = 2.7 \times 10^{-4}$, $a_2 = -3.618 \times 10^{-6}$,
$b_0 = -0.1483$, $b_1 = 0.3220133$, $b_2 = -3.0062 \times 10^{-2}$, $b_3 = 9.34458 \times 10^{-4}$.

In Equation 18, the wet deposition coefficient for small particles ($r \leq 1.4\mu m$) and for large particles ($10.0\mu m < r$) does not depend on the particle size, but on precipitation intensity. Only for particles in the range ($1.4\mu m < r \leq 10.0\mu m$), the wet deposition coefficient is a function of both particle size and precipitation intensity.

Wet deposition process between cloud base and cloud top (rainout) depends on the type of precipitation - dynamic or convective. The wet deposition coefficient for dynamic precipitation is close to wet deposition coefficient below the cloud and be also estimated by Eq. 18. The wet deposition is more effective for convective than dynamic precipitation. Therefore, wet deposition coefficient for convective precipitation between cloud base and top is estimated according to Maryon et. al. [21] in the following way:

$$k_w(r,q) = a_0 q^{0.79} \tag{19}$$

where $a_0 = 3.36 \times 10^{-4}$. The wet deposition coefficient within the cloud is not dependent on the particle size as it was suggested by Crandall et. al. [11].

In many cases and in convective situation especially, precipitation does not occur in the entire model grid square. The area of the model grid square covered by precipitation as a function of precipitation intensity was originally estimated in [18]. In the SNAP model we use a probability curve Fig. 2 based on this estimation. From the probability curve we can find the probability of the model particle to be affected by precipitation in a given model grid as a function of precipitation intensity. If the probability ϕ of precipitation for a given location of the model particle is above zero, we replace the precipitation intensity q in Equation 18 by the effective precipitation intensity $q_{eff} = q/\phi$.

In addition, there is an elevation limit for model particles to be a subject of wet deposition. In the volcano version of SNAP, we have assumed that only those particles located below the model level $\eta = 0.76$ are losing mass due to wet deposition. This η level corresponds roughly to 2000 m.

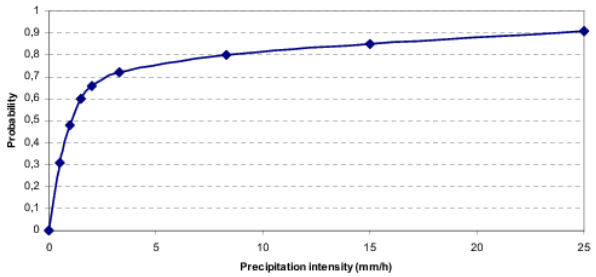

Figure 2: The probability curve for precipitation used in the SNAP, model and taken from [18].

2.8. Radioactive decay

All isotopes included in the SNAP model are subject to radioactive decay. In the SNAP version run directly at met.no, this process is specified in the "snap.input" file as in the example shown below:

```
...
COMPONENT= 'Xe-133'
...
RADIOACTIVE.DECAY.ON
HALF.LIFE.TIME.DAYS= 5.243
...
```

In the example above, a half-life time for Xe-133 is given in days. Other units e.g. hours and years can be also used for the specification of half-life time. For remote applications of SNAP from NRPA the radionuclides specified in Appendix A are used in the model runs. This specification also includes information about the decay constant. The relation between half-life time $T_{1/2}$ and decay constant λ is the following:

$$T_{1/2} = \frac{ln2}{\lambda} = \frac{0.693}{\lambda} \tag{20}$$

The activity of any isotope remaining in the air after time t is calculated according to the following equation:

$$A(t) = A_0 e^{-\lambda t} \tag{21}$$

where $A(t)$ is the activity at time T and A_0 is the initial activity of the considered isotope. The calculations are performed at every time step Δt, so:

$$A(t+\Delta t) = A(t) e^{-\lambda t} \tag{22}$$

The radioactive decay is also affecting a part of each isotope already deposited to the ground, so the same approach is applied to matrices of wet and dry deposition for each isotope at each model time step.

$$\begin{aligned} D_{dry}(i,j,t+\Delta t) &= D_{dry}(i,j,t) e^{-\lambda t} \\ D_{wet}(i,j,t+\Delta t) &= D_{wet}(i,j,t) e^{-\lambda t} \end{aligned} \tag{23}$$

where $D_{dry}(i,j,t)$ and $D_{wet}(i,j,t)$ are matrices of dry and wet deposition respectively.

3. Remote Applications of SNAP

In the old system, only one application of SNAP was available for remote runs from NRPA - simulation of nuclear accident. In the new version, in addition to nuclear accident, SNAP can be run for simulation nuclear explosion and for calculating three dimensional trajectories.

3.1. Nuclear accident

Simulation of atmospheric dispersion of radioactive debris from nuclear accident is the most important task for the SNAP model. In fact, nuclear accident in Chernobyl in 1986 was the main reason for developing SNAP. A practical importance of this kind of modelling was confirmed by the latest accident in Fukushima in May 2011.

3.1.1. Computational scheme for nuclear accident

The sequence of events starts at NRPA in the frame of ARGOS system and is illustrated in Fig. 3 in the computational diagram for the accident case.

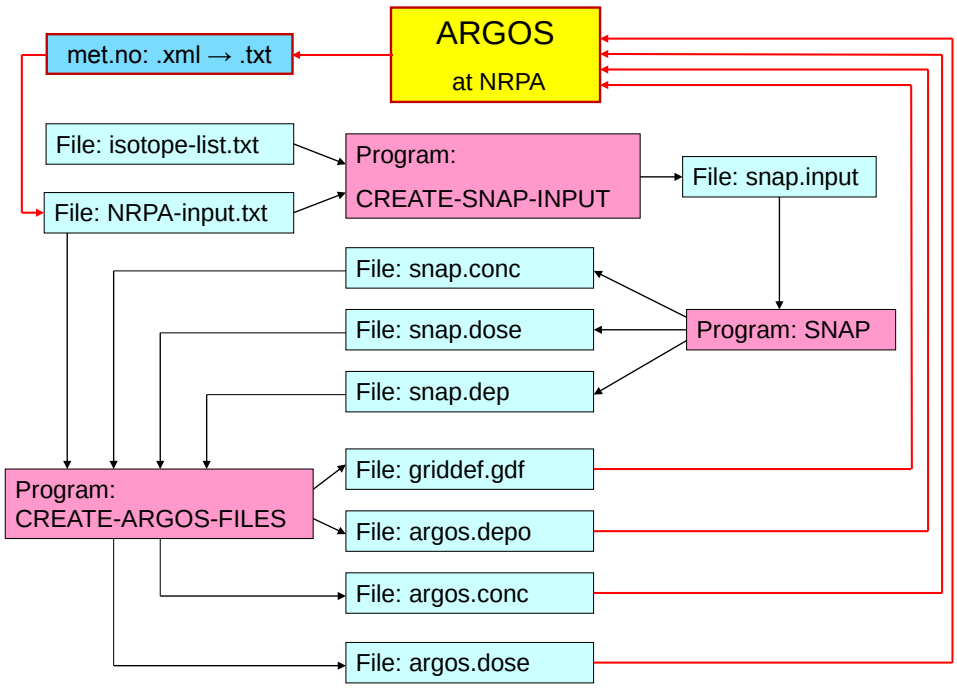

Figure 3: Computational diagram at met.no for the accident case.

In the remote SNAP applications from NRPA, the SNAP run for the nuclear accident is initiated when the new input file for the nuclear accident appears on the met.net server. This file is originally in .xml format, but it is converted to a simple text file at met.no. A test example of such input file (NRPA-input.txt) is shown below.

```
57.249982262757 LATITUDE
12.0998963945262 LONGITUDE
2011-10-12T06:00:00Z RELEASE START
3 ISOTOPES
748 I -131a
158 Xe-133
169 Cs-137
2 RELEASE INTERVALS
INTERVAL
10 0 HOUR,MINUTE
10 45 RELEASE HEIGHT MIN,MAX
748 57667598327
158 44058874033996
169 5814817158
INTERVAL
5 0 HOUR,MINUTE
10 35 RELEASE HEIGHT MIN,MAX
748 5000000000
158 4000000000000
169 600000000
```

The first two lines of the file give the geographical co-ordinates of the accident and at the same time the release location. The third line specifies the date and time (in hours, minutes and seconds) of the accident and beginning of release. The fourth line gives the number of isotopes to be simulated. In this case, there are three isotopes with the identification numbers and names specified in three following lines and taken from the isotope list, which will be explained later. Next line gives the total number of release intervals, which are two in this test case. In the first interval the release duration is 10 hours and 0 minutes. The minimum elevation of release is 10 m and maximum elevation of release is 45 m. Next three lines specify the release rate (in Bq s^{-1}) for each simulated isotope with corresponding identification number. The duration of release in the second interval is 5 hours and 0 minutes with vertical range 10-35 m and there are also three different release rates for each isotope. They are specified in the last three lines of the file.

Two input files are necessary to start the SNAP run at met.no: `NRPA_input.txt` and `isotope_list.txt`. The file `isotope_list.txt` is presented as a table in Appendix A. Altogether there are 382 isotopes listed in Appendix A which can be used in remote applications of SNAP from NRPA. The identification number of each isotope is given in the first column and name of the isotope in the second column. There can be three forms of the isotope denoted by a single digit number: 0-noble gas, 1-gas and 2-aerosol. This information is included in the third column. The decay coefficient (s^{-1}) is given in column four.

Program `CREATE_SNAP_INPUT` (Fig. 3) is creating the input file (`snap.input`) for the SNAP model using the information included in the files: `NRPA_input.txt` and `isotope_list.txt`. Next step is the SNAP model run producing three intermediate output files: `snap.conc`, `snap.dose` and `snap.dep`, including calculated instantaneous concentrations, time integrated concentrations and deposition, respectively. These files are very large, because they contain many unnecessary zeros in the model grid system. The intermediate output files are then converted to final output files by program `CREATE_ARGOS_FILES`. The

final output files are much smaller because they include only non-zero values of concentration and deposition. Program `CREATE-ARGOS-FILES` is also producing an additional file `isotope-griddef.gdf` with model grid definition in geographical coordinates. The final output files are sent to the ARGOS system at NRPA as soon as they are created.

In principle the sequence of actions illustrated in Fig. 3 can be simplified so, that the ARGOS files are produced directly by the `SNAP` model and program `CREATE-ARGOS-FILES` is not used at all. However, this will require some additional changes in the SNAP hard code and therefore it is not done in the test phase.

3.1.2. An example of remote application for nuclear accident

An example of the remote application from NRPA for nuclear accident is shown in Fig. 4 and Fig. 5. In this example atmospheric dispersion of radioactive debris from hypothetical accident in Ringhals (Sweden) nuclear power plant has been simulated. The start of the accident was assumed on 24 September 2011 at 13:00 UTC. Two isotopes Cs-137 and I-131 were released into the air for the period of 10 hours. Compared to the previous SNAP version, a better and more precise specification of the source term geometry is available in the new model version. Both isotopes were released into the abstract cylinder with the base at 10 m and top at 20 m. The cylinder radius was 20 m. The SNAP simulation of this accident was performed for 63 hours. The final results of the model run were available on 27 September 2011 at 04:00 UTC.

In Fig. 4 the results of SNAP simulation (time integrated concentration and deposition of I-131) are shown using the graphics available at met.no. The radioactive debris from this accident is mainly transported and deposited over Swedish territory, reaching a small area of Northern Norway at the end of the simulation. There is also a small part of Southern Norway affected at the beginning of the transport. The range of the deposition is longer than the range of time integrated concentration, because a part of the radioactivity is transported higher in the air. It means zero concentration on the ground, but still possible wet deposition. In this case, the wet deposition process above the ground is quite effective, showing relatively high deposition values far away from the source in Northern Sweden, where time integrated concentrations were equal to zero. Both in the concentration and deposition maps, but especially in the deposition maps, two separate plums can be seen corresponding to different periods of the transport. The earlier tang is going south and then east whereas the later tang is going first south-north for a short period and then to the north.

In Fig. 5, the same results as in Fig. 4 are illustrated using the ARGOS graphics. Both, maps created at met.no and those in ARGOS system are very similar, however more details are visible on the ARGOS maps. The spatial distributions, as well as the gradients are very similar on the met.no's and NRPA's maps.

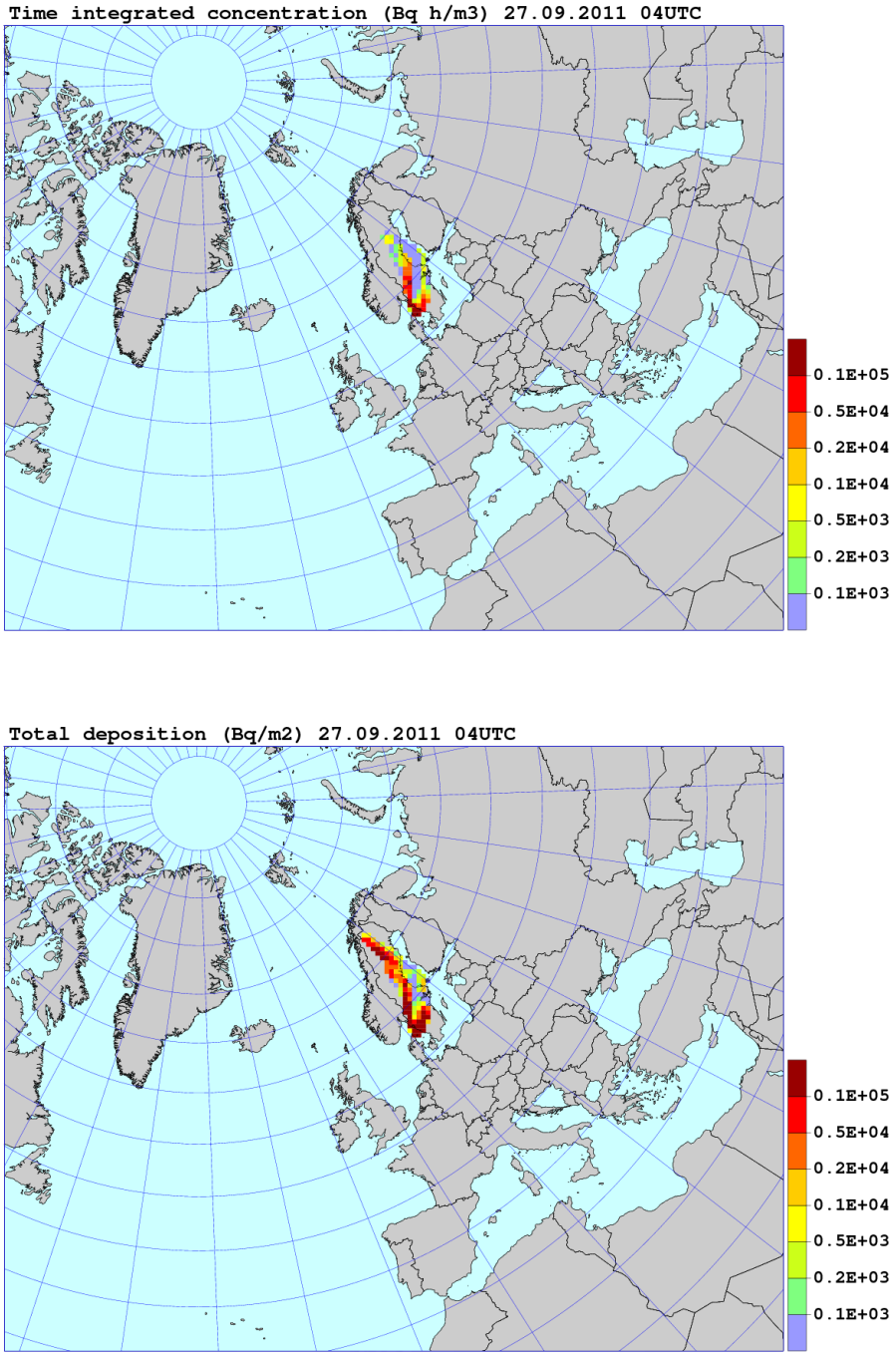

Figure 4: Maps of time integrated I-131 concentration (above) and total deposition (below). Results of SNAP run performed at met.no for the test accident submitted by NRPA.

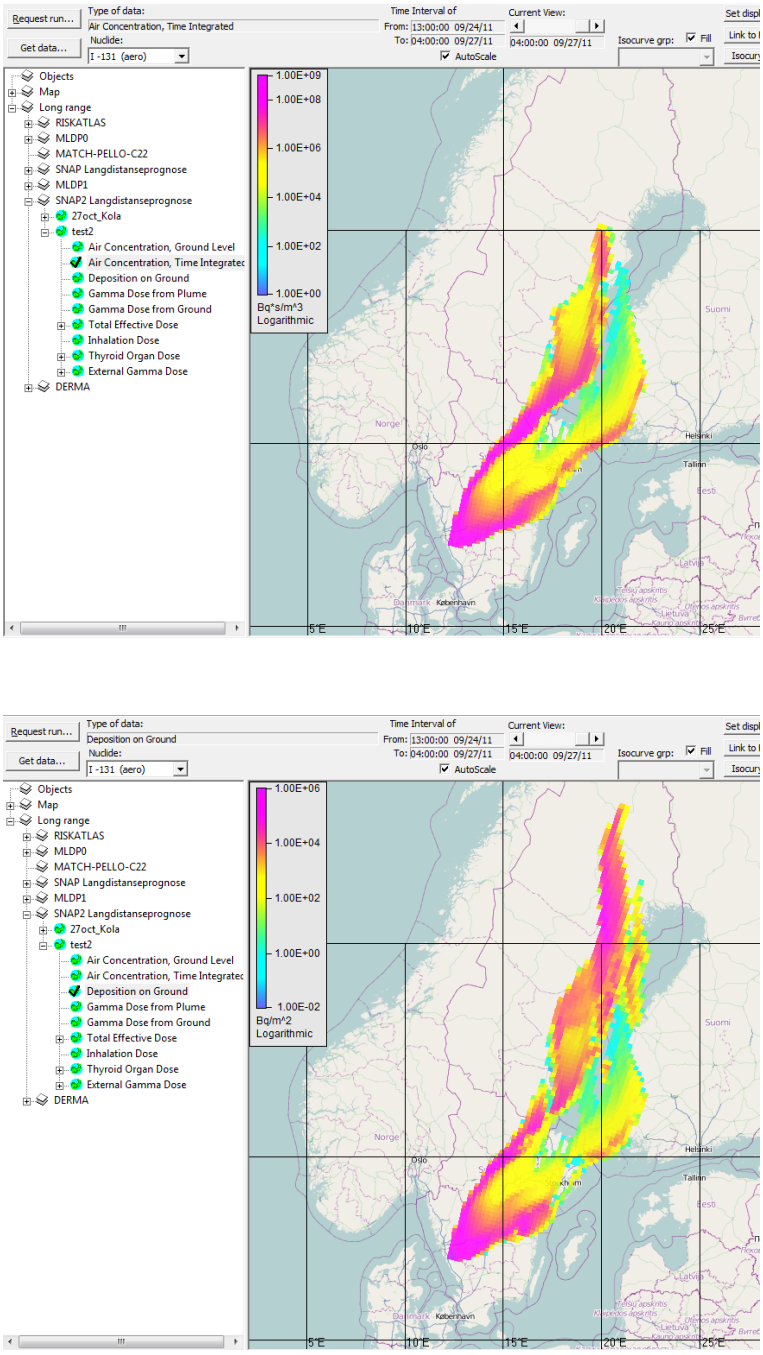

Figure 5: Screen dumps of the time integrated I-131 concentration (above) and deposition (below) from the test accident run post processed in the ARGOS system at NRPA. Results of the same SNAP run as presented in Fig. 4.

3.2. Nuclear explosion

Possibility of simulating nuclear explosion is a new and important feature in the remote SNAP applications from NRPA. Fortunately up to now, SNAP has never been used for simulating a real nuclear explosion in operational model, but it has been used to simulate historical nuclear explosions in Novaya Zemlya. In the new model version, NRPA can simulate a nuclear explosion which takes place within the model domain shown in Fig. 1.

3.2.1. Computational scheme for nuclear explosion

The procedure and computational diagram for nuclear explosion (Fig. 6) is very similar to the case of nuclear accident (Fig. 3) and there are only two small differences visible in the bomb diagram.

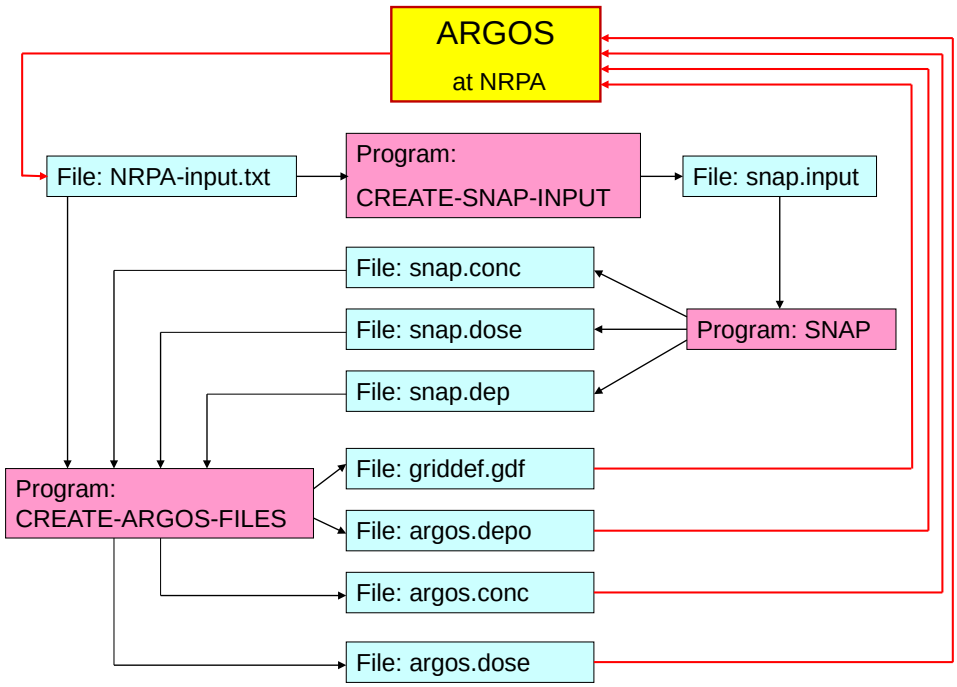

Figure 6: Computational diagram at met.no for nuclear explosion case.

The first difference is in the lack of the file `isotope-list.txt`, which is not necessary for nuclear explosion. The second is in the fact, that the file `NRPA-input.txt` is created by ARGOS directly in the text format, so conversion from the html to text file is not necessary. The computational procedure at met.no starts when the file `NRPA-input.txt` arrives. Program `CREATE-SNAP-INPUT.txt` generates file `snap.input` and the run of the SNAP model starts at once. The relatively longest time in the entire procedure is necessary for the SNAP run. When this run is finished, three SNAP output files are converted to ARGOS for-

mat by the program `CREATE-ARGOS-FILES.txt` and these files are immediately sent to NRPA.

An example of the input file for remote nuclear explosion application is shown below:

```
61.972          Latitude (dec.deg.)
10.810          Longitude (dec.deg.)
201111041214    Start (UTC)
201111061214    End (UTC)
3 Output time step (hr)
10 kt Yield of source
100.00 Fission proportion
```

The first two lines of the file above give the geographical coordinates of the explosion. The third line specifies the time of explosion and the next one gives the required end time of the simulation and time of the final output from the model run. If the meteorological data are not available for the required end time, the model is run until the end of available meteorological data. The line number five gives the time interval between consecutive outputs from the model run. The one before last line gives the most important information for the explosion, namely the explosive yield in kt. The last line, fission proportion, is not used in the SNAP model at present.

3.2.2. Examples of remote applications for nuclear explosion

For all examples of remote applications from NRPA we have chosen a hypothetical nuclear explosions over London. There was no particular reason for selecting London as the place of explosion, except for some interesting weather patterns which created large differences for different explosion yields. In these examples we have tested all explosive yields available in the SNAP menu, starting from 1 kt and ending in 3000 kt. It means that, in this example, we have performed eight model runs with different explosive yields with London as a detonation place, or to be more precise the sky over London. The results of these runs as maps of time integrated concentrations and deposition are shown in Figs. 7-14 for different explosive yields In Fig. 7-14, the same scale is kept for all time integrated concentration maps and the same scale for all deposition maps.

The direction of the transport is south-west for the first three explosive yields in the range 1-30 kt, however, the west component is getting stronger with the higher explosive yield. The southern part of UK, small area of Western France and also small area of Northern Spain are affected in this explosive range.

An interesting effect can be seen in Figs. 10 and 11 showing the results of 30 kt and 100 kt explosions. Namely, in addition to south-west direction there is also a clear and strong transport to the east. This is caused by the easterly wind direction in the upper troposphere, where a large part of the initial cloud is located for these explosions. The similar features are seen for 300 kt explosion (Fig. 12). Much larger part of France and many additional countries (Belgium, Germany, Switzerland, Italy, Austria Czech Republic, Slovak Republic, Hungary, Poland and Ukraine) are covered by the radioactive cloud in this explosive yield range.

For very high explosive yield like 1000 kt and 3000 kt, there is only transport to the east with the radioactive cloud reaching Russia at the end.

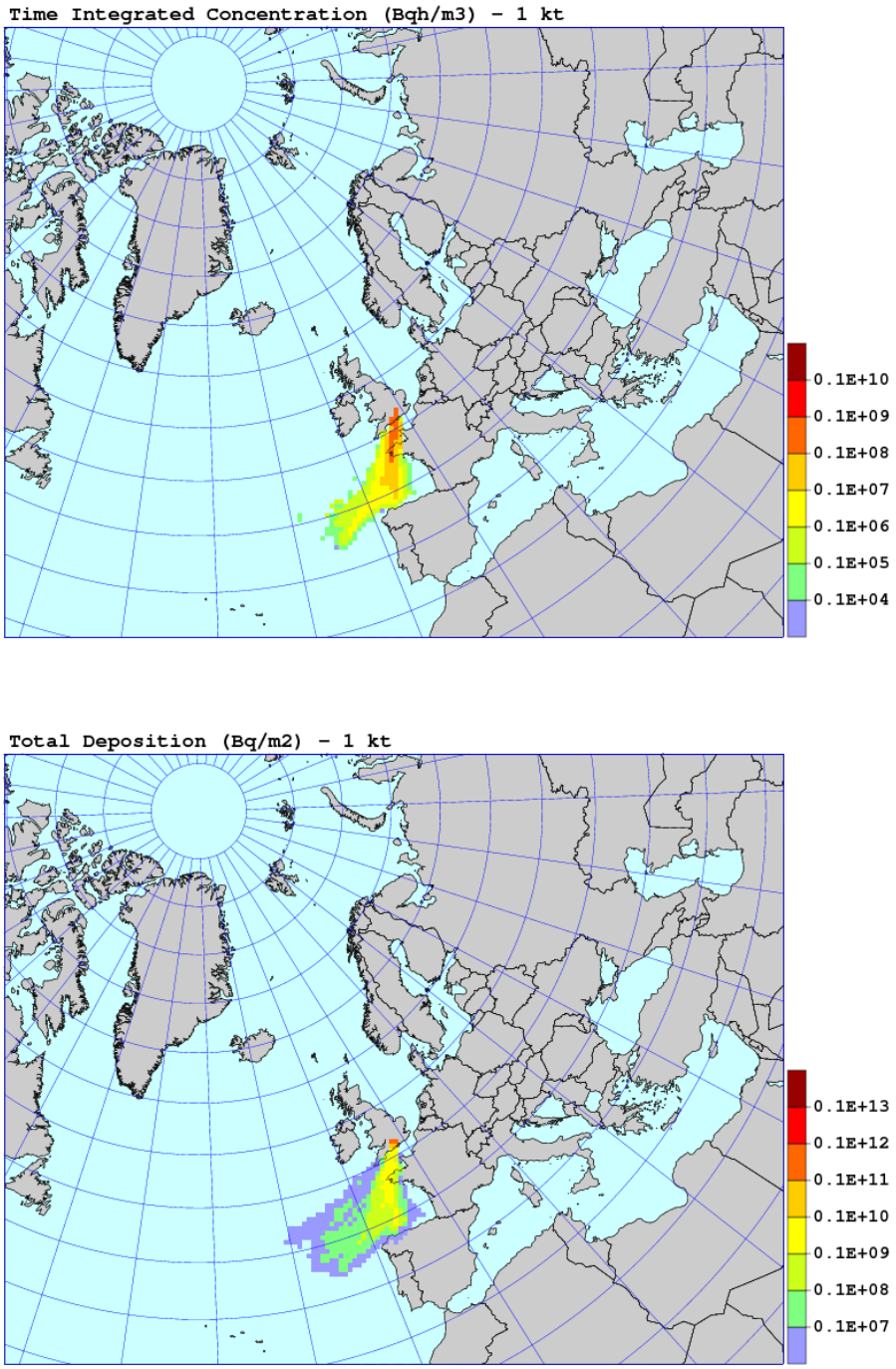

Figure 7: An example of SNAP run for 1 kt nuclear explosion, 48 hours after the detonation. Time integrated concentrations in Bq h m^{-3} above and total deposition in Bq m^{-3} in the bottom.

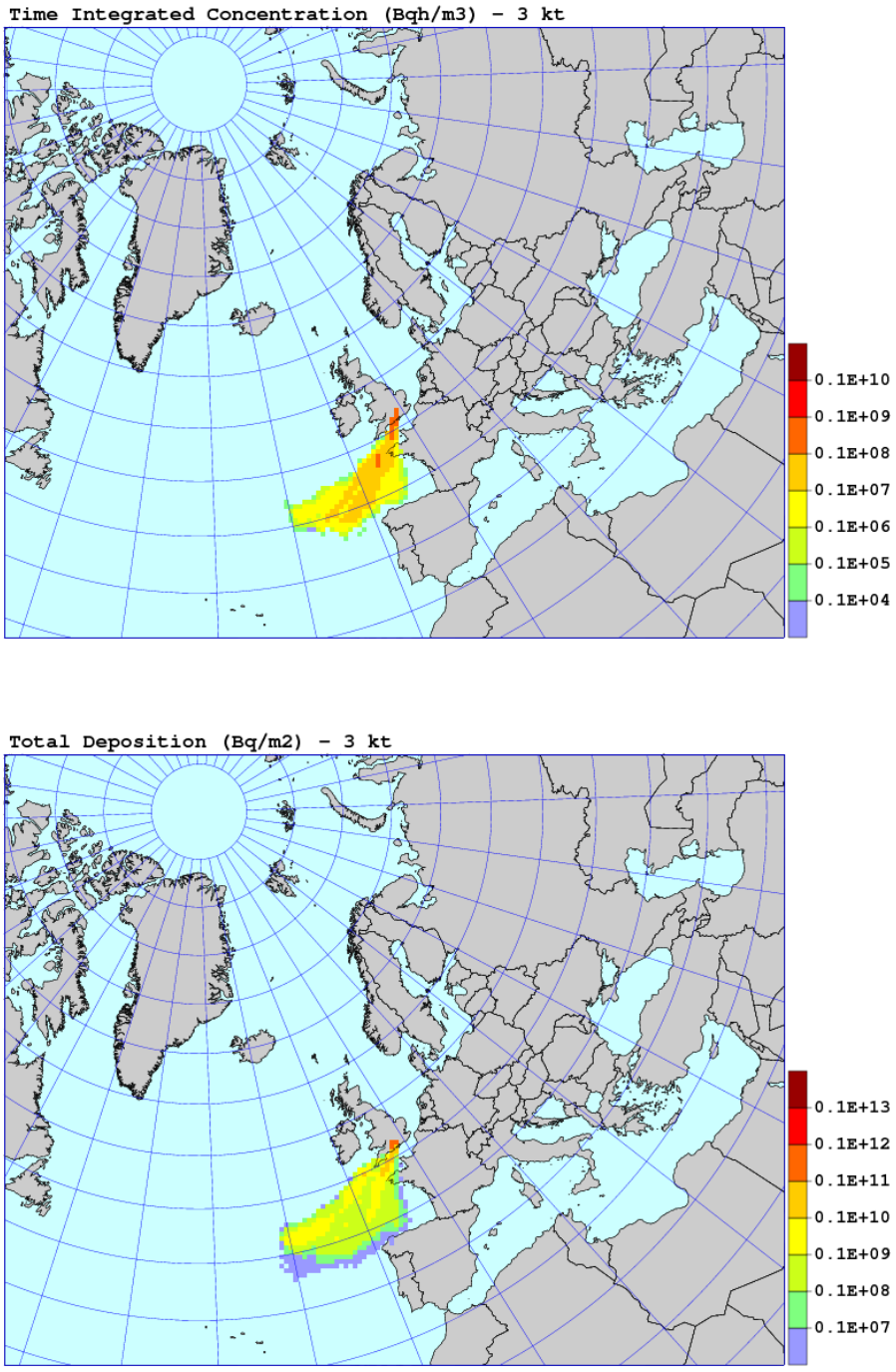

Figure 8: An example of SNAP run for 3 kt nuclear explosion, 48 hours after the detonation. Time integrated concentrations in Bq h m^{-3} above and total deposition in Bq m^{-3} in the bottom.

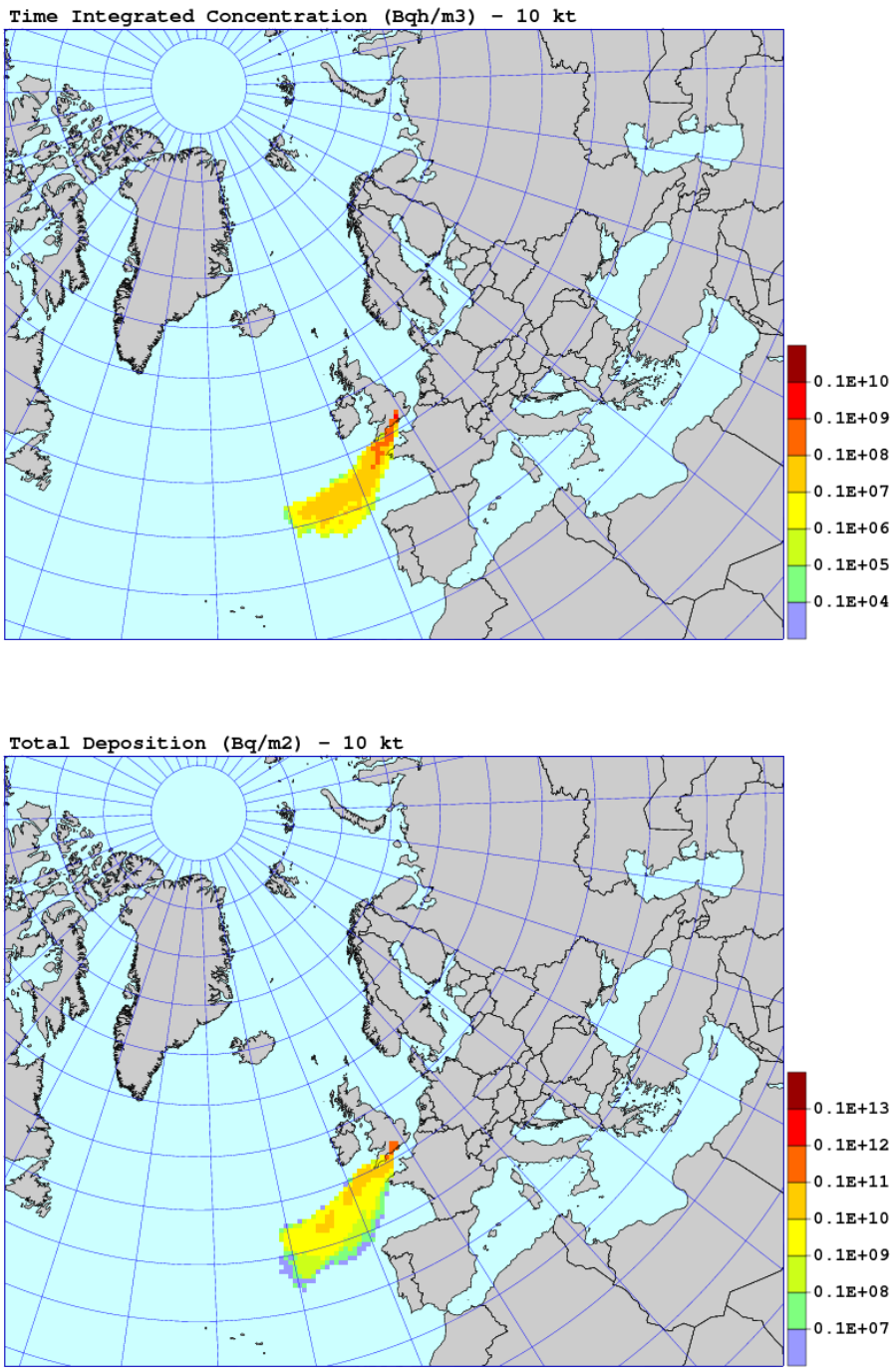

Figure 9: An example of SNAP run for 10 kt nuclear explosion, 48 hours after the detonation. Time integrated concentrations in Bq h m^{-3} above and total deposition in Bq m^{-3} in the bottom.

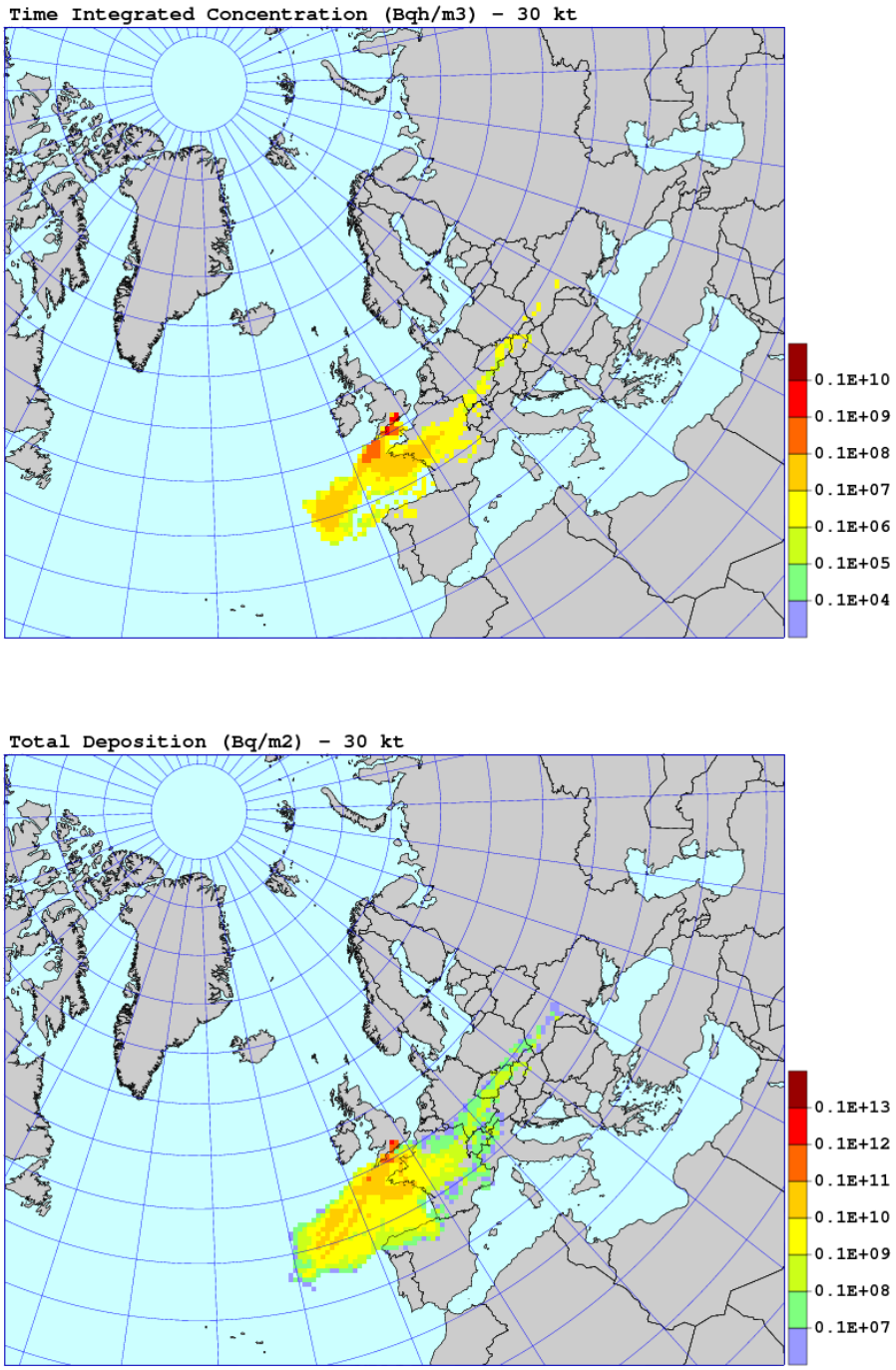

Figure 10: An example of SNAP run for 30 kt nuclear explosion, 48 hours after the detonation. Time integrated concentrations in Bq h m^{-3} above and total deposition in Bq m^{-3} in the bottom.

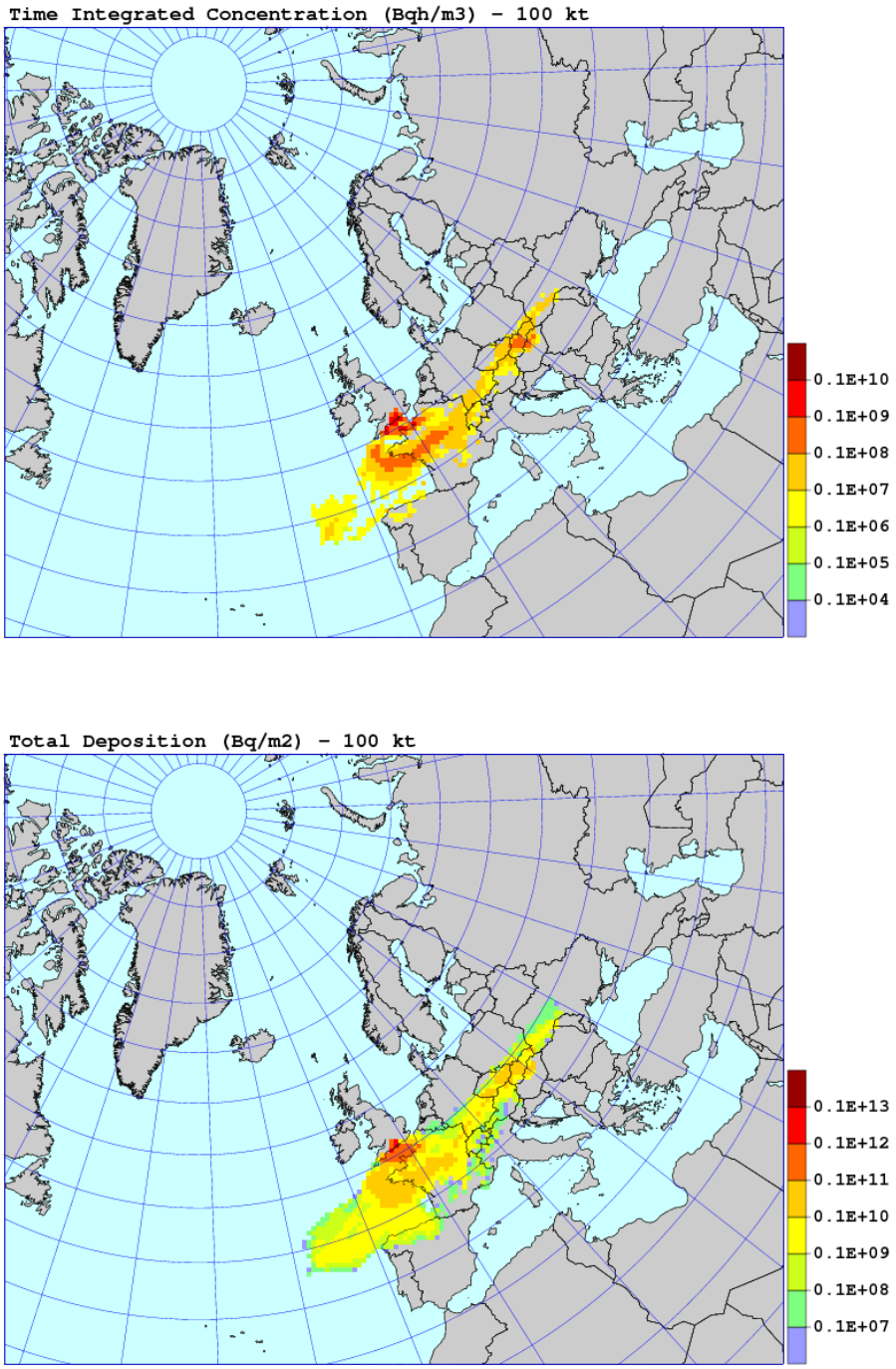

Figure 11: An example of SNAP run for 100 kt nuclear explosion, 48 hours after the detonation. Time integrated concentrations in Bq h m^{-3} above and total deposition in Bq m^{-3} in the bottom.

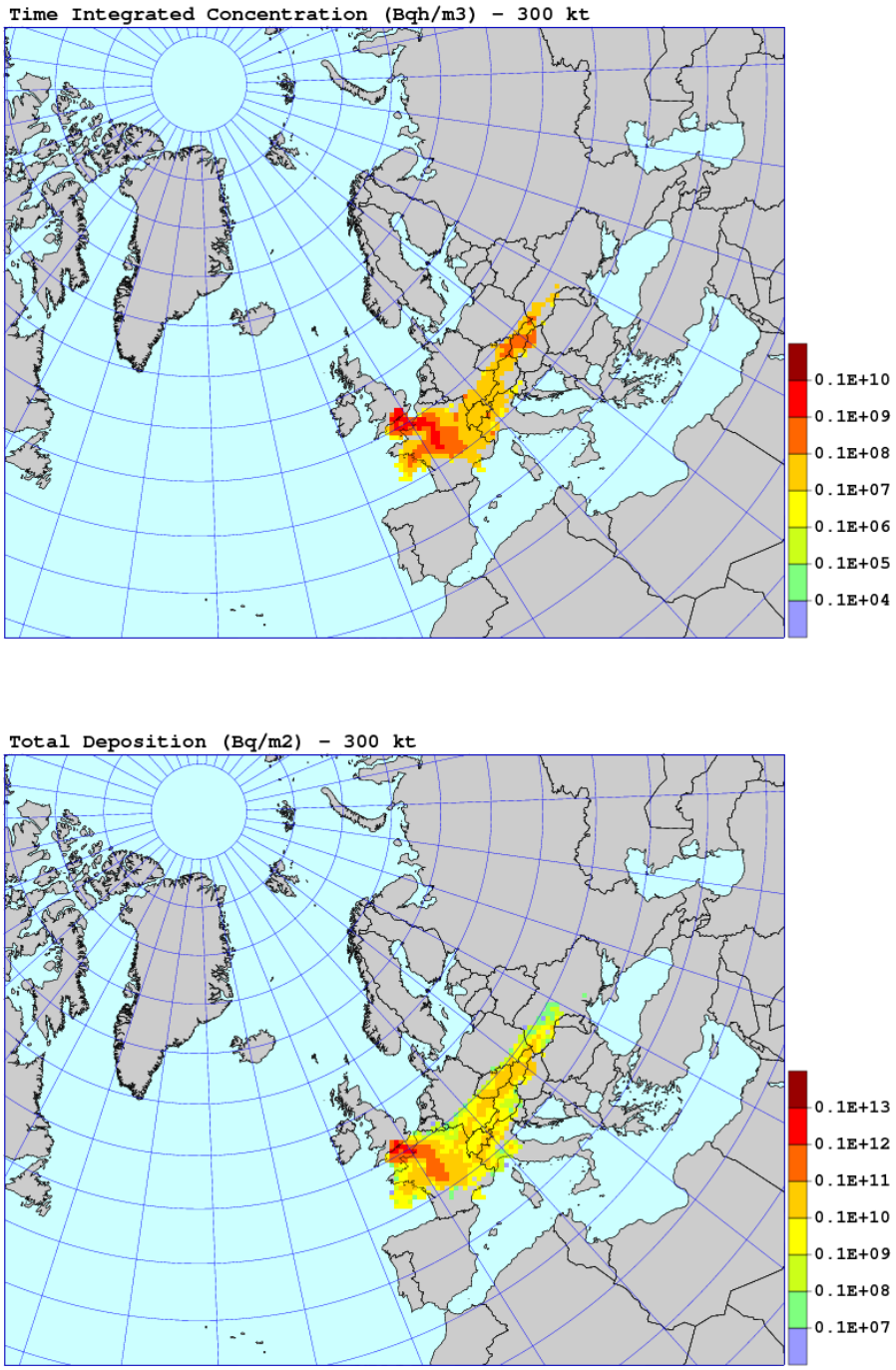

Figure 12: An example of SNAP run for 300 kt nuclear explosion, 48 hours after the detonation. Time integrated concentrations in Bq h m^{-3} above and total deposition in Bq m^{-3} in the bottom.

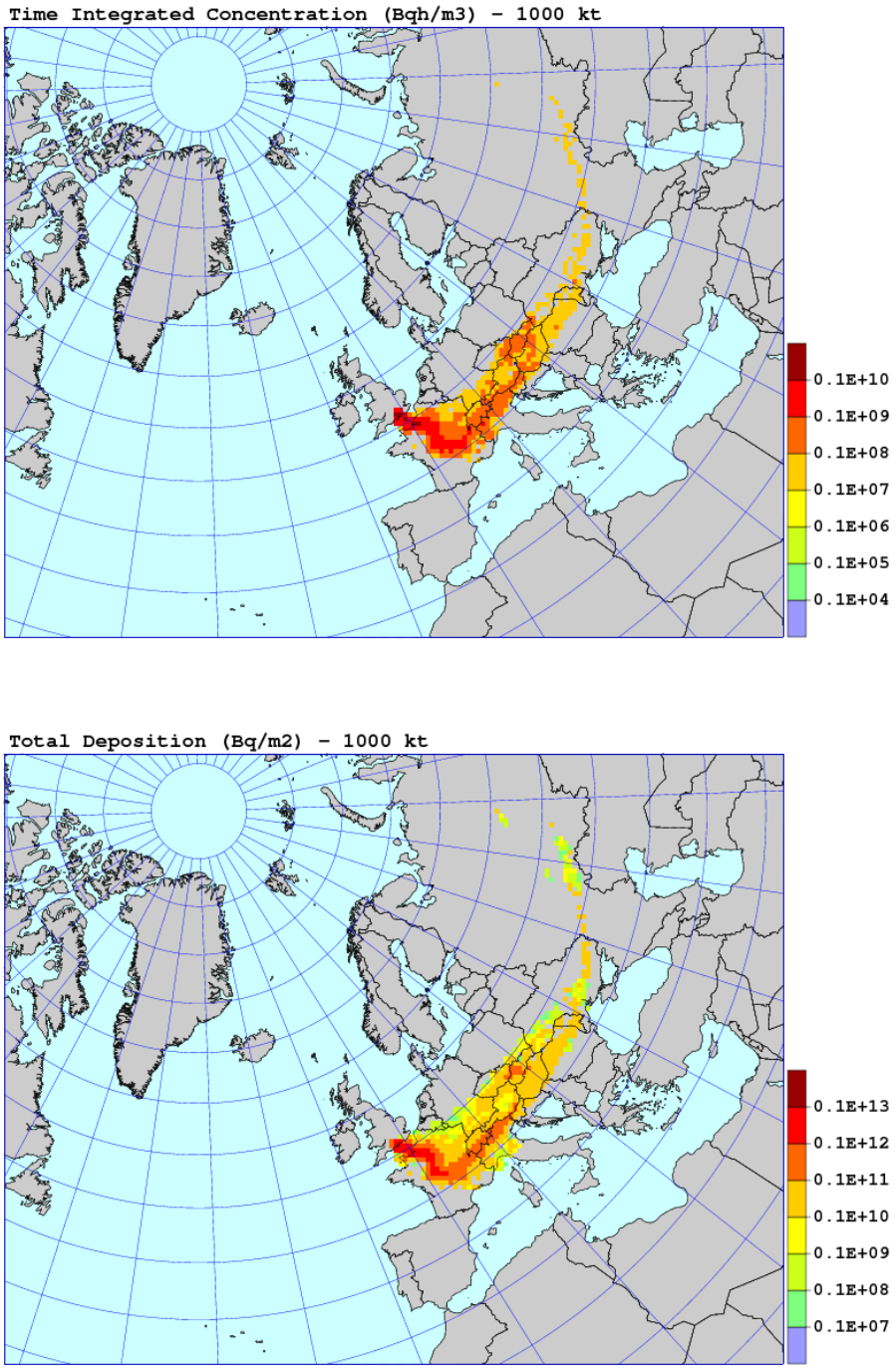

Figure 13: An example of SNAP run for 1000 kt nuclear explosion, 48 hours after the detonation. Time integrated concentrations in Bq h m^{-3} above and total deposition in Bq m^{-3} in the bottom.

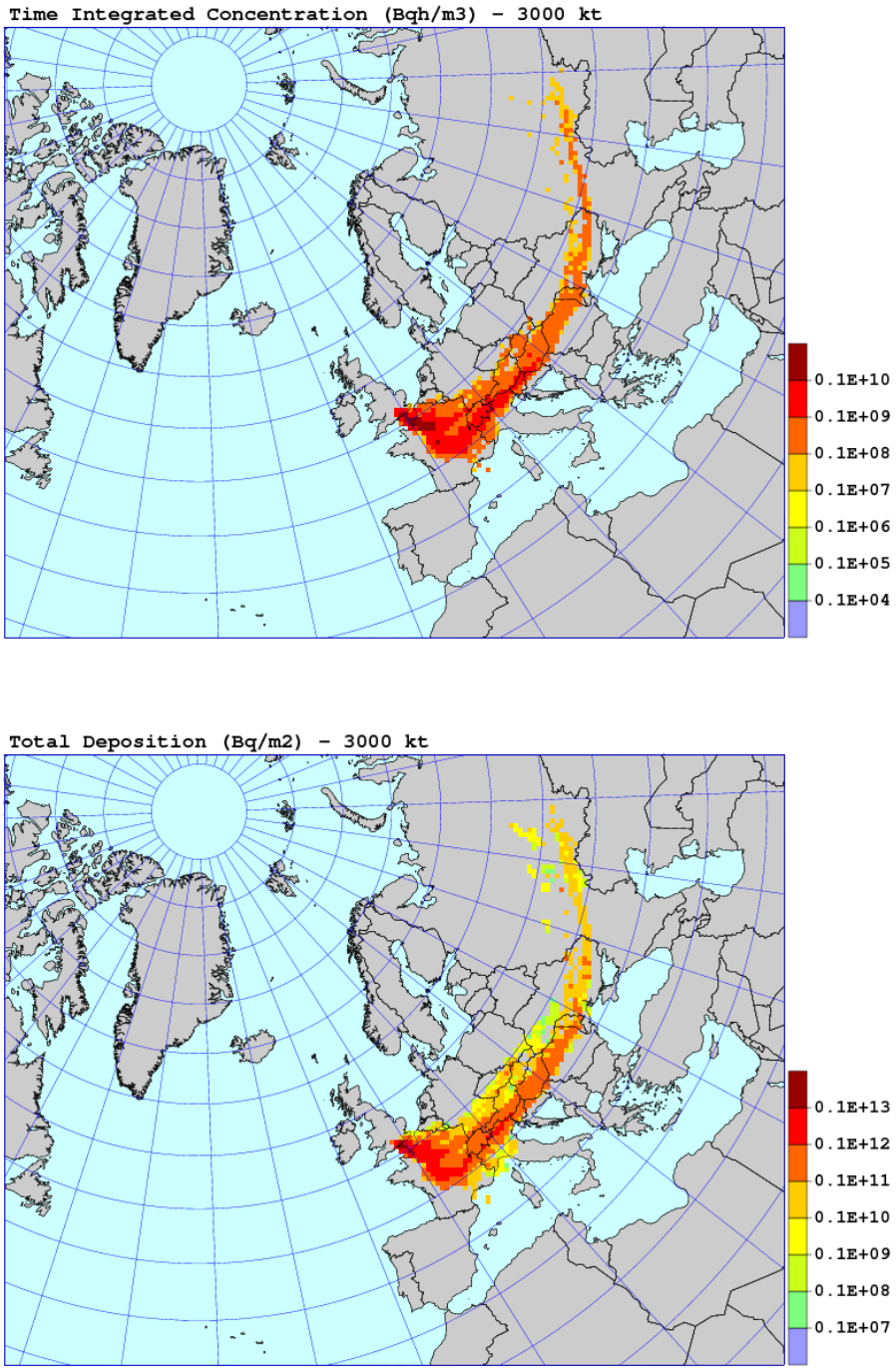

Figure 14: An example of SNAP run for 3000 kt nuclear explosion, 48 hours after the detonation. Time integrated concentrations in Bq h m^{-3} above and total deposition in Bq m^{-3} in the bottom.

3.3. Trajectories

In the frame of current project, there was a plan for implementation of both, forward and backward trajectory calculations in SNAP. However, some difficulties occurred concerning development of backward trajectories. First, because of the limited storage space, met.no does not store more than one day of old meteorological output from HIRLAM-12. It means that calculation of backward trajectories would be very limited in time for present situation. Second difficulty is related to the present structure of the FORTRAN code of SNAP. Reading meteorological data takes more time than the computation and therefore only data for the period of 6 hours are available for the computation at the arbitrary model time step and in the strictly forward order. This is enough for calculating the forward trajectories, but not enough for backward, in which case we need to reverse the order of reading meteorological data and change the sign of the velocity field. Theoretically it is not a problem, but technically it is quite a problem in the present code structure of SNAP. Therefore, we decided to postpone the implementation of the backward trajectories until the new version of SNAP code will be developed and new dedicated server ready for use.

3.3.1. Calculation of forward trajectories

Three-dimensional trajectories are calculated in the SNAP model and in case meteorological data from the NWP of HIRLAM-12 model, these calculations are originally performed in the η vertical co-ordinates. The forward three-dimensional trajectory is calculated in SNAP by solving the following set of equations:

$$\begin{cases} \frac{dx}{dt} = u(x,y,\eta,t) \\ \frac{dy}{dt} = v(x,y,\eta,t) \\ \frac{d\eta}{dt} = \dot{\eta}(x,y,\eta,t) \end{cases} \tag{24}$$

where $x = x(t)$, $y = y(t)$, $\eta = \eta(t)$ represent a parametric description of the trajectory; u and v are the horizontal components of the velocity field and η is the vertical component. To solve the set of equations (24) we have used the same numerical method as applied in the EMEP trajectory model [2]. In the numerical solution, each forward trajectory is represented by a set of discrete points. These points are calculated from Eq. 24 using an interactive procedure described by Pettersen [23]. Denoting the initial point on the trajectory at time t as (x_0, y_0, η_0), the initial change of the position is defined as:

$$\begin{cases} \triangle x_0 = u(x_0,y_0,\eta_0,t)\triangle t \\ \triangle y_0 = v(x_0,y_0,\eta_0,t)\triangle t \\ \triangle \eta_0 = \dot{\eta}(x_0,y_0,\eta_0,t)\triangle t \end{cases} \tag{25}$$

Bi-linear interpolation in space from the four nearest nodes is used to calculate the wind com-

ponents in Eq. 25 and linear interpolation in time between consecutive 3-hourly wind fields. The time step between the points on the trajectory is 5 minutes. The following iterative procedure for i in Eq. 26 is applied to correct the first guess for $(\triangle x_0, \triangle y_0, \triangle \eta_0)$:

$$\begin{cases} \triangle x_i = \frac{\triangle x_0 + u(x_0+\triangle x_{i-1}, y_0+\triangle y_{i-1}, \eta_0+\triangle \eta_{i-1}, t+\triangle t)\triangle t}{2} \\ \triangle y_i = \frac{\triangle y_0 + v(x_0+\triangle x_{i-1}, y_0+\triangle y_{i-1}, \eta_0+\triangle \eta_{i-1}, t+\triangle t)\triangle t}{2} \\ \triangle \eta_i = \frac{\triangle y_0 + v(x_0+\triangle x_{i-1}, y_0+\triangle y_{i-1}, \eta_0+\triangle \eta_{i-1}, t+\triangle t)\triangle t}{2} \end{cases} \tag{26}$$

After N iterations, the next point on the trajectory can be calculated as:

$$\begin{cases} x(t+\triangle t) = x(t) + \triangle x_N \\ y(t+\triangle t) = y(t) + \triangle y_N \\ \eta(t+\triangle t) = \eta(t) + \triangle \eta_N \end{cases} \tag{27}$$

In the EMEP model [2], five iterations ($N = 5$) are assumed to be sufficient for the conversion. In our experiments [**?**], we have not found much difference in accuracy between five and two iterations and therefore we used only two iterations to calculate for convergence to the final position. Each trajectory is calculated for the period specified in the input file or shorter if it reaches the boundary of the model domain or the end of available meteorological data. The minimum possible time step between the consecutive points on the trajectory is 5 minutes, but the distance between the consecutive trajectory points in the output file is 1 hour.

3.3.2. An Example of forward trajectories calculated by SNAP

One of the MetNet scenarios was chosen for testing remote calculation of the trajectories. In this scenario, a radioactive release from the accident at nuclear powered ship located close to the coast of Norway is assumed. All parameters necessary for calculating three dimensional trajectories are specified in the compressed input file send from NRPA. The original compressed file, sent from NRPA is decompressed and further proceed at met.no in the similar way as for nuclear accident or explosion. An example of such a file in the text format is shown below. The first line in the file is the name of the source or scenario. Two next lines include information about origin of the trajectory (latitude and longitude). Following line gives the date and time of the release and next defines the calculation mode. There are two options for the mode parameter in the file: forward and backward. Only forward option is used at present which means that trajectories are calculated forward from the source location. The length (in time) of the trajectories is specified by the "Simulation duration (h)" and the maximum length/period for which trajectories can be calculated is 66 hrs. It is limited by the forecast horizon of HIRLAM NWP model currently operational at met.no. Number of trajectories to be calculated is specified by "Number of parcels". For practical reason, the number of trajectories to be calculated is limited to 10. The last lines in the input file define the release level (in m) for each trajectory.

```
METNET          Source name
64.15           Latitude (dec.deg.)
9.10            Longitude (dec.deg.)
2010101406      Start (UTC)
forward         Mode
48              Simulation duration (h)
4               Number of parcels
10.0            First parcel (meters above surface)
500.0           Second parcel (meters above surface)
1000.0          Third parcel (meters above surface)
1500.0          Fourth trajectory (meters above surface)
```

The above file is then used to create the input file for the SNAP model and SNAP is run to calculate specified 3-D trajectories. In this example four forward trajectories are calculated for the period of 48 hours (two days). These trajectories are released at different levels above the surface: 10m, 50m, 1000m and 1500m. The results of the model run are written in the number of files corresponding to the number of trajectories calculated, which means one output file for each trajectory. Each file includes the locations (latitude and longitude) and height above the surface of the trajectory points. These output files are available for further processing in the ARGOS system at NRPA. The results of the SNAP run are also used internally at met.no to create maps with calculated trajectories.

The example with such maps for four trajectories specified in the input file above and calculated at met.no is presented in Fig. 15. There is one trajectory on each map with different colors indicating the elevation (in m above the ground level) of the trajectory segment. Those trajectories go to different directions and their altitudes are variable in time.

Output trajectory files are sent automatically to NRPA and there used for creating maps in the ARGOS system. The same trajectories as shown on separate maps in Fig. 15 are shown in Fig. 16, but on one map and created within the ARGOS system. Each of four trajectories in Fig. 16 is marked with different color and the trajectory points (positions at each hour after release) are shown. The release location is also marked on the map. As expected, the distance traveled by the trajectory increases with the elevation of the release location because of the higher wind speed on high elevations. The destination and directions of movements are quite different for the trajectories released at different levels. The density of the points on each trajectory indicates the speed of the transport. The transport was relatively fast over Norway and Sweden on three trajectories released on 500 m and above. The transport was much slower outside the Scandinavia mainly because all trajectories went on trough much lower level than the level they were released on. The transport on the lowest trajectory was relatively slow and the speed had not changed much during the entire period.

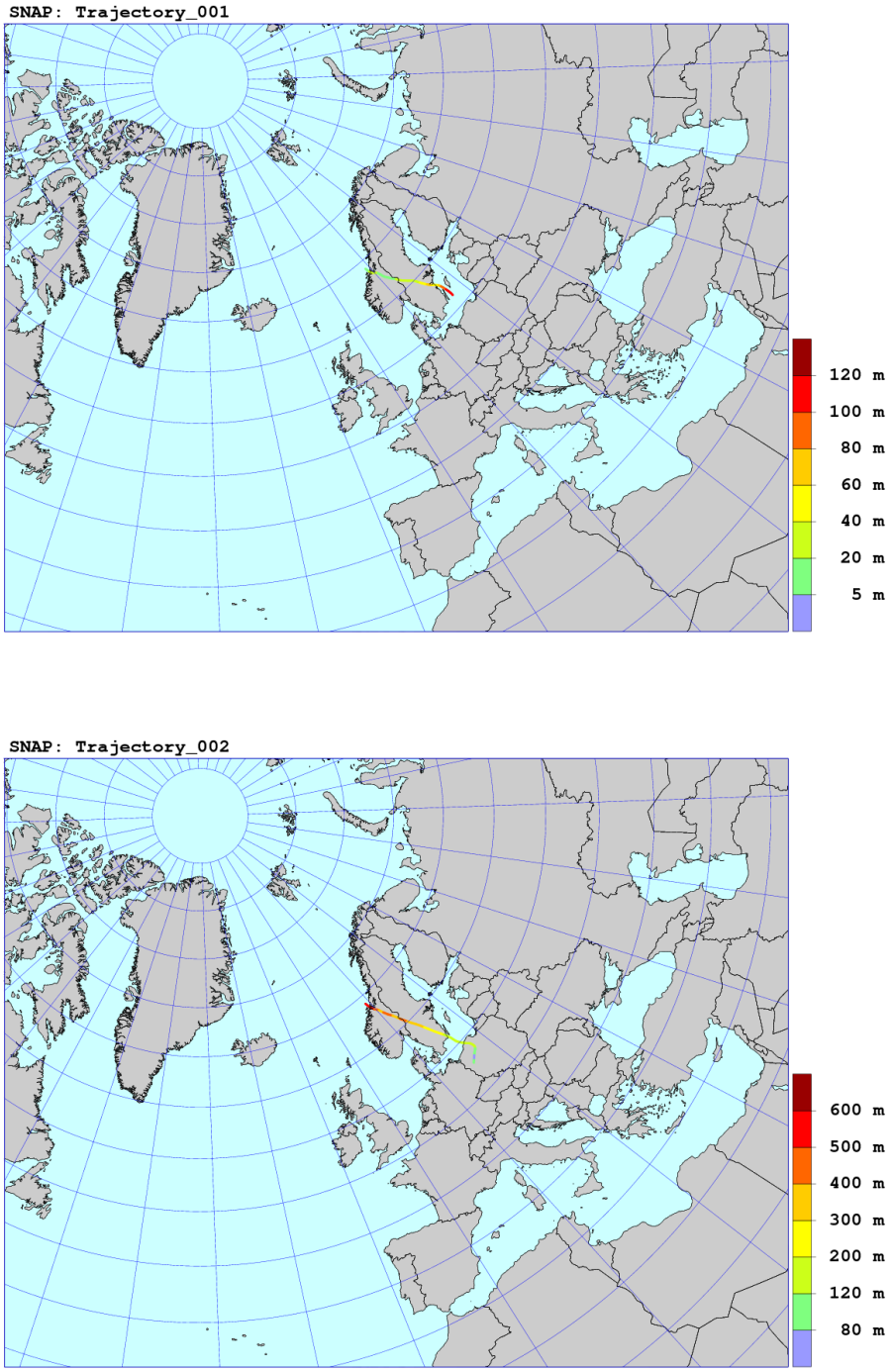

Figure 15: Test trajectories calculated by SNAP based on input file specified at NRPA and displayed locally at met.no. Different colors indicate the elevation (in m above the ground level) of the trajectory segment.

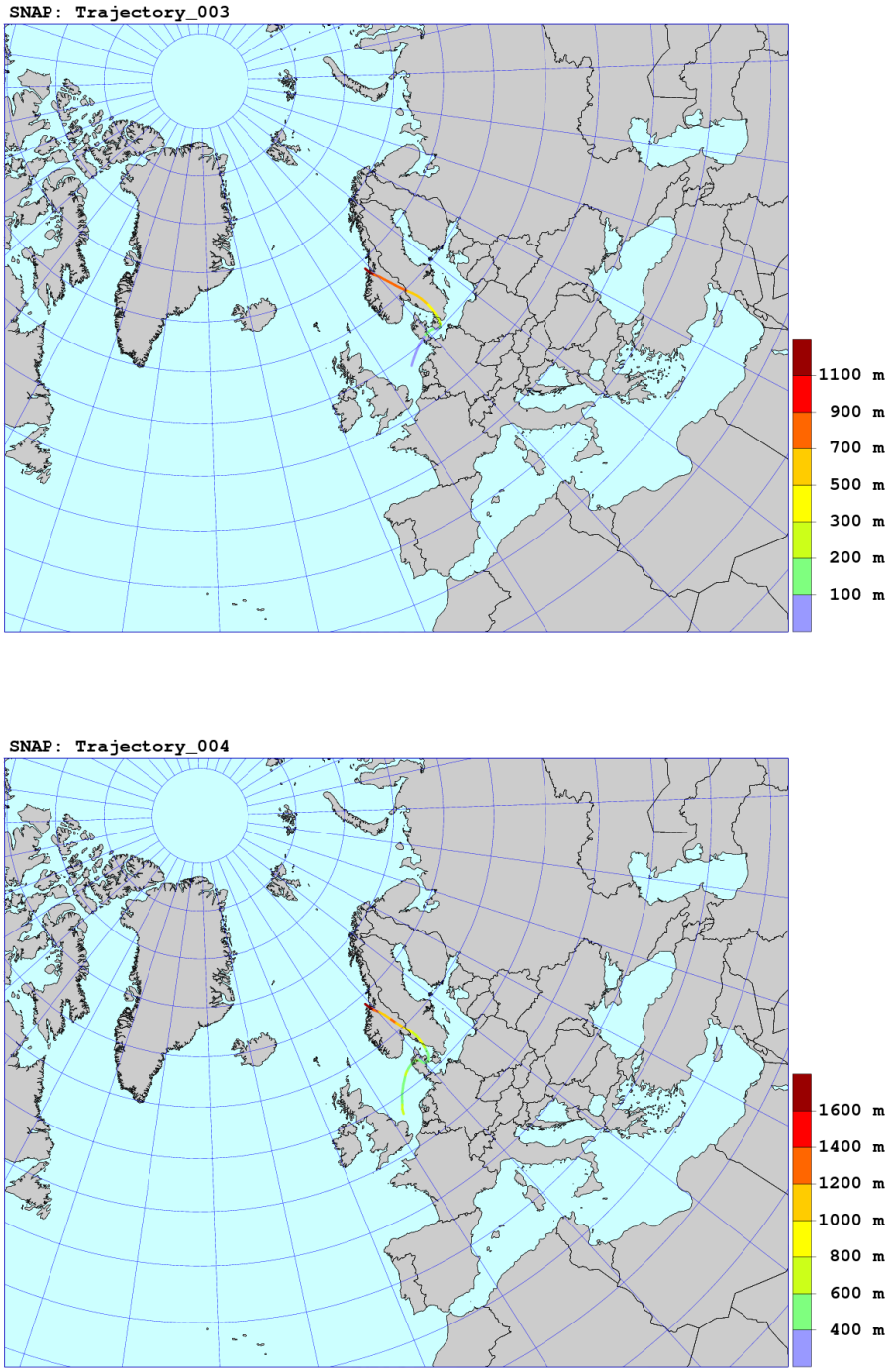

Figure 15: (cont.) Test trajectories calculated by SNAP based on input file specified at NRPA and displayed locally at met.no. Different colors indicate the elevation (in m above the ground level) of the trajectory segment.

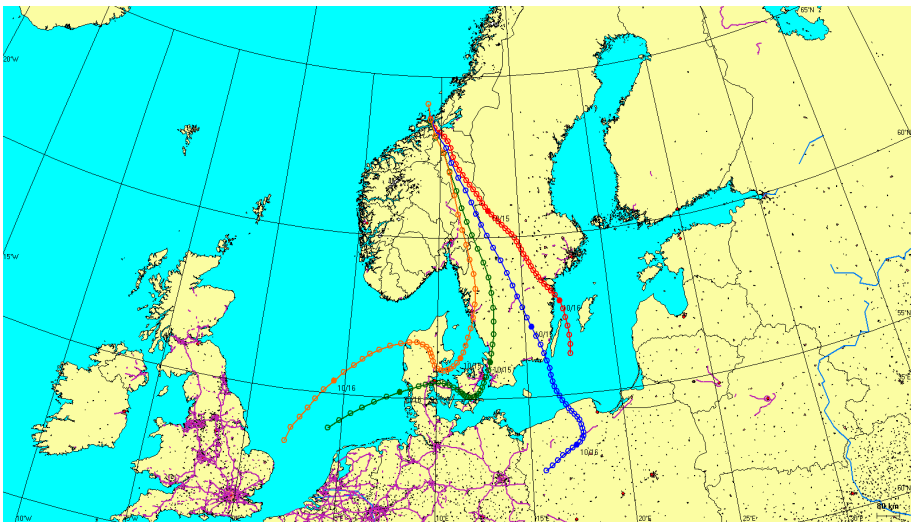

Figure 16: The same test trajectories calculated by SNAP as in Fig. 15, but displayed remotely in the ARGOS system at NRPA.

Figure 17: Vertical locations of the trajectory points in time for the same trajectories as in Fig. 16.

The levels of the trajectory segments are not shown in Fig. 16, but instead they are displayed in a separate Fig. 17. Fig. 17 shows that atmospheric transport is indeed three dimensional. Only trajectory released at the lowest level (10 m) does not change altitude much, however it is slightly higher at the and. All other trajectories tend to go down in the first period of the transport. Then the trajectory released at the top level (1500 m) remains on the 500 m level, whereas, two other trajectories end up much lower, close to the ground.

4. Sensitivity Tests and Measures

Sensitivity tests have been performed with the new SNAP version for two main remote applications from NRPA: nuclear accident and nuclear explosion. The results of these tests will be later described separately for nuclear accident and nuclear explosion. In this Chapter we describe a general procedure for the sensitivity tests and give definitions of selected sensitivity measures.

A framework for sensitivity analysis is discussed in several papers e.g. in Rao [25]. In general, sensitivity analysis examines the response of the particular model to variations of input variables or internal parameters to this model. The results of sensitivity analysis are not directly related to model accuracy, but give the indication of relative importance of input variables. This is helpful when deciding how accurately the input variables have to be estimated.

Following Rao [25], for a model with j-th output given by $C(t_i)$ where $t_i(= 1,2,...,n)$ are independent input variables, the sensitivity coefficients S_{ij} are defined as

$$S_{ij} = \partial C / \partial (\ln t_i) \tag{28}$$

and the derivatives are evaluated for the base case values of the inputs.

In our sensitivity studies we do not use Eq. 28 and perform a slightly different and more intuitive analysis having in mind possible applications to nuclear accident or explosion. The first step in this analysis is a choice of the basic case. For this purpose we have chosen one of the cases for MetNet meteorological scenario from 10 October 2010. The main reason for this choice was a fact that the radioactive cloud from this hypothetical accident came to Norway and particularly to Oslo. The second important reason was availability of meteorological data for this case. So, the SNAP model was run first for the basic case.

In the sensitivity tests, we have performed a number of additional runs. In each of them, we either excluded one of the most important processes responsible for transport and deposition of radioactive debris or intensity of this process. Then, we compared the results of such runs with the results of the standard run performed for the basic case. The maps of deposition and concentration were used for visual comparison and estimation of differences and sensitivities. I addition, the values of total deposition and time integrated concentration were compared for the model grid square were the city of Oslo is located.

The results of the SNAP model are not only sensitive to the presence and correct parameterisation of basic physical processes, but also to the number of model particles used for the simulations. The number of model particles should be as large as possible in the Lagrangian models, but it is limited for the practical and mainly computational (time and memory) reasons. It is important to know how the model results are changing with different number of model particles used. This kind of sensitivity to number of model particles was also taken into account.

To compare sensitivities quantitatively, four sensitivity measures were established, two of global nature for comparisons of the fields and two local for comparison of the values in the Oslo grid square. Definitions of these sensitivity measures are given below:

Sensitivity of **D**eposition **F**ield (**SDF**):

$$SDF = 100 \cdot \frac{\sqrt{(\frac{1}{M \cdot N} \sum_{i=1}^{M} \sum_{j=1}^{N} (d_t(i,j) - d_s(i,j))^2)}}{\frac{1}{M \cdot N} \sum_{i=1}^{M} \sum_{j=1}^{N} d_s(i,j)} \tag{29}$$

Sensitivity of Time Integrated **C**oncentration **F**ield (**SCF**):

$$SCF = 100 \cdot \frac{\sqrt{(\frac{1}{M \cdot N} \sum_{i=1}^{M} \sum_{j=1}^{N} (c_t(i,j) - c_s(i,j))^2)}}{\frac{1}{M \cdot N} \sum_{i=1}^{M} \sum_{j=1}^{N} c_s(i,j)} \tag{30}$$

Sensitivity of **D**eposition in the **G**rid square with Oslo (**SDG**):

$$SDG = 100 \cdot \frac{d_t(i_o, j_o)}{d_s(i_o, j_o))} \tag{31}$$

Sensitivity of Time Integrated **C**oncentration in the **G**rid square with Oslo (**SCG**):

$$SCG = 100 \cdot \frac{c_t(i_o, j_o)}{c_s(i_o, j_o))} \tag{32}$$

In the above equations:
M - is the model grid size in x-direction,
N - is the model grid size in y-direction,
$d_s(i,j)$ - is the standard (from the base run) deposition in the model grid square (i,j),
$d_t(i,j)$ - is the test (from the sensitivity run) deposition in the model grid square (i,j),
$c_s(i,j)$ - is the standard (from the base run) time integrated concentration in the model grid square (i,j),
$c_t(i,j)$ - is the test (from the sensitivity run) time integrated concentration in the model grid square (i,j),
(i_o, j_o) - coordinates of the model grid where Oslo is located.

The **SDF** measure is calculated only in the grids where, either standard deposition $d_s(i,j) > 0$, or test deposition $d_t(i,j) > 0$. The same applies to **SCF** measure and concentrations. The **SDF** measure can be roughly interpreted as a standard deviation between the standard deposition field and the deposition field from the sensitivity test, expressed in percent of the average value of the standard deposition field. The **SCF** measure can be interpreted in the same way, but for time integrated concentration. The **SDG** and **SCG** measures are the changes between the value of sensitivity run and value of the standard run, expressed in percent of the standard run value.

The above defined sensitivity measures were calculated for each sensitivity run. The same measures were used in the sensitivity tests for the accident case and sensitivity tests for nuclear explosion.

5. Sensitivity Tests for Nuclear Accident

The choice of the basic case, as well as the resulting source term for the standard run are described in this Chapter, together with the results of sensitivity runs. A brief summary, comparison and ranking of model sensitivities to different processes are also included at the end of the Chapter.

5.1. Standard run for nuclear accident

As a basic case for the standard run we assumed a hypothetical nuclear accident in the ship located close to Norwegian coast, as described in the MetNet exercise which took place in October 2010. Original description of the simulated accident was the following: "A serious accident has occurred aboard a transport ship carrying nuclear waste to Murmansk. The ship is on fire and is reported to leak Cs-137 from a storage tank". To make this basic case a bit more general we have also assumed the release of two other radionuclides iodine and xenon. In this way, we could take into account radionuclides in the form of gas, aerosol and noble gas. Atmospheric transport of these radionuclides is simulated for 48 hours in the standard run and in the test runs.

5.1.1. Source term

Participants of the MetNet exercise in October 2010 were asked to report long range dispersion results based on the original source term:

```
Location: Coast of Norway
Longitude: E 9 deg 10 min 00 sec (9,167)
Latitude: N 64 deg 15 min 00 sec (64,250)
Date and time of release start: 14.10.2010 06:00 UTC
Height of release: 15 meters
Plume rise: up to 500 meters
Length of release: 10 hours
Total amount of nuclides: 9.4E+15 Bq Cs-137 = 2.6E+11 Bq/s
```

In addition, the release of iodine and xenon was assumed from the same location with the rates given below:

```
5.0E17 Bq of iodine (I-131) => Release rate = 1.39E+13 Bq/sec
3.6E17 Bq of xenon (Xe-133) => Release rate = 1.00E+13 Bq/sec
```

The decay constants for selected radionuclides were taken from Appendix A and converted to a half-life time as traditional input for the SNAP model. Both, decay constants and half-life times for selected three radionuclides are given in Table 22. Compared to I-131 and Xe-133, Cs-137 has much longer half-life time and in practice its radioactive decay during the 48 hours simulation can be neglected. Therefore one can expect a low sensitivity of model results to radioactive decay for concentration and deposition of Cs-137.

The above specified source term for nuclear accident was used for the standard run in sensitivity tests.

Table 4: Decay constants and half-life times for three radionuclides selected for sensitivity tests.

Decay variable	Cs-137	I-131	Xe-133
Decay constant (s^{-1})	0.729×10^{-9}	0.944×10^{-6}	0.729×10^{-5}
Half-life time (days)	10954.88	8.07	4.57

5.1.2. Results of the standard run

The source term described in the previous section was used to calculate time integrated concentrations and total deposition for the standard run. The results for Cs-137, I-131 and Xe-133 are presented in Figures. 42, 43, and 44, respectively, in the form of time integrated concentration and deposition maps after 48 hours from the release start.

Time integrated concentrations and deposition calculated in the standard SNAP run show similar spatial pattern for all selected radionuclides. However, calculated values are different for each radionuclide reflecting differences in their release rates. In the initial phase of the transport, the plume is relatively narrow and directed mainly to the south and little bit to the east. In the later phase, prevailing wind direction is changing, horisontal diffusion becomes stronger and the plume is reaching Northern part of Germany in the south, covering Denmark on the way. In the east, the plume is reaching Baltic Sea and in the west it covers almost entire North Sea area, being close to the United Kingdom.

For comparison of sensitivity results, time integrated concentrations and deposition were calculated in the model grid square where the city of Oslo is located. The results for the standard run in the Oslo grid are presented in Table 23.

Table 5: Time integrated concentrations and deposition, 48 hours after the start of release, in the model grid cell where the city of Oslo is located. Results of the standard run.

Radionuclide selected	Time integrated concentration (Bq h m^{-3})	Total deposition (Bq m^{-2})
Cs-137	0.27×10^{1}	0.10×10^{3}
I-131	0.99×10^{2}	0.13×10^{5}
Xe-133	0.15×10^{3}	0.0

The values of time integrated concentrations and deposition for each radionuclide in Table 23 reflect roughly their release rates in the source term for the standard run. However, the highest values of time integrated concentration can be noticed for Xe-133, although total release for I-131 (5.0e17 Bq) is higher than the total release for Xe (3.6e17 Bq). This is because Xe-133 is a noble gas which is neither dry nor wet deposited, with zero deposition value in Table 23. Therefore, the relative amount of Xe-133 radioactivity remaining in the air during the transport is significantly higher than the amount of radioactivity of regular gas or aerosol.

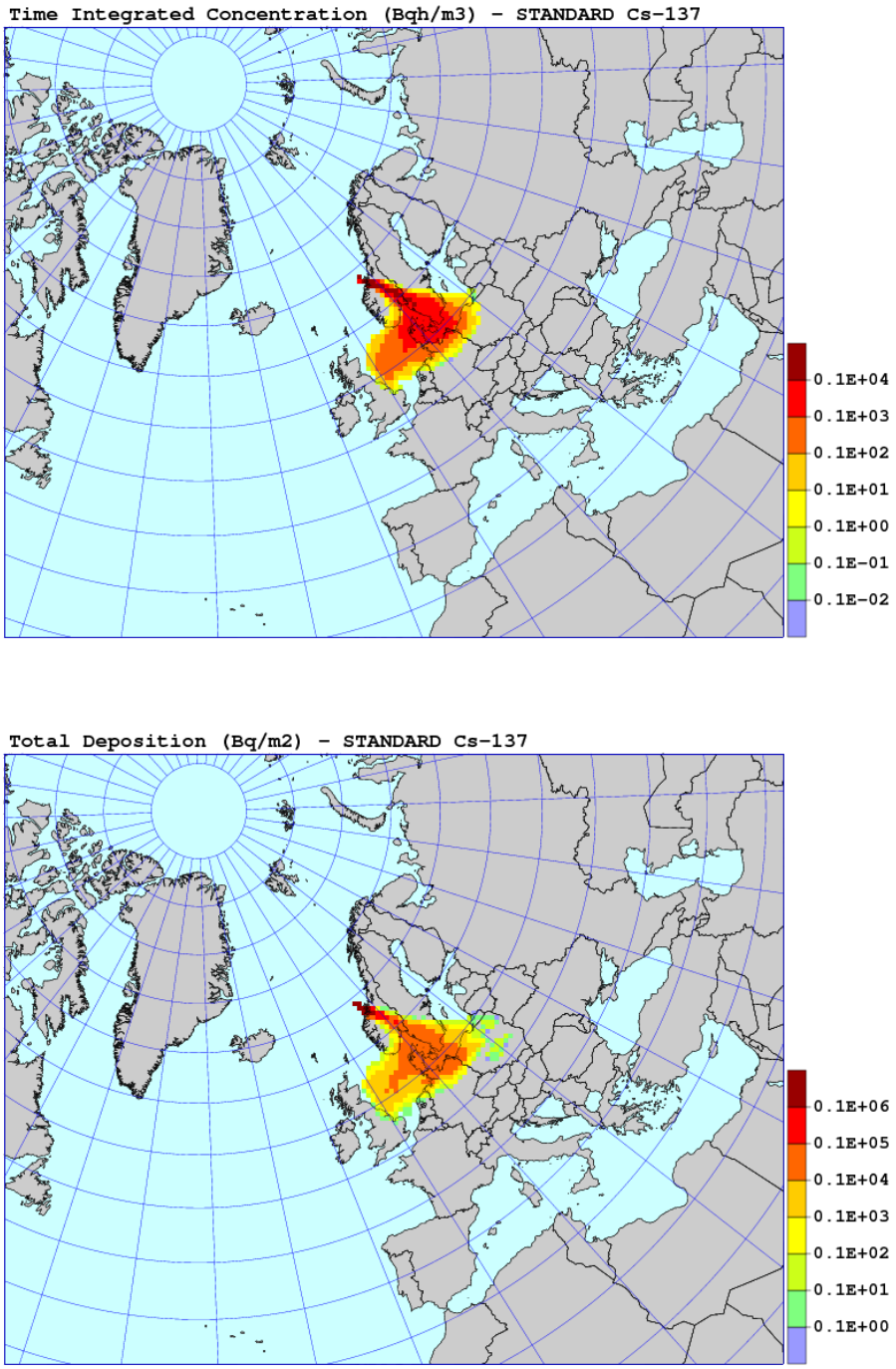

Figure 18: The results of the standard SNAP run for Cs-137 after 48 hours from the accident start. Time integrated concentrations in Bq h m^{-3} above and total deposition in Bq m^{-3} in the bottom.

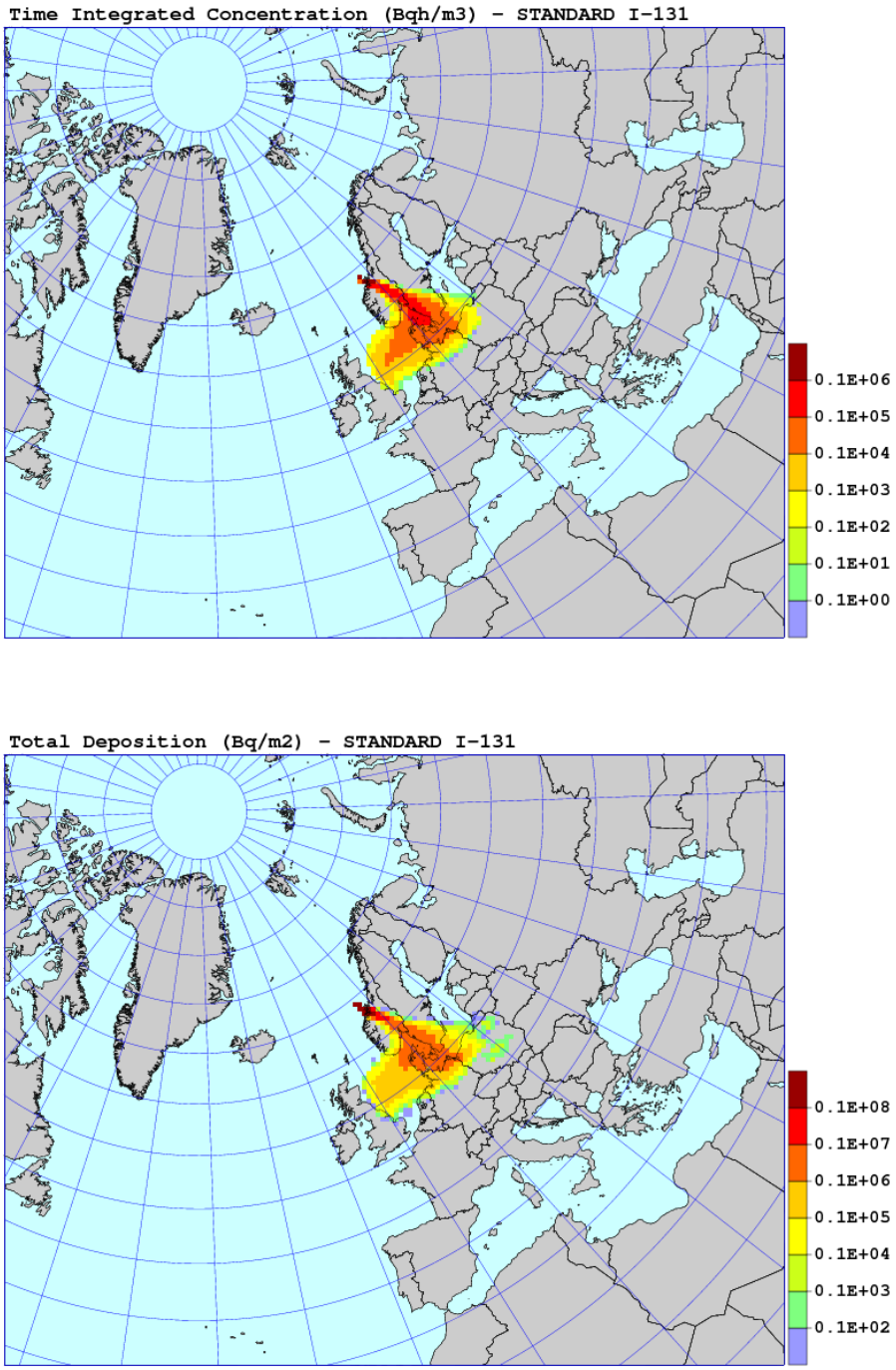

Figure 19: The results of the standard SNAP run for I-131 after 48 hours from the accident start. Time integrated concentrations in Bq h m^{-3} above and total deposition in Bq m^{-3} in the bottom.

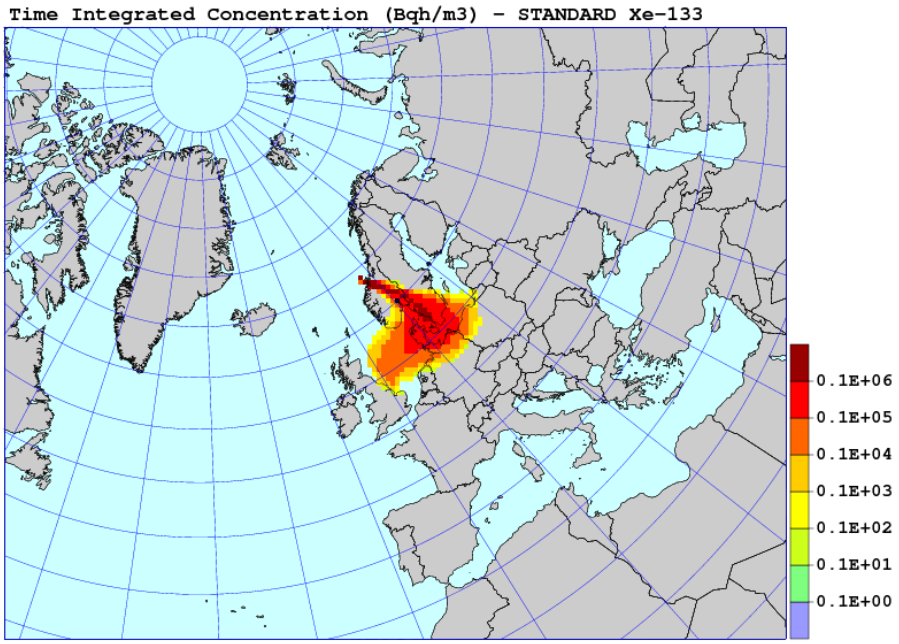

Figure 20: The results of the standard SNAP run for Xe-133 after 48 hours from the accident start. Time integrated concentrations in Bq h m^{-3}.

5.2. Sensitivity to dry deposition

Sensitivity to dry deposition was tested in the model run without dry deposition process. The maps of time integrated concentration and total deposition for Cs-137 are shown in Fig. 45 and the maps of time integrated concentration and total deposition for I-131 are shown in Fig. 46. Since Xe-133 is a noble gas, it is not sensitive to dry deposition and the deposition and concentration maps are not shown here for Xe-133.

Time integrated concentrations and deposition in the model grid cell where the city of Oslo is located are shown in Table 24 for the model run without dry deposition, 48 hours after the start of release. Sensitivity measures for the run without dry deposition are shown in Table 25.

Table 6: Time integrated concentrations and deposition, 48 hours after the start of release, in the model grid cell where the city of Oslo is located. Results of the model run without dry deposition.

Radionuclide selected	Time integrated concentration (Bq h m^{-3})	Total deposition (Bq m^{-2})
Cs-137	0.29×10^{1}	0.0
I-131	0.12×10^{3}	0.0
Xe-133	0.15×10^{3}	0.0

SENS SDF SCF SDG SCG Cs-137 58.4 77.1 -100.0 5.0 I-131 136.0 292.7 -100.0 18.9 Xe-133 0 0 0 0

Table 7: Sensitivity measures as defined in Eqs. (29) - (32), for the run without dry deposition.

Radionuclide selected	SDF	SCF	SDG	SCG
Cs-137	58.4	77.1	-100.0	5.0
I-131	136.0	292.7	-100.0	18.9
Xe-133	0	0	0	0

Elimination of dry deposition from the model processes results in higher air concentrations of Cs-137 and I-131, visible in the concentration maps (Fig. 45 and 46) and in the sensitivity measures (Table 25). The SCF values in Table 25 show that time integrated concentration of I-131 is definitely more sensitive to dry deposition process than time integrated concentration of Cs-137. The same conclusion applies to deposition, as indicated by SDF measure in Table 25. Sensitivity of Cs-137 and I-131 deposition to dry deposition is also clearly visible in the deposition maps for those radionuclides (Fig. 45 and 46). Total deposition pattern is the same as wet deposition pattern on those maps and it reflects the precipitation distribution during the transport. Since it does not rain in Oslo, total deposition in Oslo grid in the run without dry deposition is zero, which explains -100.0 values of SDG measure in Table 25.

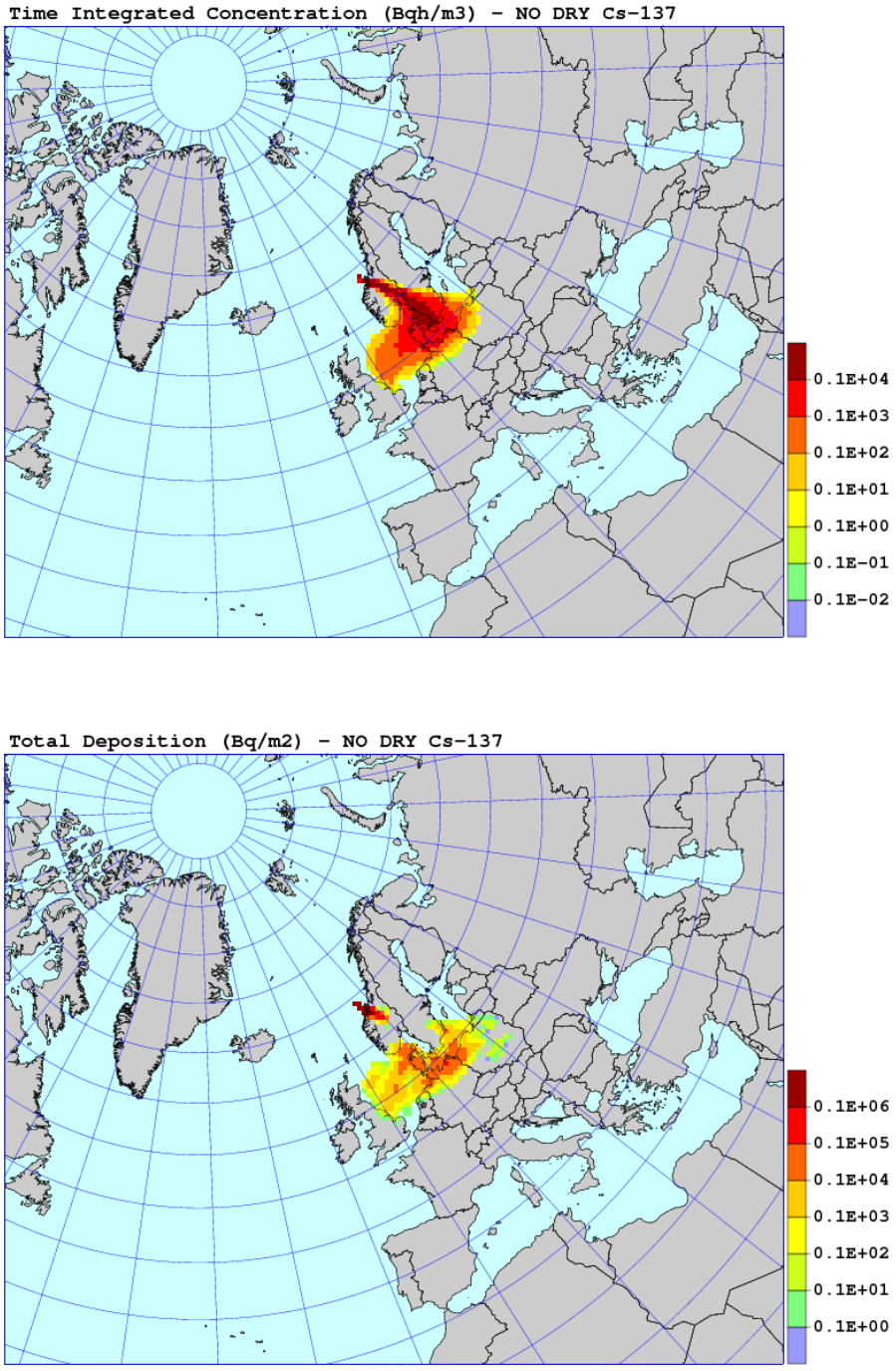

Figure 21: Results of the sensitivity run without dry deposition. Maps of time integrated concentration and deposition of Cs-137, 48 hours from the accident start.

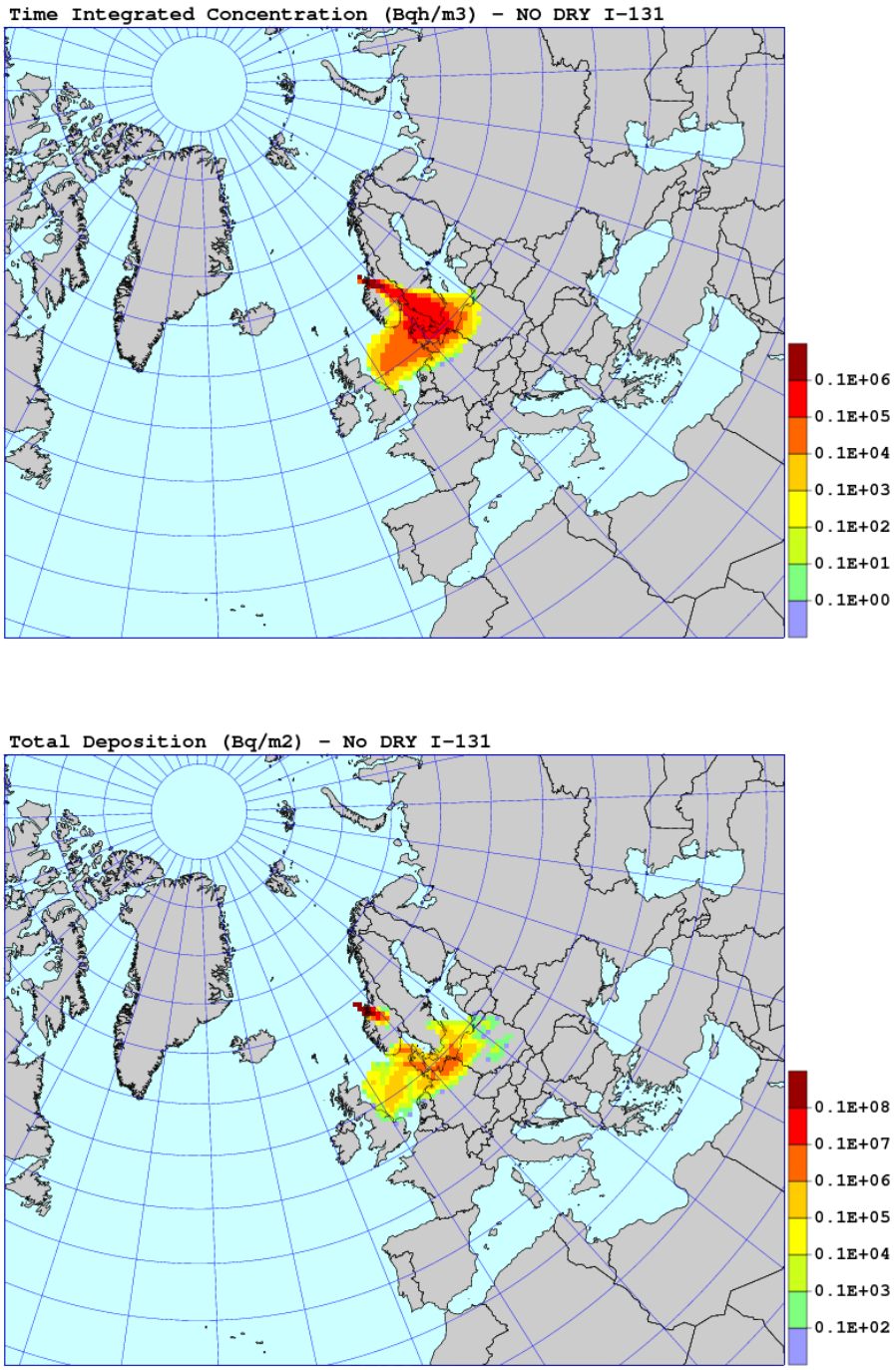

Figure 22: Results of the sensitivity run without dry deposition. Maps of time integrated concentration and deposition of I-131, 48 hours from the accident start.

5.3. Sensitivity to wet deposition

Sensitivity to dry deposition was tested in the model run without wet deposition process. The maps of time integrated concentration and total deposition for Cs-137 run are shown in Fig. 47 and the maps of time integrated concentration and total deposition for I-131 run are shown in Fig. 48. Since Xe-133 is a noble gas, it is not sensitive to wet deposition and the deposition and concentration maps are not shown here for Xe-133. Compared to the results of standard run, time integrated concentrations of Cs-137 and I-131 is higher and smoother in the run without wet deposition, especially in the centre of the plume. The deposition maps shown in the same figures indicate, on the other hand, slightly lower deposition values compared to the standard run.

Time integrated concentrations and deposition in the model grid cell where the city of Oslo is located are shown in Table 26 for the model run without wet deposition, 48 hours after the start of release. Both, time integrated concentrations and deposition of Cs-137 and I-131 in the Oslo grid are higher in the run without wet deposition than in the standard run. Sensitivity measures for the run without wet deposition are shown in Table 27.

Table 8: Time integrated concentrations and deposition, 48 hours after the start of release, in the model grid cell where the city of Oslo is located. Results of the model run without wet deposition.

Radionuclide selected	Time integrated concentration (Bq h m^{-3})	Total deposition (Bq m^{-2})
Cs-137	0.62×10^{1}	0.17×10^{3}
I-131	0.29×10^{3}	0.27×10^{5}
Xe-133	0.15×10^{3}	0.0

Table 9: Sensitivity measures as defined in Eq. (29) - (32), for the run without wet deposition.

Radionuclide selected	SDF	SCF	SDG	SCG
Cs-137	545.2	234.5	68.8	126.4
I-131	464.8	341.5	102.7	189.6
Xe-133	0	0	0	0

The sensitivity measures in Table 27 show that the model is more sensitive to wet deposition than to dry deposition. Especially, the SDF values in Table 27 are very high, which means that the sensitivity of both radionuclides is higher for deposition than concentration, however, the sensitivity of concentrations to wet deposition is also relatively high. High sensitivity to wet deposition is also confirmed by local SDG and SCG measures in Table 27 which apply to the model grid square with Oslo location. In this case sensitivity is slightly higher for concentration than for deposition.

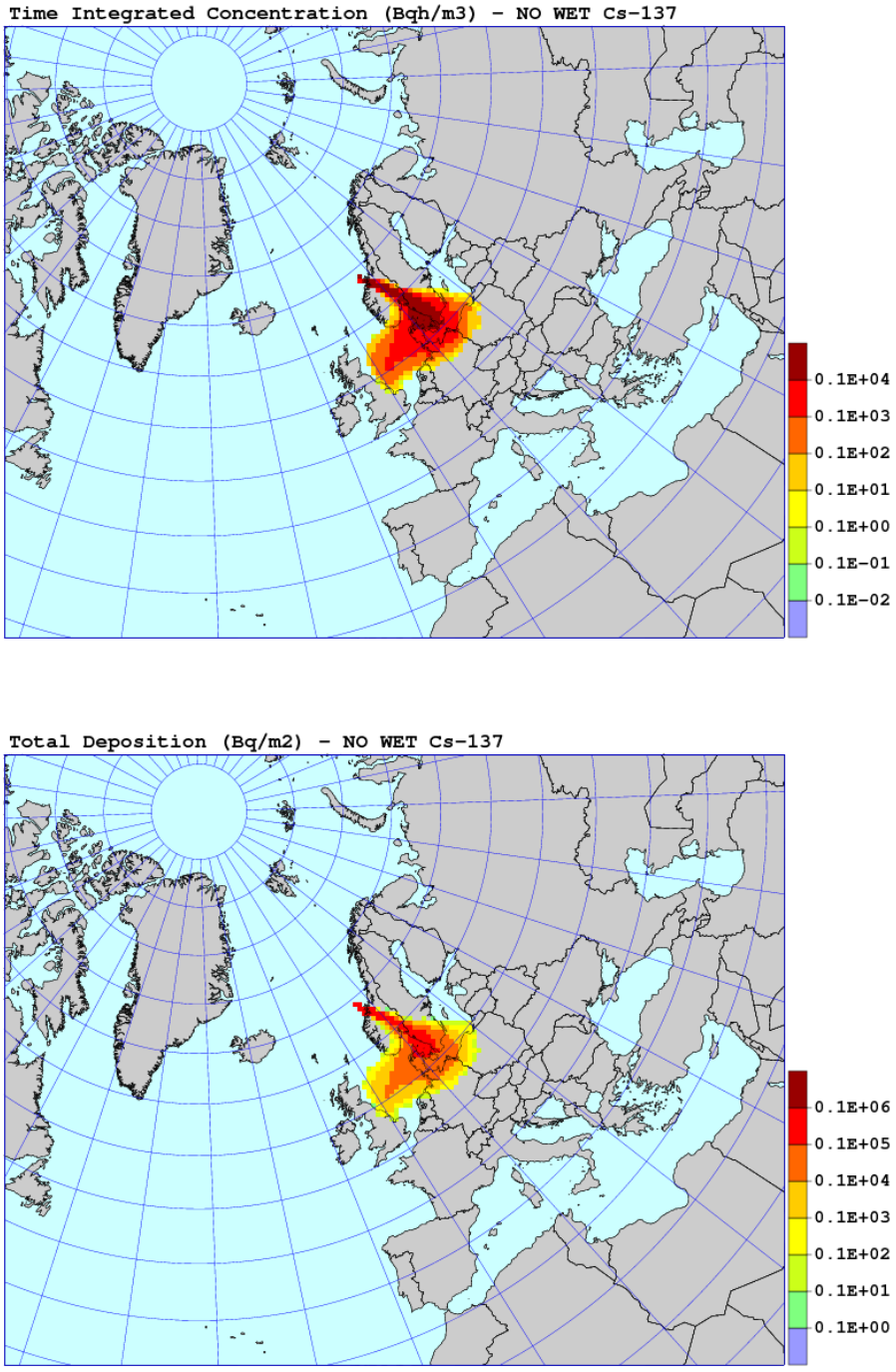

Figure 23: Results of the sensitivity run without wet deposition. Maps of time integrated concentration and deposition of Cs-137, 48 hours from the accident start.

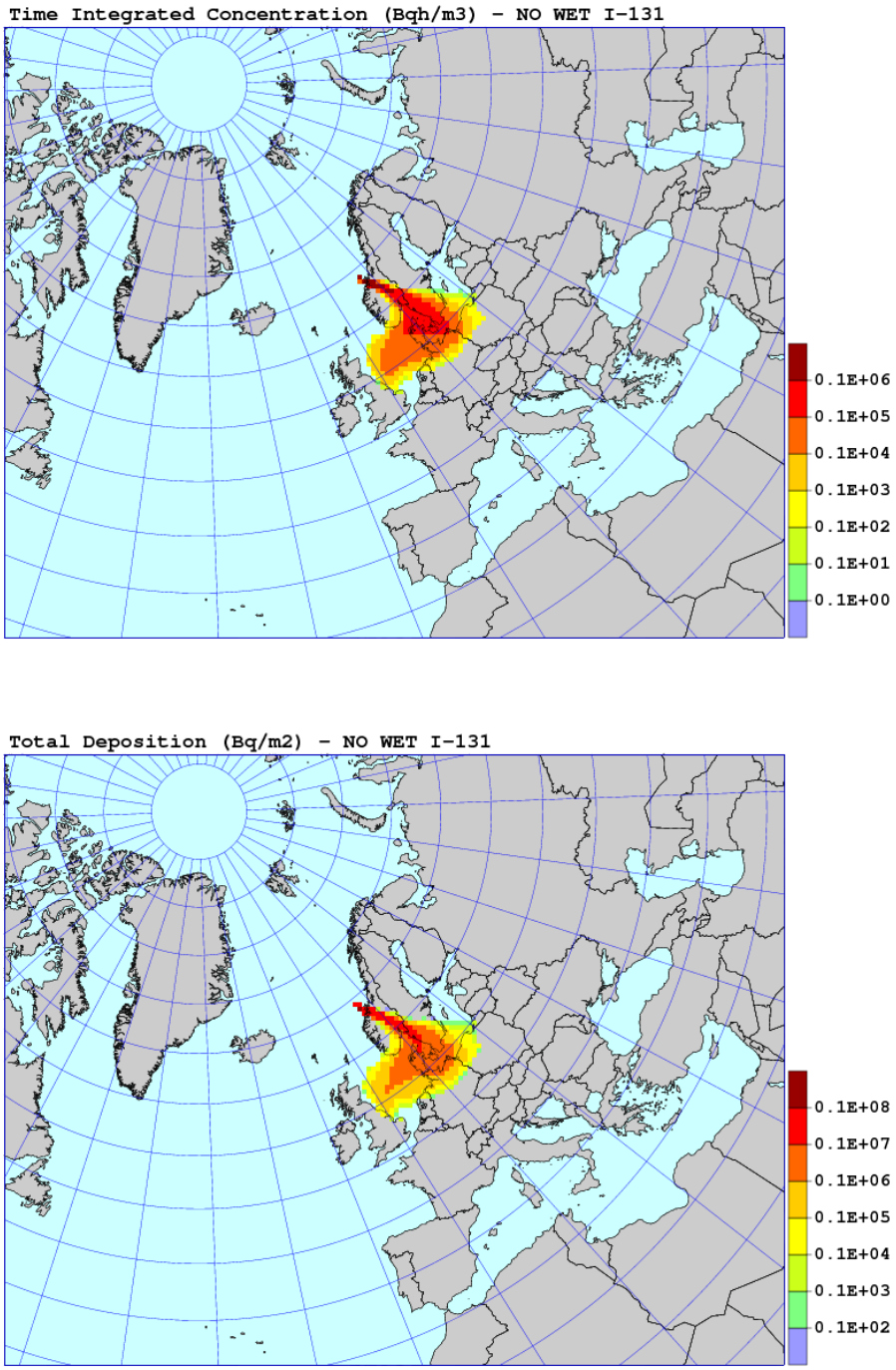

Figure 24: Results of the sensitivity run without wet deposition. Maps of time integrated concentration and deposition of I-131, 48 hours from the accident start.

5.4. Sensitivity to radioactive decay

Sensitivity to radioactive decay was tested in the model run without a decay process. The maps of time integrated concentration and total deposition for Cs-137 run are shown in Fig. 49. The maps of time integrated concentration and total deposition for I-131 are shown in Fig. 50 and finally the map of time integrated concentration for Xe-133 is shown in Fig. 51. Since Xe-133 is a noble gas the deposition field for this radionuclide is not shown. Practically, there are no differences between the standard run and the test run for Cs-137 in time integrated concentration and in deposition maps. Also for I-131 the differences between maps from the standard and test runs are small and they are not large either for the maps of time integrated concentrations of Xe-133.

Time integrated concentrations and deposition, 48 hours after the start of release, in the model grid cell where the city of Oslo is located are shown in Table 28 for the model run without radioactive decay. For Cs-137, both time integrated concentrations and deposition are practically the same in the standard run and in the test run. For I-131, there is only 1% difference in time integrated concentration, but deposition in the run without radioactive decay is 15% higher than in the standard run. However, time integrated concentration of Xe-131 in the Oslo grid is almost two times higher in the test run than in the standard run.

Sensitivity measures for the run without radioactive decay are given in Table 29. As expected, the model results for Cs-137 are definitely not sensitive to radioactive decay. Certain model sensitivity to radioactive decay can be noticed in case of I-131 and some more sensitivity in case of time integrated concentration of Xe-133.

Table 10: Time integrated concentrations and deposition, 48 hours after the start of release, in the model grid cell where the city of Oslo is located. Results of the model run without radioactive decay.

Radionuclide selected	Time integrated concentration (Bq h m^{-3})	Total deposition (Bq m^{-2})
Cs-137	0.27×10^{1}	0.10×10^{3}
I-131	0.10×10^{3}	0.15×10^{5}
Xe-133	0.27×10^{3}	0.0

Table 11: Sensitivity measures as defined in Eqs. (29) - (32), for the run without radioactive decay.

Radionuclide selected	SDF	SCF	SDG	SCG
Cs-137	0.1	0.0	0.0	0.0
I-131	10.8	8.4	15.1	4.1
Xe-133	0.0	26.0	0.0	79.4

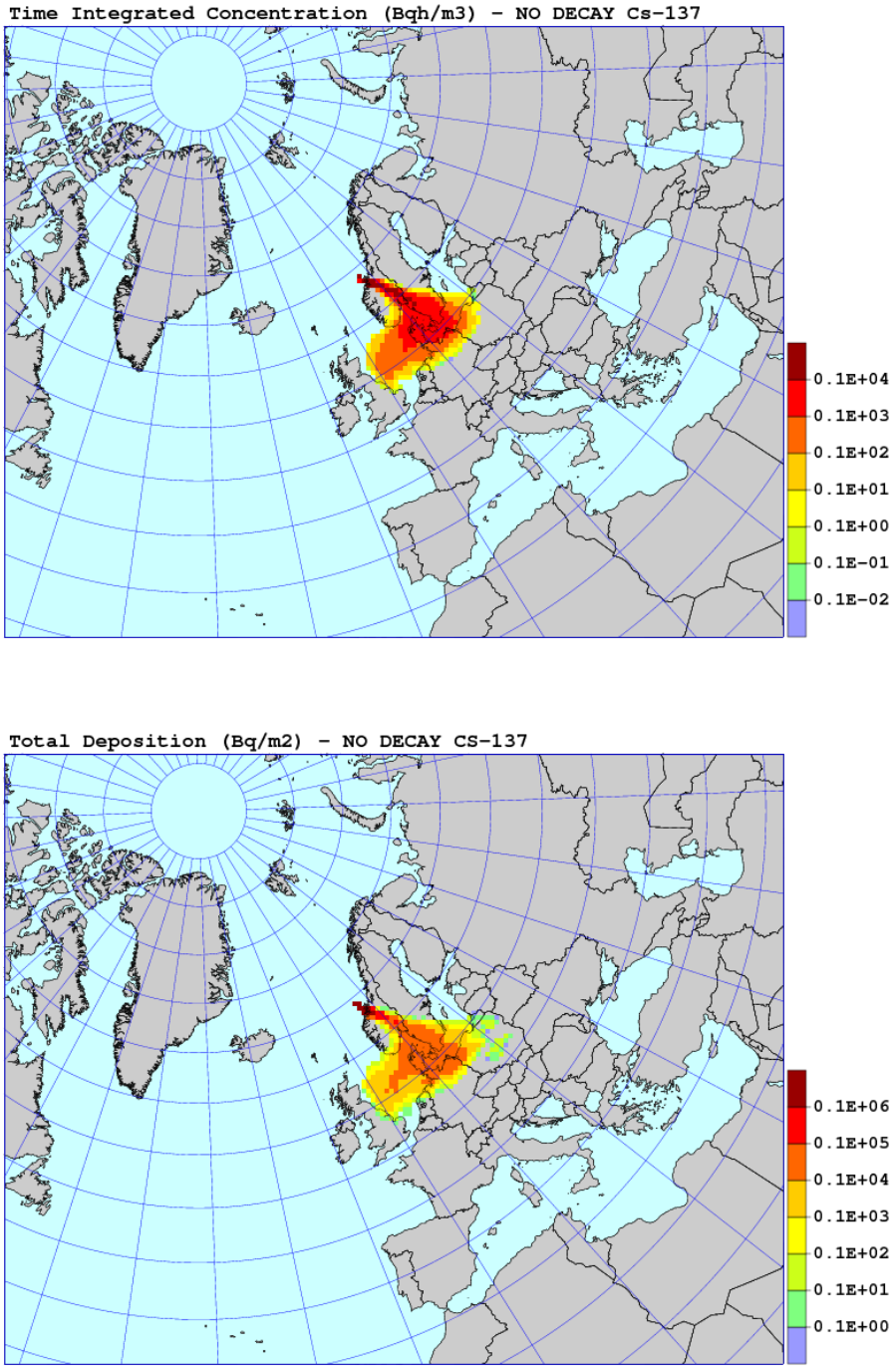

Figure 25: Results of the sensitivity run without radioactive decay. Maps of time integrated concentration and deposition of Cs-137, 48 hours from the accident start.

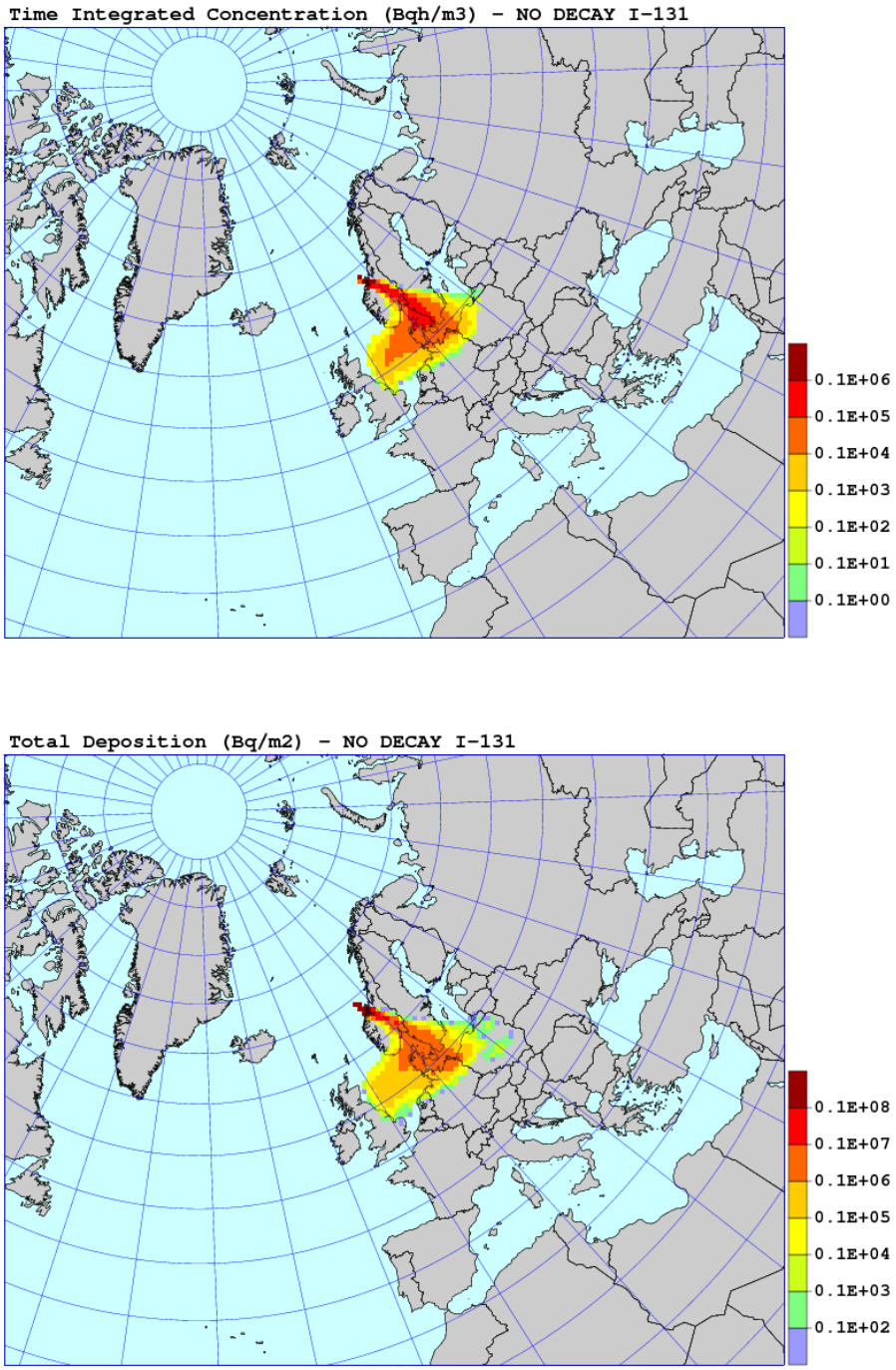

Figure 26: Results of the sensitivity run without radioactive decay. Maps of time integrated concentration and deposition of I-131, 48 hours from the accident start.

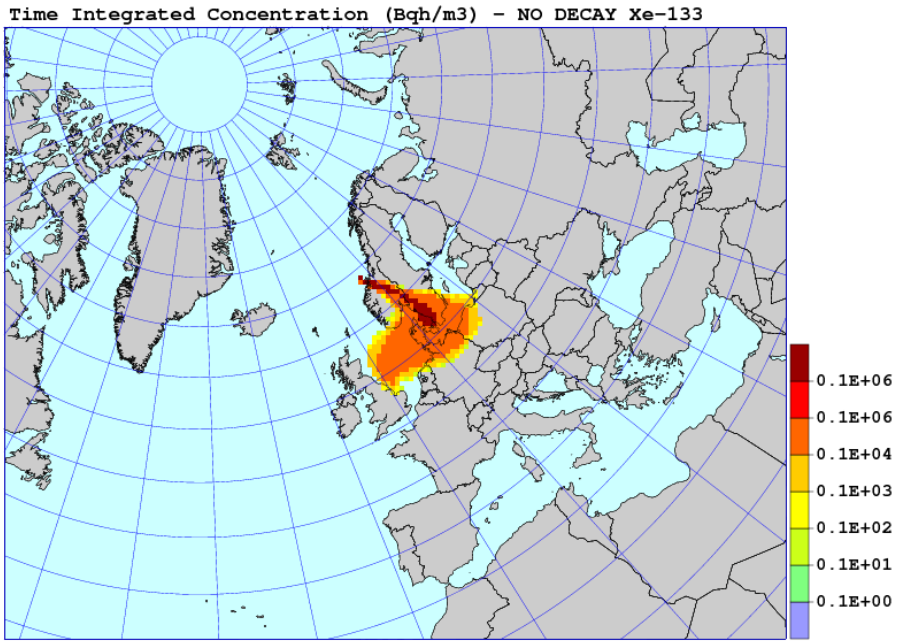

Figure 27: Results of the sensitivity run without radioactive decay. Maps of time integrated concentration and deposition of Xe-133, 48 hours from the accident start.

5.5. Sensitivity to horisontal diffusion

Sensitivity to horisontal diffusion was tested in two model runs. In the first run, the process of horisontal diffusion was switched off, both below and above the mixing height. In the second run, horisontal diffusion was increased by applying double value to horisontal diffusion coefficient, again in the boundary layer and above.

The maps of time integrated concentrations and total deposition for Cs-137 for the run without horisontal diffusion are shown in Fig. 52. The maps of time integrated concentration and total deposition for I-131, for the same run, are shown in Fig. 55. Both, for Cs-137 and I-131 the differences between the standard run the run without horisontal diffusion are very small. It applies to the maps of time integrated concentration and deposition maps, as well.

The maps of time integrated concentrations and total deposition for Cs-137 for the run with increased horisontal diffusion are shown in Fig. 54. The maps of time integrated concentration and total deposition for I-131, for the same run, are shown in Fig. 56. The differences between the standard run and the test run with increased horisontal diffusion are also small in this case for both radionuclides.

The maps of time integrated concentration for Xe-133 are shown in Fig. 57 for the runs without horisontal diffusion and increased horisontal diffusion. Once again, differences between the maps of time integrated concentrations calculated in the run with no horisontal diffusion, in the run with increased horisontal diffusion and in the standard run are very small.

Time integrated concentrations and deposition, 48 hours after the start of release, in the model grid cell where the city of Oslo is located are shown in Table 30, for the model run without horisontal diffusion and in Table 31, for the model run with increased horisontal diffusion. As in case of Cs-137 and I-131, also there are only small differences between time integrated concentrations maps from the standard run and the runs without and with increase horisontal diffusion.

Table 12: Time integrated concentrations and deposition, 48 hours after the start of release, in the model grid cell where the city of Oslo is located. Results of the model run without horisontal diffusion.

Radionuclide selected	Time integrated concentration (Bq h m^{-3})	Total deposition (Bq m^{-2})
Cs-137	0.22×10^{1}	0.12×10^{3}
I-131	0.85×10^{2}	0.15×10^{5}
Xe-133	0.22×10^{3}	0.0

In general there is not much difference between the deposition values from the standard and test runs for all radionuclides and for both, run without deposition and run with increased deposition. However, all depositions in the Oslo grid from the test run are slightly higher - 10-20%, than the depositions from the standard run. On the other hand, calculated time integrated concentrations in the test runs in the Oslo grid differ, sometimes significantly from those in the standard run. The largest difference -87% can be noticed for I-131 and the run with increased horisontal diffusion.

Table 13: Time integrated concentrations and deposition, 48 hours after the start of release, in the model grid cell where the city of Oslo is located. Results of the model run with increased horisontal diffusion.

Radionuclide selected	Time integrated concentration (Bq h m^{-3})	Total deposition (Bq m^{-2})
Cs-137	0.33×10^{1}	0.11×10^{3}
I-131	0.13×10^{2}	0.14×10^{5}
Xe-133	0.31×10^{3}	0.0

Sensitivity measures, for the runs without horisontal diffusion and with increased horisontal diffusion are shown in Tables32 and 33. These measures are relatively (compared to dry and wet deposition) low for SCF and all three isotopes. For SDF, the measures for Cs-137 and I-131 are similar to those for dry deposition, but much lower than those for wet deposition. Three sensitivity measures (SDF, SCF and SDG), for the runs without horisontal diffusion and with increased horisontal diffusion, are a bit higher for I-131 than for Cs-137. The SCG measure is higher for Cs-137. Sensitivity measures for Xe-133 are lower for the runs with and without horisontal diffusion than for the run without a radioactive decay.

Table 14: Sensitivity measures as defined in Eqs. (29) - (32), for the run without horisontal diffusion.

Radionuclide selected	SDF	SCF	SDG	SCG
Cs-137	122.2	11.5	11.0	-17.8
I-131	150.0	16.3	11.8	-13.6
Xe-133	0.0	10.2	0.0	44.4

Table 15: Sensitivity measures as defined in Eqs. (29) - (32), for the run with increased horisontal diffusion.

Radionuclide selected	SDF	SCF	SDG	SCG
Cs-137	135.4	20.0	5.8	20.9
I-131	139.2	26.0	7.5	27.0
Xe-133	0.0	14.6	0.0	104.0

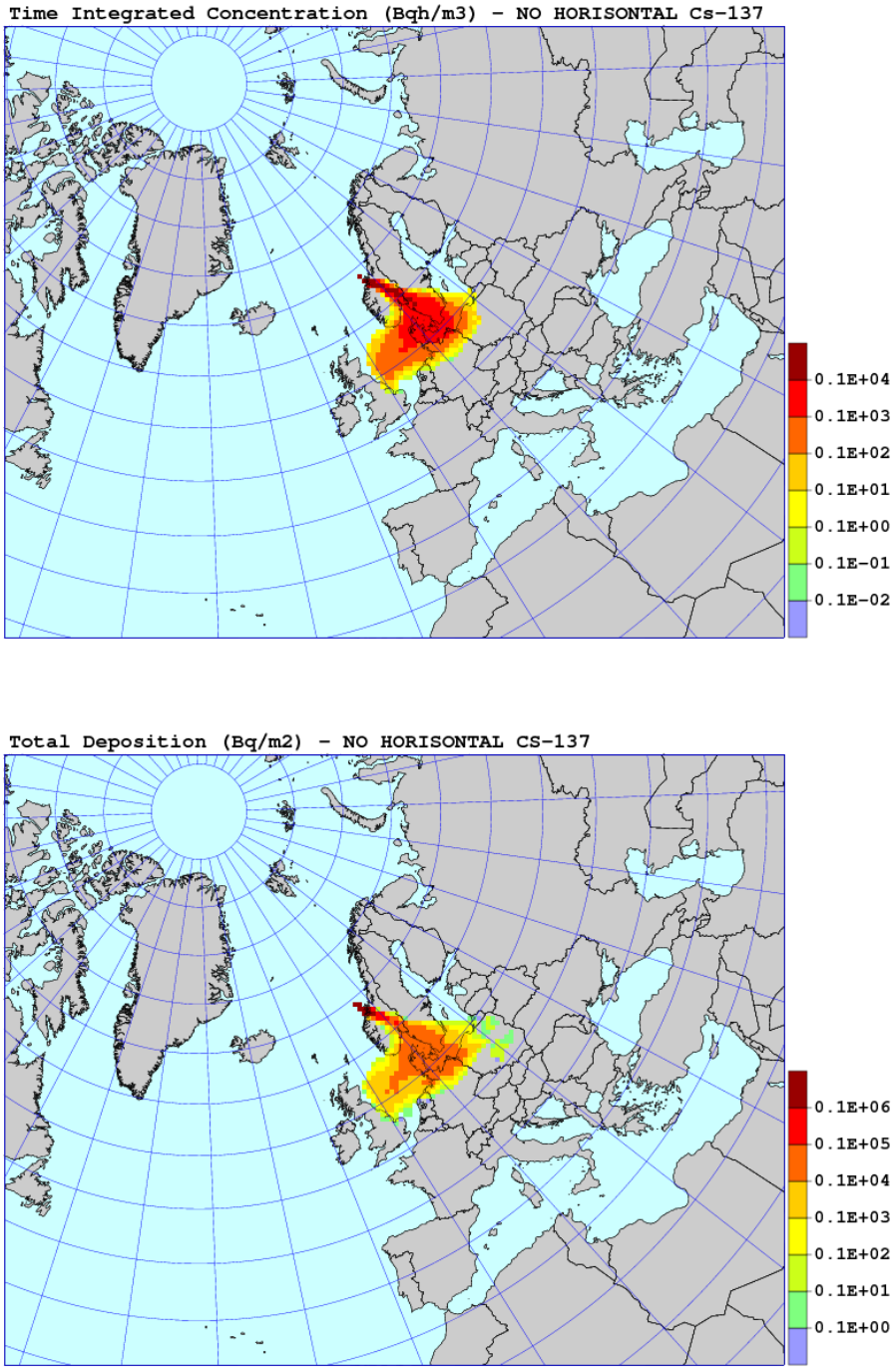

Figure 28: Results of the sensitivity run without horisontal diffusion. Maps of time integrated concentration and deposition of Cs-137, 48 hours from the accident start.

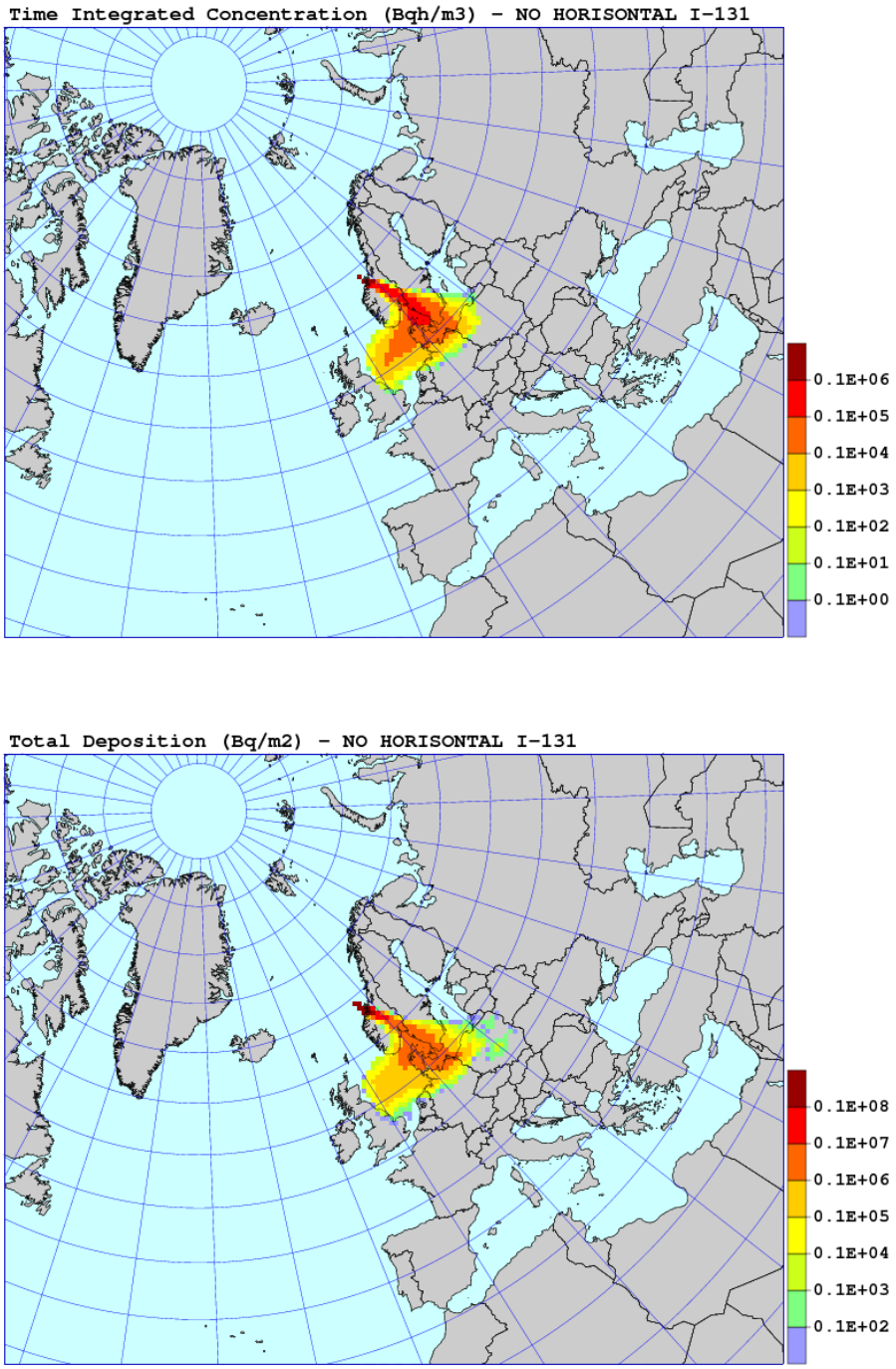

Figure 29: Results of the sensitivity run without horisontal diffusion. Maps of time integrated concentration and deposition of I-131, 48 hours from the accident start.

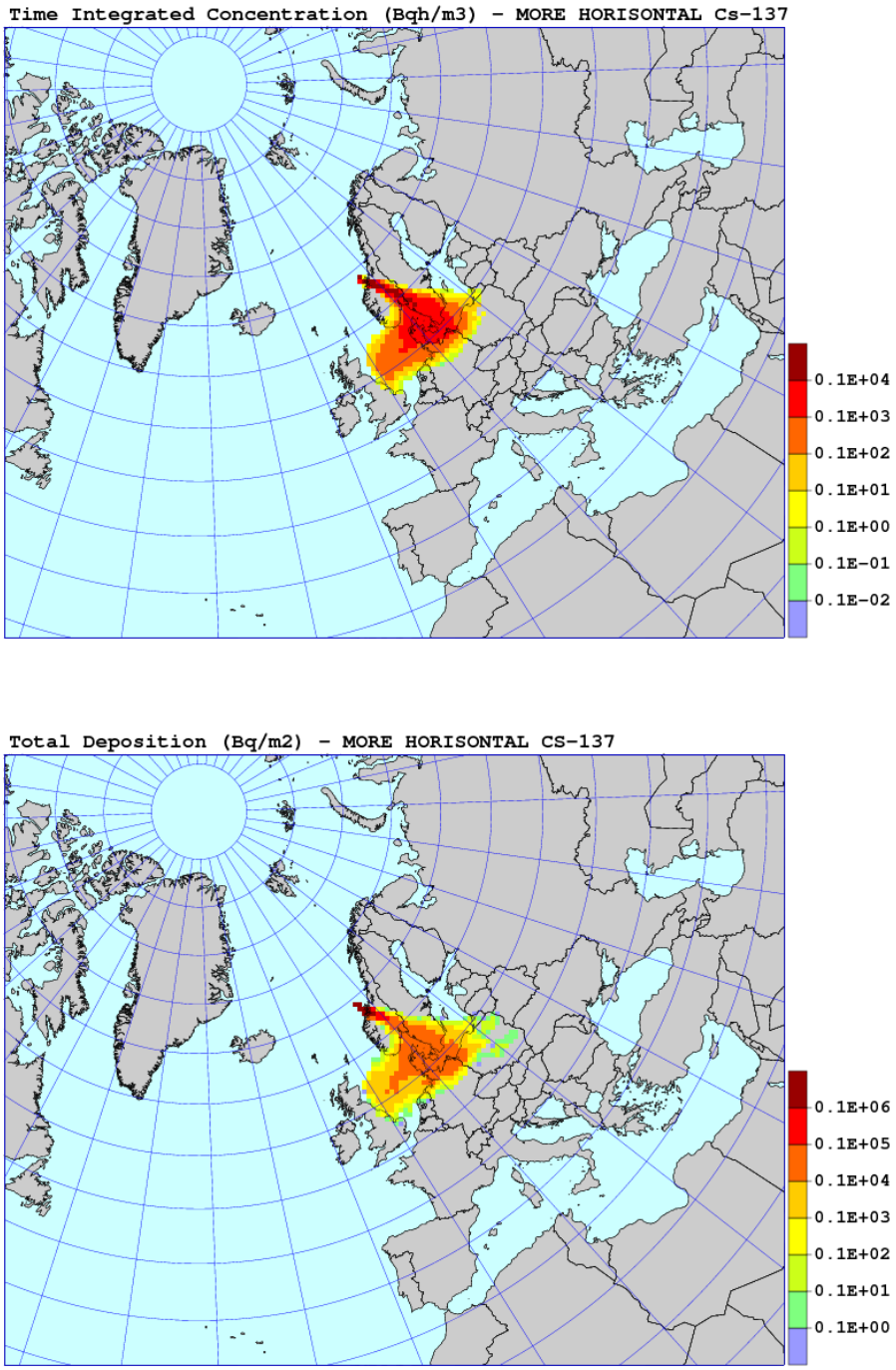

Figure 30: Results of the sensitivity run with increased horisontal diffusion. Maps of time integrated concentration and deposition of Cs-137, 48 hours from the accident start.

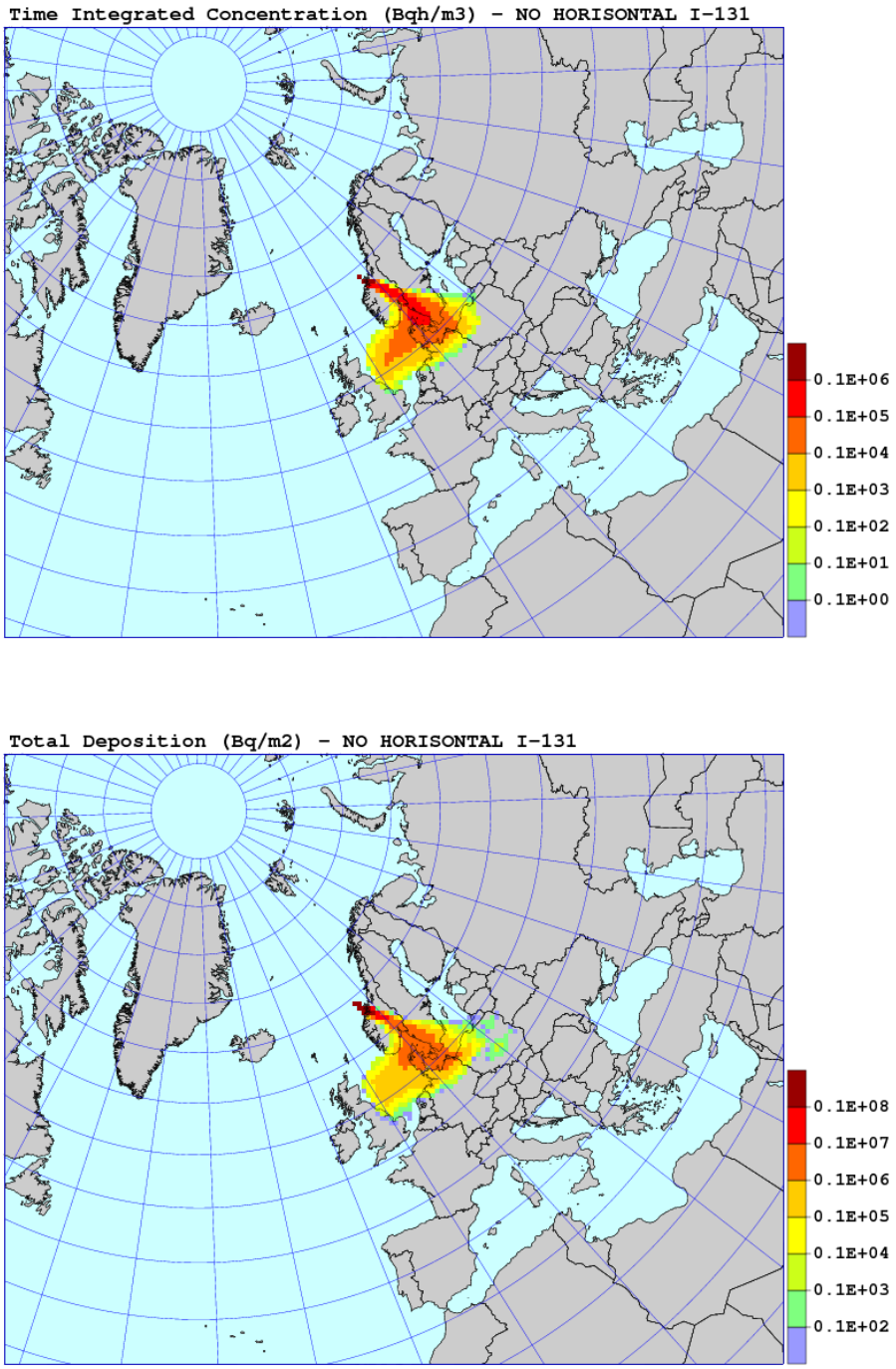

Figure 31: Results of the sensitivity run without horisontal diffusion. Maps of time integrated concentration and deposition of I-131, 48 hours from the accident start.

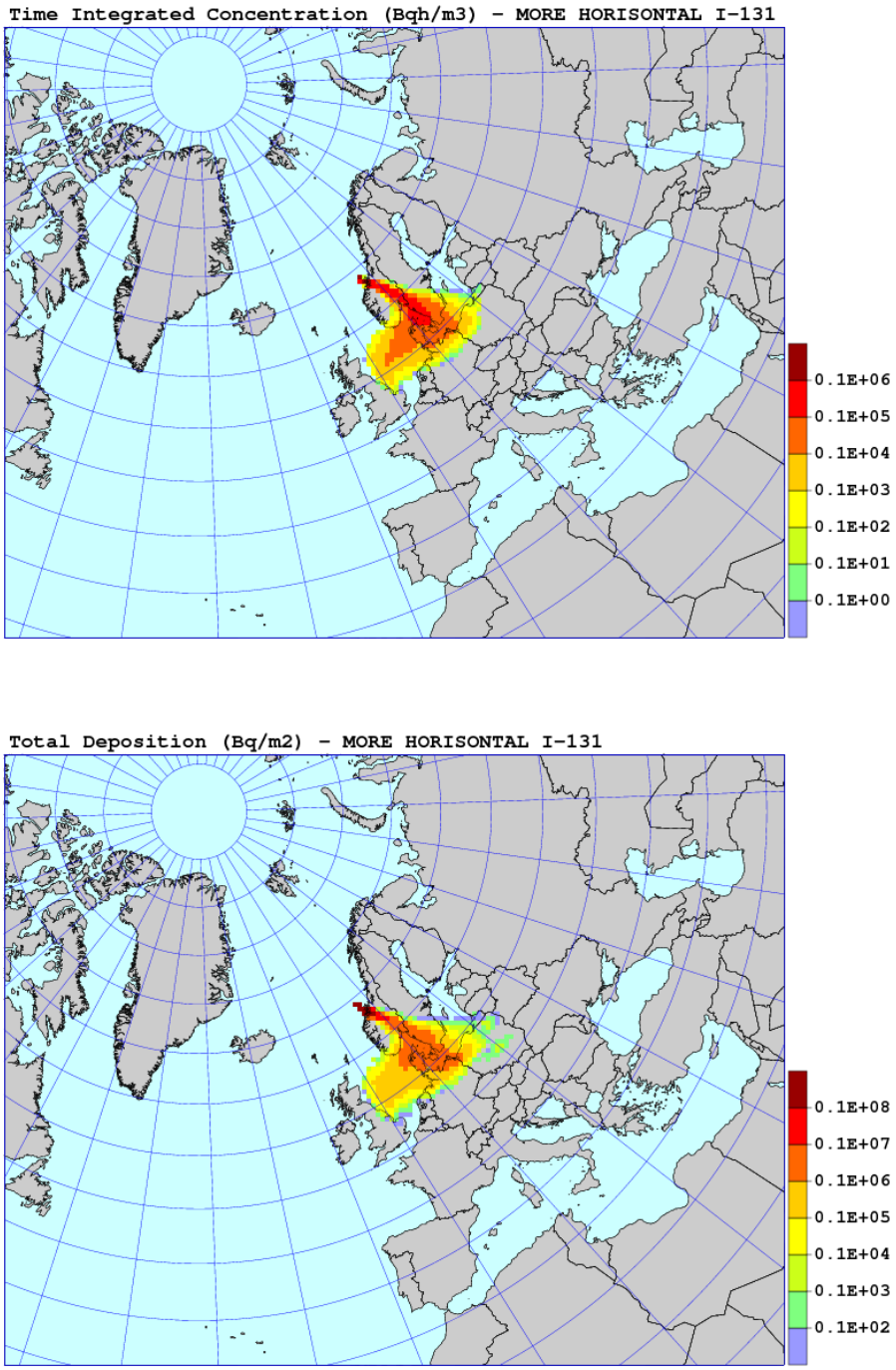

Figure 32: Results of the sensitivity run with increased horisontal diffusion. Maps of time integrated concentration and deposition of I-131, 48 hours from the accident start.

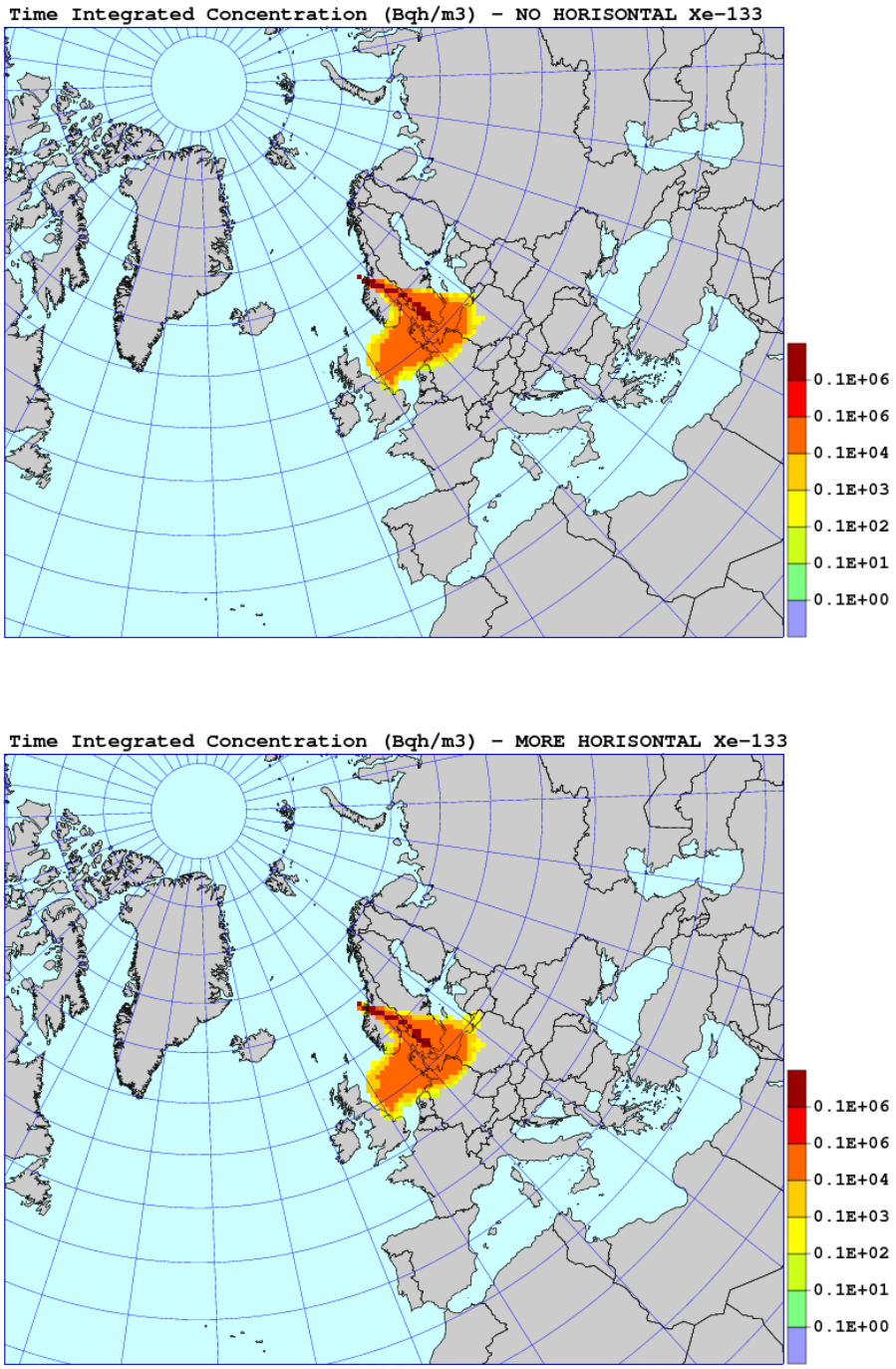

Figure 33: Results of the sensitivity run without horisontal diffusion (above) and increased horisontal diffusion (below). Maps of time integrated concentration and deposition of Xe-133, 48 hours from the accident start.

5.6. Sensitivity to vertical diffusion

As in case of horisontal diffusion, sensitivity to vertical diffusion was also tested in two model runs. In the first run, the process of vertical diffusion was switched off, both below and above the mixing height. In the second run, vertical diffusion was increased by applying double value to vertical diffusion coefficient, in the boundary layer and above.

The maps of time integrated concentration and total deposition for Cs-137 for the run without vertical diffusion are shown in Fig. 58. The maps of time integrated concentration and total deposition for I-131, for the same run, are shown in Fig. 59. All test maps for Cs-137 and I-131 differ significantly from the standard run maps. The plumes in the test runs are narrower and gradients are steeper. This applies, both to the maps of deposition and maps of time integrated concentration.

The maps of time integrated concentration and total deposition for Cs-137 and the run with increased vertical diffusion are shown in Fig. 60. The maps of time integrated concentration and total deposition for I-131, for the same run, are shown in Fig. 61. Also in this case, the results for Cs-137 and I-131 on the maps from test runs are quite different from the results on the maps from the standard run. However, in the run with increased vertical diffusion, the plumes are wider than the plumes from the standard run.

The maps of time integrated concentration for Xe-133 are shown in Fig. 62, for the runs without vertical diffusion and the runs with increased vertical diffusion. The differences in Xe-133 time integrated concentrations between the standard run and the test runs without vertical diffusion and with increased vertical diffusion are very similar like in case of Cs-137 and I-131. Compared to the standard run results, narrower plume can be noticed in the run without vertical diffusion and wider plume in the run with increased vertical diffusion.

Time integrated concentrations and deposition, 48 hours after the start of release, in the model grid cell where the city of Oslo is located are shown in Table 34 - for the model run without vertical diffusion and in Table 35 - for the model run with increased vertical diffusion.

Table 16: Time integrated concentrations and deposition, 48 hours after the start of release, in the model grid cell where the city of Oslo is located. Results of the model run without vertical diffusion.

Radionuclide selected	Time integrated concentration (Bq h m^{-3})	Total deposition (Bq m^{-2})
Cs-137	0.00E+00	0.00E+00
I-131	0.00E+00	0.00E+00
Xe-133	0.00E+00	0.00e+00

Only zeros can be found in Table 34, because in the model run without vertical diffusion, radioactive debris did not arrive to Oslo grid at all. On the other hand, time integrated concentrations and deposition in the Oslo grid from the model run with increased vertical diffusion (Table 35) are much higher than corresponding values from the standard run. It means that for Oslo location, model sensitivity to vertical diffusion is relatively high.

Table 17: Time integrated concentrations and deposition, 48 hours after the start of release, in the model grid cell where the city of Oslo is located. Results of the model run with increased vertical diffusion.

Radionuclide selected	Time integrated concentration (Bq h m^{-3})	Total deposition (Bq m^{-2})
Cs-137	0.79×10^{1}	0.28×10^{3}
I-131	0.30×10^{3}	0.36×10^{5}
Xe-133	0.60×10^{3}	0.0

Sensitivity measures for the run without vertical diffusion and run with enhanced vertical diffusion are shown in Table 36. Compared to other sensitivity tests, the local measures (SDG and SCG) are relatively high, both for the run without vertical diffusion and run with increased vertical diffusion. The global measures - SDF and SCF - are approximately 100% higher in the run without vertical diffusion than in the run with increased vertical diffusion. In both runs, the global measure for time integrated concentration (SCF) is more sensitive to vertical diffusion than the global measure for deposition SDF.

Table 18: Sensitivity measures as defined in Eqs. (29) - (32), for the run without vertical diffusion and the model run with enhanced vertical diffusion.

Radionuclide selected	SDF	SCF	SDG	SCG
No vertical diffusion				
Cs-137	88.2	188.4	-100.0	-100.0
I-131	96.0	273.1	-100.0	-100.0
Xe-133	0.0	204.0	0.0	-100.0
More vertical diffusion				
Cs-137	48.2	93.9	174.7	190.3
I-131	46.0	90.7	172.5	202.5
Xe-133	0.0	102.5	0.0	291.5

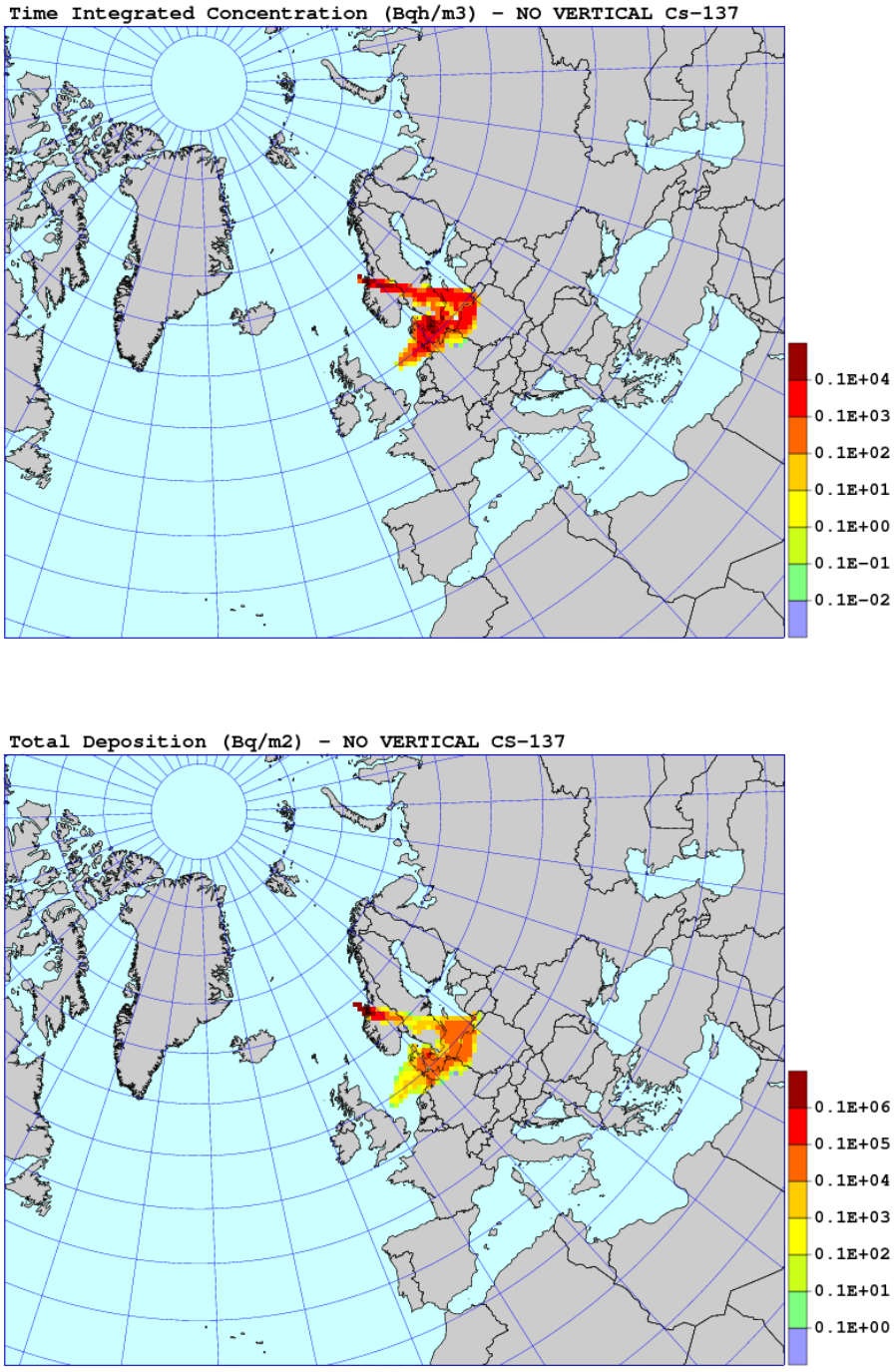

Figure 34: Results of the sensitivity run without vertical diffusion. Maps of time integrated concentration and deposition of Cs-137, 48 hours from the accident start.

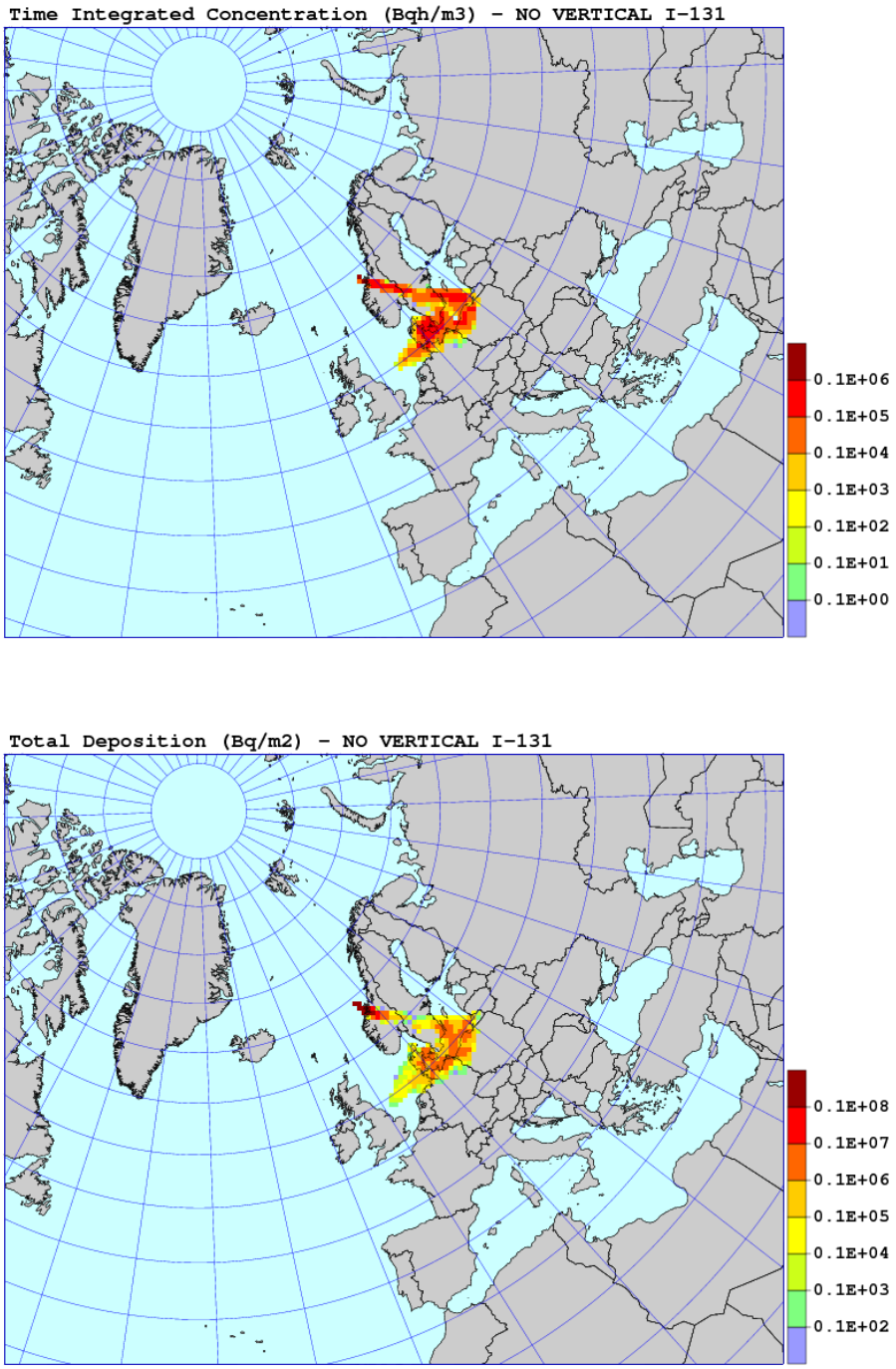

Figure 35: Results of the sensitivity run without vertical diffusion. Maps of time integrated concentration and deposition of I-131, 48 hours from the accident start.

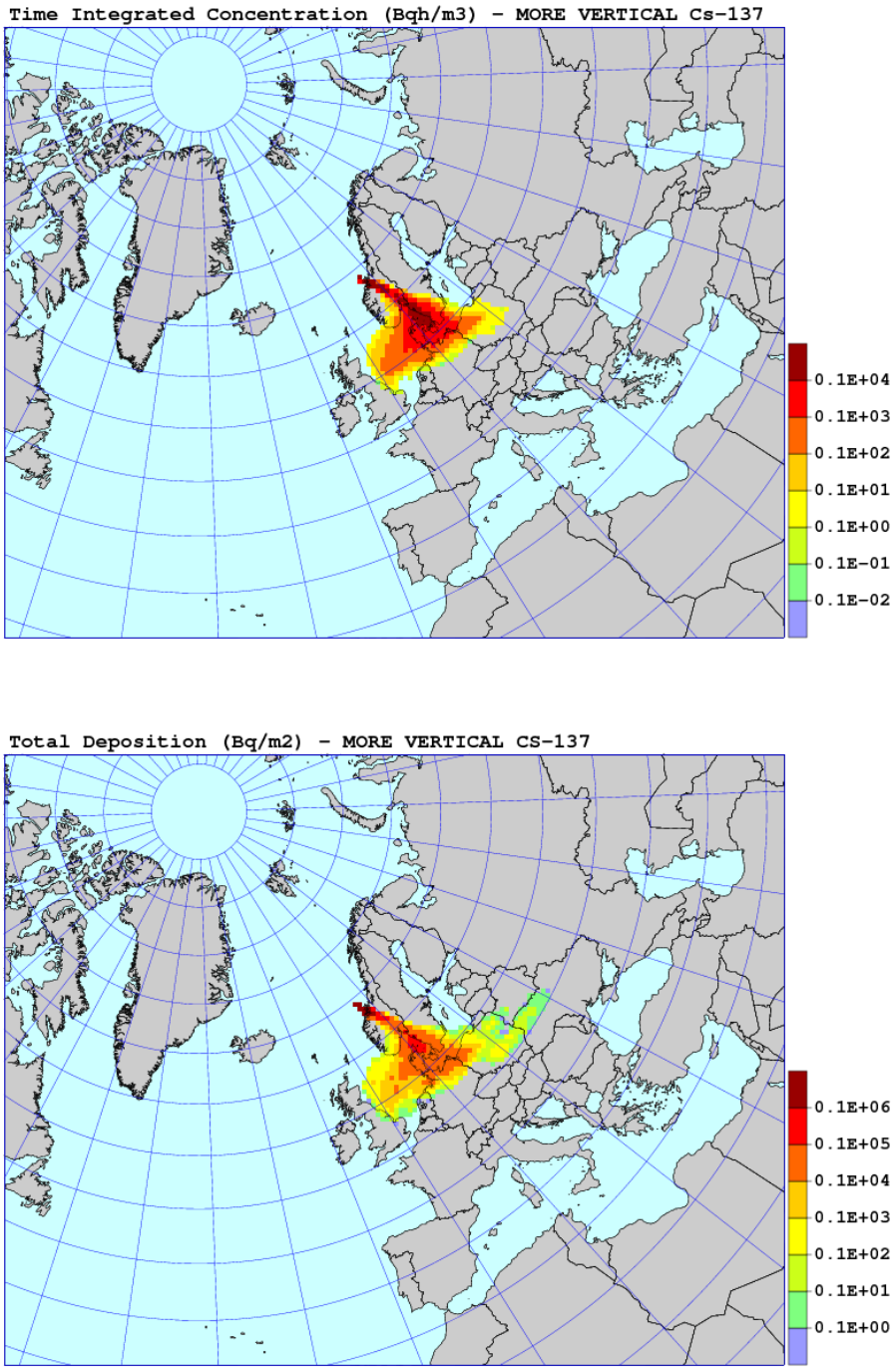

Figure 36: Results of the sensitivity run with increased vertical diffusion. Maps of time integrated concentration and deposition of Cs-137, 48 hours from the accident start.

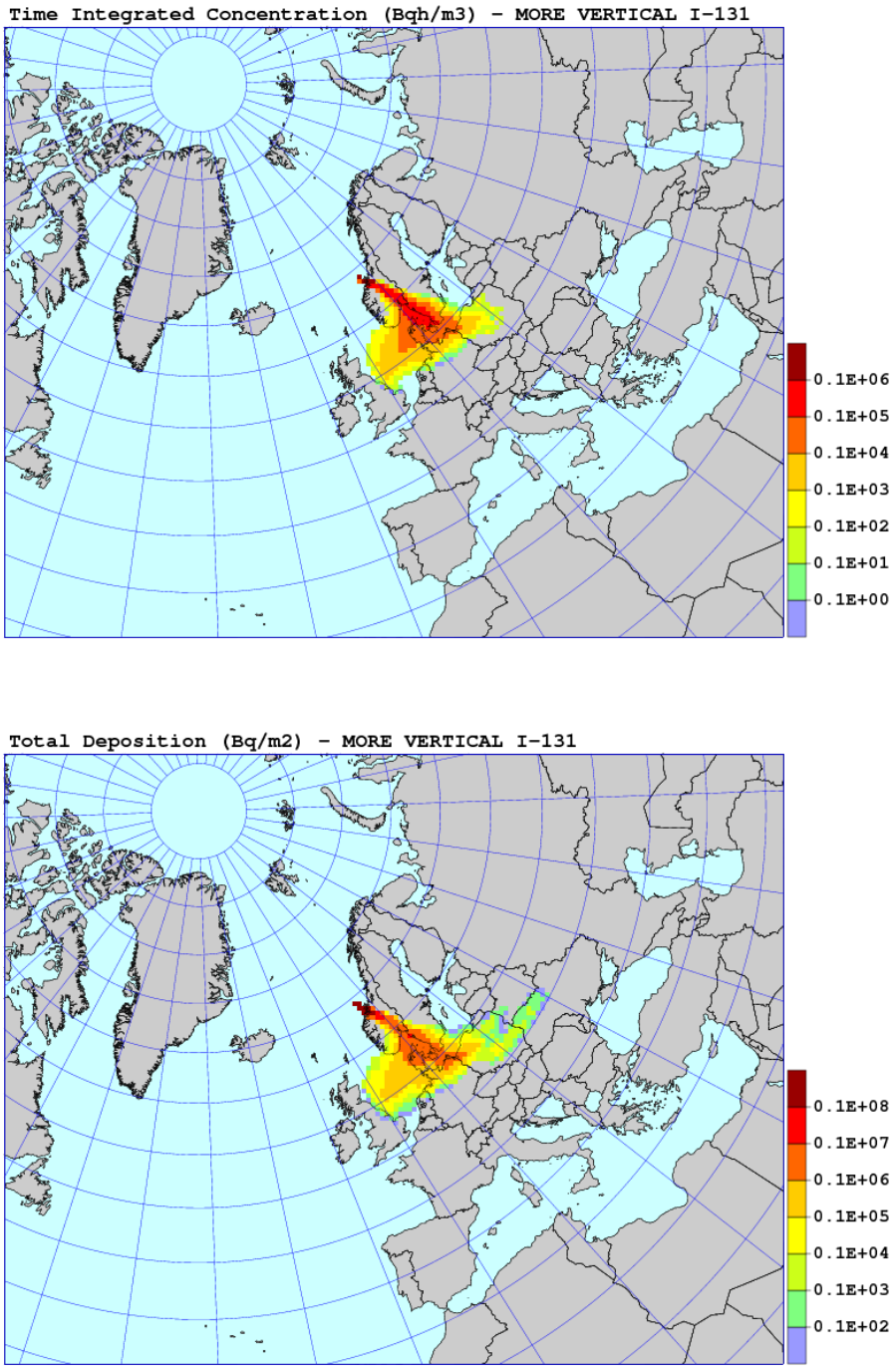

Figure 37: Results of the sensitivity run with increased vertical diffusion. Maps of time integrated concentration and deposition of I-131, 48 hours from the accident start.

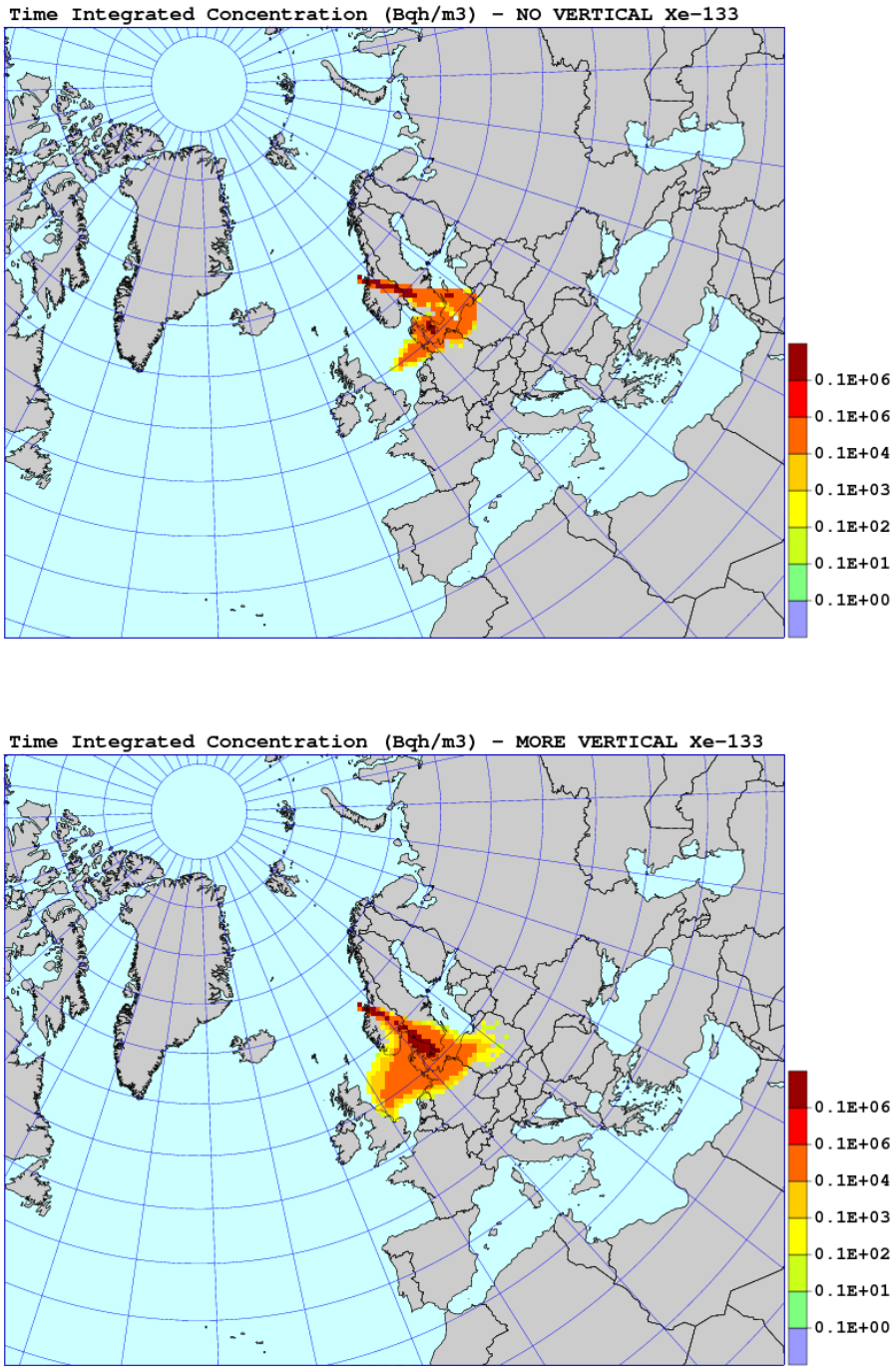

Figure 38: Results of the sensitivity run without vertical diffusion (above) and increased vertical diffusion (below). Maps of time integrated concentration and deposition of Xe-133, 48 hours from the accident start.

5.7. Sensitivity to number of model particles

The number of model particles is not related to any particular physical process, but it decides about the accuracy of the approximation of the model equations. The accuracy of the model results increases with the number of model particles and it should be as large as possible. Unfortunately, this number is limited for technical reasons, mainly computational time and available CPU memory. For the model applications, it is important to know how the model results are changing with the number of model particles used in the simulation. In the standard model run, the number of model particles was set to 2000 for each model time step. It means that total number of the model particles released was 240 000. In the sensitivity tests, we have tried both lower and higher number of model particles as shown in Table 37. The number of model particles used in the standard run is highlighted in Table 37.

Table 19: The number of model particles used in the sensitivity tests. The number of model particles in the standard run is highlighted.

Per time step	500	1000	**2000**	4000	8000
Total	60 000	120 000	**240 000**	480 000	960 000

The results of sensitivity runs with different number of the model particles are shown in Fig. (63) - (66) - for Cs-137, in Fig. (67) - (70) - for I-131, and in Fig. (71) - (72) - for Xe-133. For all numbers of model particles tested and for all radionuclides selected, the maps of time integrated concentration and deposition look very similar to those form the standard run. In some cases, only very small differences can noticed at the edge of the plume, where the concentration and deposition values are small. However, these small differences can be neglected in practical applications of the SNAP model.

The results of the SNAP runs, for different number of model particles are summarised in Table 38 - in the model grid square where the city of Oslo is located. The results are shown 48 hours after the release start. The most significant differences between the test run and the standard run for time integrated concentration can be noticed in the run with 500 particles per time step - for Cs-137 and I-131, and in the run with 200 particles in case of Xe-133. Calculated deposition in the Oslo grid is not so sensitive to the number of model particles and differences between the test runs and the standard run are much smaller compared to time integrated concentration.

Sensitivity measures for the SNAP runs with different number of model particles are shown in Table 56. Global sensitivity measures (SDF and SCF) are relatively small, especially for SDF measure and the test runs with the number of model particles lower than standard. For CS-137 and I-131, the global deposition measures are higher than global concentration measures for the number of model particles higher than standard. For Xe-131, the SCF measure remains on the same level for all test model runs and is very small.

Table 20: Time integrated concentrations, 48 hours after the start of release, in the model grid cell where the city of Oslo is located. Results of the model runs with different number of model particles (N). Values for the standard run are highlighted. The unit for time integrated concentration is Bq h m^{-3} and the unit for deposition is Bq m^{-2}.

N	Cs-137	I-131	Xe-133
Time Integrated Concentration			
200	0.35E+01	0.12E+03	0.41E+03
500	0.52E+01	0.18E+03	0.83E+02
2000	**0.27E+01**	**0.99E+02**	**0.15E+03**
4000	0.30E+01	0.12E+03	0.20E+03
8000	0.27E+01	0.99E+02	0.21E+03
Deposition			
200	0.87E+02	0.11E+05	0.0
500	0.11E+03	0.14E+05	0.0
2000	**0.10E+03**	**0.13E+05**	0.0
4000	0.99E+02	0.13E+05	0.0
8000	0.10E+03	0.13E+05	0.0

Table 21: Sensitivity measures as defined in Eqs. (29) - (32), for the SNAP runs with different number of model particles (N).

N	SDF	SCF	SDG	SCG
Cs-137				
200	2.7	12.6	-16.4	27.7
500	2.4	12.0	10.2	91.5
4000	57.2	11.7	-4.8	10.9
8000	73.2	19.9	-1.5	-2.5
I-131				
200	3.3	16.0	-19.7	26.3
500	2.7	15.1	5.7	80.9
4000	50.9	15.4	-2.6	17.5
8000	65.0	25.9	-0.1	0.5
Xe-133				
200	0.0	13.4	0.0	165.7
500	0.0	10.8	0.0	-45.8
4000	0.0	17.9	0.0	33.8
8000	0.0	6.0	0.0	38.2

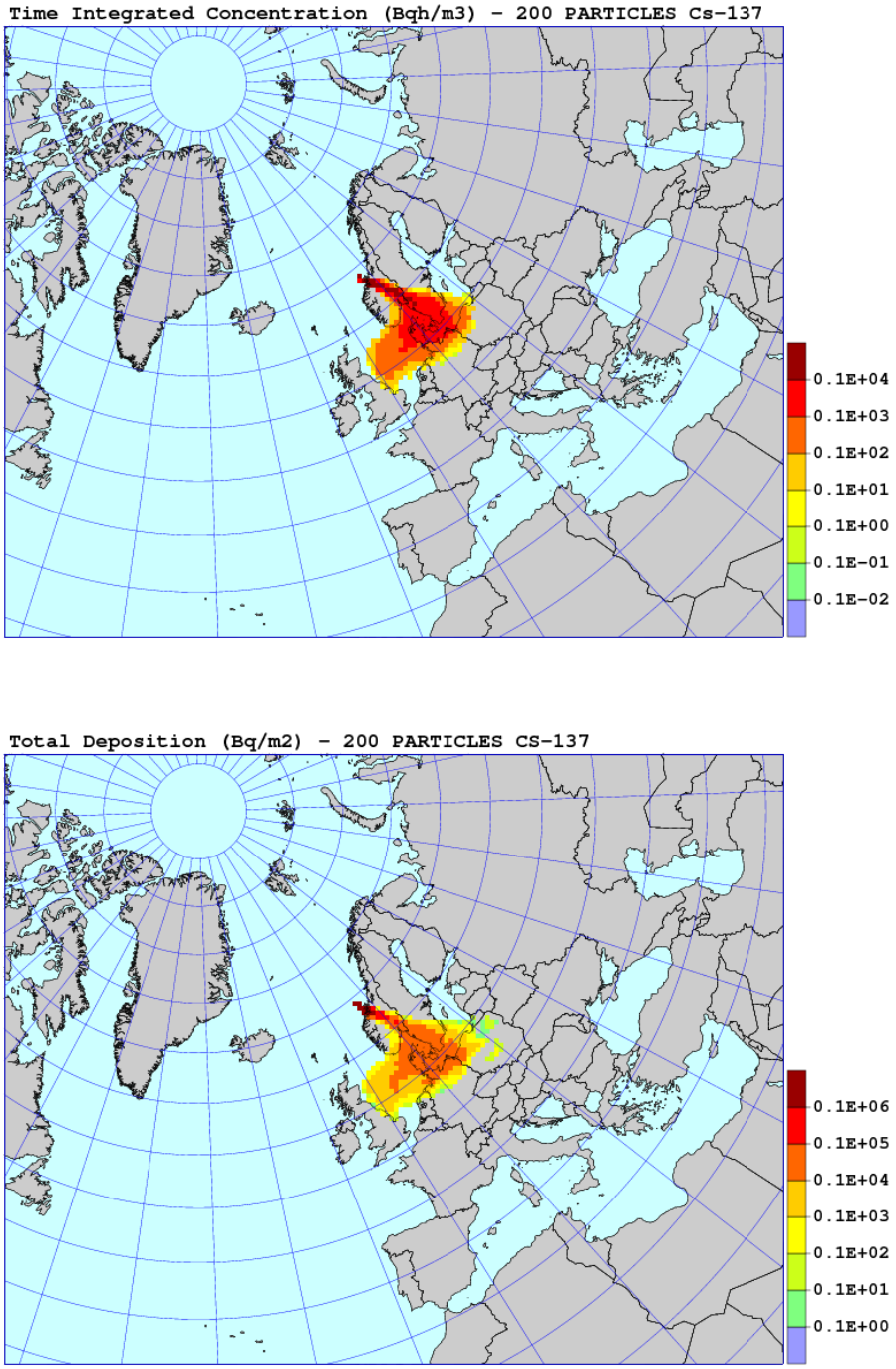

Figure 39: Results of the sensitivity run with 200 model particles. Maps of time integrated concentration and deposition of Cs-137, 48 hours from the accident start.

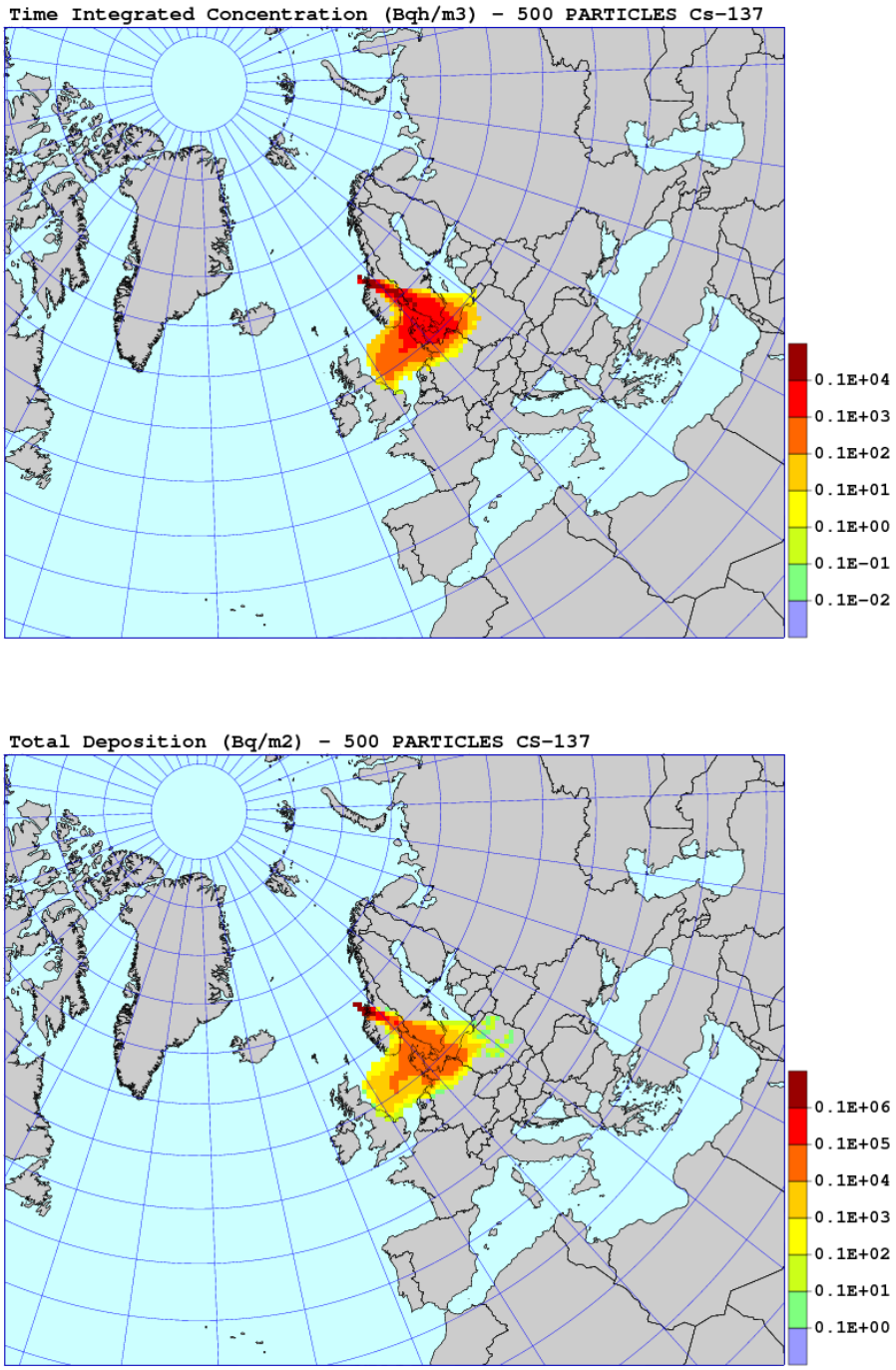

Figure 40: Results of the sensitivity run with 500 model particles. Maps of time integrated concentration and deposition of Cs-137, 48 hours from the accident start.

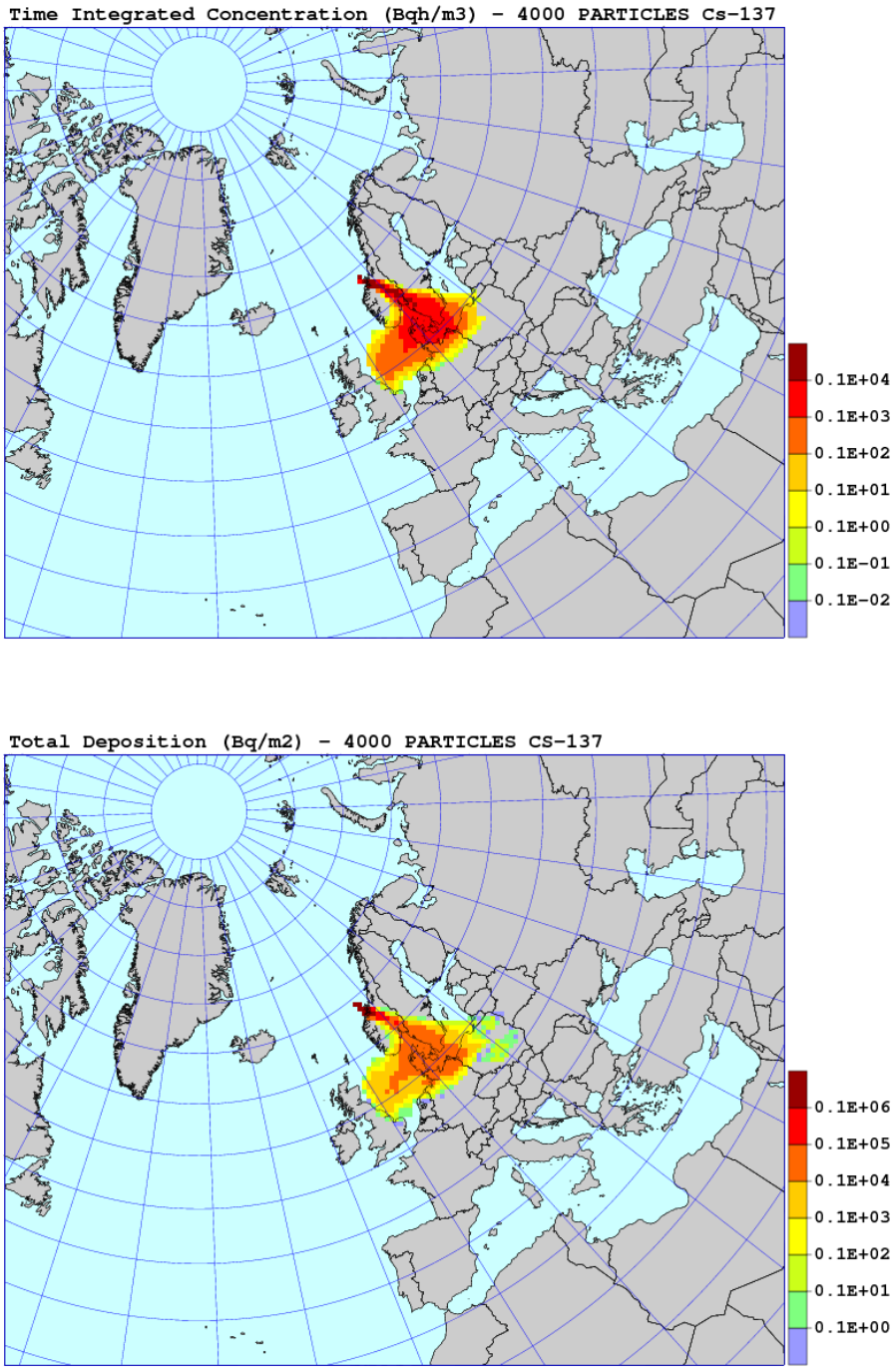

Figure 41: Results of the sensitivity run with 4000 model particles. Maps of time integrated concentration and deposition of Cs-137, 48 hours from the accident start.

The choice of the basic case, as well as the resulting source term for the standard run are described in this Chapter, together with the results of sensitivity runs. A brief summary, comparison and ranking of model sensitivities to different processes are also included at the end of the Chapter.

5.8. Standard run for nuclear accident

As a basic case for the standard run we assumed a hypothetical nuclear accident in the ship located close to Norwegian coast, as described in the MetNet exercise which took place in October 2010. Original description of the simulated accident was the following: "A serious accident has occurred aboard a transport ship carrying nuclear waste to Murmansk. The ship is on fire and is reported to leak Cs-137 from a storage tank". To make this basic case a bit more general we have also assumed the release of two other radionuclides iodine and xenon. In this way, we could take into account radionuclides in the form of gas, aerosol and noble gas. Atmospheric transport of these radionuclides is simulated for 48 hours in the standard run and in the test runs.

5.8.1. Source term

Participants of the MetNet exercise in October 2010 were asked to report long range dispersion results based on the original source term:

```
Location: Coast of Norway
Longitude: E 9 deg 10 min 00 sec (9,167)
Latitude: N 64 deg 15 min 00 sec (64,250)
Date and time of release start: 14.10.2010 06:00 UTC
Height of release: 15 meters
Plume rise: up to 500 meters
Length of release: 10 hours
Total amount of nuclides: 9.4E+15 Bq Cs-137 = 2.6E+11 Bq/s
```

In addition, the release of iodine and xenon was assumed from the same location with the rates given below:

```
5.0E17 Bq of iodine (I-131) => Release rate = 1.39E+13 Bq/sec
3.6E17 Bq of xenon (Xe-133) => Release rate = 1.00E+13 Bq/sec
```

The decay constants for selected radionuclides were taken from Appendix A and converted to a half-life time as traditional input for the SNAP model. Both, decay constants and half-life times for selected three radionuclides are given in Table 22. Compared to I-131 and Xe-133, Cs-137 has much longer half-life time and in practice its radioactive decay during the 48 hours simulation can be neglected. Therefore one can expect a low sensitivity of model results to radioactive decay for concentration and deposition of Cs-137.

The above specified source term for nuclear accident was used for the standard run in sensitivity tests.

Table 22: Decay constants and half-life times for three radionuclides selected for sensitivity tests.

Decay variable	Cs-137	I-131	Xe-133
Decay constant (s^{-1})	0.729×10^{-9}	0.944×10^{-6}	0.729×10^{-5}
Half-life time (days)	10954.88	8.07	4.57

5.8.2. Results of the standard run

The source term described in the previous section was used to calculate time integrated concentrations and total deposition for the standard run. The results for Cs-137, I-131 and Xe-133 are presented in Figures. 42, 43, and 44, respectively, in the form of time integrated concentration and deposition maps after 48 hours from the release start.

Time integrated concentrations and deposition calculated in the standard SNAP run show similar spatial pattern for all selected radionuclides. However, calculated values are different for each radionuclide reflecting differences in their release rates. In the initial phase of the transport, the plume is relatively narrow and directed mainly to the south and little bit to the east. In the later phase, prevailing wind direction is changing, horisontal diffusion becomes stronger and the plume is reaching Northern part of Germany in the south, covering Denmark on the way. In the east, the plume is reaching Baltic Sea and in the west it covers almost entire North Sea area, being close to the United Kingdom.

For comparison of sensitivity results, time integrated concentrations and deposition were calculated in the model grid square where the city of Oslo is located. The results for the standard run in the Oslo grid are presented in Table 23.

Table 23: Time integrated concentrations and deposition, 48 hours after the start of release, in the model grid cell where the city of Oslo is located. Results of the standard run.

Radionuclide selected	Time integrated concentration (Bq h m^{-3})	Total deposition (Bq m^{-2})
Cs-137	0.27×10^1	0.10×10^3
I-131	0.99×10^2	0.13×10^5
Xe-133	0.15×10^3	0.0

The values of time integrated concentrations and deposition for each radionuclide in Table 23 reflect roughly their release rates in the source term for the standard run. However, the highest values of time integrated concentration can be noticed for Xe-133, although total release for I-131 (5.0e17 Bq) is higher than the total release for Xe (3.6e17 Bq). This is because Xe-133 is a noble gas which is neither dry nor wet deposited, with zero deposition value in Table 23. Therefore, the relative amount of Xe-133 radioactivity remaining in the air during the transport is significantly higher than the amount of radioactivity of regular gas or aerosol.

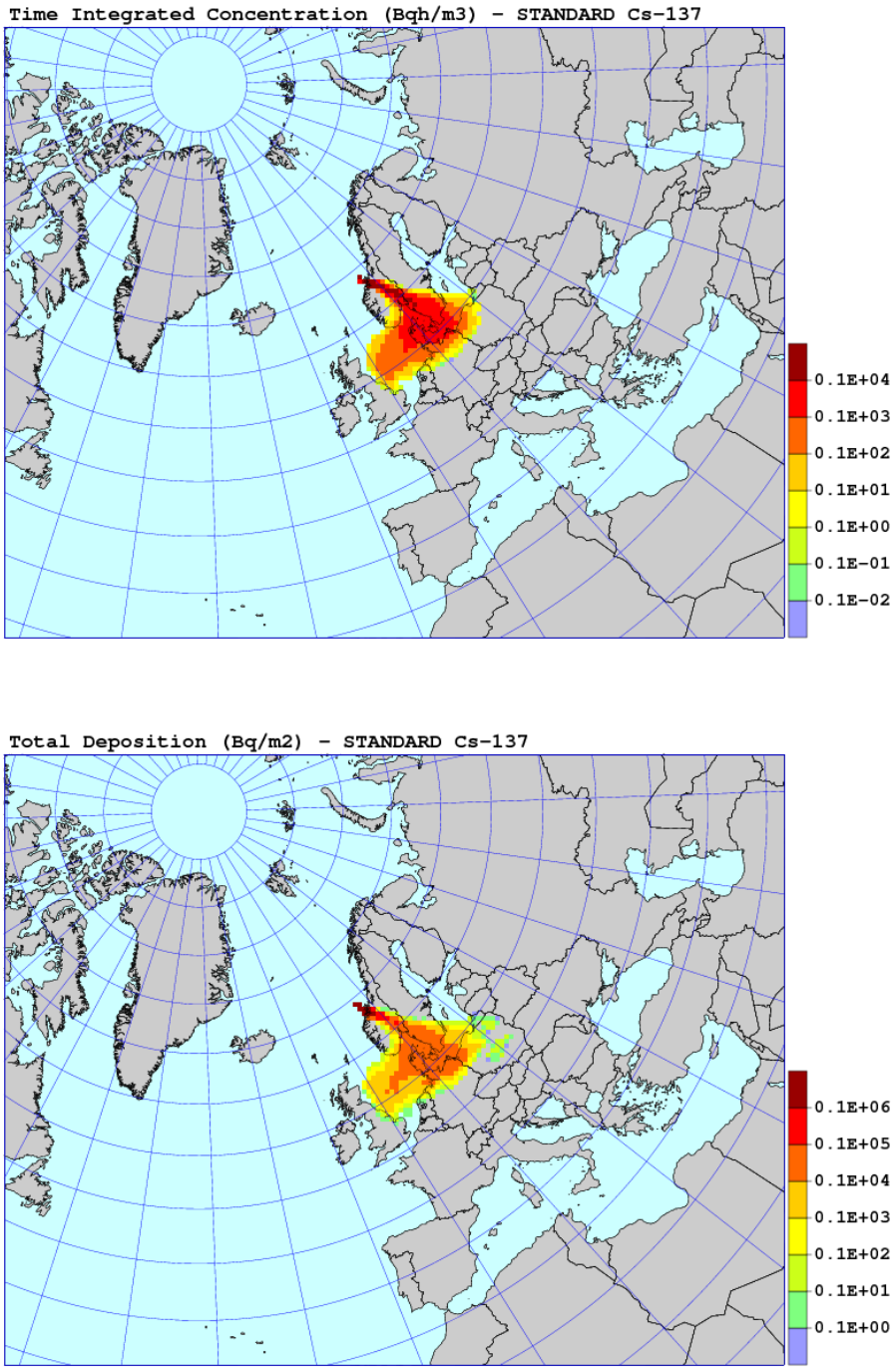

Figure 42: The results of the standard SNAP run for Cs-137 after 48 hours from the accident start. Time integrated concentrations in Bq h m^{-3} above and total deposition in Bq m^{-3} in the bottom.

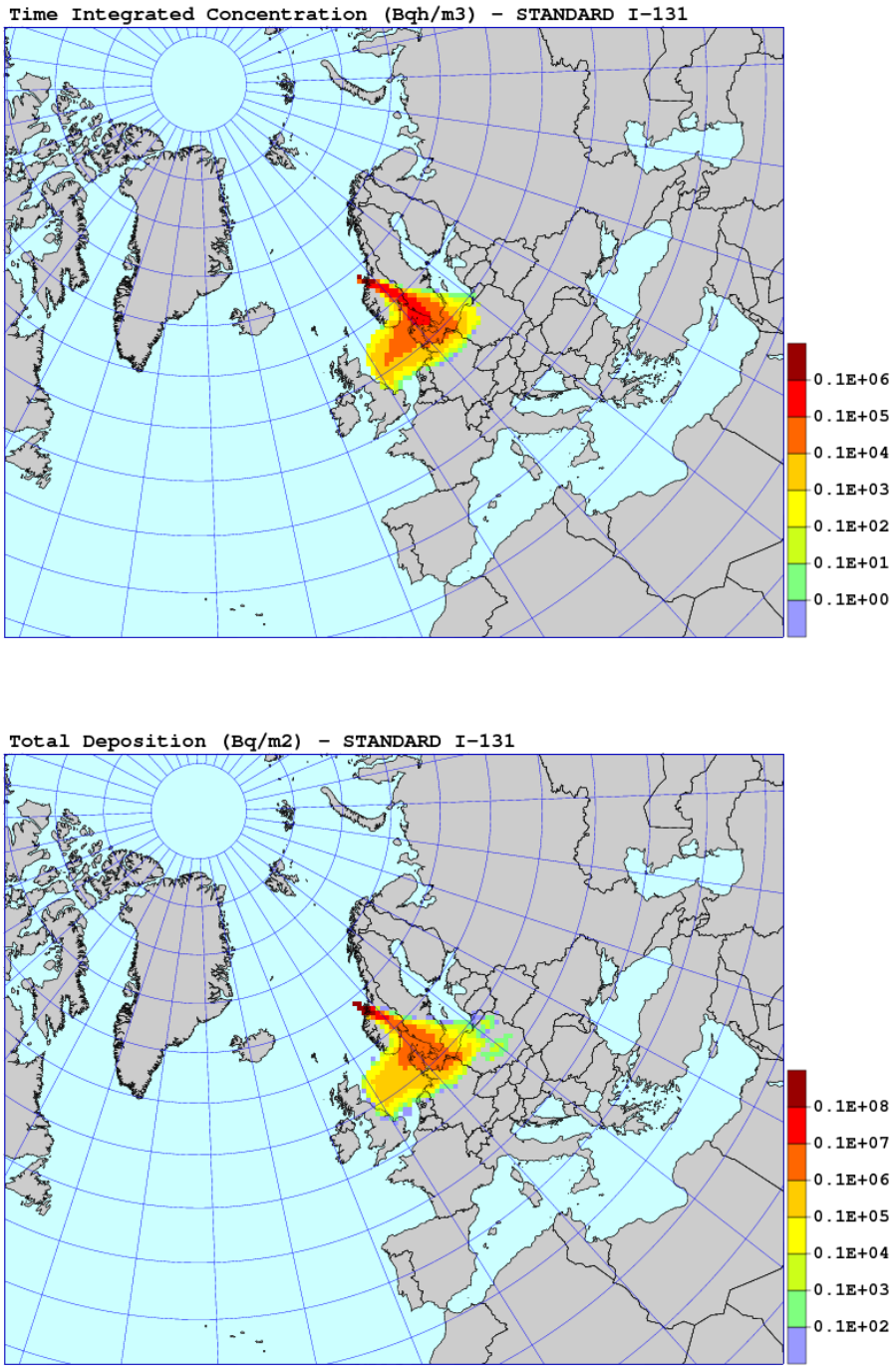

Figure 43: The results of the standard SNAP run for I-131 after 48 hours from the accident start. Time integrated concentrations in Bq h m^{-3} above and total deposition in Bq m^{-3} in the bottom.

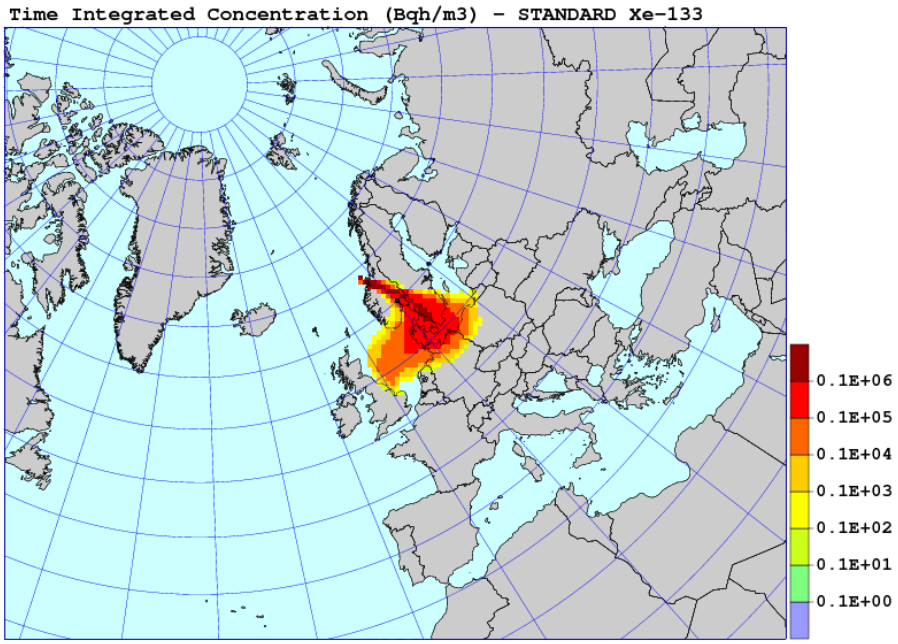

Figure 44: The results of the standard SNAP run for Xe-133 after 48 hours from the accident start. Time integrated concentrations in Bq h m^{-3}.

5.9. Sensitivity to dry deposition

Sensitivity to dry deposition was tested in the model run without dry deposition process. The maps of time integrated concentration and total deposition for Cs-137 are shown in Fig. 45 and the maps of time integrated concentration and total deposition for I-131 are shown in Fig. 46. Since Xe-133 is a noble gas, it is not sensitive to dry deposition and the deposition and concentration maps are not shown here for Xe-133.

Time integrated concentrations and deposition in the model grid cell where the city of Oslo is located are shown in Table 24 for the model run without dry deposition, 48 hours after the start of release. Sensitivity measures for the run without dry deposition are shown in Table 25.

Table 24: Time integrated concentrations and deposition, 48 hours after the start of release, in the model grid cell where the city of Oslo is located. Results of the model run without dry deposition.

Radionuclide selected	Time integrated concentration (Bq h m^{-3})	Total deposition (Bq m^{-2})
Cs-137	0.29×10^{1}	0.0
I-131	0.12×10^{3}	0.0
Xe-133	0.15×10^{3}	0.0

SENS SDF SCF SDG SCG Cs-137 58.4 77.1 -100.0 5.0 I-131 136.0 292.7 -100.0 18.9 Xe-133 0 0 0 0

Table 25: Sensitivity measures as defined in Eqs. (29) - (32), for the run without dry deposition.

Radionuclide selected	SDF	SCF	SDG	SCG
Cs-137	58.4	77.1	-100.0	5.0
I-131	136.0	292.7	-100.0	18.9
Xe-133	0	0	0	0

Elimination of dry deposition from the model processes results in higher air concentrations of Cs-137 and I-131, visible in the concentration maps (Fig. 45 and 46) and in the sensitivity measures (Table 25). The SCF values in Table 25 show that time integrated concentration of I-131 is definitely more sensitive to dry deposition process than time integrated concentration of Cs-137. The same conclusion applies to deposition, as indicated by SDF measure in Table 25. Sensitivity of Cs-137 and I-131 deposition to dry deposition is also clearly visible in the deposition maps for those radionuclides (Fig. 45 and 46). Total deposition pattern is the same as wet deposition pattern on those maps and it reflects the precipitation distribution during the transport. Since it does not rain in Oslo, total deposition in Oslo grid in the run without dry deposition is zero, which explains -100.0 values of SDG measure in Table 25.

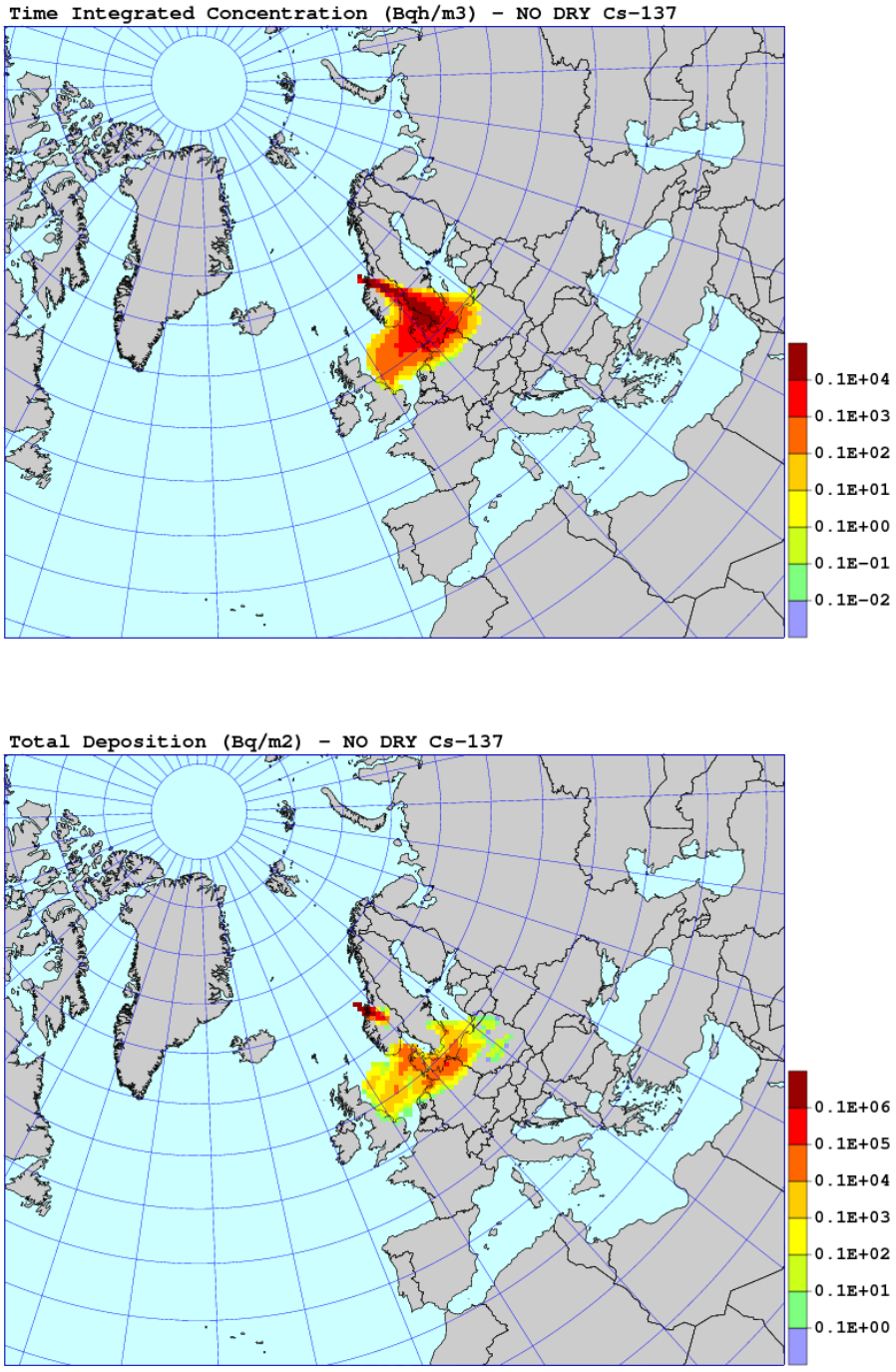

Figure 45: Results of the sensitivity run without dry deposition. Maps of time integrated concentration and deposition of Cs-137, 48 hours from the accident start.

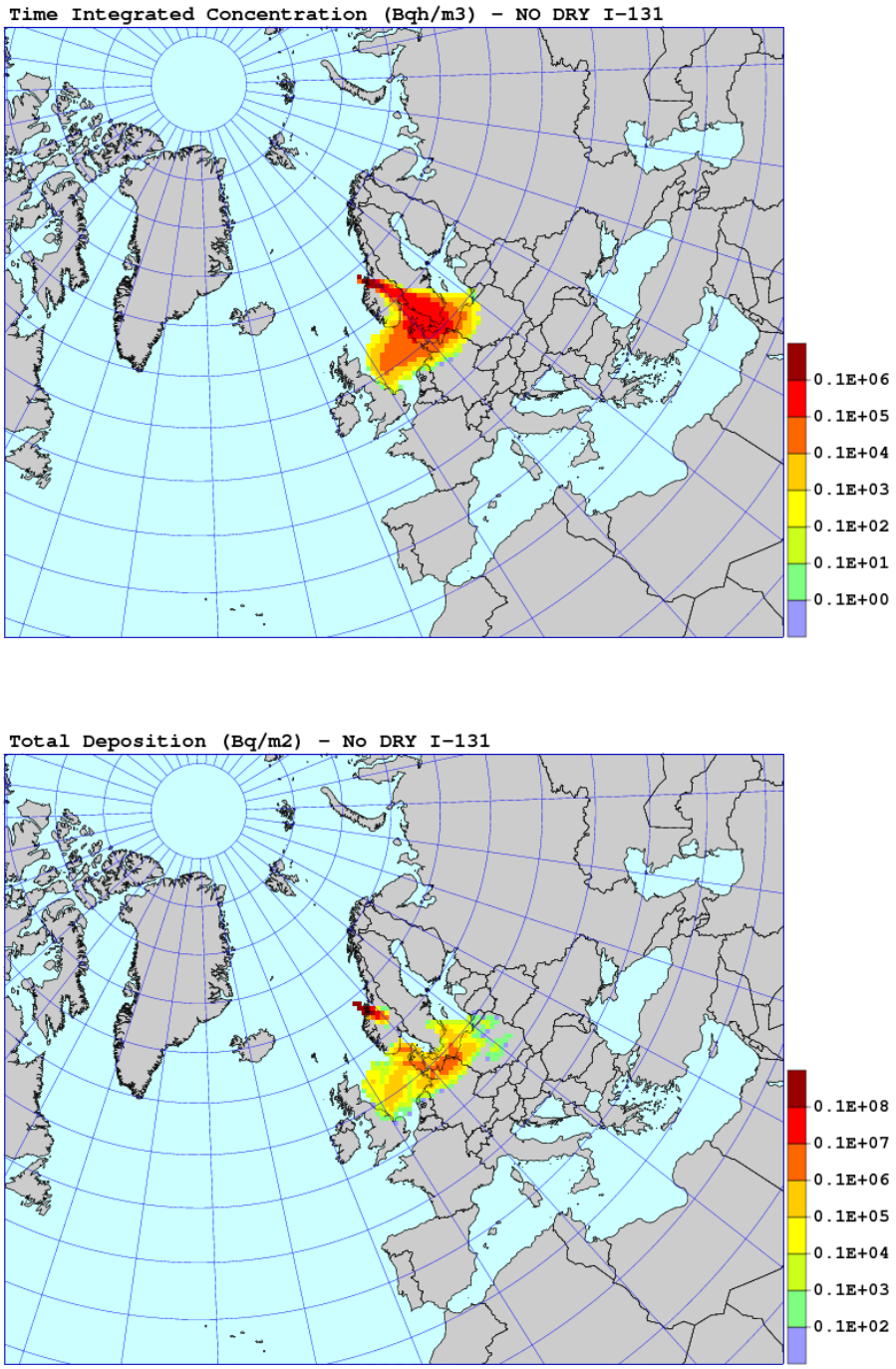

Figure 46: Results of the sensitivity run without dry deposition. Maps of time integrated concentration and deposition of I-131, 48 hours from the accident start.

5.10. Sensitivity to wet deposition

Sensitivity to dry deposition was tested in the model run without wet deposition process. The maps of time integrated concentration and total deposition for Cs-137 run are shown in Fig. 47 and the maps of time integrated concentration and total deposition for I-131 run are shown in Fig. 48. Since Xe-133 is a noble gas, it is not sensitive to wet deposition and the deposition and concentration maps are not shown here for Xe-133. Compared to the results of standard run, time integrated concentrations of Cs-137 and I-131 is higher and smoother in the run without wet deposition, especially in the centre of the plume. The deposition maps shown in the same figures indicate, on the other hand, slightly lower deposition values compared to the standard run.

Time integrated concentrations and deposition in the model grid cell where the city of Oslo is located are shown in Table 26 for the model run without wet deposition, 48 hours after the start of release. Both, time integrated concentrations and deposition of Cs-137 and I-131 in the Oslo grid are higher in the run without wet deposition than in the standard run. Sensitivity measures for the run without wet deposition are shown in Table 27.

Table 26: Time integrated concentrations and deposition, 48 hours after the start of release, in the model grid cell where the city of Oslo is located. Results of the model run without wet deposition.

Radionuclide selected	Time integrated concentration (Bq h m^{-3})	Total deposition (Bq m^{-2})
Cs-137	0.62×10^{1}	0.17×10^{3}
I-131	0.29×10^{3}	0.27×10^{5}
Xe-133	0.15×10^{3}	0.0

Table 27: Sensitivity measures as defined in Eq. (29) - (32), for the run without wet deposition.

Radionuclide selected	SDF	SCF	SDG	SCG
Cs-137	545.2	234.5	68.8	126.4
I-131	464.8	341.5	102.7	189.6
Xe-133	0	0	0	0

The sensitivity measures in Table 27 show that the model is more sensitive to wet deposition than to dry deposition. Especially, the SDF values in Table 27 are very high, which means that the sensitivity of both radionuclides is higher for deposition than concentration, however, the sensitivity of concentrations to wet deposition is also relatively high. High sensitivity to wet deposition is also confirmed by local SDG and SCG measures in Table 27 which apply to the model grid square with Oslo location. In this case sensitivity is slightly higher for concentration than for deposition.

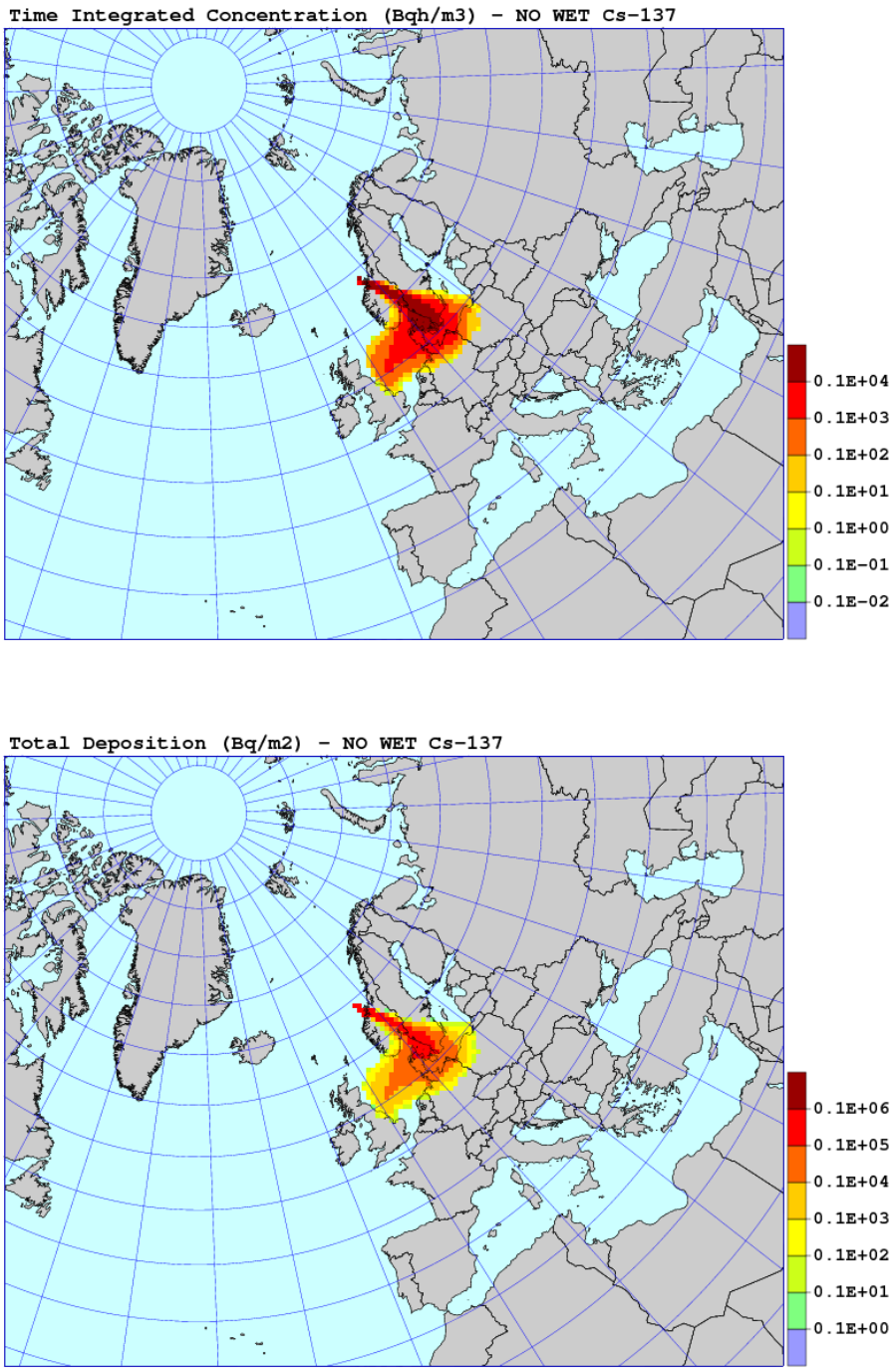

Figure 47: Results of the sensitivity run without wet deposition. Maps of time integrated concentration and deposition of Cs-137, 48 hours from the accident start.

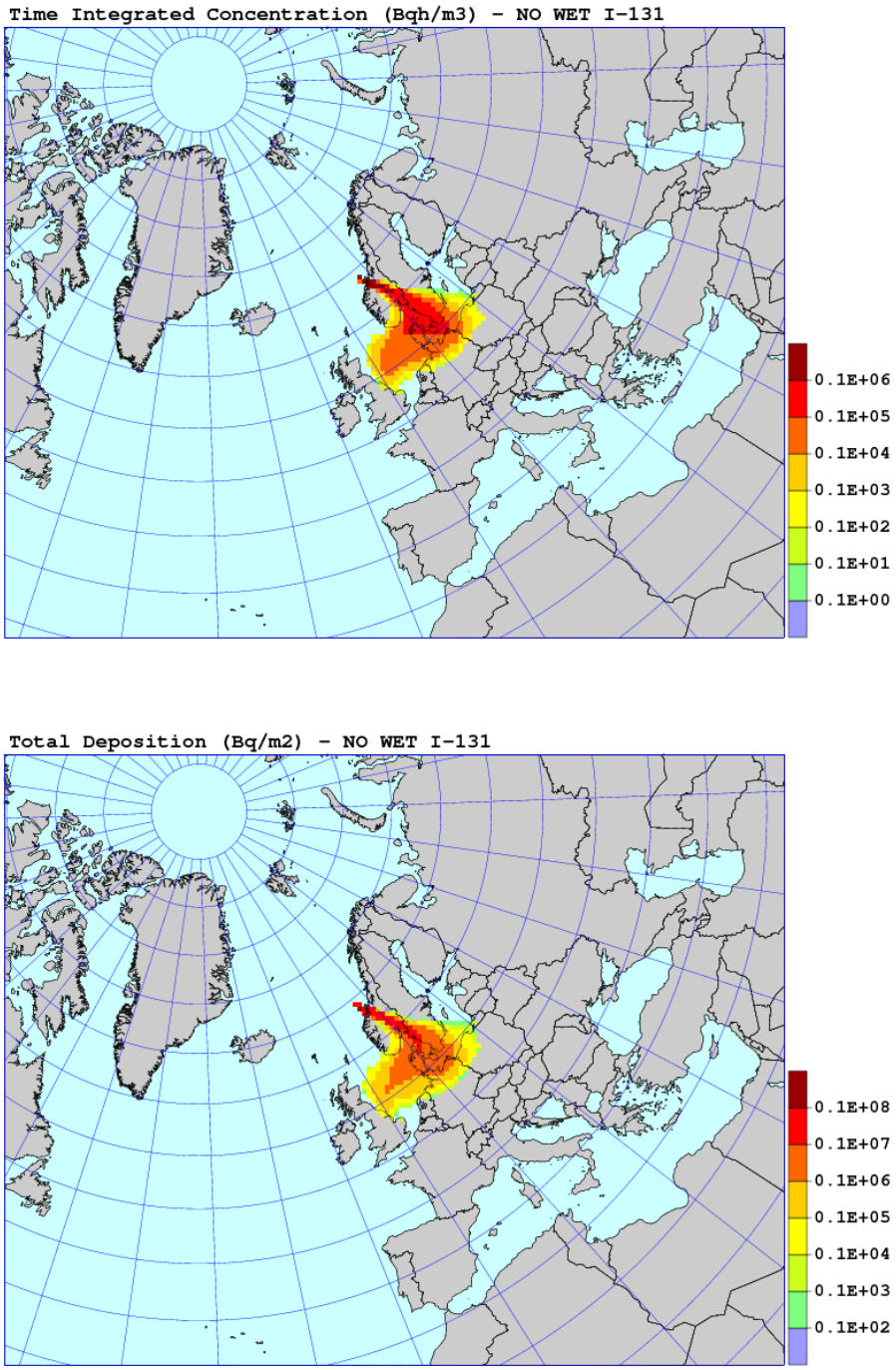

Figure 48: Results of the sensitivity run without wet deposition. Maps of time integrated concentration and deposition of I-131, 48 hours from the accident start.

5.11. Sensitivity to radioactive decay

Sensitivity to radioactive decay was tested in the model run without a decay process. The maps of time integrated concentration and total deposition for Cs-137 run are shown in Fig. 49. The maps of time integrated concentration and total deposition for I-131 are shown in Fig. 50 and finally the map of time integrated concentration for Xe-133 is shown in Fig. 51. Since Xe-133 is a noble gas the deposition field for this radionuclide is not shown. Practically, there are no differences between the standard run and the test run for Cs-137 in time integrated concentration and in deposition maps. Also for I-131 the differences between maps from the standard and test runs are small and they are not large either for the maps of time integrated concentrations of Xe-133.

Time integrated concentrations and deposition, 48 hours after the start of release, in the model grid cell where the city of Oslo is located are shown in Table 28 for the model run without radioactive decay. For Cs-137, both time integrated concentrations and deposition are practically the same in the standard run and in the test run. For I-131, there is only 1% difference in time integrated concentration, but deposition in the run without radioactive decay is 15% higher than in the standard run. However, time integrated concentration of Xe-131 in the Oslo grid is almost two times higher in the test run than in the standard run.

Sensitivity measures for the run without radioactive decay are given in Table 29. As expected, the model results for Cs-137 are definitely not sensitive to radioactive decay. Certain model sensitivity to radioactive decay can be noticed in case of I-131 and some more sensitivity in case of time integrated concentration of Xe-133.

Table 28: Time integrated concentrations and deposition, 48 hours after the start of release, in the model grid cell where the city of Oslo is located. Results of the model run without radioactive decay.

Radionuclide selected	Time integrated concentration (Bq h m^{-3})	Total deposition (Bq m^{-2})
Cs-137	0.27×10^{1}	0.10×10^{3}
I-131	0.10×10^{3}	0.15×10^{5}
Xe-133	0.27×10^{3}	0.0

Table 29: Sensitivity measures as defined in Eqs. (29) - (32), for the run without radioactive decay.

Radionuclide selected	SDF	SCF	SDG	SCG
Cs-137	0.1	0.0	0.0	0.0
I-131	10.8	8.4	15.1	4.1
Xe-133	0.0	26.0	0.0	79.4

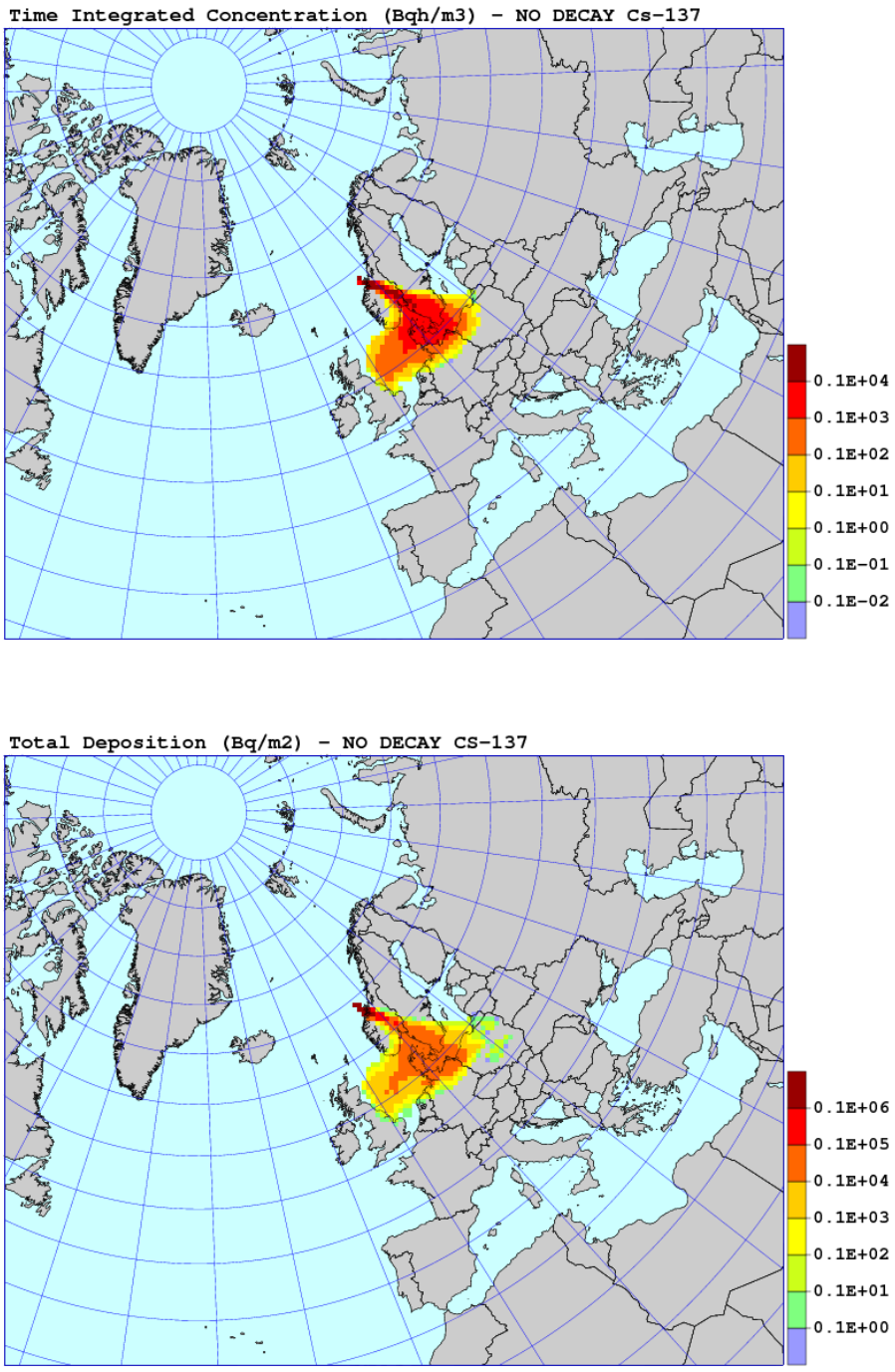

Figure 49: Results of the sensitivity run without radioactive decay. Maps of time integrated concentration and deposition of Cs-137, 48 hours from the accident start.

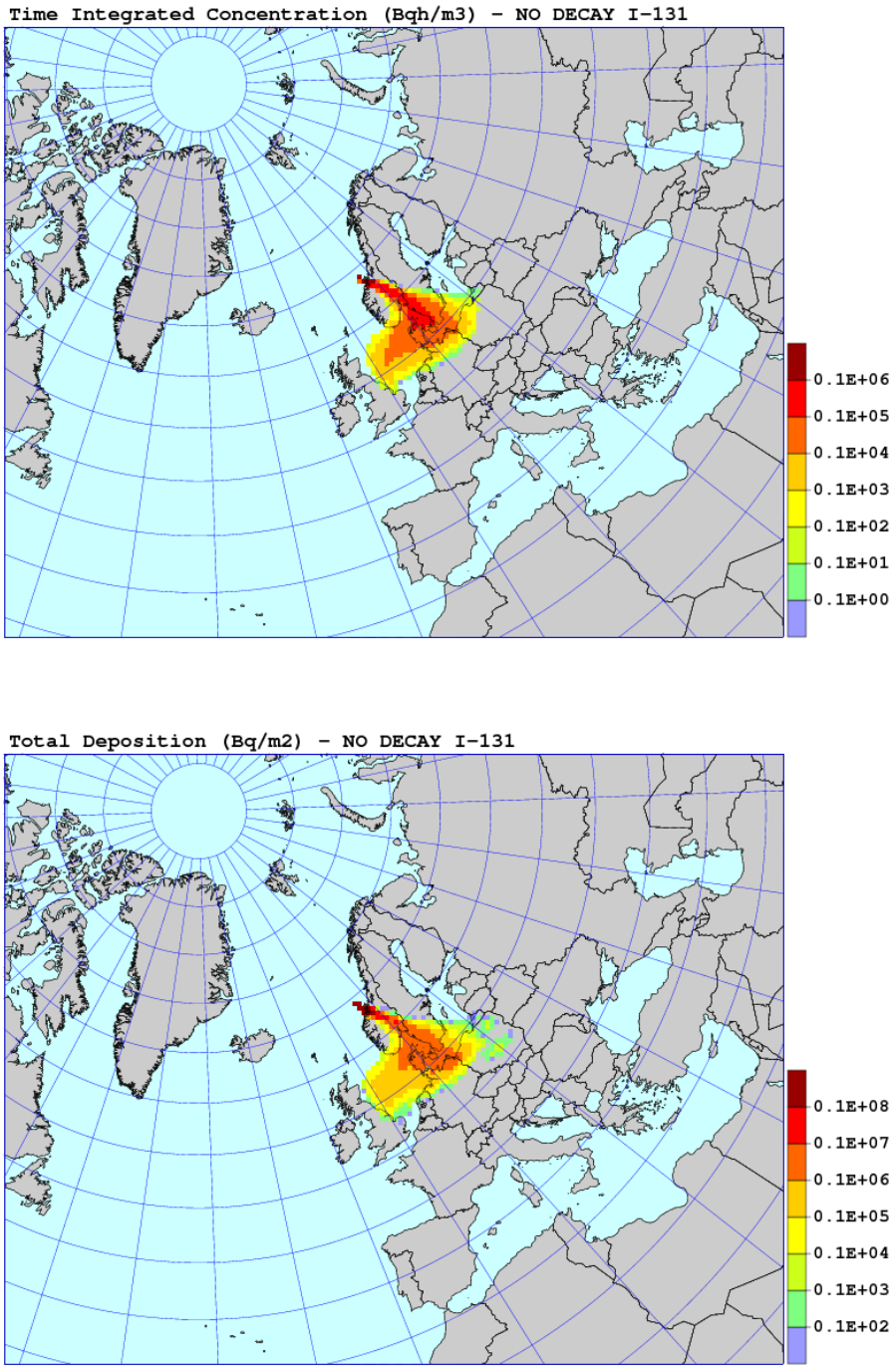

Figure 50: Results of the sensitivity run without radioactive decay. Maps of time integrated concentration and deposition of I-131, 48 hours from the accident start.

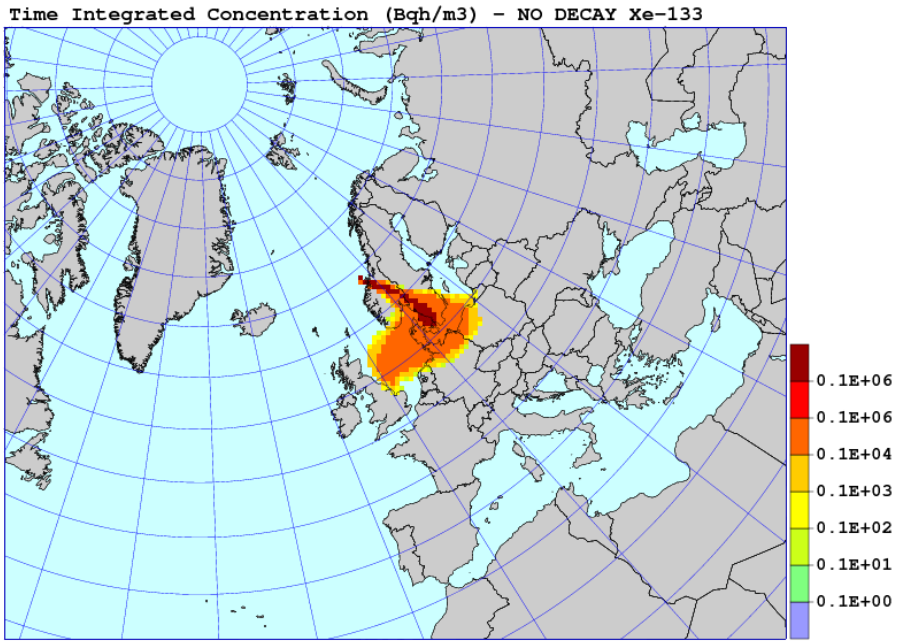

Figure 51: Results of the sensitivity run without radioactive decay. Maps of time integrated concentration and deposition of Xe-133, 48 hours from the accident start.

5.12. Sensitivity to horisontal diffusion

Sensitivity to horisontal diffusion was tested in two model runs. In the first run, the process of horisontal diffusion was switched off, both below and above the mixing height. In the second run, horisontal diffusion was increased by applying double value to horisontal diffusion coefficient, again in the boundary layer and above.

The maps of time integrated concentrations and total deposition for Cs-137 for the run without horisontal diffusion are shown in Fig. 52. The maps of time integrated concentration and total deposition for I-131, for the same run, are shown in Fig. 55. Both, for Cs-137 and I-131 the differences between the standard run the run without horisontal diffusion are very small. It applies to the maps of time integrated concentration and deposition maps, as well.

The maps of time integrated concentrations and total deposition for Cs-137 for the run with increased horisontal diffusion are shown in Fig. 54. The maps of time integrated concentration and total deposition for I-131, for the same run, are shown in Fig. 56. The differences between the standard run and the test run with increased horisontal diffusion are also small in this case for both radionuclides.

The maps of time integrated concentration for Xe-133 are shown in Fig. 57 for the runs without horisontal diffusion and increased horisontal diffusion. Once again, differences between the maps of time integrated concentrations calculated in the run with no horisontal diffusion, in the run with increased horisontal diffusion and in the standard run are very small.

Time integrated concentrations and deposition, 48 hours after the start of release, in the model grid cell where the city of Oslo is located are shown in Table 30, for the model run without horisontal diffusion and in Table 31, for the model run with increased horisontal diffusion. As in case of Cs-137 and I-131, also there are only small differences between time integrated concentrations maps from the standard run and the runs without and with increase horisontal diffusion.

Table 30: Time integrated concentrations and deposition, 48 hours after the start of release, in the model grid cell where the city of Oslo is located. Results of the model run without horisontal diffusion.

Radionuclide selected	Time integrated concentration (Bq h m^{-3})	Total deposition (Bq m^{-2})
Cs-137	0.22×10^{1}	0.12×10^{3}
I-131	0.85×10^{2}	0.15×10^{5}
Xe-133	0.22×10^{3}	0.0

In general there is not much difference between the deposition values from the standard and test runs for all radionuclides and for both, run without deposition and run with increased deposition. However, all depositions in the Oslo grid from the test run are slightly higher - 10-20%, than the depositions from the standard run. On the other hand, calculated time integrated concentrations in the test runs in the Oslo grid differ, sometimes significantly from those in the standard run. The largest difference -87% can be noticed for I-131 and the run with increased horisontal diffusion.

Table 31: Time integrated concentrations and deposition, 48 hours after the start of release, in the model grid cell where the city of Oslo is located. Results of the model run with increased horisontal diffusion.

Radionuclide selected	Time integrated concentration (Bq h m^{-3})	Total deposition (Bq m^{-2})
Cs-137	0.33×10^{1}	0.11×10^{3}
I-131	0.13×10^{2}	0.14×10^{5}
Xe-133	0.31×10^{3}	0.0

Sensitivity measures, for the runs without horisontal diffusion and with increased horisontal diffusion are shown in Tables32 and 33. These measures are relatively (compared to dry and wet deposition) low for SCF and all three isotopes. For SDF, the measures for Cs-137 and I-131 are similar to those for dry deposition, but much lower than those for wet deposition. Three sensitivity measures (SDF, SCF and SDG), for the runs without horisontal diffusion and with increased horisontal diffusion, are a bit higher for I-131 than for Cs-137. The SCG measure is higher for Cs-137. Sensitivity measures for Xe-133 are lower for the runs with and without horisontal diffusion than for the run without a radioactive decay.

Table 32: Sensitivity measures as defined in Eqs. (29) - (32), for the run without horisontal diffusion.

Radionuclide selected	SDF	SCF	SDG	SCG
Cs-137	122.2	11.5	11.0	-17.8
I-131	150.0	16.3	11.8	-13.6
Xe-133	0.0	10.2	0.0	44.4

Table 33: Sensitivity measures as defined in Eqs. (29) - (32), for the run with increased horisontal diffusion.

Radionuclide selected	SDF	SCF	SDG	SCG
Cs-137	135.4	20.0	5.8	20.9
I-131	139.2	26.0	7.5	27.0
Xe-133	0.0	14.6	0.0	104.0

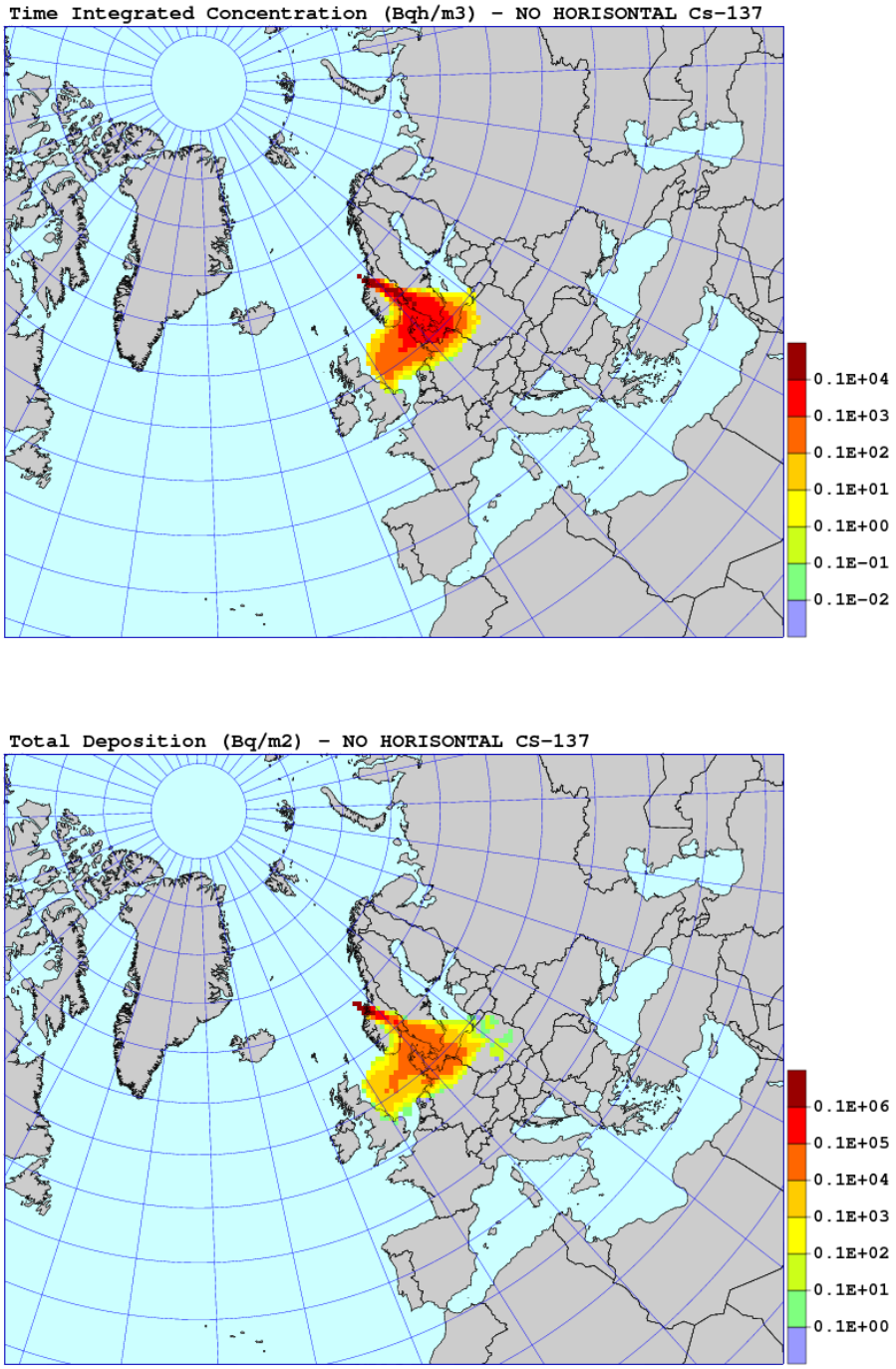

Figure 52: Results of the sensitivity run without horisontal diffusion. Maps of time integrated concentration and deposition of Cs-137, 48 hours from the accident start.

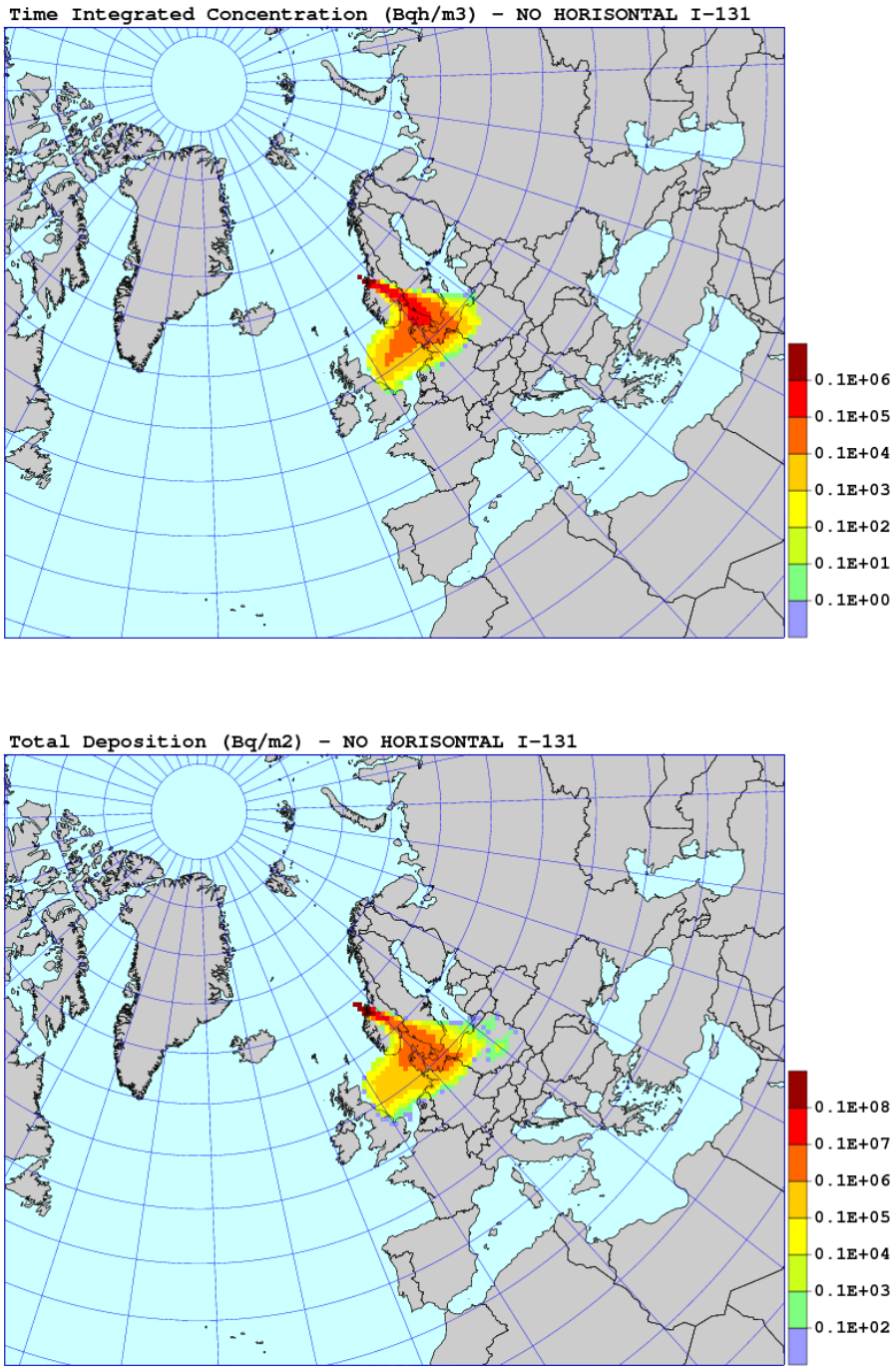

Figure 53: Results of the sensitivity run without horisontal diffusion. Maps of time integrated concentration and deposition of I-131, 48 hours from the accident start.

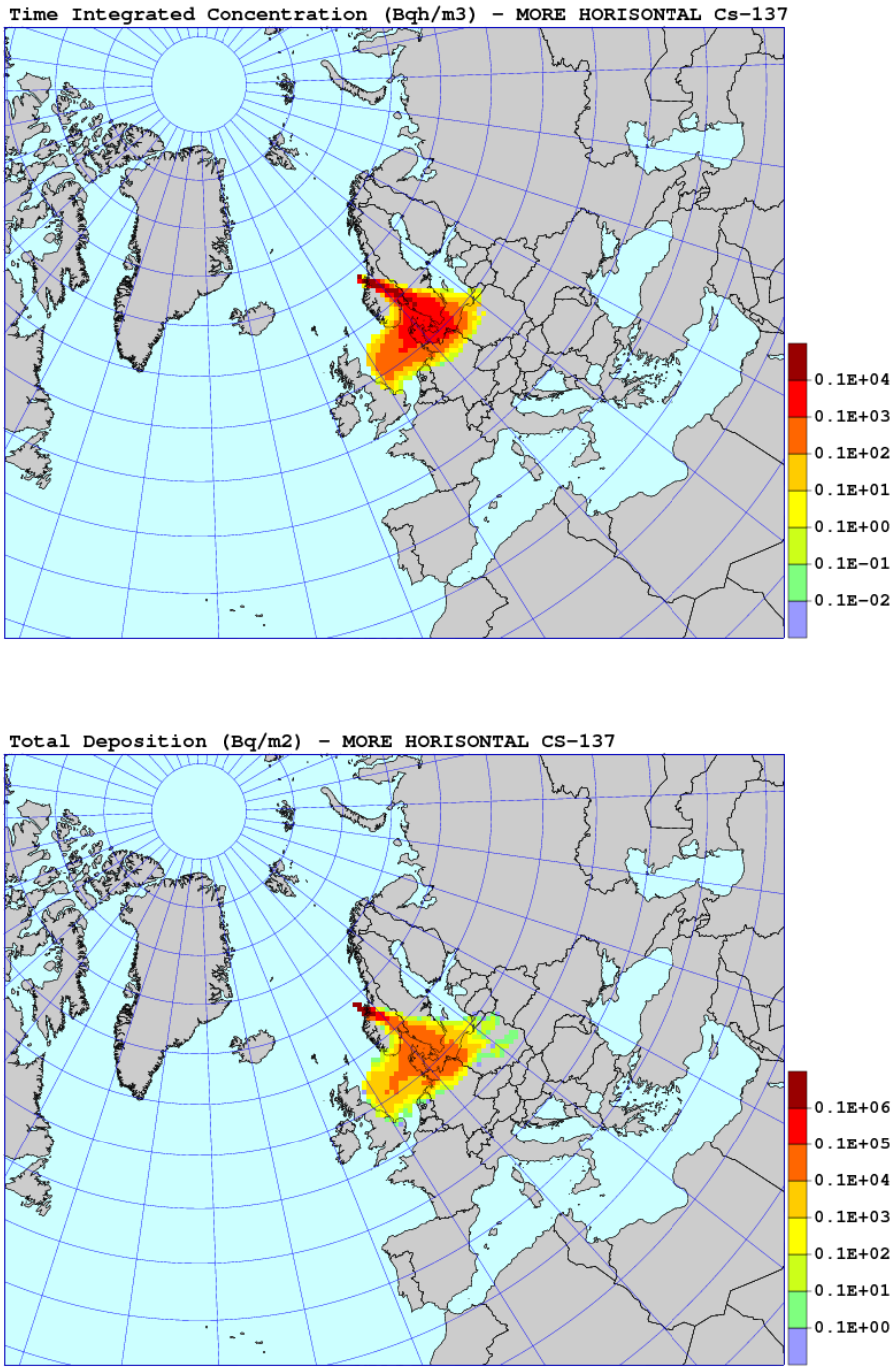

Figure 54: Results of the sensitivity run with increased horisontal diffusion. Maps of time integrated concentration and deposition of Cs-137, 48 hours from the accident start.

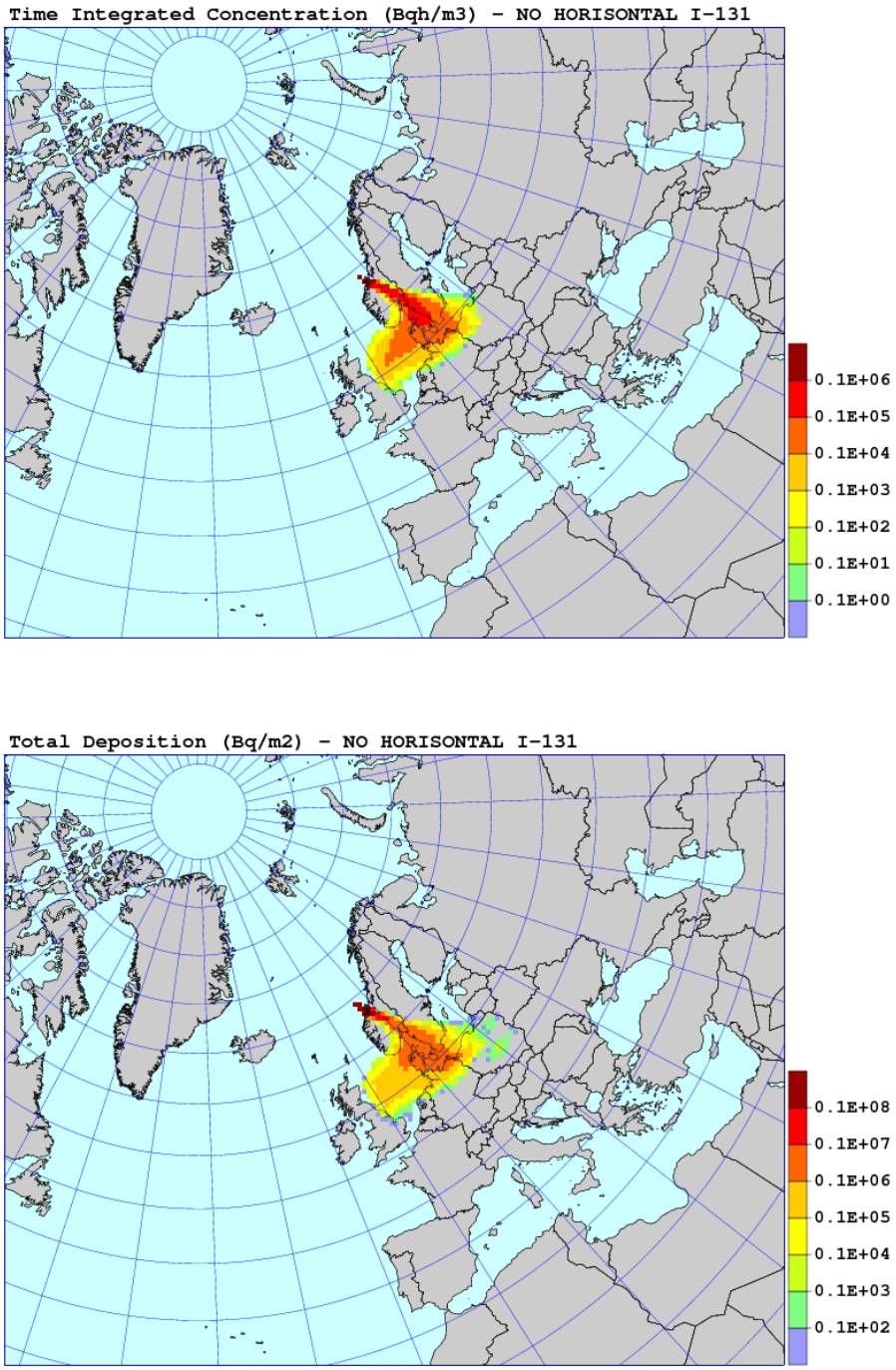

Figure 55: Results of the sensitivity run without horisontal diffusion. Maps of time integrated concentration and deposition of I-131, 48 hours from the accident start.

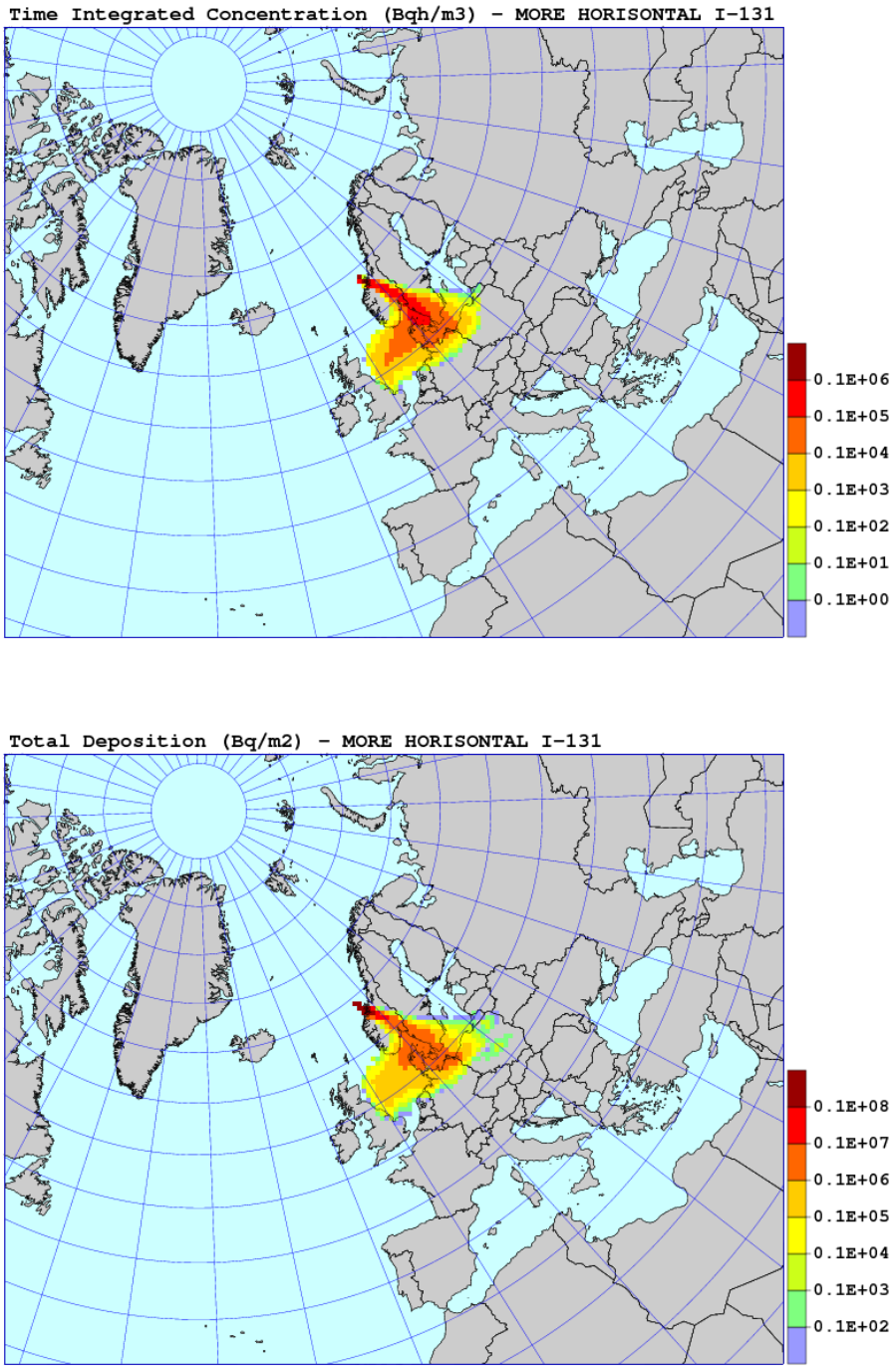

Figure 56: Results of the sensitivity run with increased horisontal diffusion. Maps of time integrated concentration and deposition of I-131, 48 hours from the accident start.

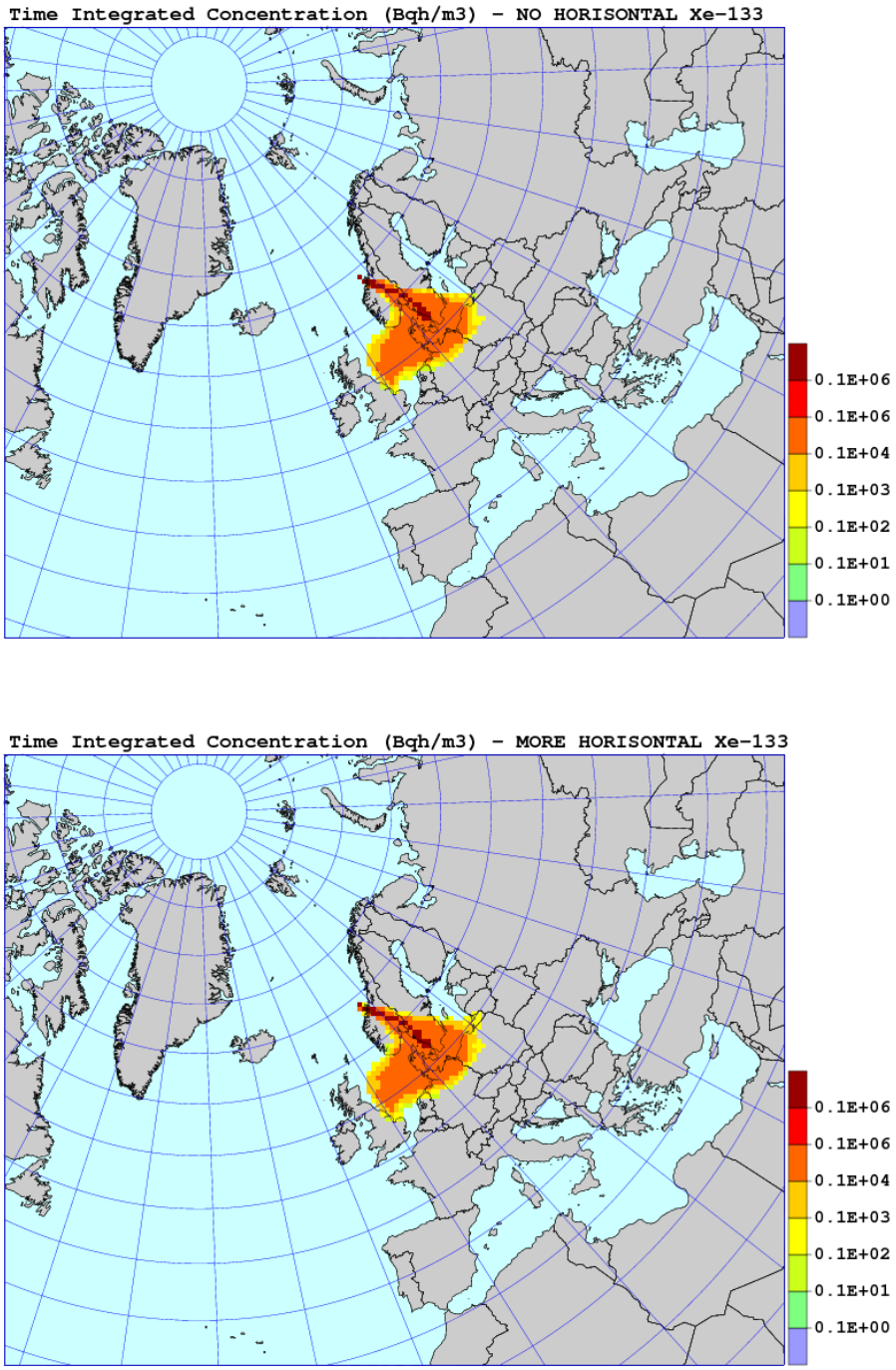

Figure 57: Results of the sensitivity run without horisontal diffusion (above) and increased horisontal diffusion (below). Maps of time integrated concentration and deposition of Xe-133, 48 hours from the accident start.

5.13. Sensitivity to vertical diffusion

As in case of horisontal diffusion, sensitivity to vertical diffusion was also tested in two model runs. In the first run, the process of vertical diffusion was switched off, both below and above the mixing height. In the second run, vertical diffusion was increased by applying double value to vertical diffusion coefficient, in the boundary layer and above.

The maps of time integrated concentration and total deposition for Cs-137 for the run without vertical diffusion are shown in Fig. 58. The maps of time integrated concentration and total deposition for I-131, for the same run, are shown in Fig. 59. All test maps for Cs-137 and I-131 differ significantly from the standard run maps. The plumes in the test runs are narrower and gradients are steeper. This applies, both to the maps of deposition and maps of time integrated concentration.

The maps of time integrated concentration and total deposition for Cs-137 and the run with increased vertical diffusion are shown in Fig. 60. The maps of time integrated concentration and total deposition for I-131, for the same run, are shown in Fig. 61. Also in this case, the results for Cs-137 and I-131 on the maps from test runs are quite different from the results on the maps from the standard run. However, in the run with increased vertical diffusion, the plumes are wider than the plumes from the standard run.

The maps of time integrated concentration for Xe-133 are shown in Fig. 62, for the runs without vertical diffusion and the runs with increased vertical diffusion. The differences in Xe-133 time integrated concentrations between the standard run and the test runs without vertical diffusion and with increased vertical diffusion are very similar like in case of Cs-137 and I-131. Compared to the standard run results, narrower plume can be noticed in the run without vertical diffusion and wider plume in the run with increased vertical diffusion.

Time integrated concentrations and deposition, 48 hours after the start of release, in the model grid cell where the city of Oslo is located are shown in Table 34 - for the model run without vertical diffusion and in Table 35 - for the model run with increased vertical diffusion.

Table 34: Time integrated concentrations and deposition, 48 hours after the start of release, in the model grid cell where the city of Oslo is located. Results of the model run without vertical diffusion.

Radionuclide selected	Time integrated concentration (Bq h m^{-3})	Total deposition (Bq m^{-2})
Cs-137	0.00E+00	0.00E+00
I-131	0.00E+00	0.00E+00
Xe-133	0.00E+00	0.00e+00

Only zeros can be found in Table 34, because in the model run without vertical diffusion, radioactive debris did not arrive to Oslo grid at all. On the other hand, time integrated concentrations and deposition in the Oslo grid from the model run with increased vertical diffusion (Table 35) are much higher than corresponding values from the standard run. It means that for Oslo location, model sensitivity to vertical diffusion is relatively high.

Table 35: Time integrated concentrations and deposition, 48 hours after the start of release, in the model grid cell where the city of Oslo is located. Results of the model run with increased vertical diffusion.

Radionuclide selected	Time integrated concentration (Bq h m^{-3})	Total deposition (Bq m^{-2})
Cs-137	0.79×10^{1}	0.28×10^{3}
I-131	0.30×10^{3}	0.36×10^{5}
Xe-133	0.60×10^{3}	0.0

Sensitivity measures for the run without vertical diffusion and run with enhanced vertical diffusion are shown in Table 36. Compared to other sensitivity tests, the local measures (SDG and SCG) are relatively high, both for the run without vertical diffusion and run with increased vertical diffusion. The global measures - SDF and SCF - are approximately 100% higher in the run without vertical diffusion than in the run with increased vertical diffusion. In both runs, the global measure for time integrated concentration (SCF) is more sensitive to vertical diffusion than the global measure for deposition SDF.

Table 36: Sensitivity measures as defined in Eqs. (29) - (32), for the run without vertical diffusion and the model run with enhanced vertical diffusion.

Radionuclide selected	SDF	SCF	SDG	SCG
No vertical diffusion				
Cs-137	88.2	188.4	-100.0	-100.0
I-131	96.0	273.1	-100.0	-100.0
Xe-133	0.0	204.0	0.0	-100.0
More vertical diffusion				
Cs-137	48.2	93.9	174.7	190.3
I-131	46.0	90.7	172.5	202.5
Xe-133	0.0	102.5	0.0	291.5

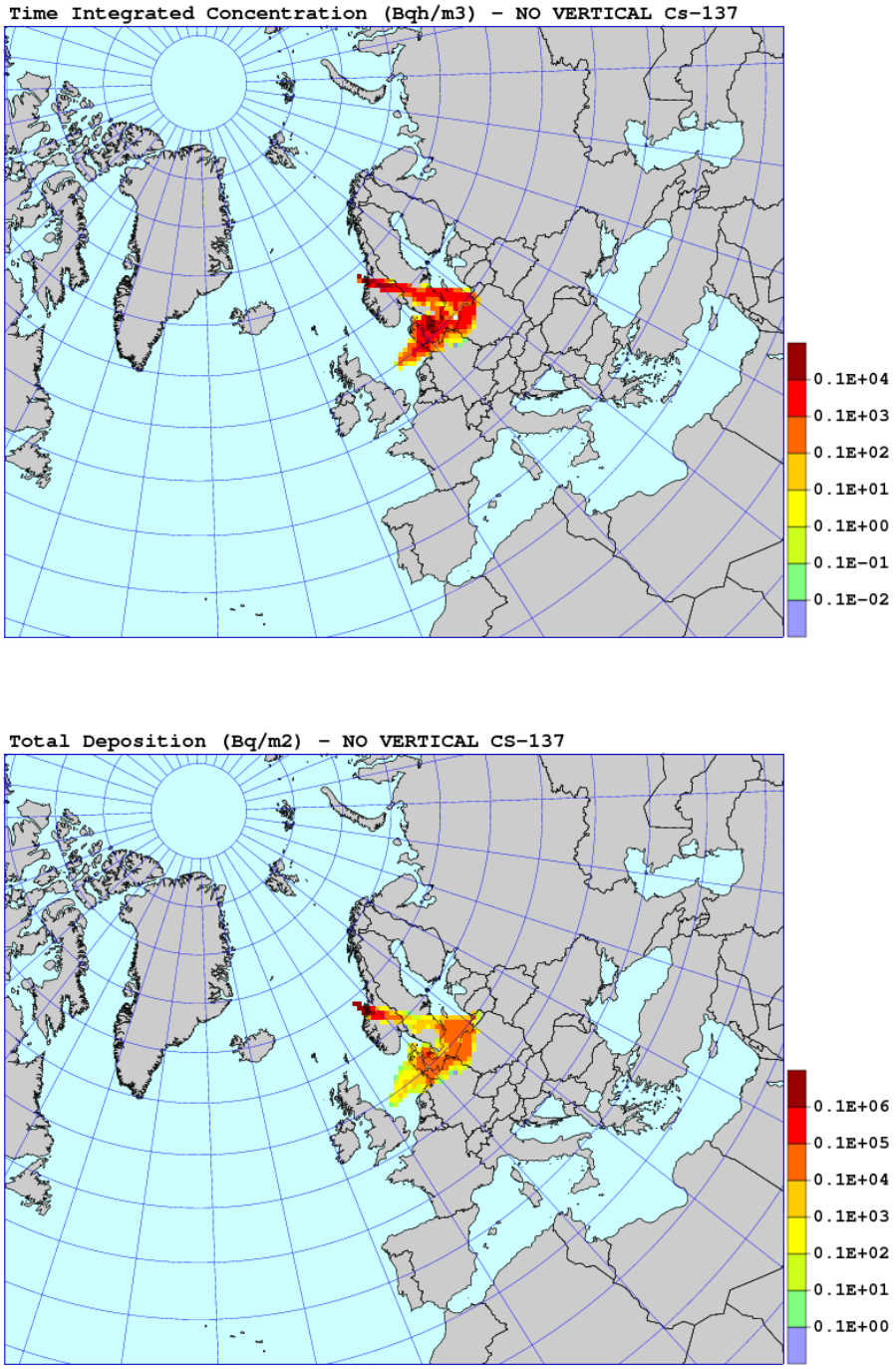

Figure 58: Results of the sensitivity run without vertical diffusion. Maps of time integrated concentration and deposition of Cs-137, 48 hours from the accident start.

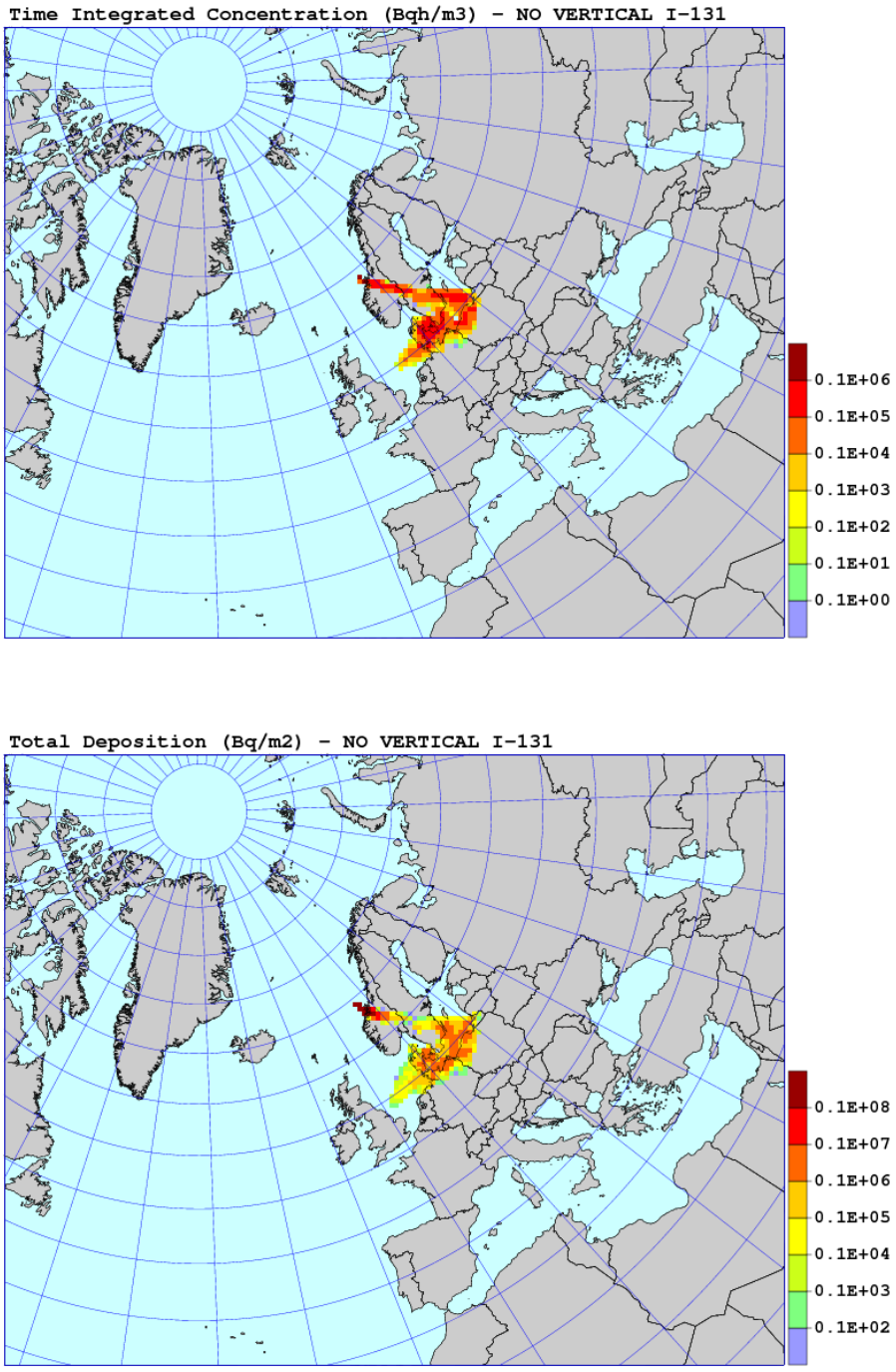

Figure 59: Results of the sensitivity run without vertical diffusion. Maps of time integrated concentration and deposition of I-131, 48 hours from the accident start.

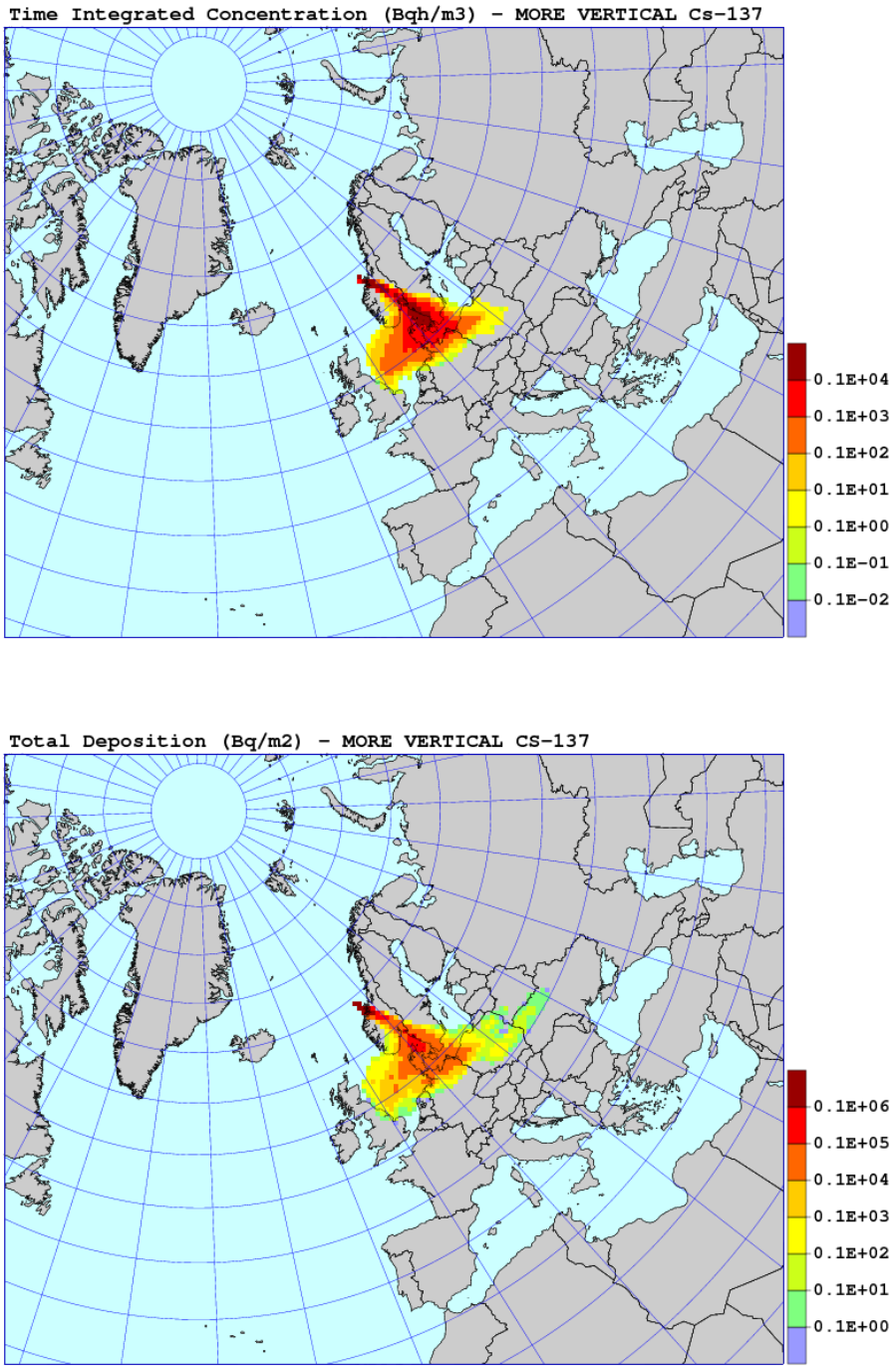

Figure 60: Results of the sensitivity run with increased vertical diffusion. Maps of time integrated concentration and deposition of Cs-137, 48 hours from the accident start.

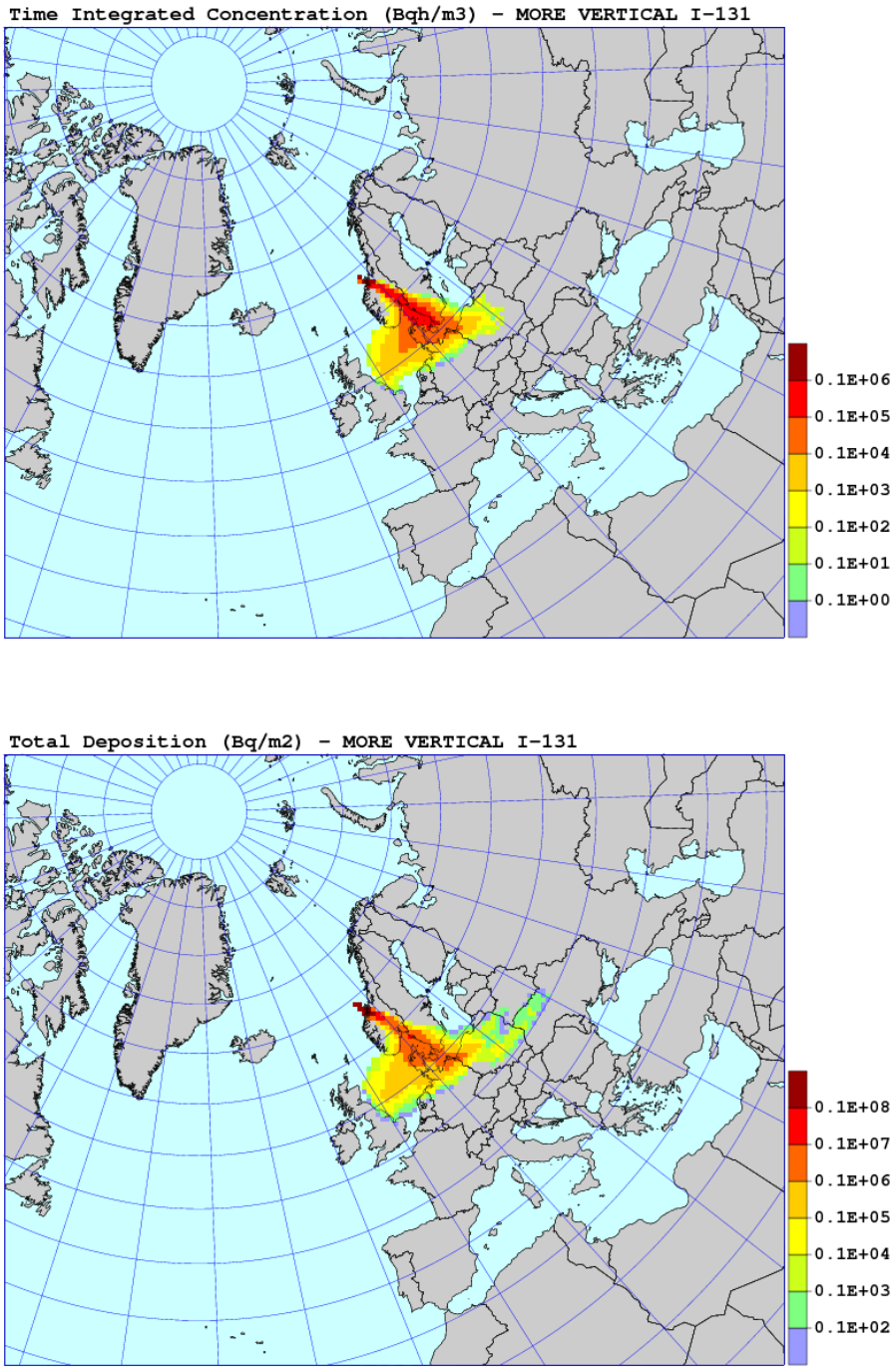

Figure 61: Results of the sensitivity run with increased vertical diffusion. Maps of time integrated concentration and deposition of I-131, 48 hours from the accident start.

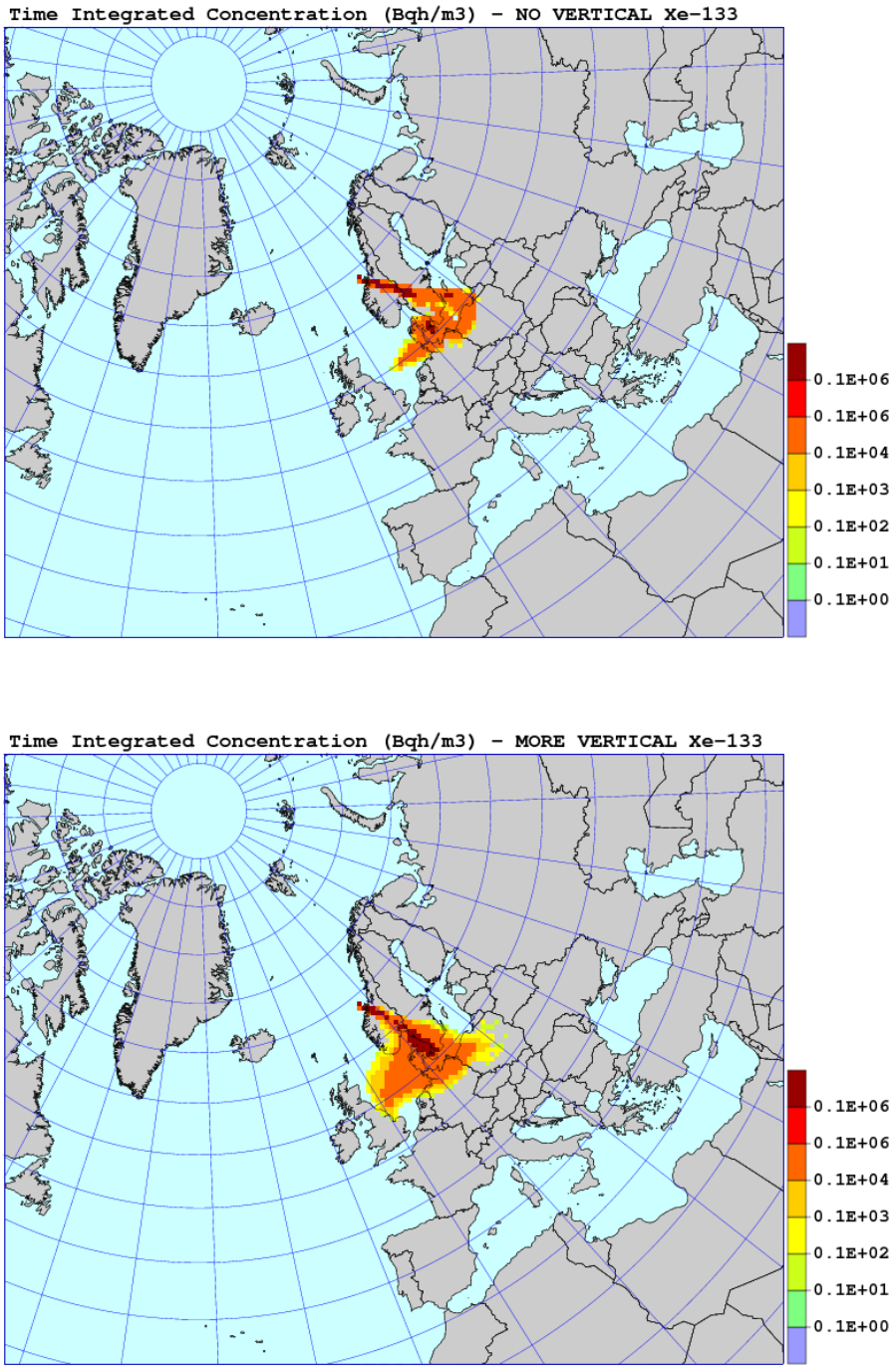

Figure 62: Results of the sensitivity run without vertical diffusion (above) and increased vertical diffusion (below). Maps of time integrated concentration and deposition of Xe-133, 48 hours from the accident start.

5.14. Sensitivity to number of model particles

The number of model particles is not related to any particular physical process, but it decides about the accuracy of the approximation of the model equations. The accuracy of the model results increases with the number of model particles and it should be as large as possible. Unfortunately, this number is limited for technical reasons, mainly computational time and available CPU memory. For the model applications, it is important to know how the model results are changing with the number of model particles used in the simulation. In the standard model run, the number of model particles was set to 2000 for each model time step. It means that total number of the model particles released was 240 000. In the sensitivity tests, we have tried both lower and higher number of model particles as shown in Table 37. The number of model particles used in the standard run is highlighted in Table 37.

Table 37: The number of model particles used in the sensitivity tests. The number of model particles in the standard run is highlighted.

Per time step	500	1000	**2000**	4000	8000
Total	60 000	120 000	**240 000**	480 000	960 000

The results of sensitivity runs with different number of the model particles are shown in Fig. (63) - (66) - for Cs-137, in Fig. (67) - (70) - for I-131, and in Fig. (71) - (72) - for Xe-133. For all numbers of model particles tested and for all radionuclides selected, the maps of time integrated concentration and deposition look very similar to those form the standard run. In some cases, only very small differences can noticed at the edge of the plume, where the concentration and deposition values are small. However, these small differences can be neglected in practical applications of the SNAP model.

The results of the SNAP runs, for different number of model particles are summarised in Table 38 - in the model grid square where the city of Oslo is located. The results are shown 48 hours after the release start. The most significant differences between the test run and the standard run for time integrated concentration can be noticed in the run with 500 particles per time step - for Cs-137 and I-131, and in the run with 200 particles in case of Xe-133. Calculated deposition in the Oslo grid is not so sensitive to the number of model particles and differences between the test runs and the standard run are much smaller compared to time integrated concentration.

Sensitivity measures for the SNAP runs with different number of model particles are shown in Table 56. Global sensitivity measures (SDF and SCF) are relatively small, especially for SDF measure and the test runs with the number of model particles lower than standard. For CS-137 and I-131, the global deposition measures are higher than global concentration measures for the number of model particles higher than standard. For Xe-131, the SCF measure remains on the same level for all test model runs and is very small.

Table 38: Time integrated concentrations, 48 hours after the start of release, in the model grid cell where the city of Oslo is located. Results of the model runs with different number of model particles (N). Values for the standard run are highlighted. The unit for time integrated concentration is Bq h m^{-3} and the unit for deposition is Bq m^{-2}.

N	Cs-137	I-131	Xe-133
Time Integrated Concentration			
200	0.35E+01	0.12E+03	0.41E+03
500	0.52E+01	0.18E+03	0.83E+02
2000	**0.27E+01**	**0.99E+02**	**0.15E+03**
4000	0.30E+01	0.12E+03	0.20E+03
8000	0.27E+01	0.99E+02	0.21E+03
Deposition			
200	0.87E+02	0.11E+05	0.0
500	0.11E+03	0.14E+05	0.0
2000	**0.10E+03**	**0.13E+05**	0.0
4000	0.99E+02	0.13E+05	0.0
8000	0.10E+03	0.13E+05	0.0

Table 39: Sensitivity measures as defined in Eqs. (29) - (32), for the SNAP runs with different number of model particles (N).

N	SDF	SCF	SDG	SCG
Cs-137				
200	2.7	12.6	-16.4	27.7
500	2.4	12.0	10.2	91.5
4000	57.2	11.7	-4.8	10.9
8000	73.2	19.9	-1.5	-2.5
I-131				
200	3.3	16.0	-19.7	26.3
500	2.7	15.1	5.7	80.9
4000	50.9	15.4	-2.6	17.5
8000	65.0	25.9	-0.1	0.5
Xe-133				
200	0.0	13.4	0.0	165.7
500	0.0	10.8	0.0	-45.8
4000	0.0	17.9	0.0	33.8
8000	0.0	6.0	0.0	38.2

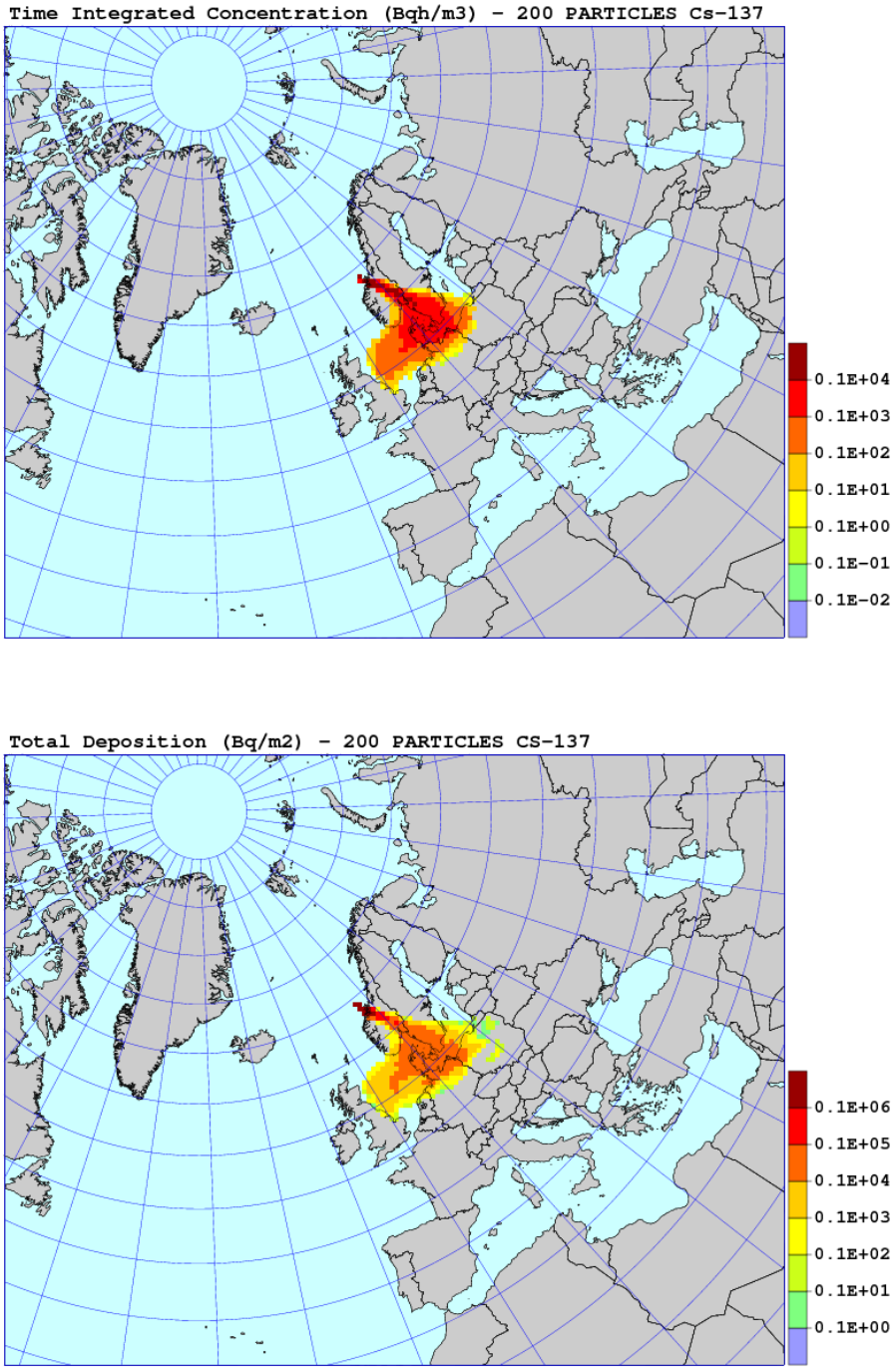

Figure 63: Results of the sensitivity run with 200 model particles. Maps of time integrated concentration and deposition of Cs-137, 48 hours from the accident start.

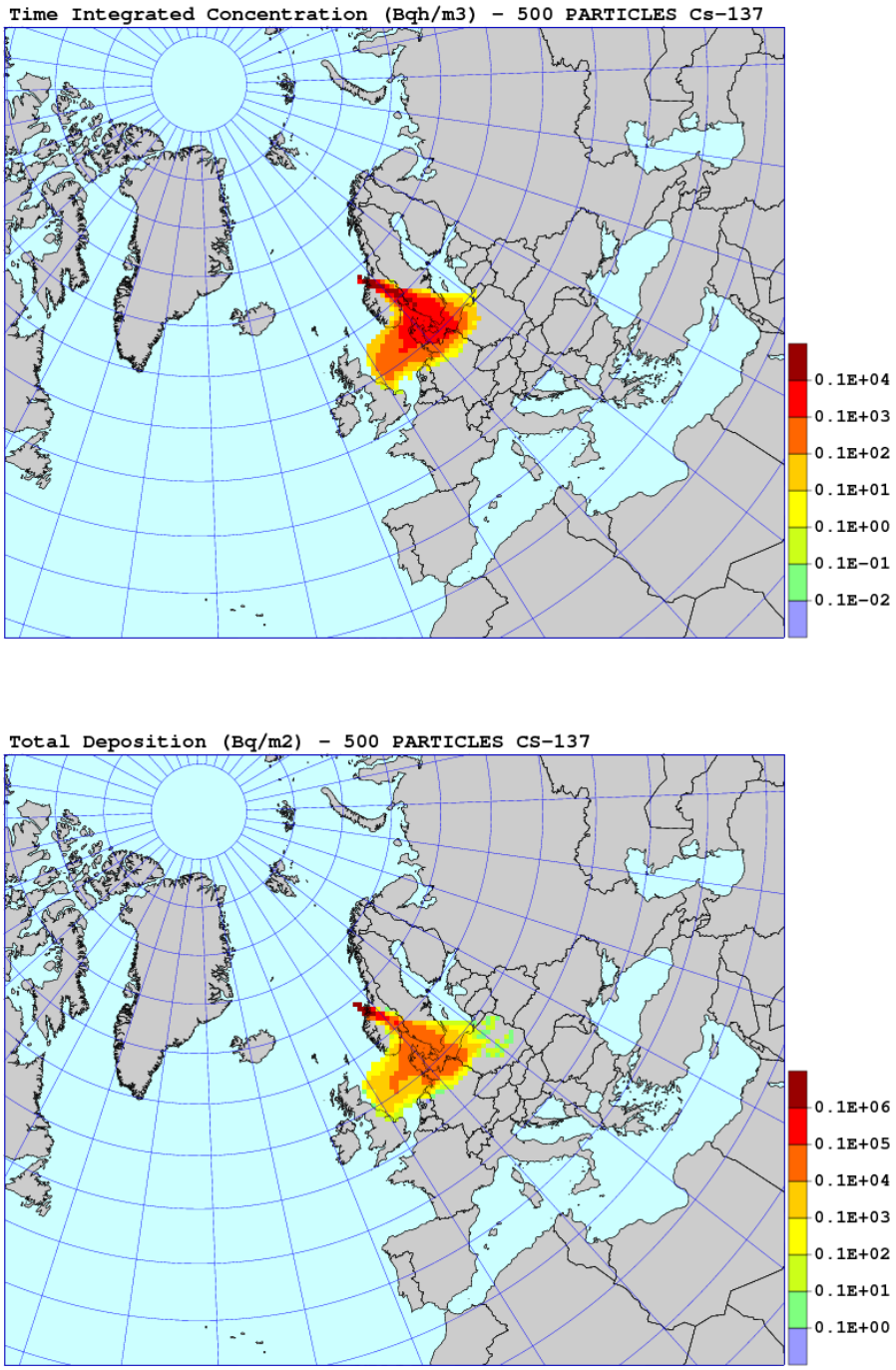

Figure 64: Results of the sensitivity run with 500 model particles. Maps of time integrated concentration and deposition of Cs-137, 48 hours from the accident start.

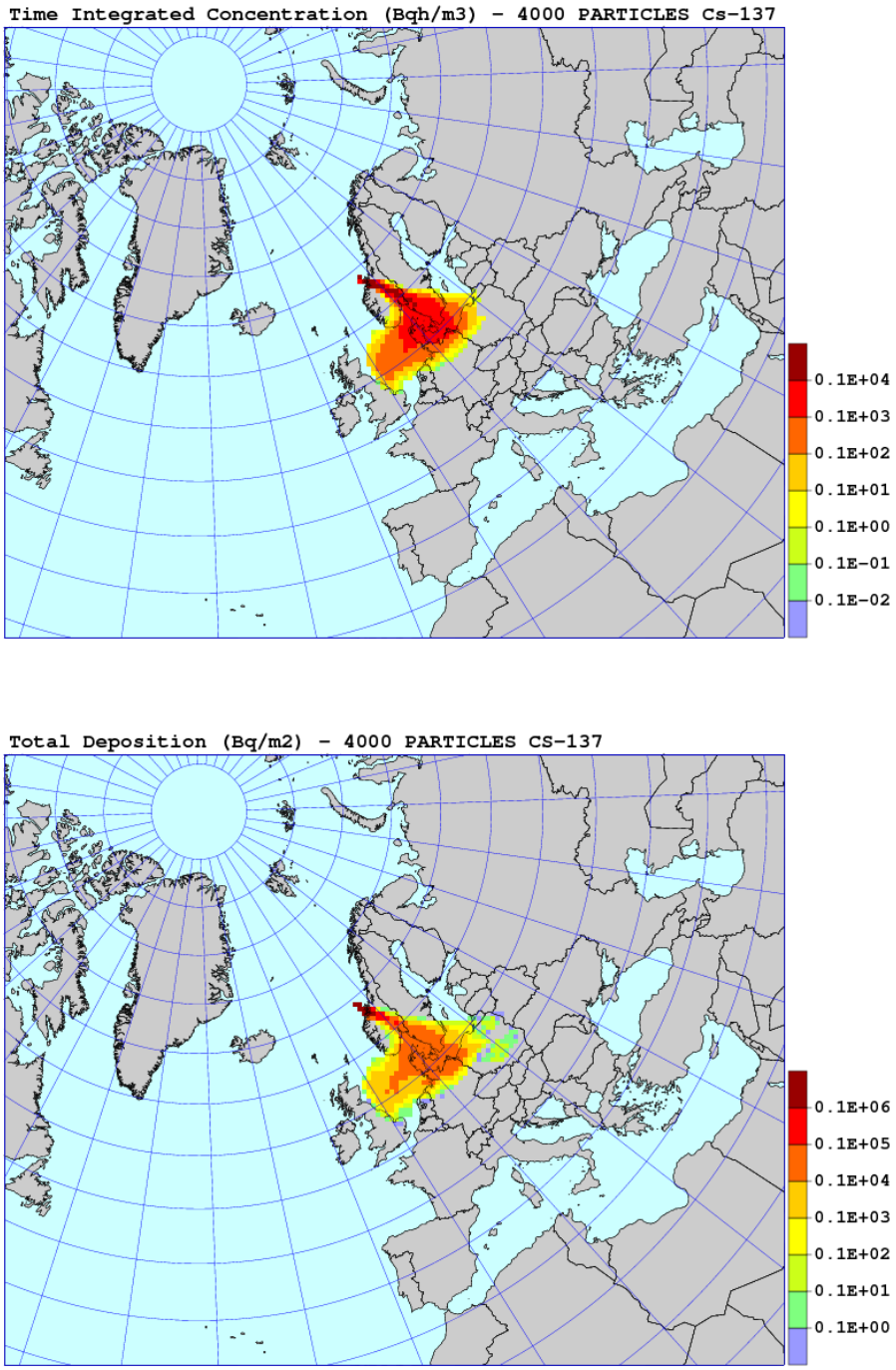

Figure 65: Results of the sensitivity run with 4000 model particles. Maps of time integrated concentration and deposition of Cs-137, 48 hours from the accident start.

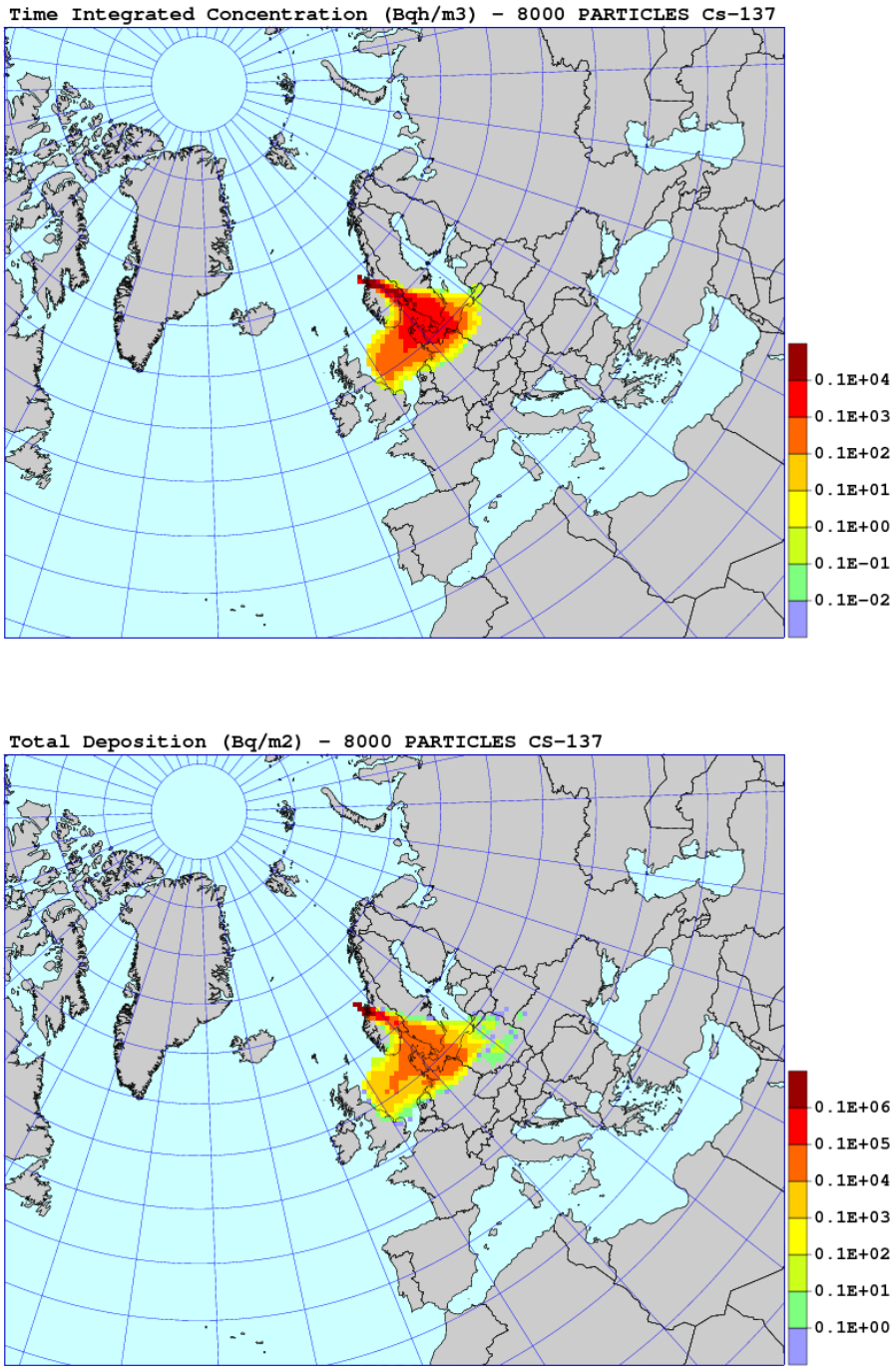

Figure 66: Results of the sensitivity run with 8000 model particles. Maps of time integrated concentration and deposition of Cs-137, 48 hours from the accident start.

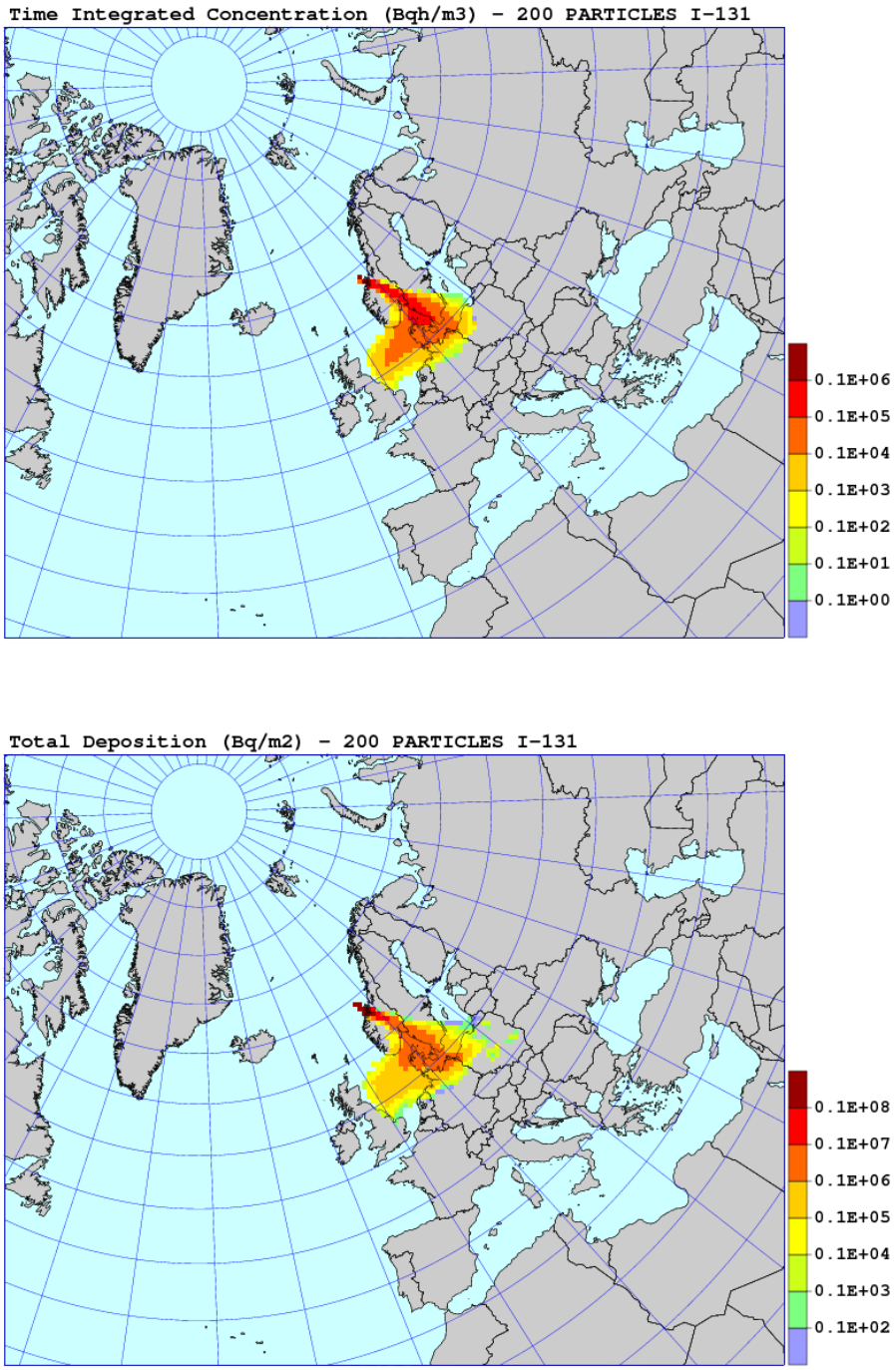

Figure 67: Results of the sensitivity run with 200 model particles. Maps of time integrated concentration and deposition of I-131, 48 hours from the accident start.

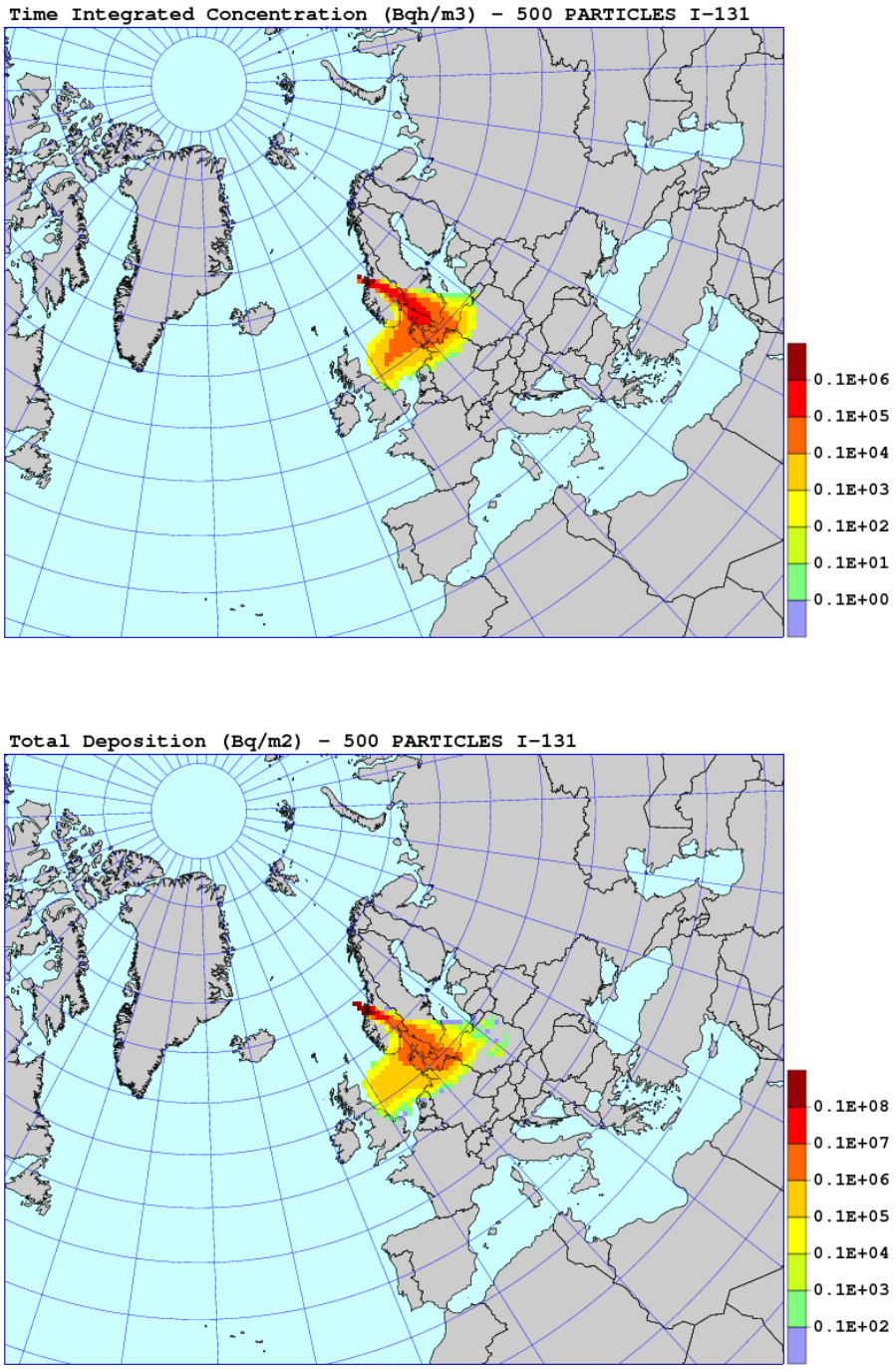

Figure 68: Results of the sensitivity run with 500 model particles. Maps of time integrated concentration and deposition of I-131, 48 hours from the accident start.

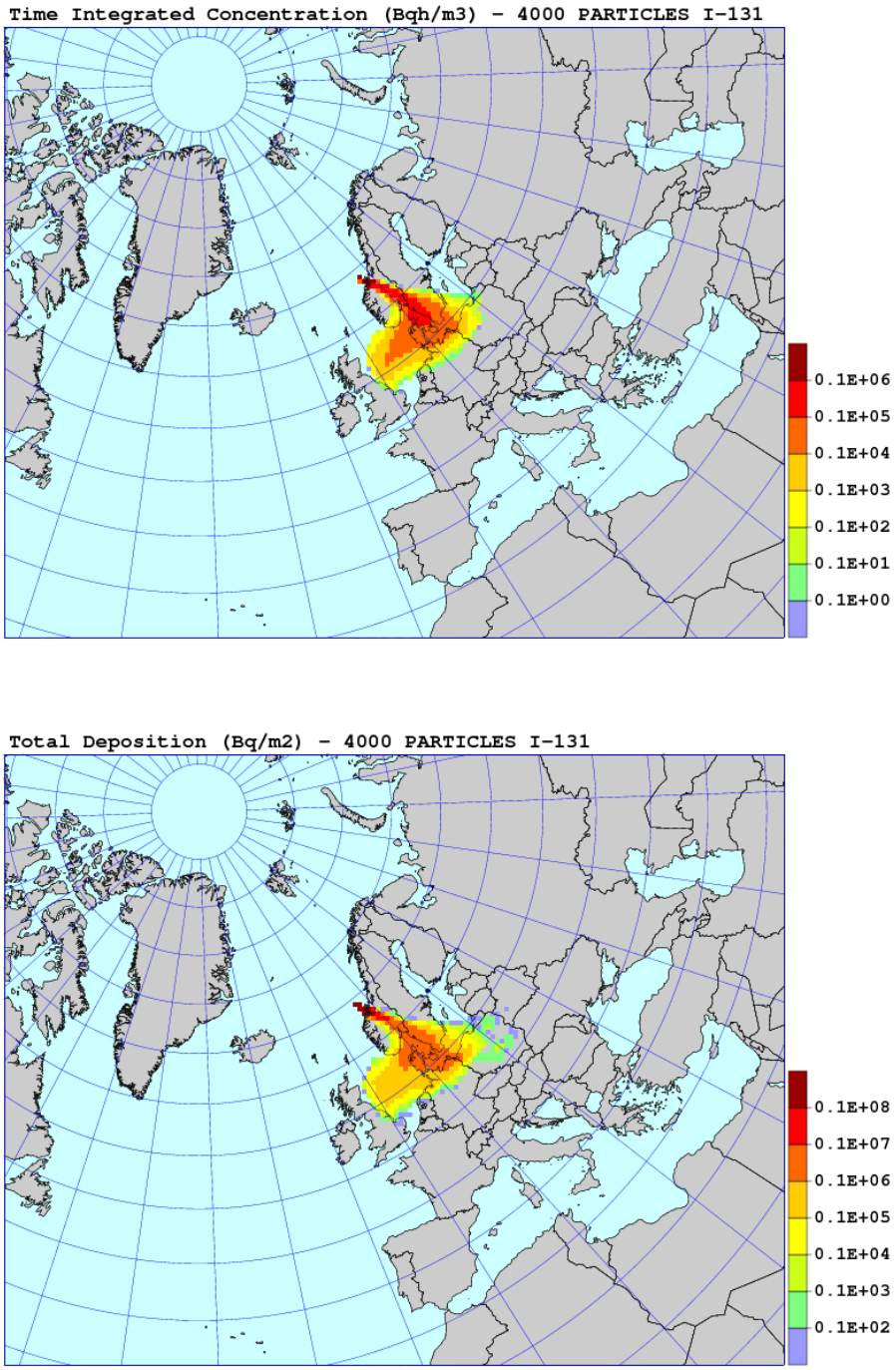

Figure 69: Results of the sensitivity run with 4000 model particles. Maps of time integrated concentration and deposition of I-131, 48 hours from the accident start.

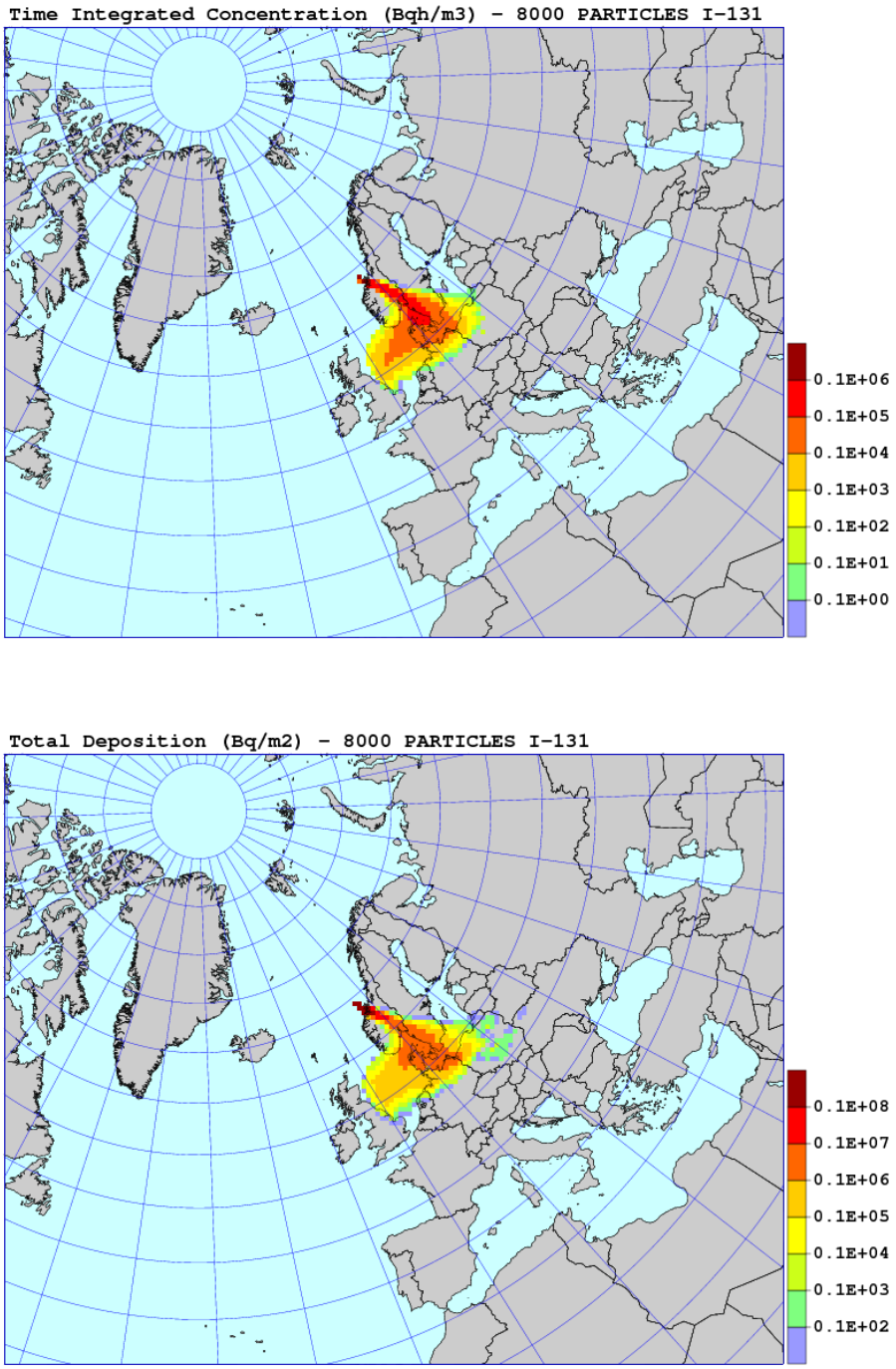

Figure 70: Results of the sensitivity run with 8000 model particles. Maps of time integrated concentration and deposition of I-131, 48 hours from the accident start.

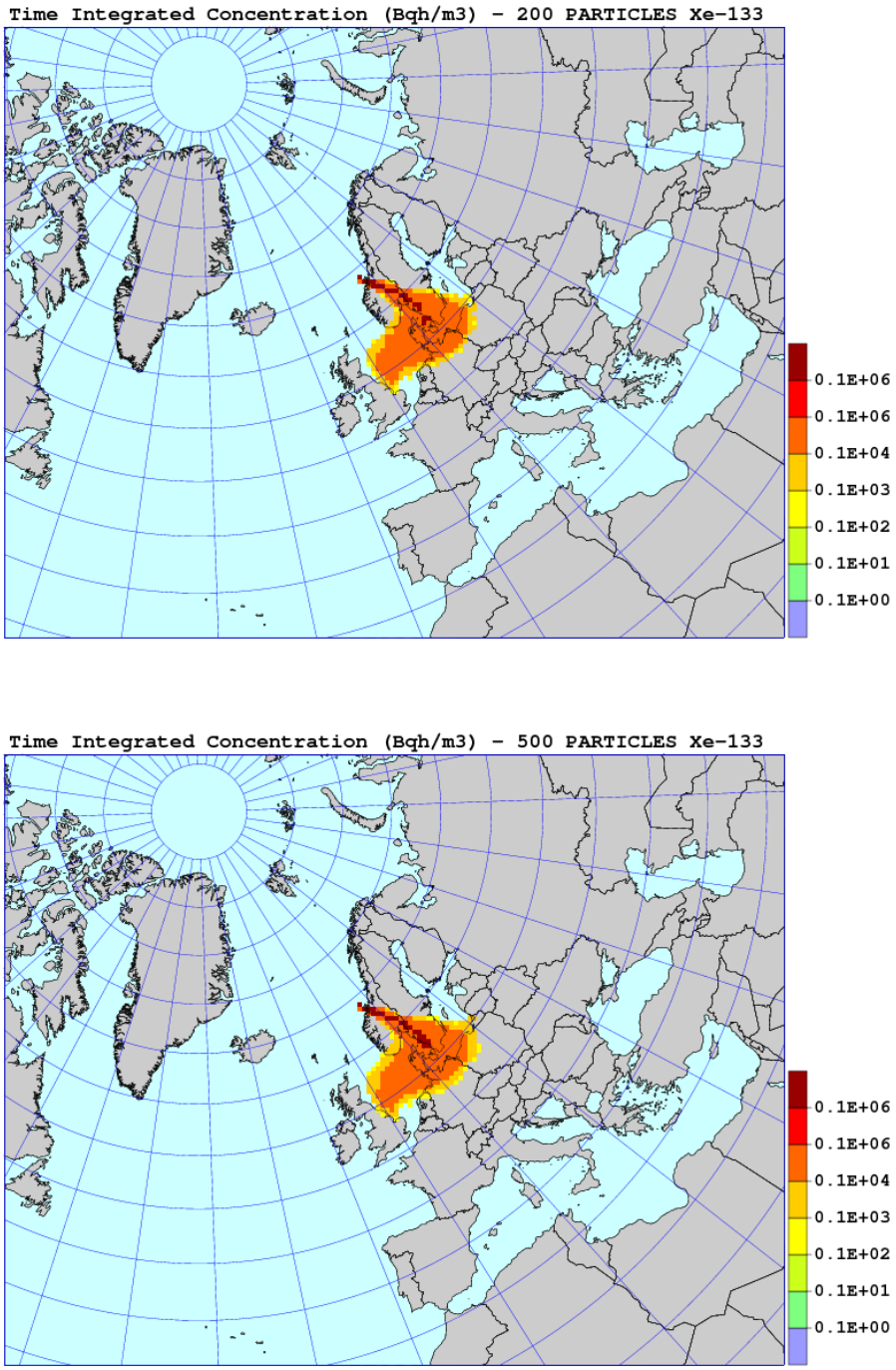

Figure 71: Results of the sensitivity run with 200 (above) and 500 (below) model particles. Maps of time integrated concentration of Xe-133, 48 hours from the accident start.

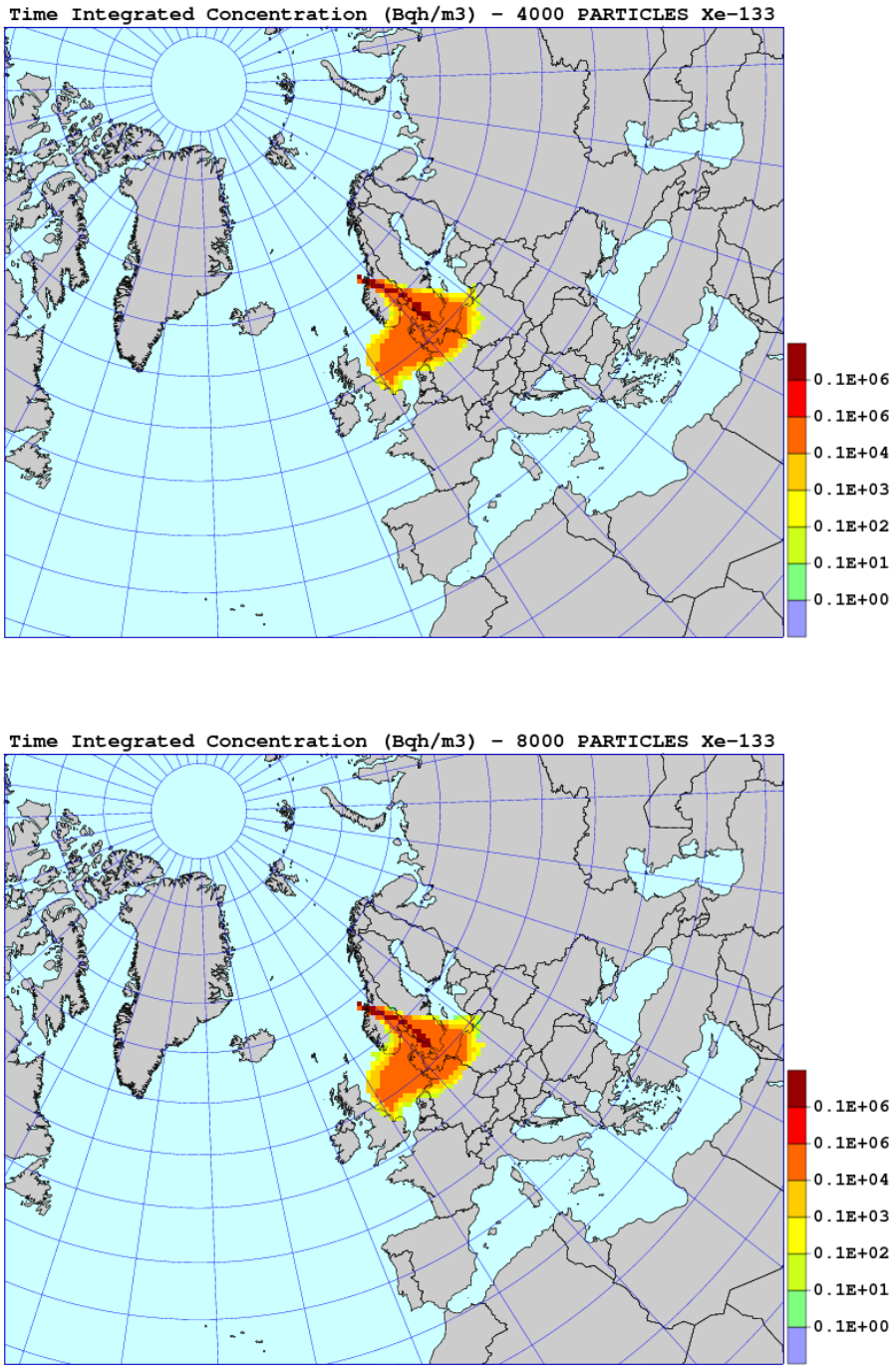

Figure 72: Results of the sensitivity run with 4000 (above) and 8000 (below) model particles. Maps of time integrated concentration of Xe-133, 48 hours from the accident start.

5.15. Sensitivity ranking for nuclear accident

Sensitivity ranking for nuclear accident is based on the comparison of sensitivity measures, as well as on visual comparison of the maps for time integrated concentration and deposition in relation to the standard run. The sensitivity measures for selected test runs are given in Table 57. In this Table, we focus our attention on the global sensitivity measures: SDF - for total deposition and SCF - for time integrated concentration.

The results of sensitivity tests are similar for Cs-137 and I-131, but quite different for Xe-133, because of the lack of deposition processes. For both, Cs-137 and I-131 isotopes, the calculated deposition and time integrated concentration is the most sensitive to wet deposition. Diffusion is the second in the sensitivity ranking, with horisontal diffusion being more important in case of Cs-137 and vertical diffusion more important in case of I-131. Next in the ranking is dry deposition for both isotopes.

For Cs-137, model is not sensitive at all to radioactive decay because of the long half-life time. Also for I-131, the model is relatively not sensitive to radioactive decay. For Xe-133, model is more sensitive to radioactive decay, because of much shorter half-life time.

For both Cs-137 and I-131, the sensitivity of calculated time integrated concentration to the number of model particles is relatively low. For calculated deposition, sensitivity to the number of model particles is slightly higher, on the same level as to dry deposition for Cs-137, but 50% lower for I-131.

For Xe-133, only SCF sensitivity measure can be considered, because there is no wet and dry deposition. In this case, calculated time integrated concentration is the most sensitive to vertical diffusion and radioactive decay, followed by horisonatal diffusion and the number of model particles.

The maps of time integrated concentration and deposition from the test runs have been compared with corresponding maps from the standard run. In general, the differences between the test runs and the standard run are small in case of Cs-137 and I-131, however, with some exceptions. Namely, the differences are large in case of the run without vertical diffusion in both, time integrated concentration and deposition maps. However smaller, the differences also can be noticed in the test runs without dry deposition, without wet deposition and with increased diffusion, but only in the deposition fields. In case of Xe-133, large differences are present in the map of time integrated concentration from the run without vertical diffusion and slightly lower in the map from the run without radioactive decay.

No differences, or only very small differences, between the test runs and standard run can be noticed for the tests with different number of model particles used, for all radionuclides selected.

The sensitivity ranking for nuclear accident is similar for Cs-137 and I-131. The model is most sensitive wet deposition then diffusion and dry deposition. For Xe-133, model is mostly sensitive to vertical diffusion and then to radioactive decay and horisontal diffusion. The sensitivity to the number of model particles used is relatively low for all radionuclides.

Table 40: Comparison of sensitivity measures for Cs-137, for different sensitivity tests.

Run	SDF	SCF	SDG	SCG
Cs-137				
No dry dep.	58.4	77.1	-100.0	5.0
No wet dep.	545.2	234.5	68.8	126.4
No radioactive decay	0.1	0.0	0.0	0.0
No hor. diff.	122.2	11.5	11.0	-17.8
More hor. diff.	135.4	20.0	5.8	20.9
No ver. diff.	88.2	188.4	-100.0	-100.0
More ver. diff.	48.2	93.9	174.7	190.3
200 part.	2.7	12.6	-16.4	27.7
500 part.	2.4	12.0	10.2	91.5
4000 part.	57.2	11.7	-4.8	10.9
8000 part.	73.2	19.9	-1.5	-2.5
I-131				
No dry dep.	136.0	292.7	-100.0	18.9
No wet dep.	464.8	341.5	102.7	189.6
No radioactive decay	10.8	8.4	15.1	4.1
No hor. diff.	150.0	16.3	11.8	-13.6
More hor. diff.	139.2	26.0	7.5	27.0
No ver. diff.	96.0	273.1	-100.0	-100.0
More ver. diff.	46.0	90.7	172.5	202.5
200 part.	3.3	16.0	-19.7	26.3
500 part.	2.7	15.1	5.7	80.9
4000 part.	50.9	15.4	-2.6	17.5
8000 part.	65.0	25.9	-0.1	0.5
Xe-133				
No dry dep.	0.0	0.0	0.0	0.0
No wet dep.	0.0	0.0	0.0	0.0
No radioactive decay	0.0	26.0	0.0	79.4
No hor. diff.	0.0	10.2	0.0	44.4
More hor. diff.	0.0	14.6	0.0	104.0
No ver. diff.	0.0	204.0	0.0	-100.0
More ver. diff.	0.0	102.5	0.0	291.5
200 part.	0.0	13.4	0.0	165.7
500 part.	0.0	10.8	0.0	-45.8
4000 part.	0.0	17.9	0.0	33.8
8000 part.	0.0	6.0	0.0	38.2

6. Sensitivity Tests for Nuclear Explosion

There are at least three important differences between nuclear accident and nuclear explosion from the modelling point of view. First, the radioactive debris from the nuclear explosion is emitted much higher into the atmosphere. Second, the release time is very short and for modelling purpose it can be set to zero in case of nuclear explosion and third, the size of particles emitted in case of nuclear explosion is significantly larger than in case of nuclear accident. Therefore the sensitivity tests for nuclear accident and explosion were performed and described separately.

6.1. Standard run for nuclear explosion

As a basic case for the standard run we assumed a nuclear explosion at the same place as the location of the ship described in the previous Chapter. The main reason for such a choice is availability of the meteorological data for the model runs in the sensitivity tests. In addition, it is interesting to see the differences in atmospheric dispersion from accident and nuclear explosion taking place in the same location and time.

6.1.1. Source term

The source term for nuclear explosion is very much dependent on the explosive yield. Three different explosive yields were used in the sensitivity tests: 1 kt, 10 kt and 100 kt. The explosive yield of 1 kt is typical for improvised nuclear device which might be used in potential terrorist attack. The explosive yield of 10 kt is typical for most of the military bombs and the explosive yield of 100 kt represents the upper limit of the explosion in the sensitivity tests. The initial shape of the radioactive cloud was in the form of cylinder with parameters dependent of the explosive yield. These parameters are given in in Table 41, together with the activities which differ one order of magnitude between the chosen explosive yields.

Table 41: Parameters for the cylinder representing the radioactive cloud shortly after the explosion in the standard run for sensitivity tests. Corresponding activities for explosive yield classes are also given.

Explosive yield (kt)	Base of cylinder (km)	Top of cylinder (km)	Radius (km)	Activity (Bq)
1	0.50	1.50	0.6	2×10^{19}
10	2.25	4.75	1.4	2×10^{20}
100	5.95	12.05	3.2	2×10^{21}

There are large differences in the cylinder parameters and especially in the cylinder top for different explosive yields in Table 41. For the explosive yield of 1 kt, the initial activity is released mainly in the mixing layer, at least for most of the meteorological situations. For the explosive yield of 10 kt, the major part of initial activity is released just above the mixing

layer in the troposphere. The initial radioactive cloud after 100 kt explosion is mostly located in the upper part of the troposphere or slightly above. Also the radius of the cylinder changes significantly (more than five times) between explosions with different yield.

Large differences in vertical location of the initial cloud for selected explosive yields can result in significant changes of direction and range of the transport of radioactive particles. This is mainly caused by different wind directions and magnitudes at different vertical layers in the SNAP model [40]. In addition, radioactive particles from relatively small explosion (1 kt) can reach the ground much faster than the particles from relatively large explosion (100 kt). This difference is more significant for the particles of small size, because large particles are mainly removed from the air by gravitational settling, not far away from the place of detonation.

6.1.2. Results of the standard run

The source term described in the previous section was used to calculate time integrated concentrations and total deposition for the standard run. The results for 1 kt, 10 kt and 100 kt nuclear explosions are presented in Fig. 73, 74 and 75, respectively, in the form of time integrated concentration and deposition maps, 48 hours after the detonation.

As expected, time integrated concentrations and deposition calculated in the standard SNAP run are significantly different in spatial patterns for selected explosive yields. Both, the range of the transport and the area affected by radioactive cloud are significantly increasing with higher explosive yields. Also direction of the transport differs as a result of the increased range for higher explosive yield. The differences between selected explosive yields are more significant for deposition maps than for the maps of time integrated concentration.

Time integrated concentrations and deposition were also calculated in the model grid square where the city of Oslo is located. The results are presented in Table 42.

Table 42: Time integrated concentrations and deposition, 48 hours after the start of release, in the model grid cell where the city of Oslo is located. Results of the standard run for selected explosive yields.

Explosive yield (kt)	Time integrated concentration (Bq h m^{-3})	Total deposition (Bq m^{-2})
1	0.41E+06	0.81E+07
10	0.16E+07	0.28E+09
100	0.20E+07	0.91E+09

Both, time integrated concentrations and deposition in the Oslo grid increase with increasing explosive yield. The differences between 1kt and 100 kt explosions in Table 42 are large, one order of magnitude for time integrated concentrations and two orders of magnitude for the deposition.

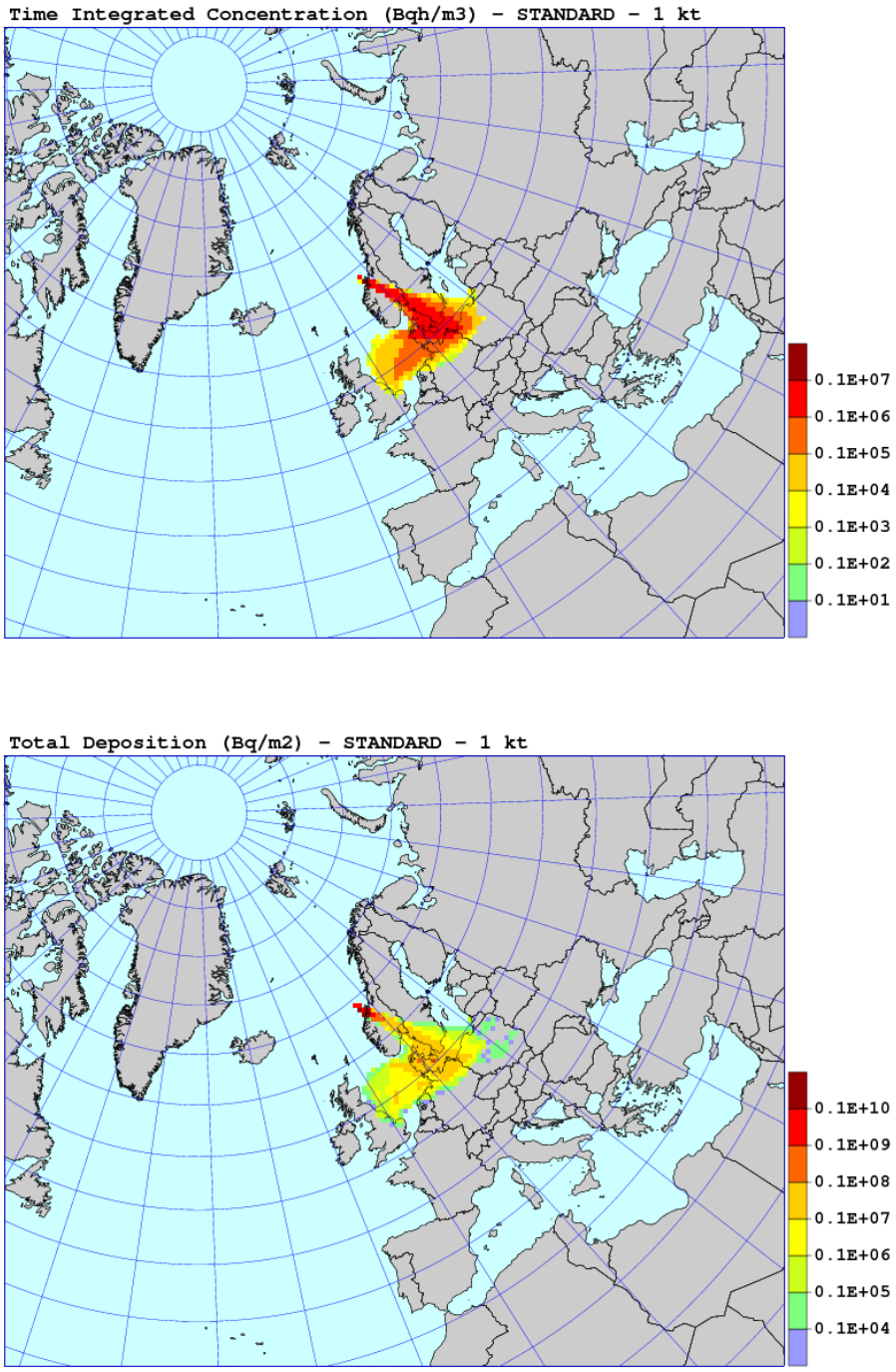

Figure 73: The results of the standard SNAP run for 1 kt nuclear explosion, 48 hours after the detonation. Time integrated concentrations in Bq h m^{-3} above and total deposition in Bq m^{-3} in the bottom.

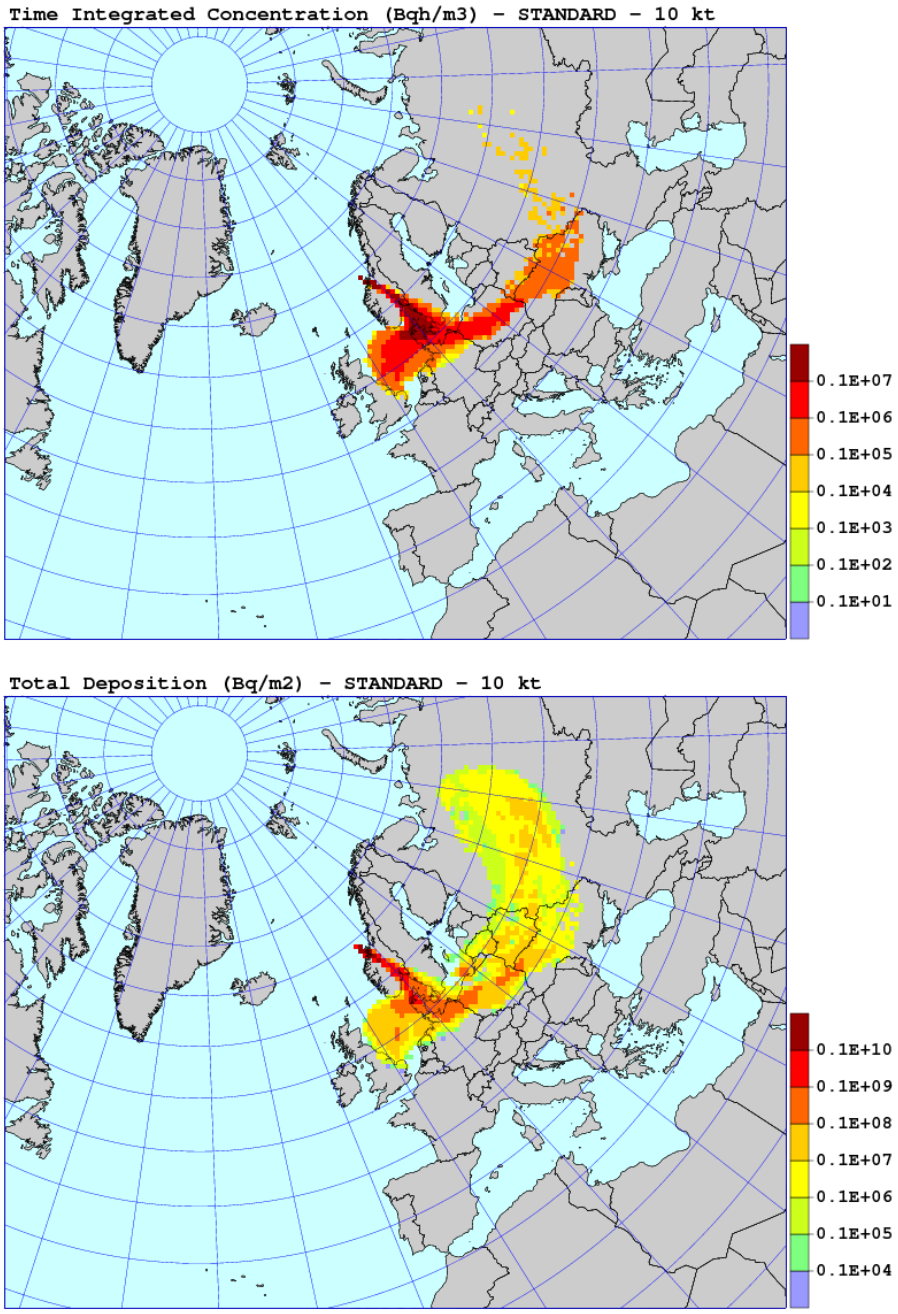

Figure 74: The results of the standard SNAP run for 10 kt nuclear explosion, 48 hours after the detonation. Time integrated concentrations in Bq h m^{-3} above and total deposition in Bq m^{-3} in the bottom.

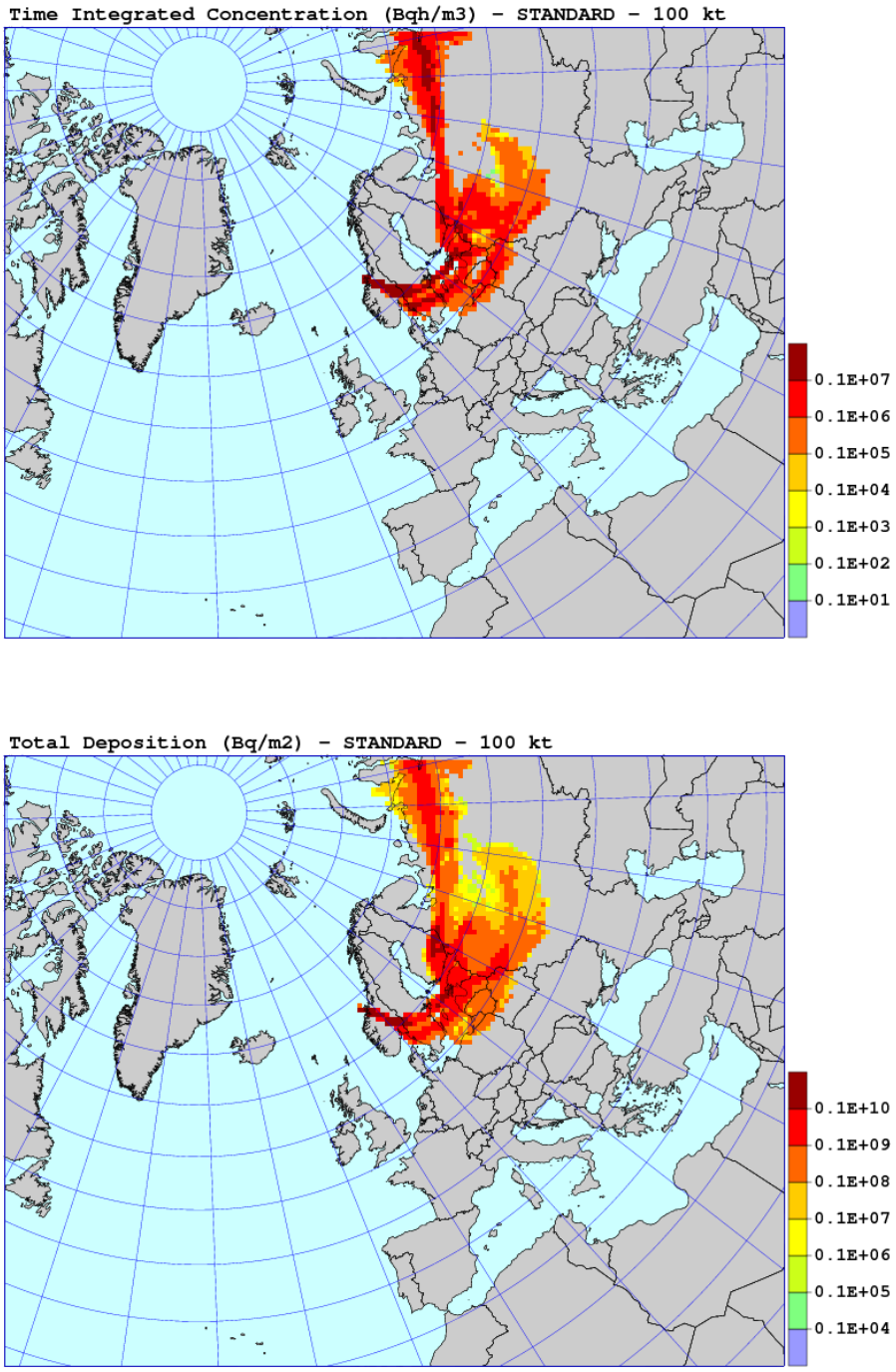

Figure 75: The results of the standard SNAP run for 100 kt nuclear explosion, 48 hours after the detonation. Time integrated concentrations in Bq h m^{-3} above and total deposition in Bq m^{-3} in the bottom.

6.2. Sensitivity to dry deposition

Sensitivity to dry deposition was tested in the model run without dry deposition process. The maps of time integrated concentration and total deposition for 1 kt, 10 kt and 100 kt explosion are shown in Fig. 76, 77 and 78, respectively.

There are visible differences between the standard and test runs, both for time integrated concentration and deposition. These differences are small in time integrated concentration fields, compared to deposition fields. The values of time integrated concentrations are slightly higher in the test runs, but there is almost no difference in the spatial pattern. The differences in the deposition fields are much larger compared to time integrated concentrations, both in magnitude and spatial distribution. They are mainly present because of irregular pattern of the precipitation field and effectiveness of wet deposition.

Time integrated concentrations and deposition in the model grid cell where the city of Oslo is located are shown in Table 43 for the model run without dry deposition. For time integrated concentration, the difference between the standard run and test run is mostly visible for 1 kt explosion. The relatively low transport and greater exposure for precipitation is the main reason for this.

Table 43: Time integrated concentrations and deposition, 48 hours after the start of release, in the model grid cell where the city of Oslo is located. Results of the model run without dry deposition.

Explosive yield (kt)	Time integrated concentration (Bq h m^{-3})	Total deposition (Bq m^{-2})
1	0.43E+06	0.00E+00
10	0.16E+07	0.00E+00
100	0.20E+07	0.00E+00

Sensitivity measures for the run without dry deposition are shown in Table 44. The absolute values of measures for deposition (SDF, SDG) are much higher than measures for time integrated concentration (SDF, SDG). The global measure for deposition SDF is decreasing with increasing explosive yield. Again, the reason for it is a low vertical location of the initial plume for 1 kt explosion, which is getting higher with the increasing explosive yield.

Table 44: Sensitivity measures as defined in Eqs. (29) - (32), for the run without dry deposition.

Explosive yield (kt)	SDF	SCF	SDG	SCG
1	289.3	15.3	-100.0	4.3
10	173.4	29.2	-100.0	3.1
100	120.4	22.1	-100.0	0.0

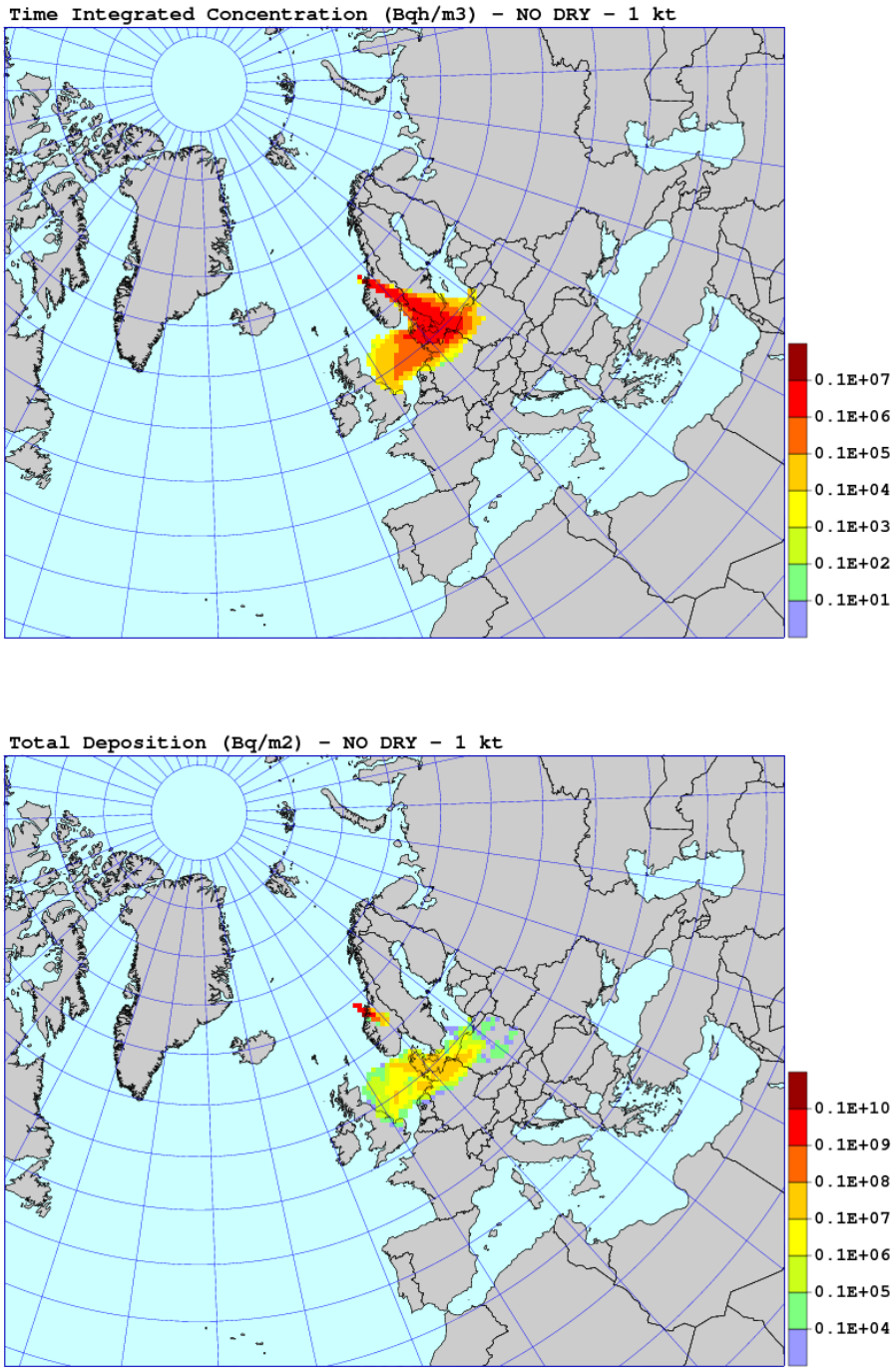

Figure 76: The results of the SNAP run without dry deposition for 1 kt nuclear explosion, 48 hours after the detonation. Time integrated concentrations in Bq h m^{-3} above and total deposition in Bq m^{-3} in the bottom.

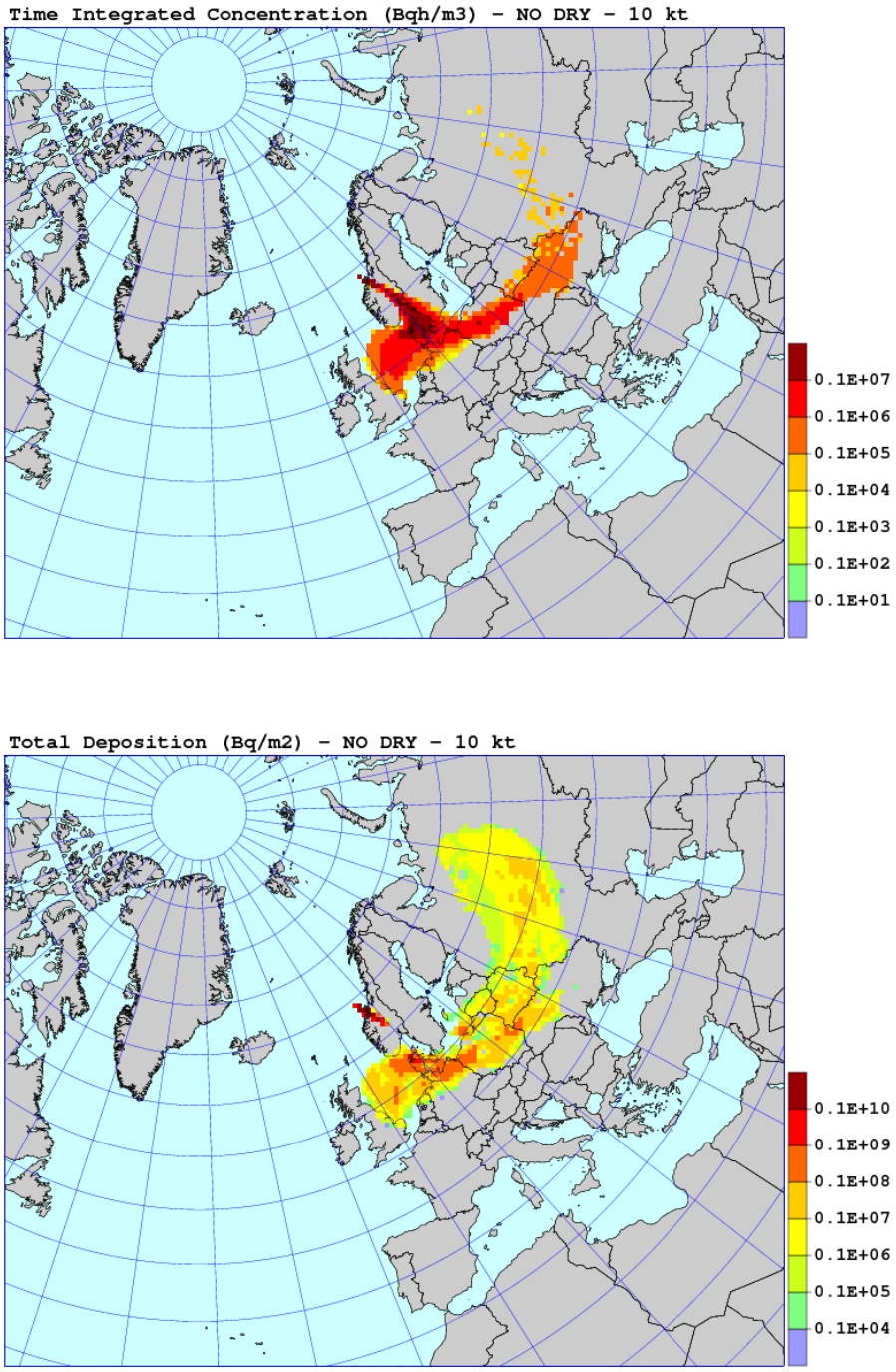

Figure 77: The results of the SNAP run without dry deposition for 10 kt nuclear explosion, 48 hours after the detonation. Time integrated concentrations in Bq h m^{-3} above and total deposition in Bq m^{-3} in the bottom.

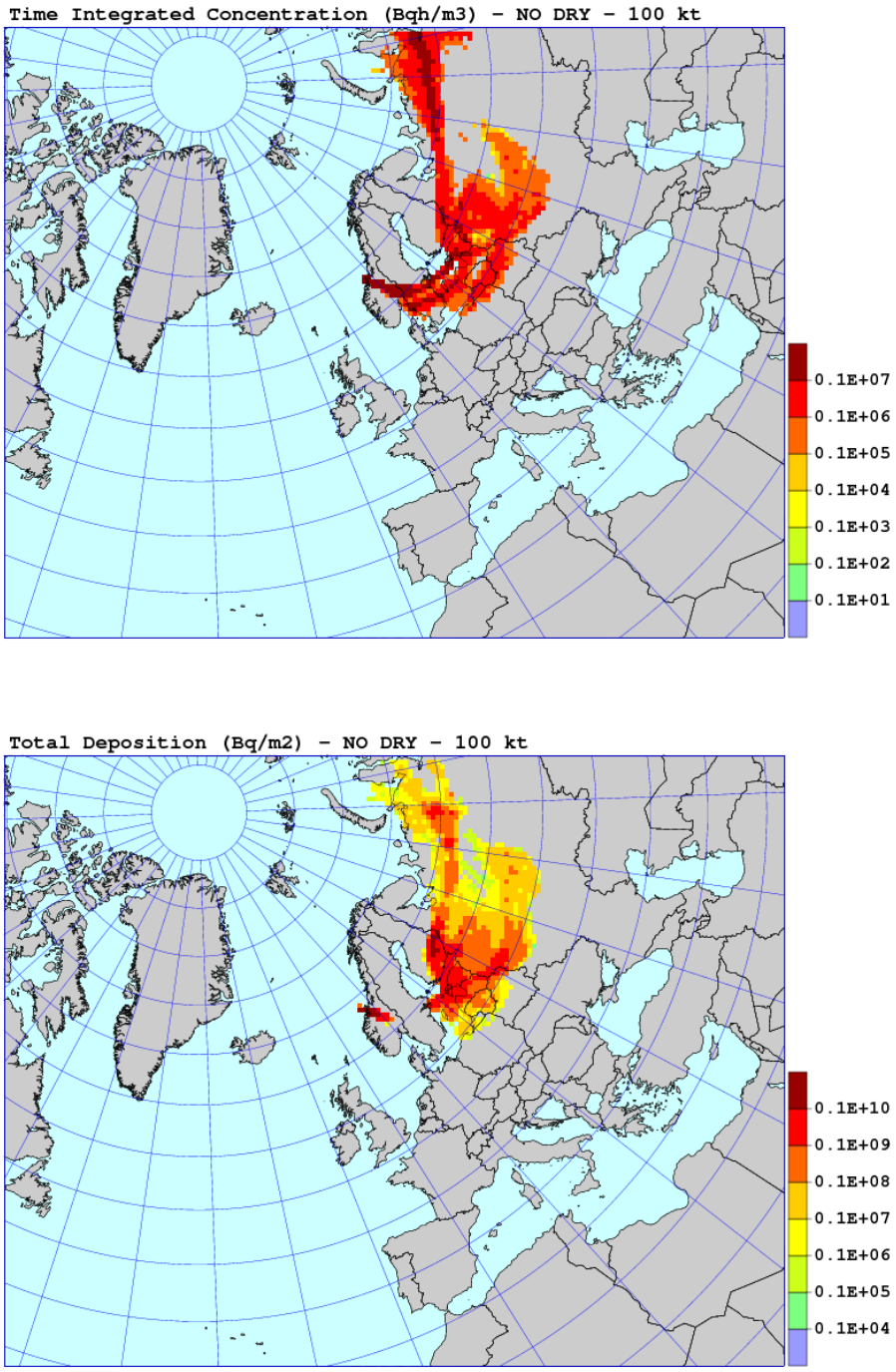

Figure 78: The results of the SNAP run without dry deposition for 100 kt nuclear explosion, 48 hours after the detonation. Time integrated concentrations in Bq h m^{-3} above and total deposition in Bq m^{-3} in the bottom.

6.3. Sensitivity to gravitational settling

Gravitational settling is an important and effective process responsible for removal of large particles from the air. In addition, gravitational settling contributes to dry deposition and gravitational settling velocity is also present in Eq. 13, used for calculating dry deposition velocity in the model. Model sensitivity to gravitational settling was tested in two runs. In the first run, gravitational settling velocity was completely neglected and switched off. In the second run, constant values of gravitational settling velocities for each particle class (as specified in Table 3) were replaced by calculating gravitational settling velocity for each model particle and at each model time step (on-line).

The results of the runs without gravity process, as maps of time integrated concentrations and deposition, are shown in Fig. 79-81. The lack of gravity keeps the large particles in air much longer and this is visible in the concentration and deposition fields for 1 kt and 10 kt explosions. Compared to standard run, both concentrations and deposition are a bit higher, in some distance away from the source. There is a dramatic difference in the maps for standard run and maps for the run without dry deposition in case of 100 kt explosion. Since there is no gravitational settling and the initial level of release is very high, all particles remain above the precipitation level for the entire period of the simulation and there is no wet deposition. Also the transport time is too short for the effective transition of model particles to the ground, so there is only a trace of dry and wet deposition at the end of the simulation - far away from the source.

The results of the runs with on-line calculated gravitational settling velocity for each model particle are shown, as maps of time integrated concentrations and deposition, in Fig. 82-84. The differences between the standard runs and sensitivity runs are rather small for all explosive yields, with slightly higher deposition for the runs with on-line calculated gravitational settling velocity. It justifies the use of fixed gravitational settling velocities in the operational applications.

The results of sensitivity tests, in the model grid cell where the city of Oslo is located are shown in Table 45. They include time integrated concentrations and deposition, 48 hours after the start of release. The differences between the standard runs and sensitivity runs are very much dependent on the explosive yield. For 1 kt explosion, both time integrated concentration and deposition in the run without dry deposition are much higher in the Oslo grid than those calculated from the standard run. The opposite relation takes place for 10 kt explosion. In this case, both time integrated concentration and deposition in the run without dry deposition are much lower in the Oslo grid than those calculated from the standard run. For 100 kt explosion, the Oslo grid is not affected at all by the radioactive cloud, because it is too high above when passing Oslo.

Comparison of the standard runs and sensitivity runs with on-line calculated gravitational settling velocity shows higher values of time integrated concentrations and deposition in the Oslo grid for sensitivity runs. It means that although spatial patterns of time integrated concentrations and depositions are rather similar (Fig. 82-84), the differences in individual model grids can be slightly larger (Table 45).

Sensitivity measures for the run without gravitational settling process and run with on-line calculated gravitational settling velocity are shown in Table 46. These measures are relatively

Table 45: Time integrated concentrations and deposition, 48 hours after the start of release, in the model grid cell where the city of Oslo is located. Results of the model run without gravitational settling and model run with on-line calculation of gravitational settling velocity.

Explosive yield (kt)	Time integrated concentration (Bq h m^{-3})	Total deposition (Bq m^{-2})
No gravitational settling		
1 kt	0.19E+07	0.16E+08
10 kt	0.41E+05	0.38E+06
100 kt	0.00E+00	0.00E+00
On-line gravitational settling		
1 kt	0.91E+06	0.28E+08
10 kt	0.17E+07	0.38E+09
100 kt	0.37E+07	0.13E+10

high, especially for time integrated concentrations and the run without gravitational settling. Compared to sensitivity run without dry deposition, sensitivity measures for gravitational settling are higher. It means that the model results are more sensitive to gravitational settling than to dry deposition.

Table 46: Sensitivity measures as defined in Eqs. (29) - (32), for the model run without gravitational settling process and model run with on-line calculation of gravitational settling velocity.

Explosive yield (kt)	SDF	SCF	SDG	SCG
No gravitational settling				
1 kt	421.0	557.4	84.2	163.9
10 kt	480.9	246.1	-99.9	-97.6
100 kt	477.1	209.4	-100.0	-100.0
On-line gravitational settling				
1 kt	206.5	73.7	212.6	26.5
10 kt	126.9	55.5	-25.4	-1.6
100 kt	214.7	188.7	9.7	36.5

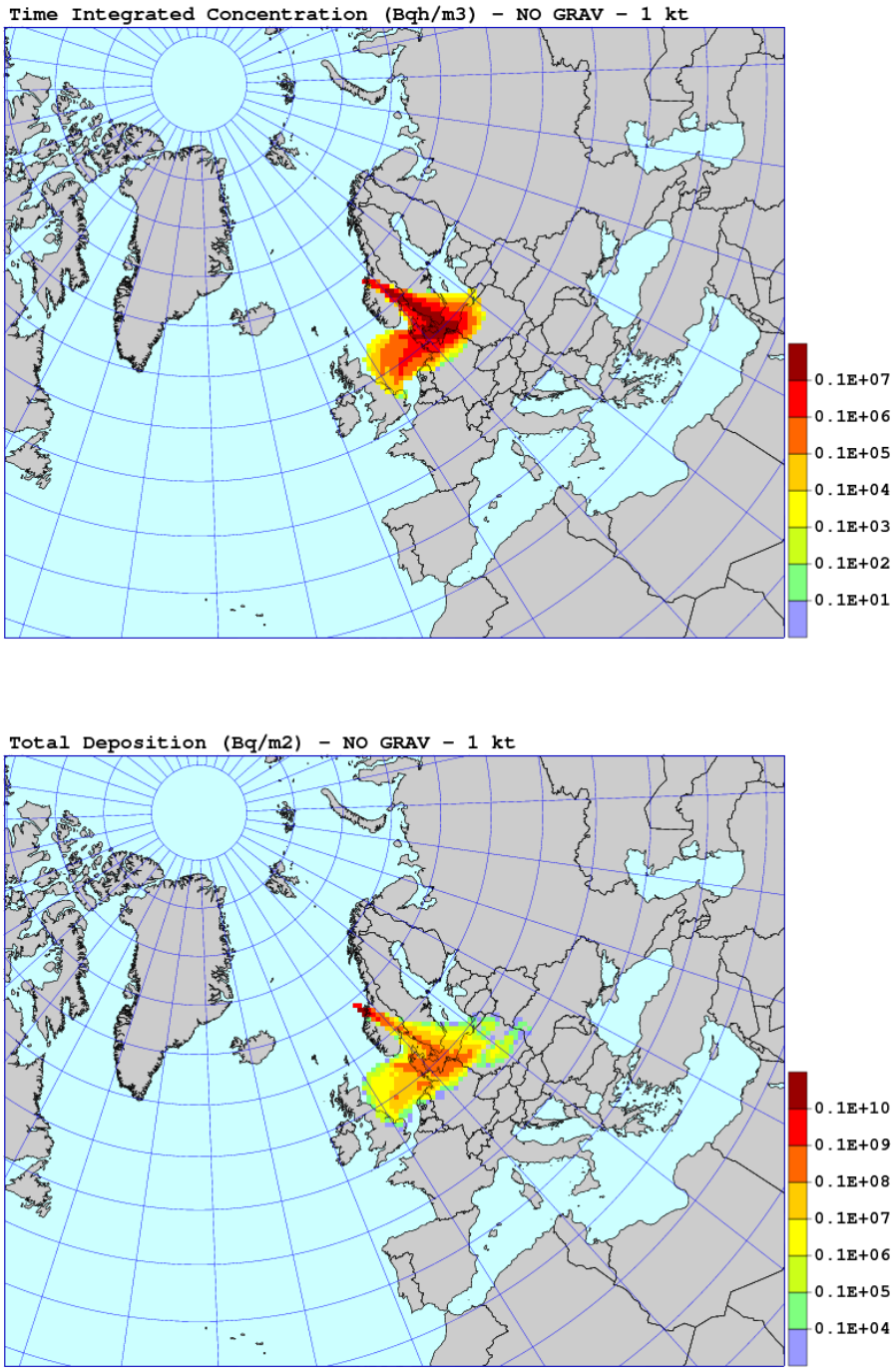

Figure 79: The results of the SNAP run without gravitational settling for 1 kt nuclear explosion, 48 hours after the detonation. Time integrated concentrations in Bq h m^{-3} above and total deposition in Bq m^{-3} in the bottom.

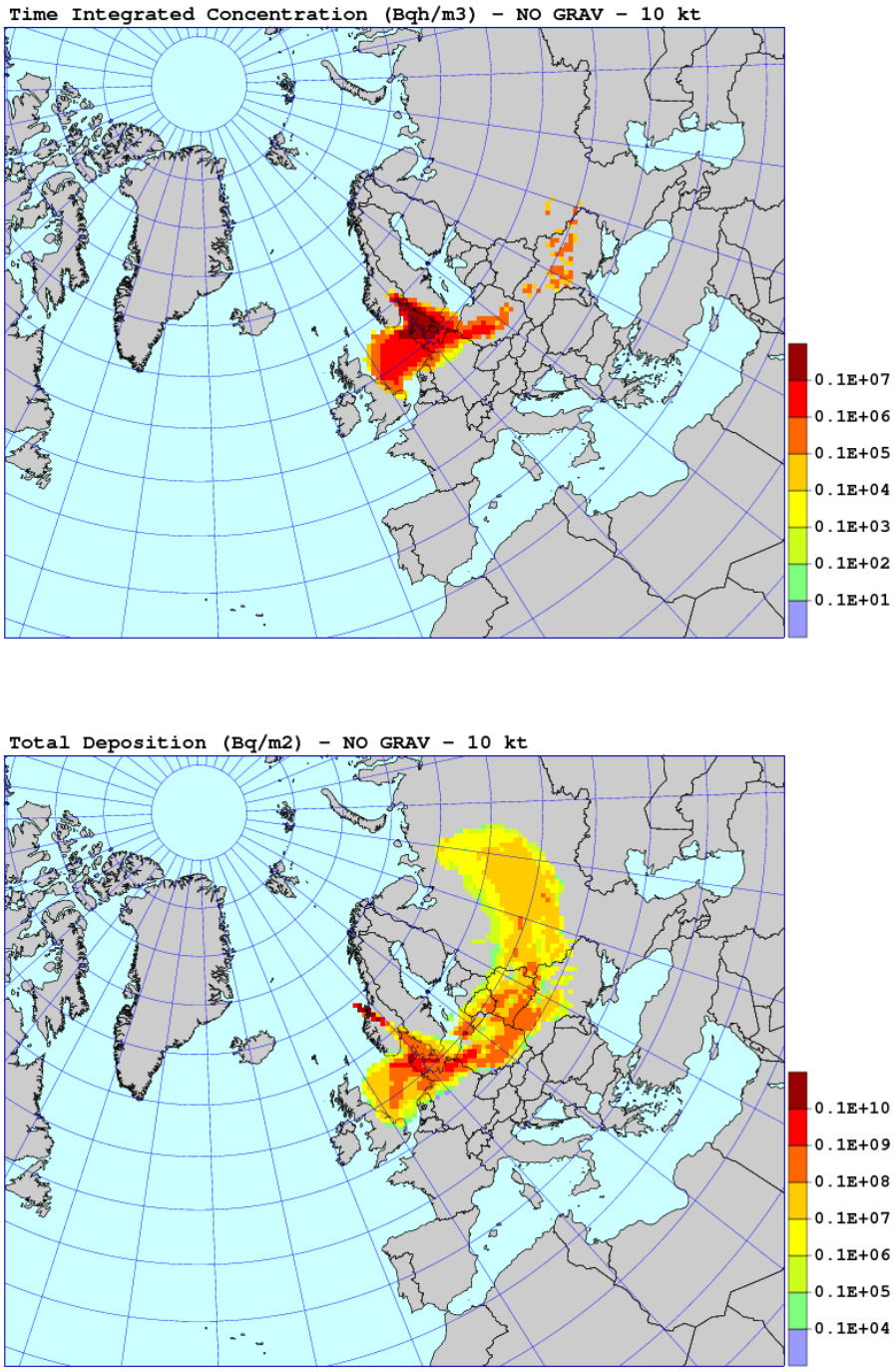

Figure 80: The results of the SNAP run without gravitational settling for 10 kt nuclear explosion, 48 hours after the detonation. Time integrated concentrations in Bq h m^{-3} above and total deposition in Bq m^{-3} in the bottom.

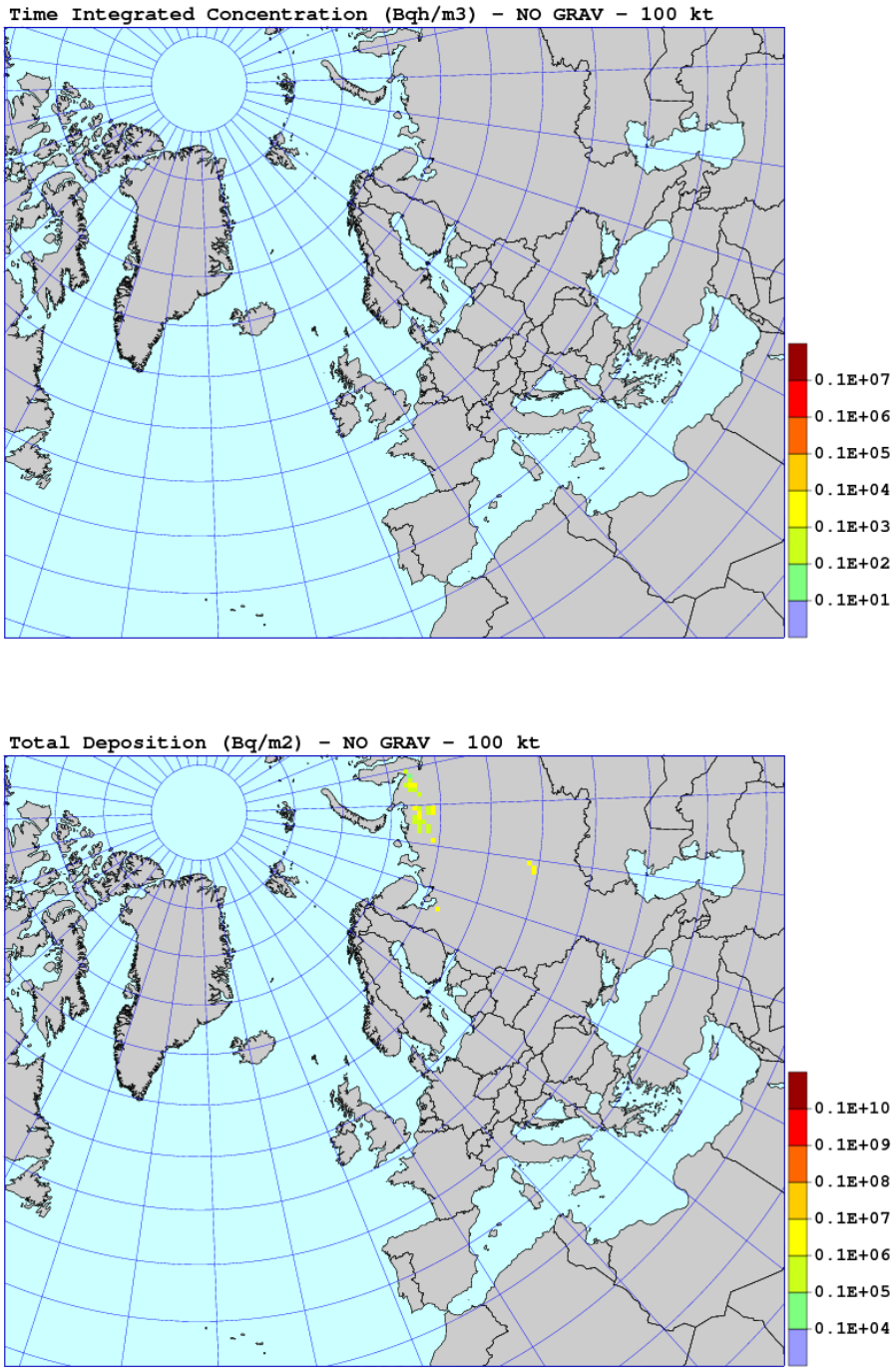

Figure 81: The results of the SNAP run without gravitational settling for 100 kt nuclear explosion, 48 hours after the detonation. Time integrated concentrations in Bq h m^{-3} above and total deposition in Bq m^{-3} in the bottom.

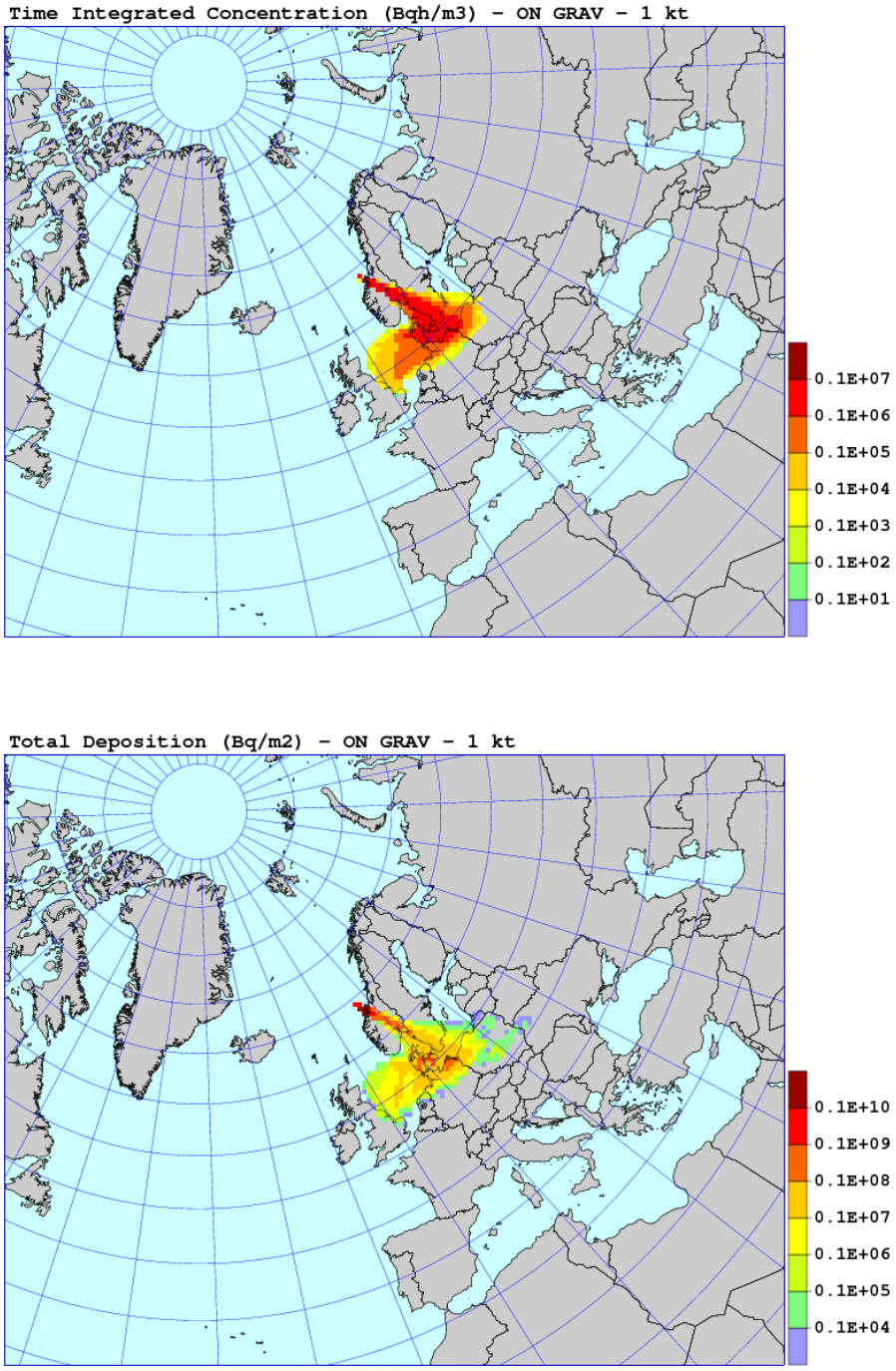

Figure 82: The results of the SNAP run with on-line gravitational settling for 1 kt nuclear explosion, 48 hours after the detonation. Time integrated concentrations in Bq h m^{-3} above and total deposition in Bq m^{-3} in the bottom.

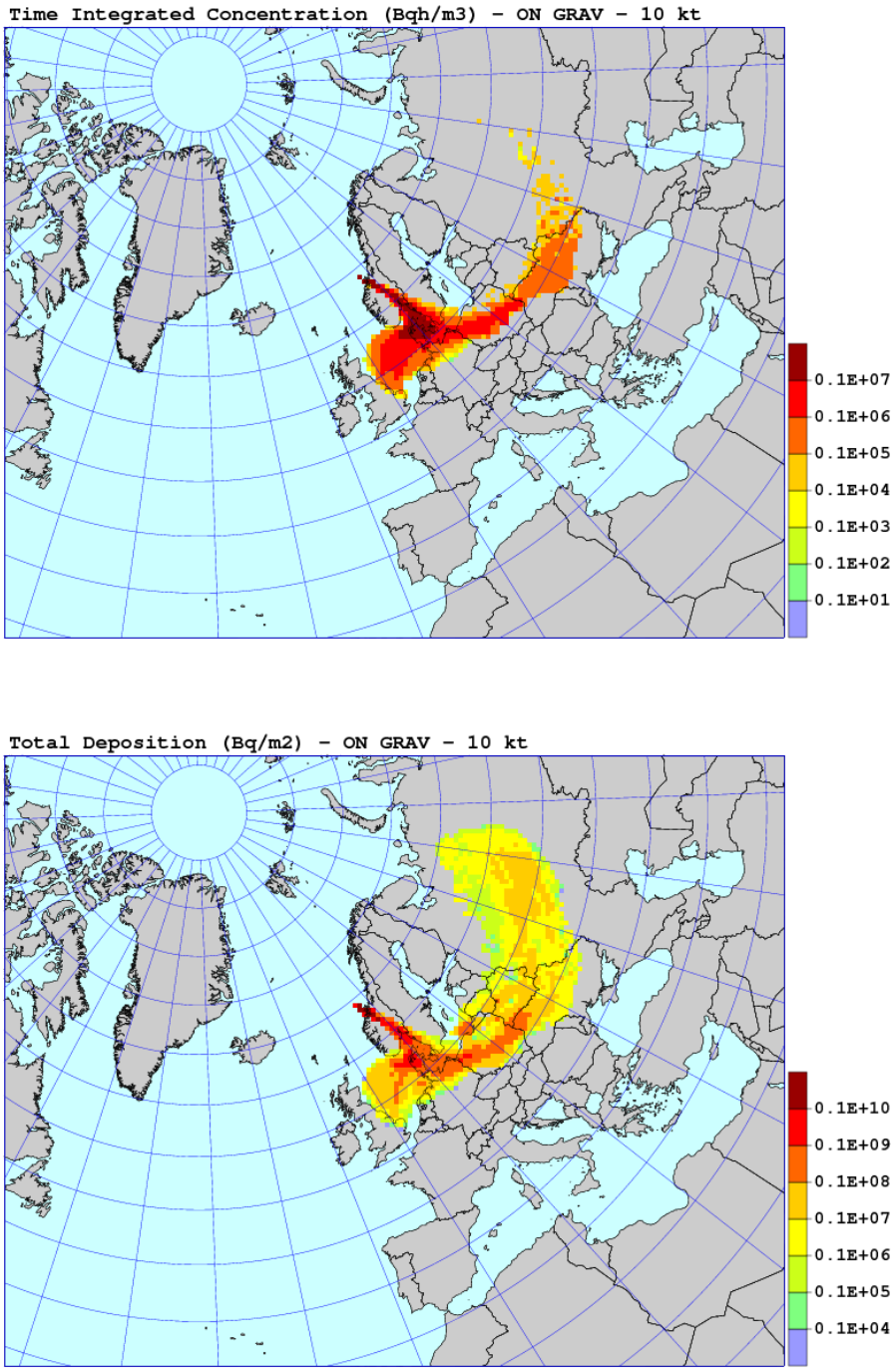

Figure 83: The results of the SNAP run with on-line gravitational settling for 10 kt nuclear explosion, 48 hours after the detonation. Time integrated concentrations in Bq h m^{-3} above and total deposition in Bq m^{-3} in the bottom.

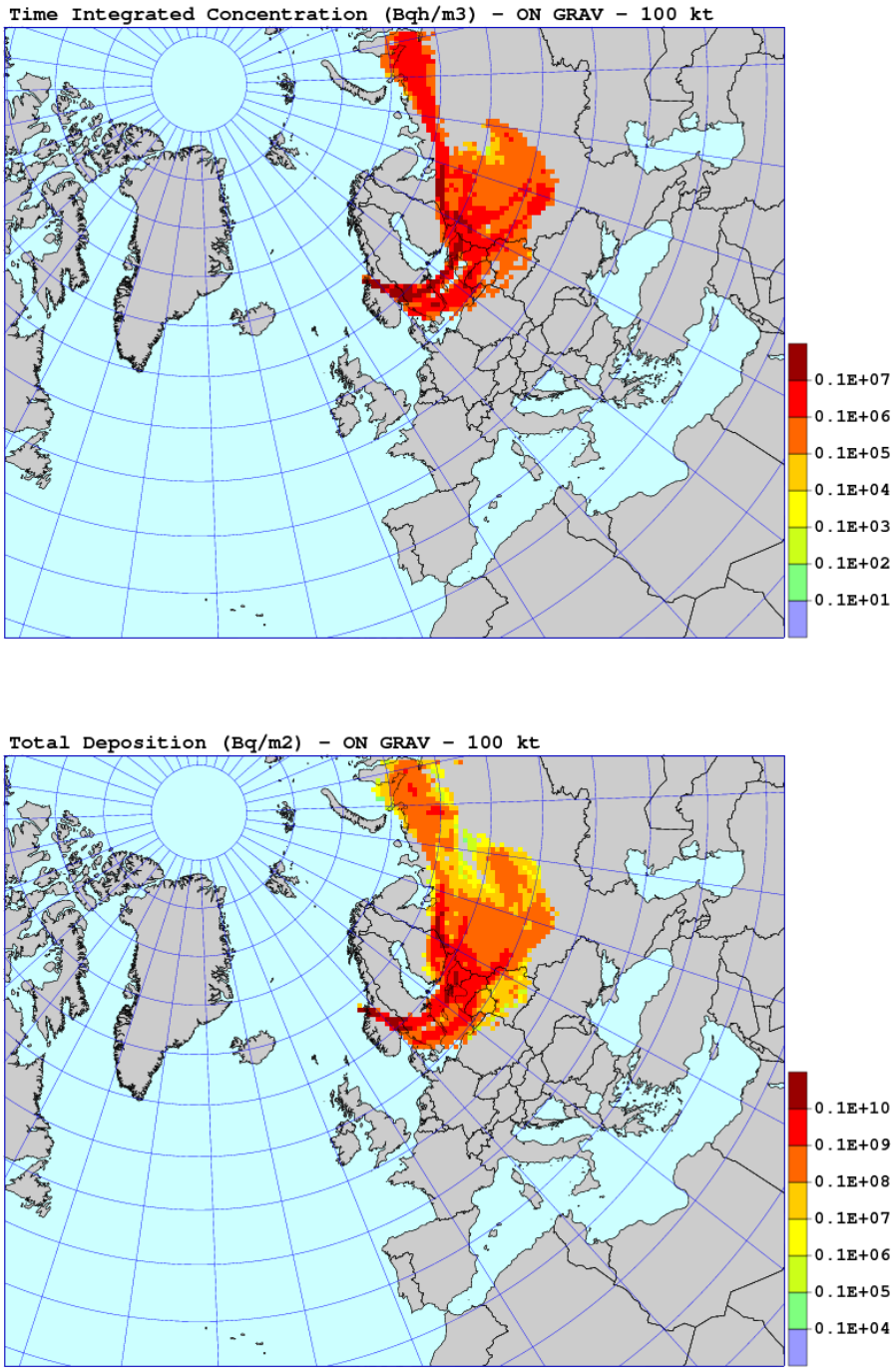

Figure 84: The results of the SNAP run with on-line gravitational settling for 100 kt nuclear explosion, 48 hours after the detonation. Time integrated concentrations in Bq h m^{-3} above and total deposition in Bq m^{-3} in the bottom.

6.4. Sensitivity to wet deposition

Sensitivity to wet deposition was tested in the model run without wet deposition process. The maps of time integrated concentration and total deposition for 1 kt, 10 kt and 100 kt explosion are shown in Fig. 85, 86 and 87, respectively.

There are some differences between the standard and test runs, both for time integrated concentration and deposition. These differences are relatively small for time integrated concentrations, but only for 1 kt explosion. For 10 kt and 100 kt explosions, the differences are significant. The differences in the deposition fields are much larger, for all explosive yields, because of the irregular pattern of precipitation field. These differences increase with the increased explosive yield, being largest for 100 kt explosion.

Time integrated concentrations and deposition in the model grid cell where the city of Oslo is located are shown in Table 47 for the model run without wet deposition, 48 hours after the start of release. The differences between the standard run and the test run are more visible for the deposition. However, both time integrated concentrations and deposition are higher in the run without wet deposition. The most likely reason for that is the area with intensive precipitation close to the source. In the model run without wet deposition, particles are not removed close to the source and transported farther away than in the standard run.

Table 47: Time integrated concentrations and deposition, 48 hours after the start of release, in the model grid cell where the city of Oslo is located. Results of the model run without wet deposition.

Explosive yield (kt)	Time integrated concentration (Bq h m^{-3})	Total deposition (Bq m^{-2})
1	0.78E+06	0.18E+08
10	0.39E+07	0.74E+09
100	0.30E+07	0.11E+10

Sensitivity measures for the run without wet deposition are given in Table 54. These measures are relatively high, especially for 10 kt explosion. In general, model is rather sensitive to wet deposition process.

Table 48: Sensitivity measures as defined in Eqs. (29) - (32), for the run without wet deposition.

Explosive yield (kt)	SDF	SCF	SDG	SCG
1	468.3	225.3	125.4	89.3
10	952.7	369.7	160.6	150.8
100	399.9	97.1	26.2	48.9

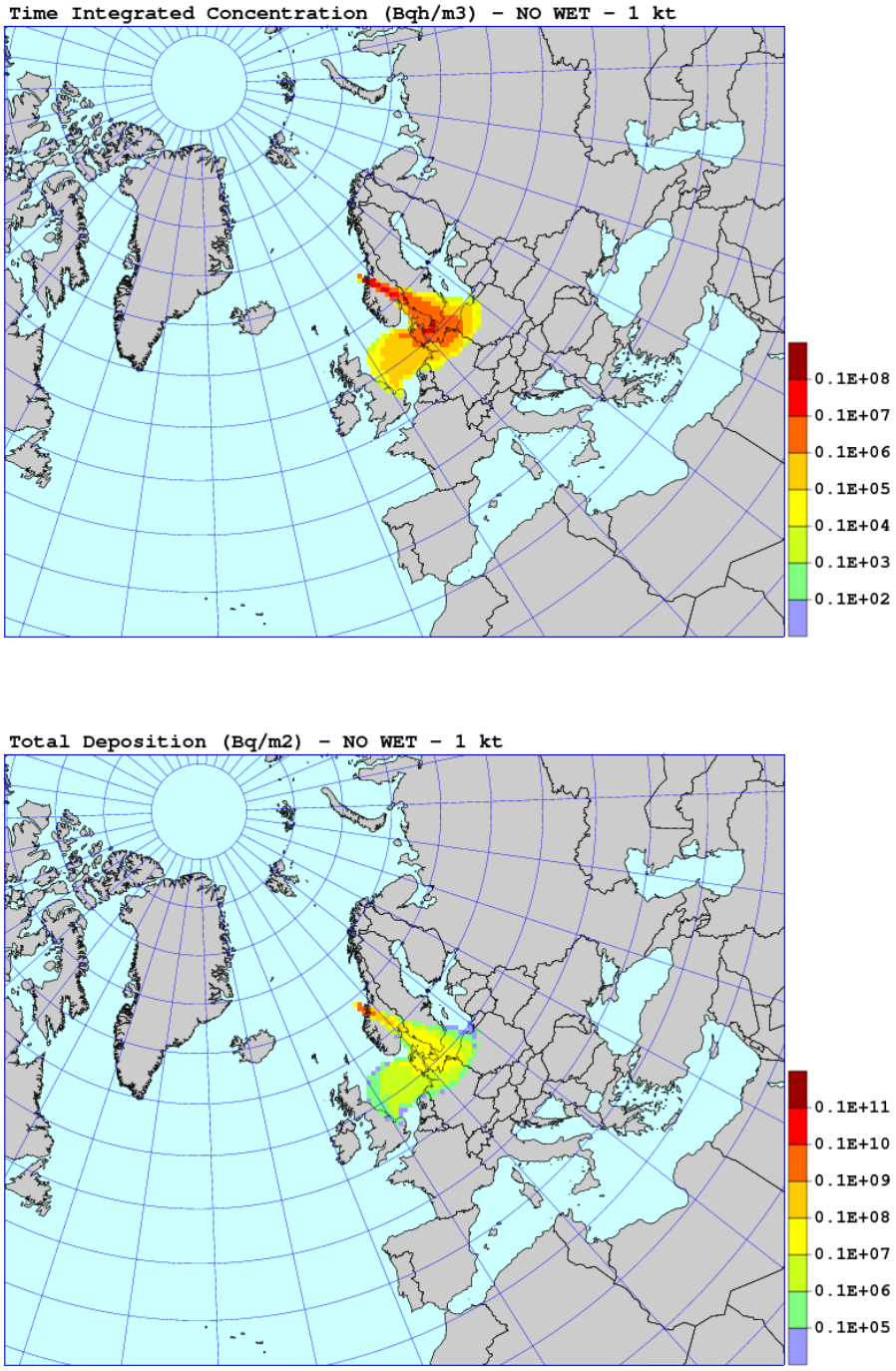

Figure 85: The results of the SNAP run without wet deposition for 1 kt nuclear explosion, 48 hours after the detonation. Time integrated concentrations in Bq h m^{-3} above and total deposition in Bq m^{-3} in the bottom.

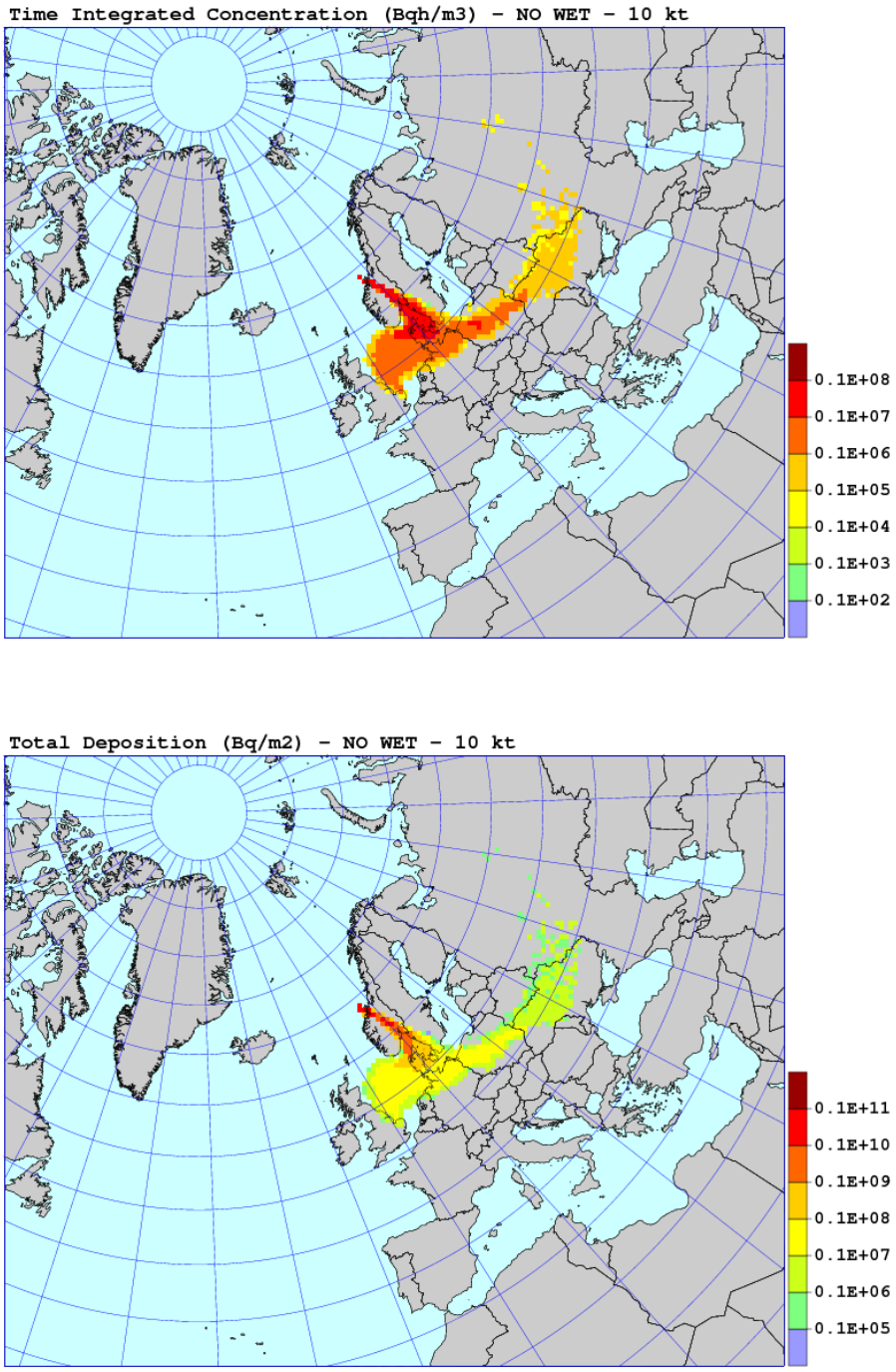

Figure 86: The results of the SNAP run without wet deposition for 10 kt nuclear explosion, 48 hours after the detonation. Time integrated concentrations in Bq h m^{-3} above and total deposition in Bq m^{-3} in the bottom.

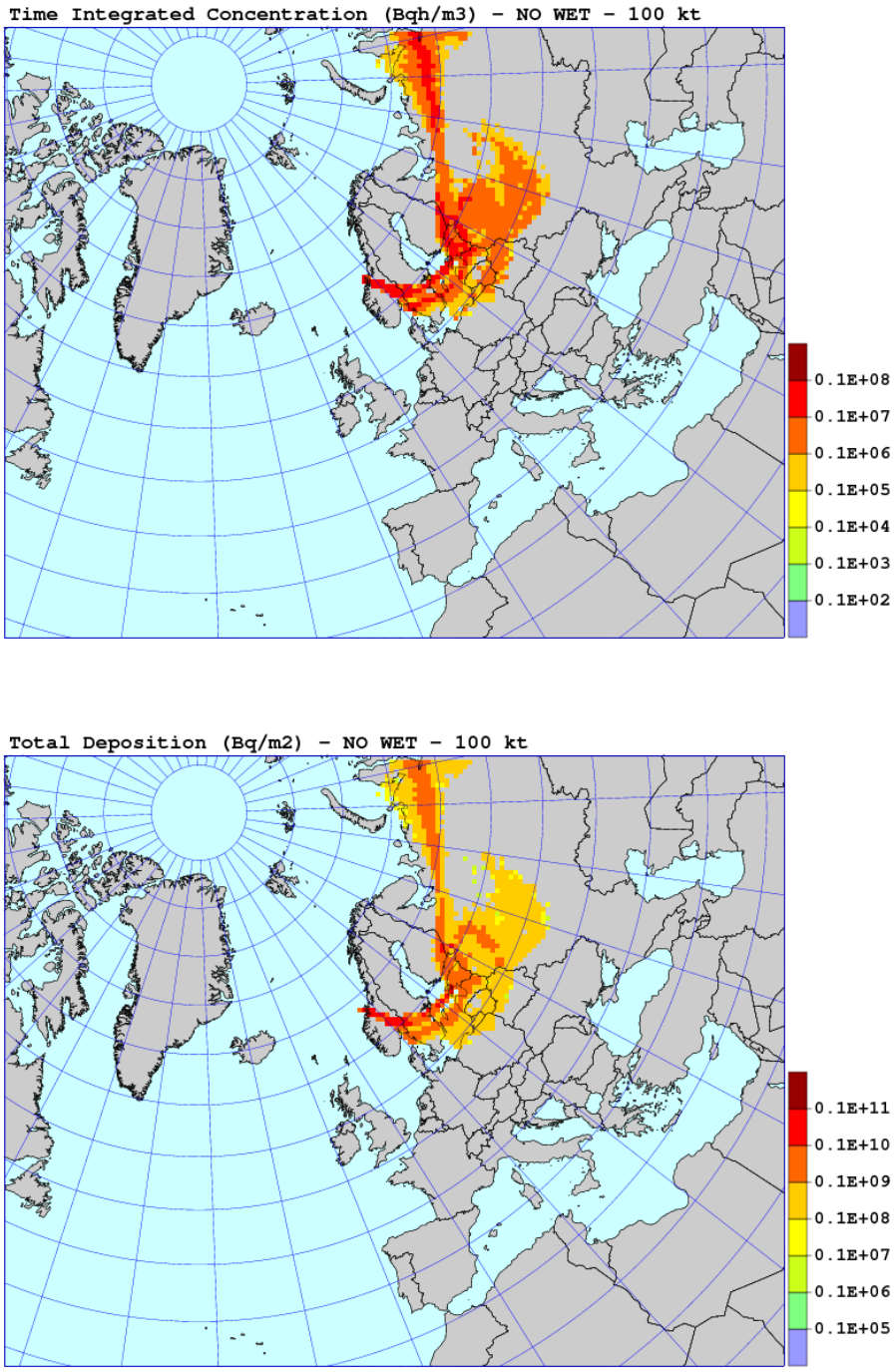

Figure 87: The results of the SNAP run without wet deposition for 100 kt nuclear explosion, 48 hours after the detonation. Time integrated concentrations in Bq h m^{-3} above and total deposition in Bq m^{-3} in the bottom.

6.5. Sensitivity to horisontal diffusion

Model sensitivity to horisontal diffusion was tested in two runs. In the first run, horisontal diffusion was completely neglected. In the second run, the coefficient of horisontal diffusion was amplified two times.

The results of sensitivity runs without horisontal diffusion are shown in Fig. 88-90 as maps of time integrated concentration and deposition. For all explosive yields, the differences between spatial distributions in the standard run and in the run without horisontal diffusion are very small, both for time integrated concentrations and deposition.

The results of sensitivity runs with enhanced horisontal diffusion are shown in Fig. 91-93 as maps of time integrated concentrations and deposition. Also in this case, the differences between spatial distributions in the standard run and in the run with enhanced horisontal diffusion are very small, for all explosive yields.

The results of sensitivity runs without and with enhanced horisonatal diffusion, in the model grid cell where the city of Oslo is located are shown in Table 49. They include time integrated concentrations and deposition, 48 hours after the detonation. Both, for the run without horisonatal diffusion and the run with enhanced horisontal diffusion, time integrated concentrations and deposition are slightly higher than in the standard run. The differences are a bit larger for the run with enhanced horisontal diffusion.

Table 49: Time integrated concentrations and deposition, 48 hours after the detonation, in the model grid cell where the city of Oslo is located. Results of the model run without horisontal diffusion and model run with enhanced horisontal diffusion.

Explosive yield (kt)	Time integrated concentration (Bq h m^{-3})	Total deposition (Bq m^{-2})
No horisontal diffusion		
1 kt	0.73E+06	0.91E+07
10 kt	0.17E+07	0.52E+09
100 kt	0.28E+07	0.11E+10
More horisontal diffusion		
1 kt	0.69E+06	0.84E+07
10 kt	0.16E+07	0.37E+09
100 kt	0.22E+07	0.10E+10

Sensitivity measures for the run without horisontal diffusion and run with enhanced horisontal diffusion are shown in Table 50. These measures are slightly higher for the run with enhanced horisontal diffusion. Compared to other sensitivity runs, the measures for horisontal diffusion are on the same level as for dry deposition, but lower than for gravitational settling and wet deposition.

The above results suggests that the model is relatively not so sensitive to horisontal diffusion. In fact, some of the Eulerian emergency models neglect horisontal diffusion completely in the model equations.

Table 50: Sensitivity measures as defined in Eqs. (29) - (32), for the model run without horisontal diffusion and model run with enhanced horisontal diffusion.

Explosive yield (kt)	SDF	SCF	SDG	SCG
No horisontal diffusion				
1 kt	158.7	30.7	3.4	1.0
10 kt	151.0	18.8	2.6	1.8
100 kt	37.2	35.4	-6.3	1.7
More horisontal diffusion				
1 kt	191.9	16.9	-5.0	-4.5
10 kt	372.1	26.3	-26.0	-4.1
100 kt	82.4	37.3	-16.3	-19.5

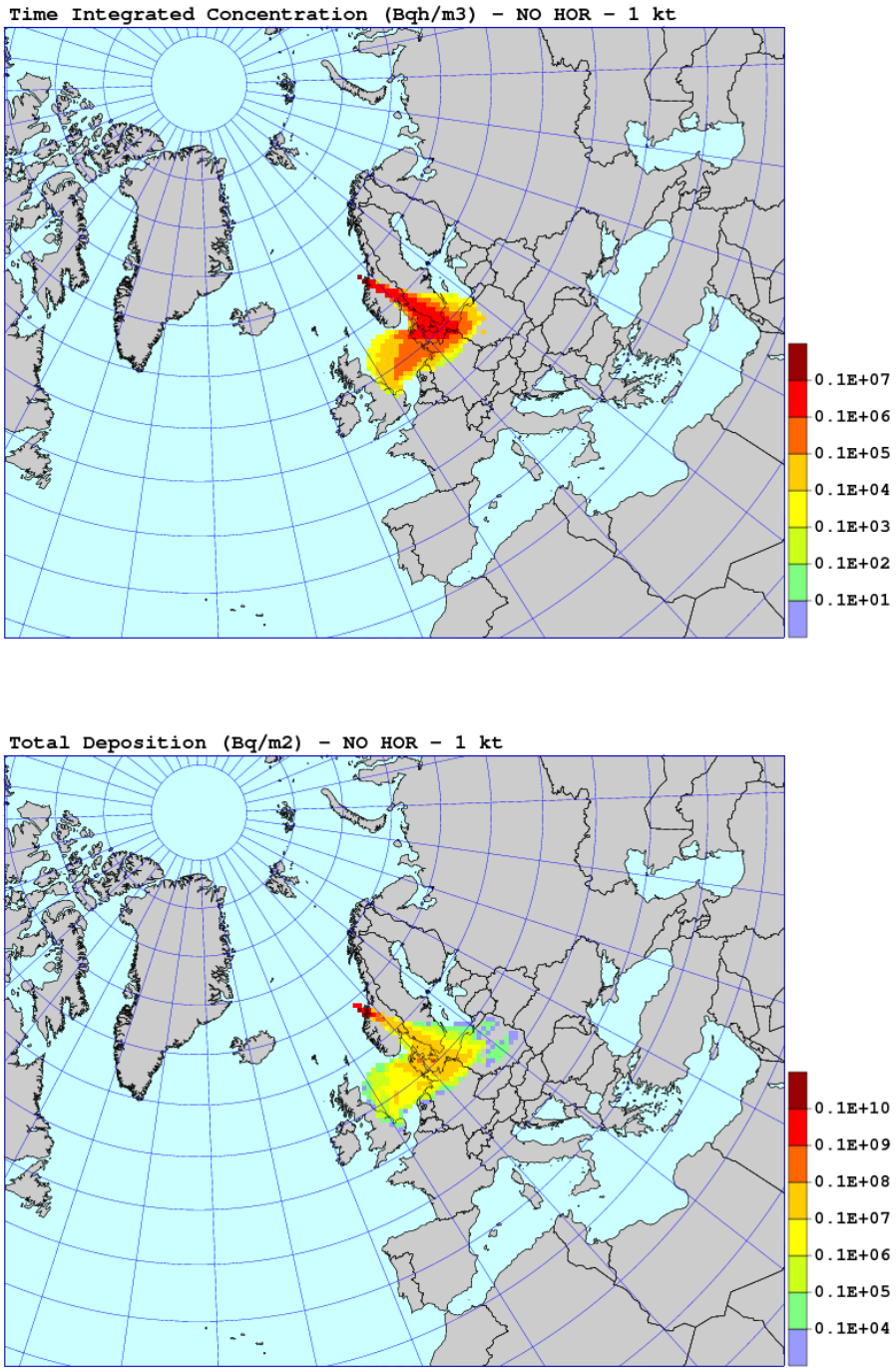

Figure 88: The results of the SNAP run without horisontal diffusion for 1 kt nuclear explosion, 48 hours after the detonation. Time integrated concentrations in Bq h m^{-3} above and total deposition in Bq m^{-3} in the bottom.

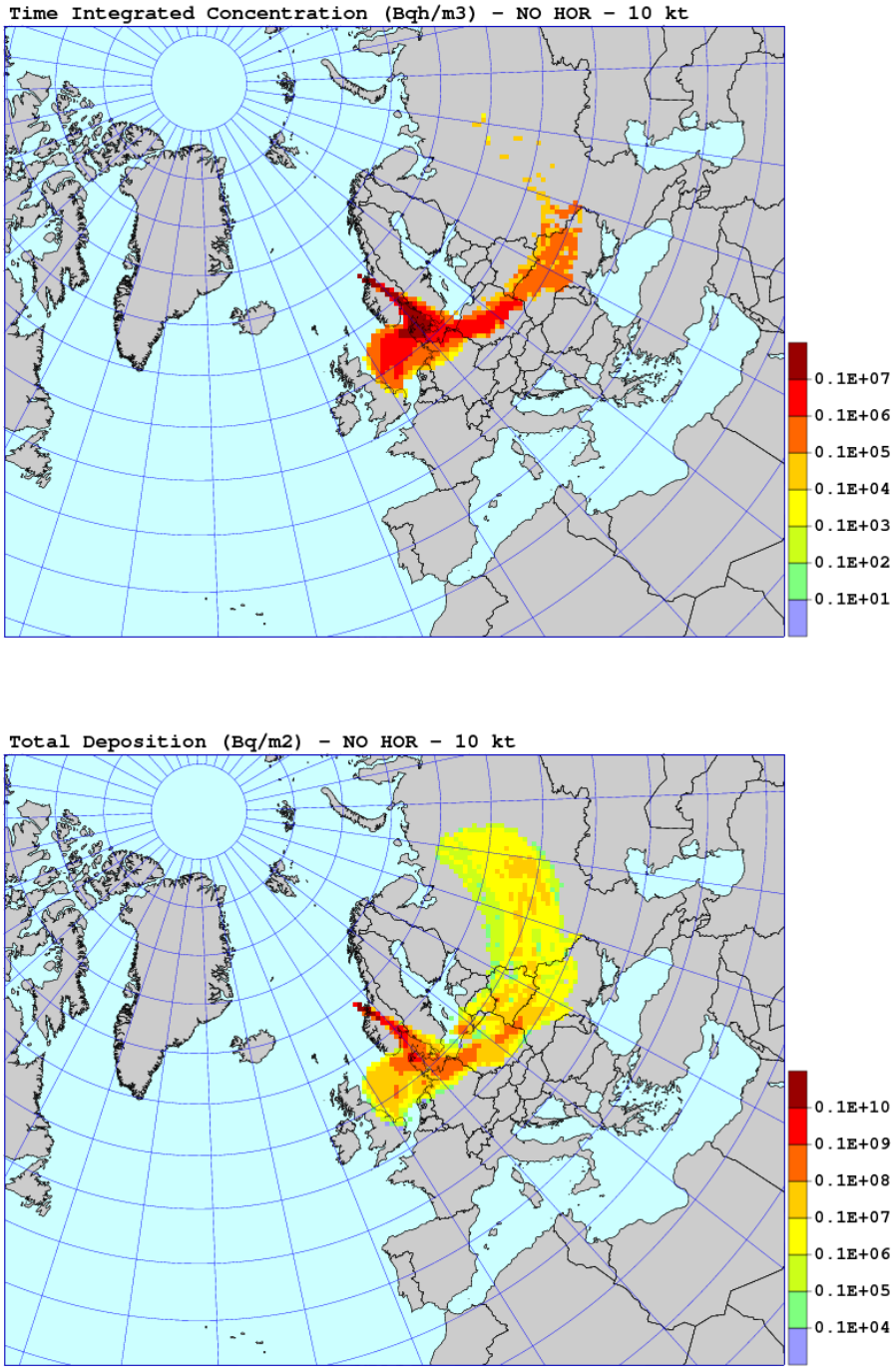

Figure 89: The results of the SNAP run without horisontal diffusion for 10 kt nuclear explosion, 48 hours after the detonation. Time integrated concentrations in Bq h m^{-3} above and total deposition in Bq m^{-3} in the bottom.

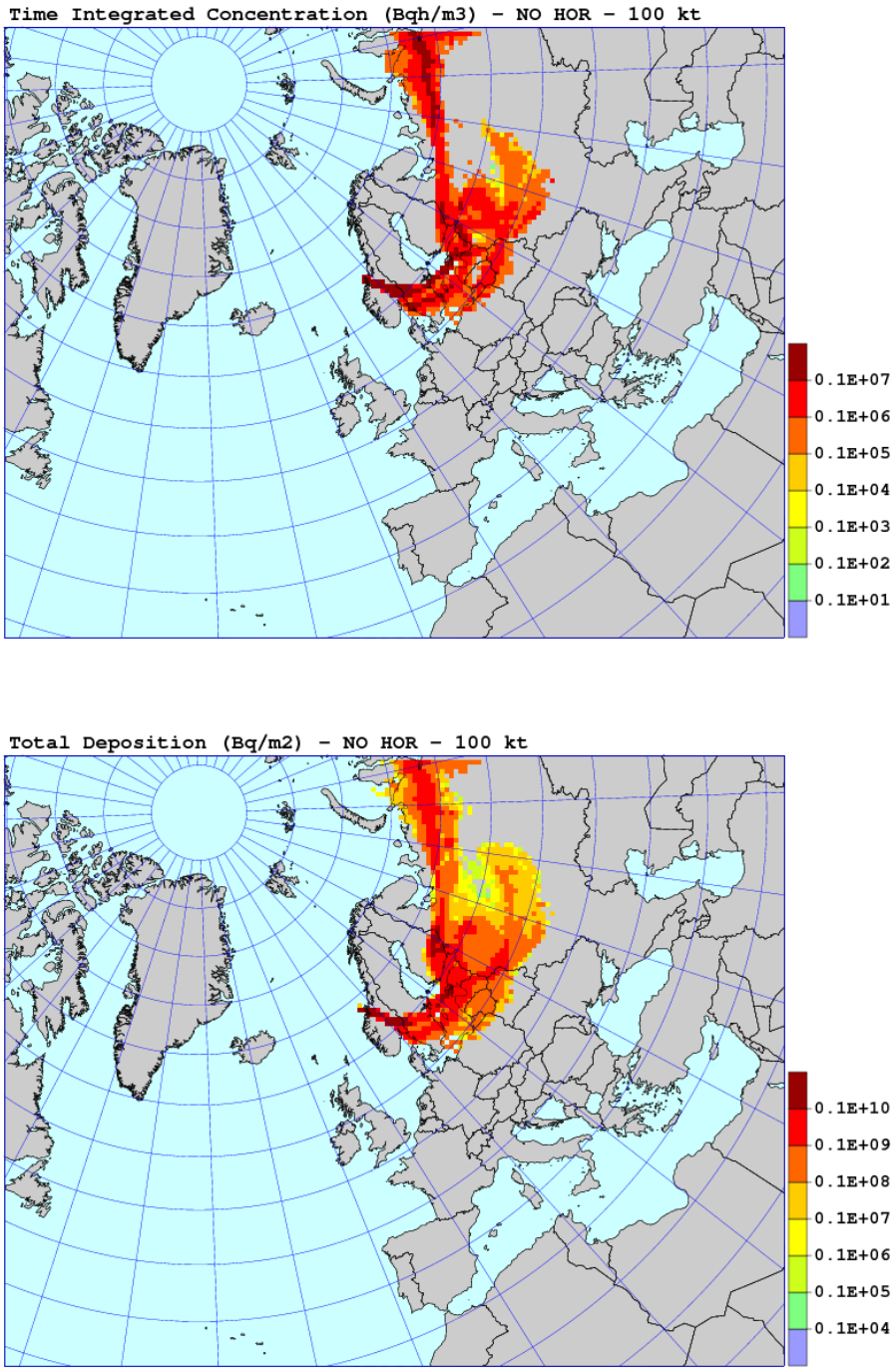

Figure 90: The results of the SNAP run without horisontal diffusion for 100 kt nuclear explosion, 48 hours after the detonation. Time integrated concentrations in Bq h m^{-3} above and total deposition in Bq m^{-3} in the bottom.

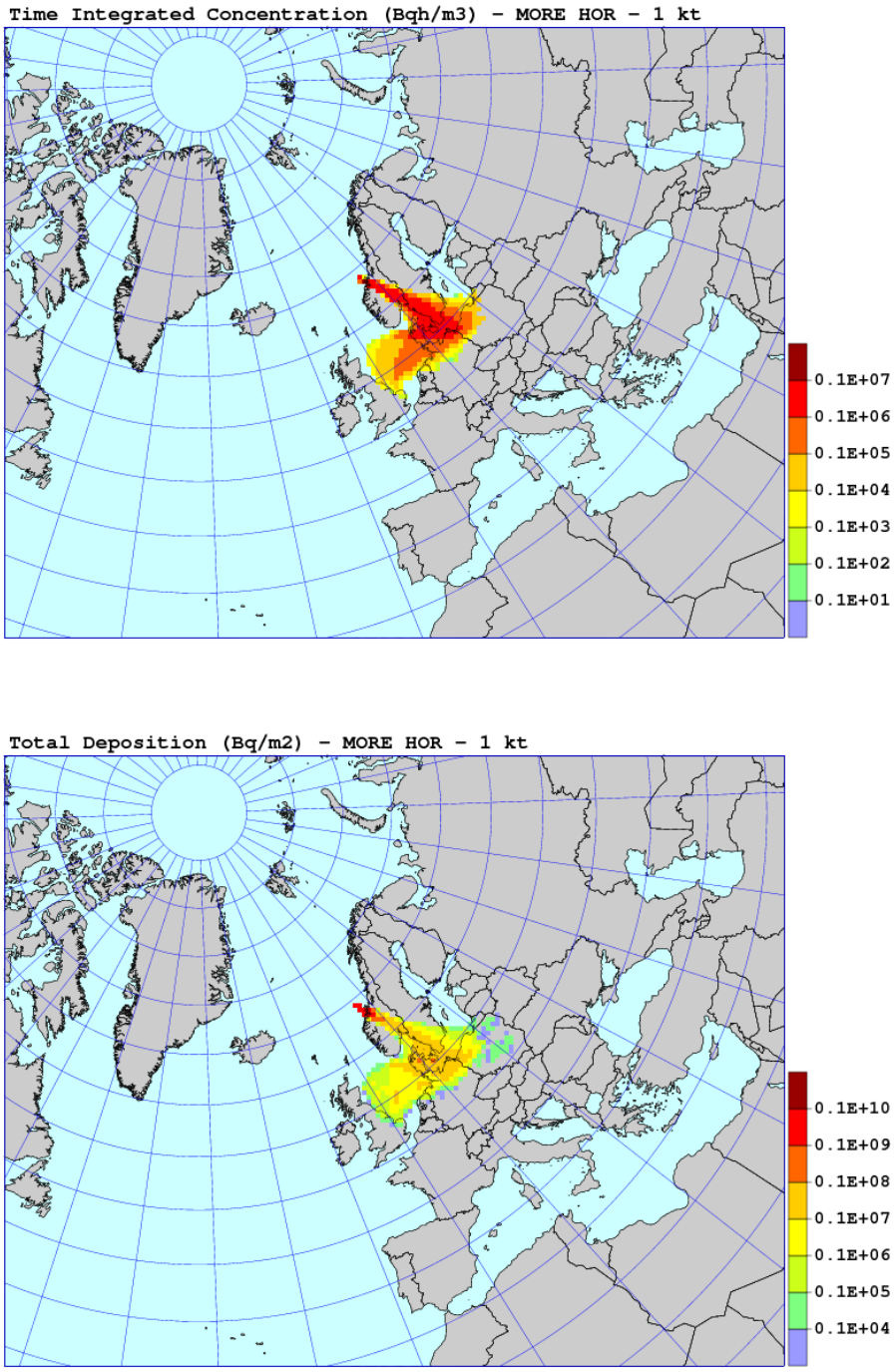

Figure 91: The results of the SNAP run with more horisontal diffusion for 1 kt nuclear explosion, 48 hours after the detonation. Time integrated concentrations in Bq h m^{-3} above and total deposition in Bq m^{-3} in the bottom.

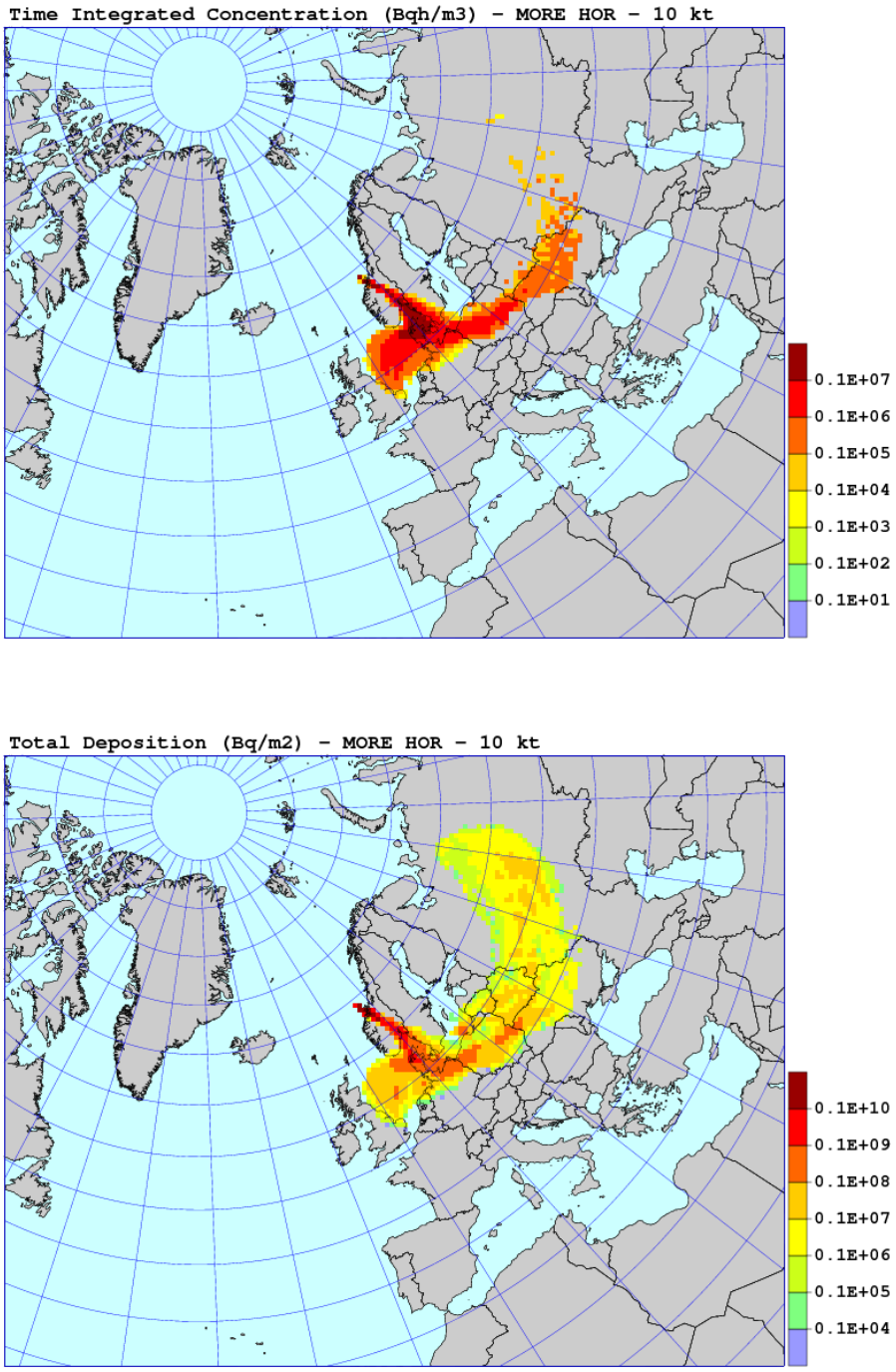

Figure 92: The results of the SNAP run with more horisontal diffusion for 10 kt nuclear explosion, 48 hours after the detonation. Time integrated concentrations in Bq h m^{-3} above and total deposition in Bq m^{-3} in the bottom.

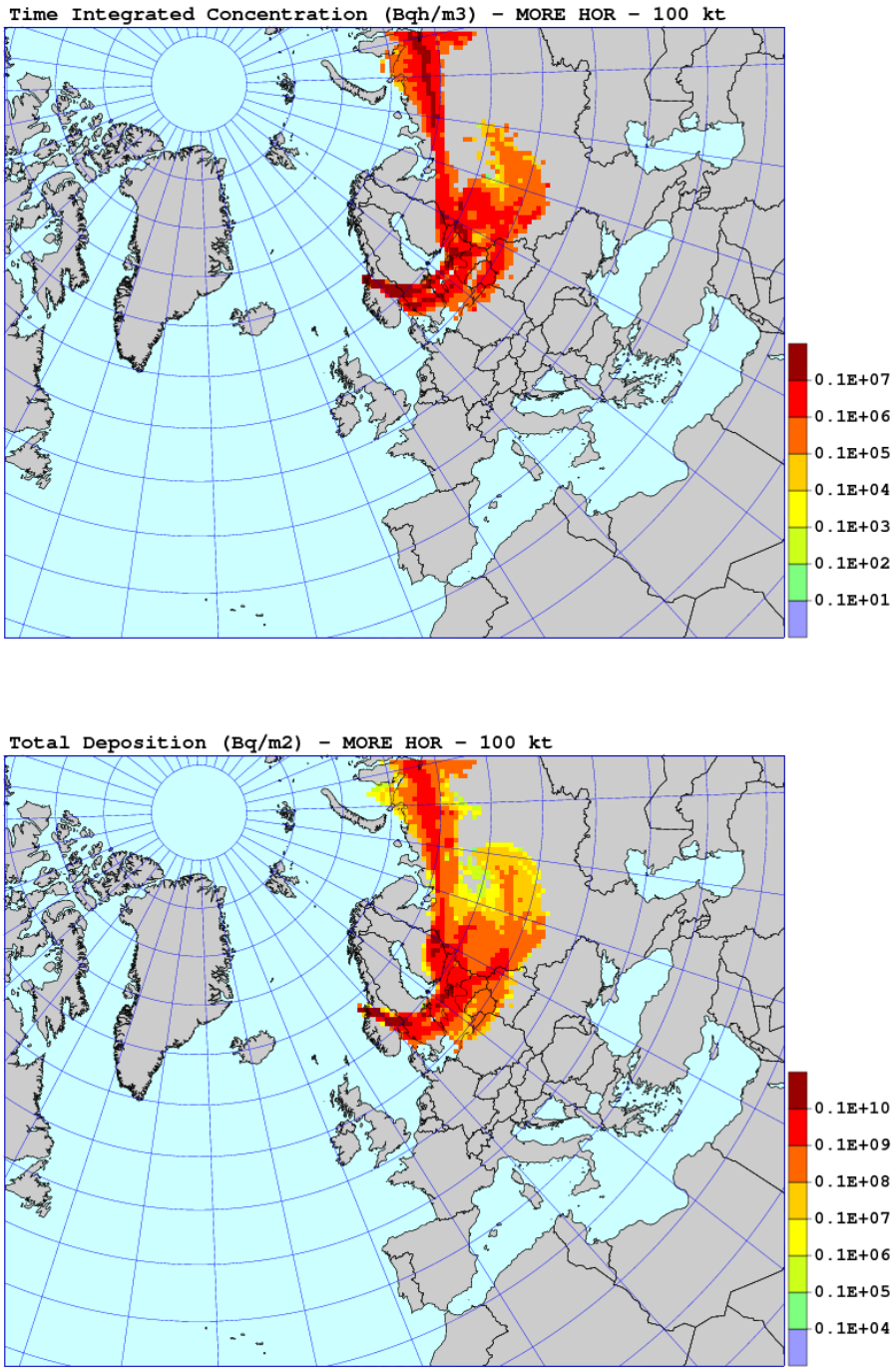

Figure 93: The results of the SNAP run with more horisontal diffusion for 100 kt nuclear explosion, 48 hours after the detonation. Time integrated concentrations in Bq h m^{-3} above and total deposition in Bq m^{-3} in the bottom.

6.6. Sensitivity to vertical diffusion

Model sensitivity to vertical diffusion was tested in two runs. In the first run, vertical diffusion was completely neglected. In the second run, the coefficient of vertical diffusion was amplified two times.

The results of sensitivity runs without vertical diffusion are shown in Fig. 94-96 as maps of time integrated concentration and deposition. For all explosive yields, the differences between spatial distributions in the standard run and in the run without vertical diffusion are very large, both for time integrated concentrations and deposition. The plume is much narrower for the run without vertical diffusion with significantly higher concentrations in the centre, compared to standard run.

The results of sensitivity runs with enhanced vertical diffusion are shown in Fig. 97-99 as maps of time integrated concentration and deposition. Also in this case, the differences between spatial distributions in the standard run and in the run with enhanced vertical diffusion are large, for all explosive yields. However, in this case the plume in the run with enhanced vertical diffusion is more spread than the plume in the standard run.

The results of sensitivity runs without and with enhanced vertical diffusion, in the model grid cell where the city of Oslo is located are shown in Table 51. They include time integrated concentrations and deposition, 48 hours after the detonation. The values from the sensitivity runs are more different from the results of the standard run in the test without vertical diffusion.

Table 51: Time integrated concentrations and deposition, 48 hours after the start of release, in the model grid cell where the city of Oslo is located. Results of the model run without vertical diffusion and model run with enhanced vertical diffusion.

Explosive yield (kt	Time integrated concentration (Bq h m^{-3})	Total deposition (Bq m^{-2})
No vertical diffusion		
1 kt	0.39E+06	0.33E+07
10 kt	0.24E+07	0.62E+09
100 kt	0.35E+07	0.14E+10
More vertical diffusion		
1 kt	0.64E+06	0.98E+07
10 kt	0.21E+07	0.33E+09
100 kt	0.20E+07	0.11E+10

Sensitivity measures for the run without vertical diffusion and in the run with enhanced vertical diffusion are shown in Table 52. Compared to other sensitivity runs, these measures are not very high. This is a bit of surprise taking into account large differences between this run and standard run in the time concentration and deposition maps.

Table 52: Sensitivity measures as defined in Eqs. (29) - (32), for the model run without vertical diffusion and model run with enhanced vertical diffusion.

Explosive yield	SDF	SCF	SDG	SCG
No vertical diffusion				
1 kt	56.6	317.0	-62.1	-45.8
10 kt	188.4	216.3	22.4	43.1
100 kt	162.4	356.4	11.7	27.7
More vertical diffusion				
1 kt	42.7	118.7	11.5	-11.6
10 kt	163.1	159.6	-35.1	23.1
100 kt	49.1	75.5	-6.9	-24.7

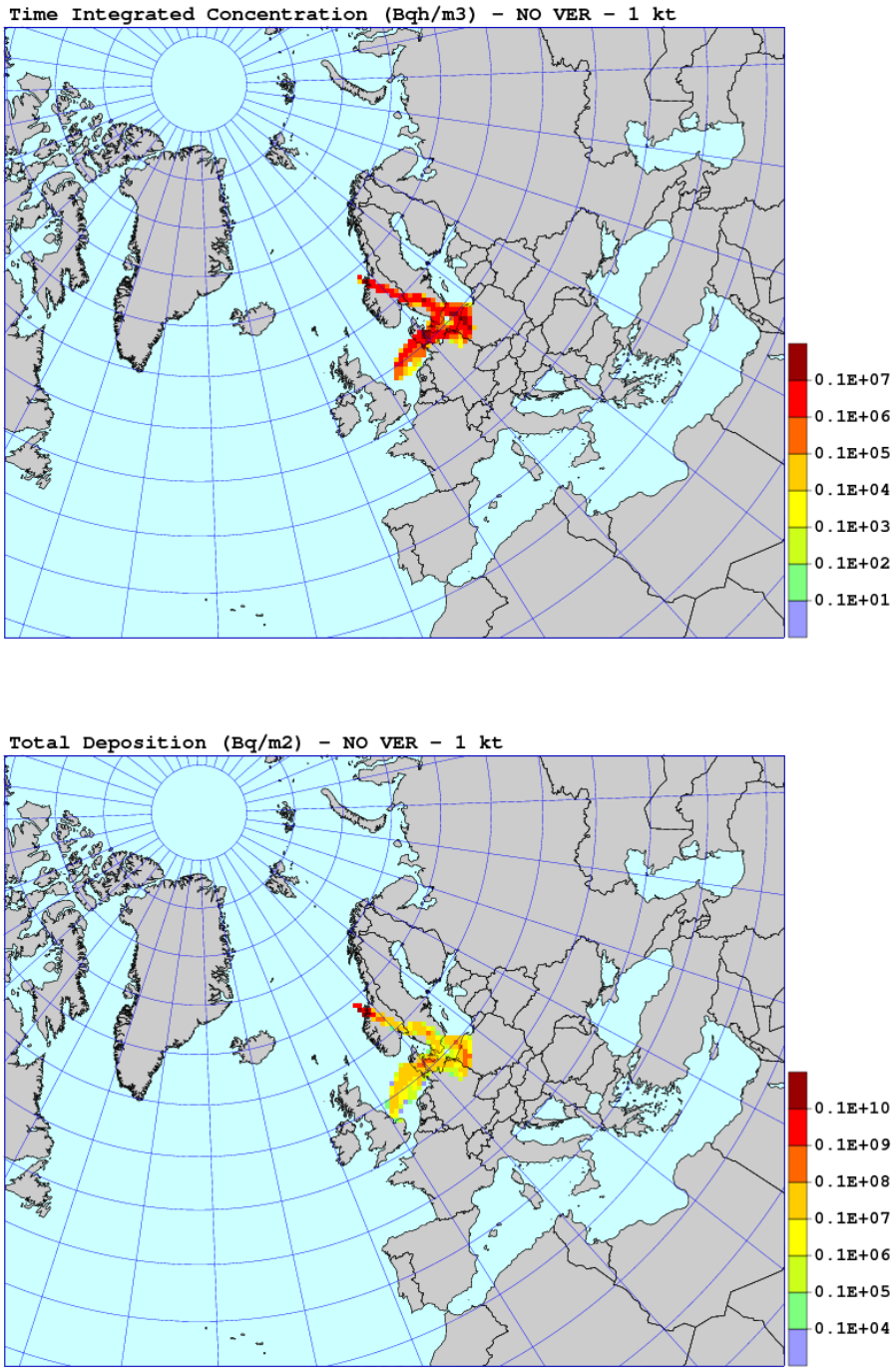

Figure 94: The results of the SNAP run without vertical diffusion for 1 kt nuclear explosion, 48 hours after the detonation. Time integrated concentrations in Bq h m^{-3} above and total deposition in Bq m^{-3} in the bottom.

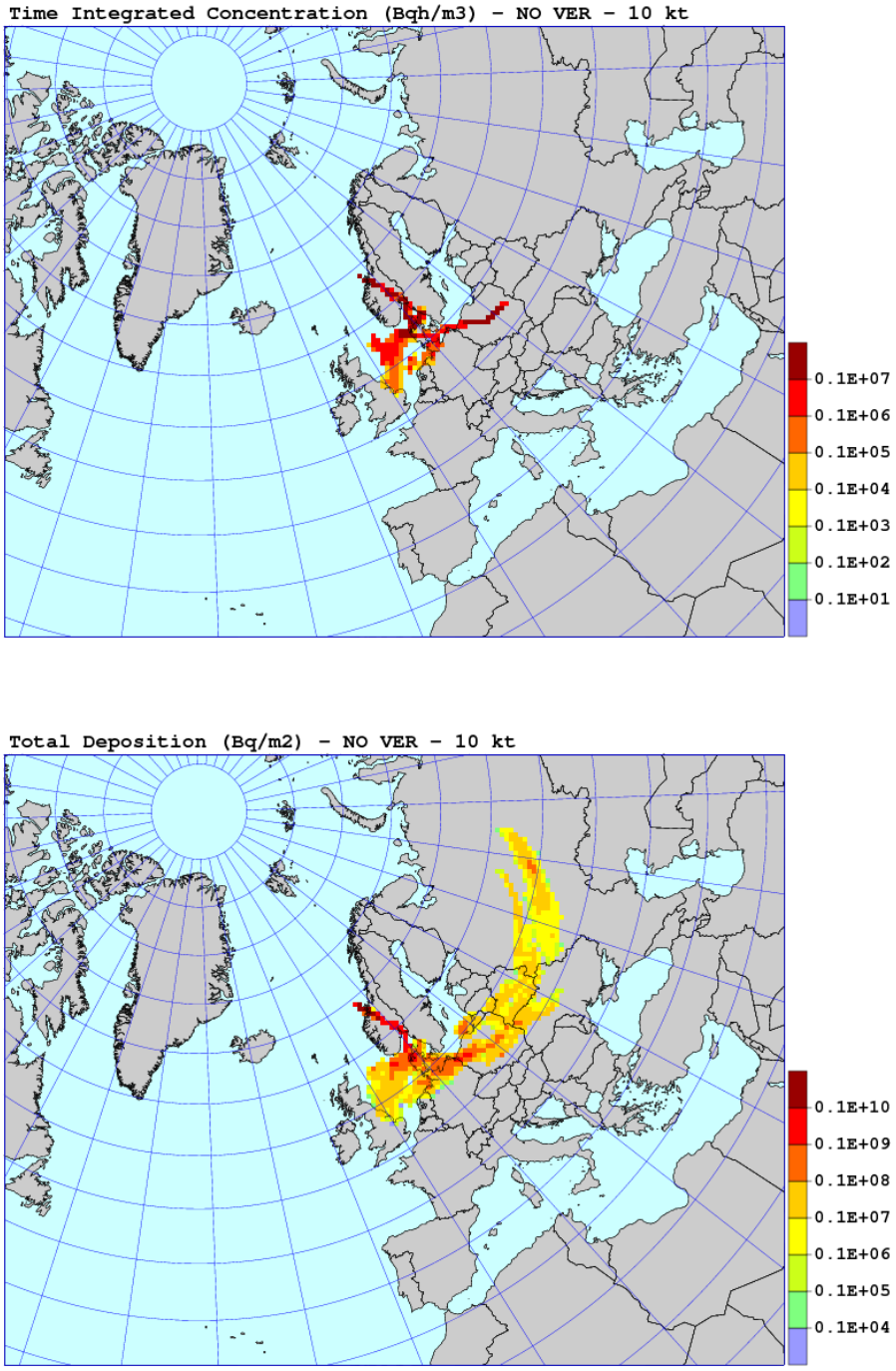

Figure 95: The results of the SNAP run without vertical diffusion for 10 kt nuclear explosion, 48 hours after the detonation. Time integrated concentrations in Bq h m^{-3} above and total deposition in Bq m^{-3} in the bottom.

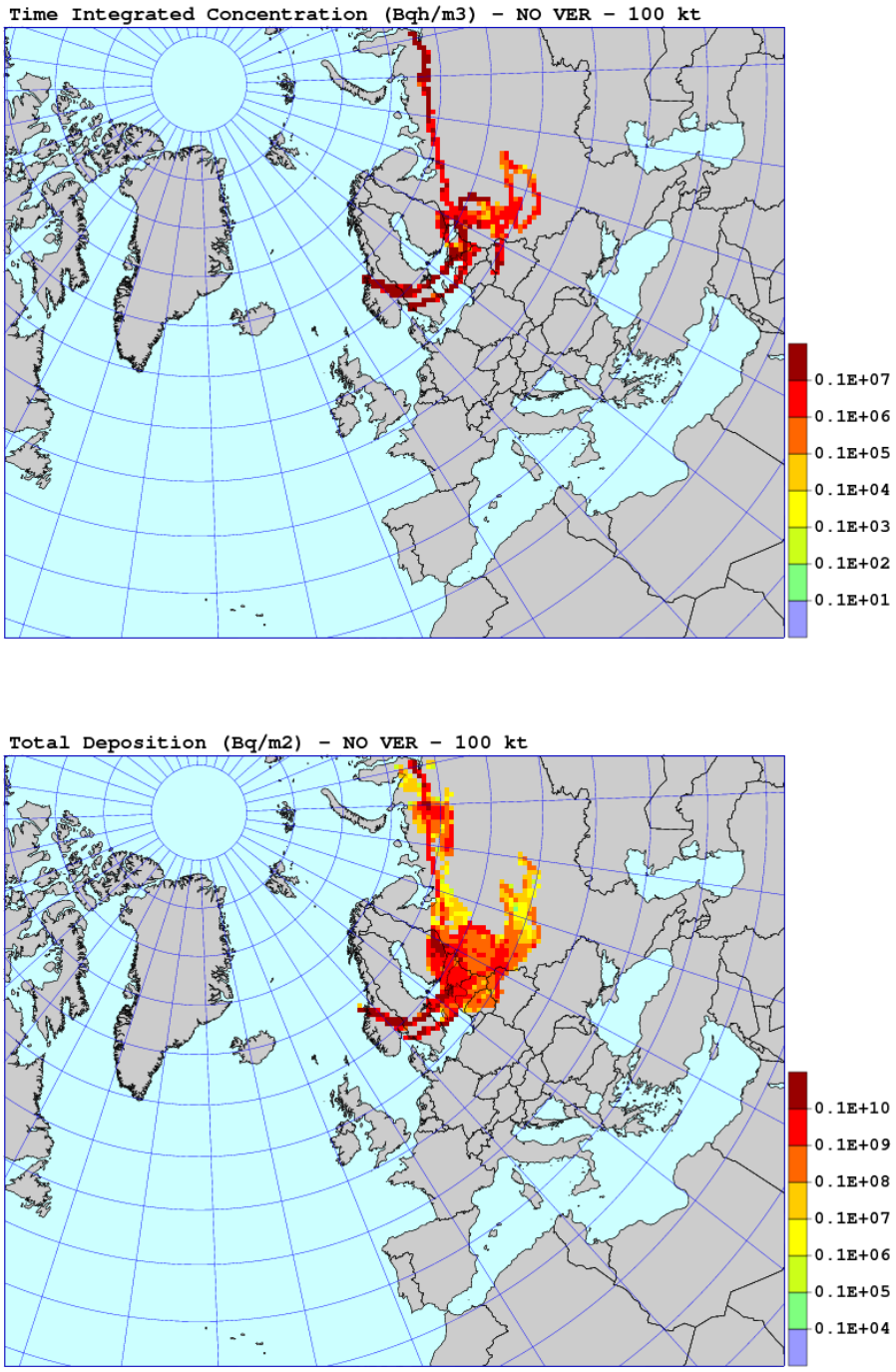

Figure 96: The results of the SNAP run without vertical diffusion for 100 kt nuclear explosion, 48 hours after the detonation. Time integrated concentrations in Bq h m^{-3} above and total deposition in Bq m^{-3} in the bottom.

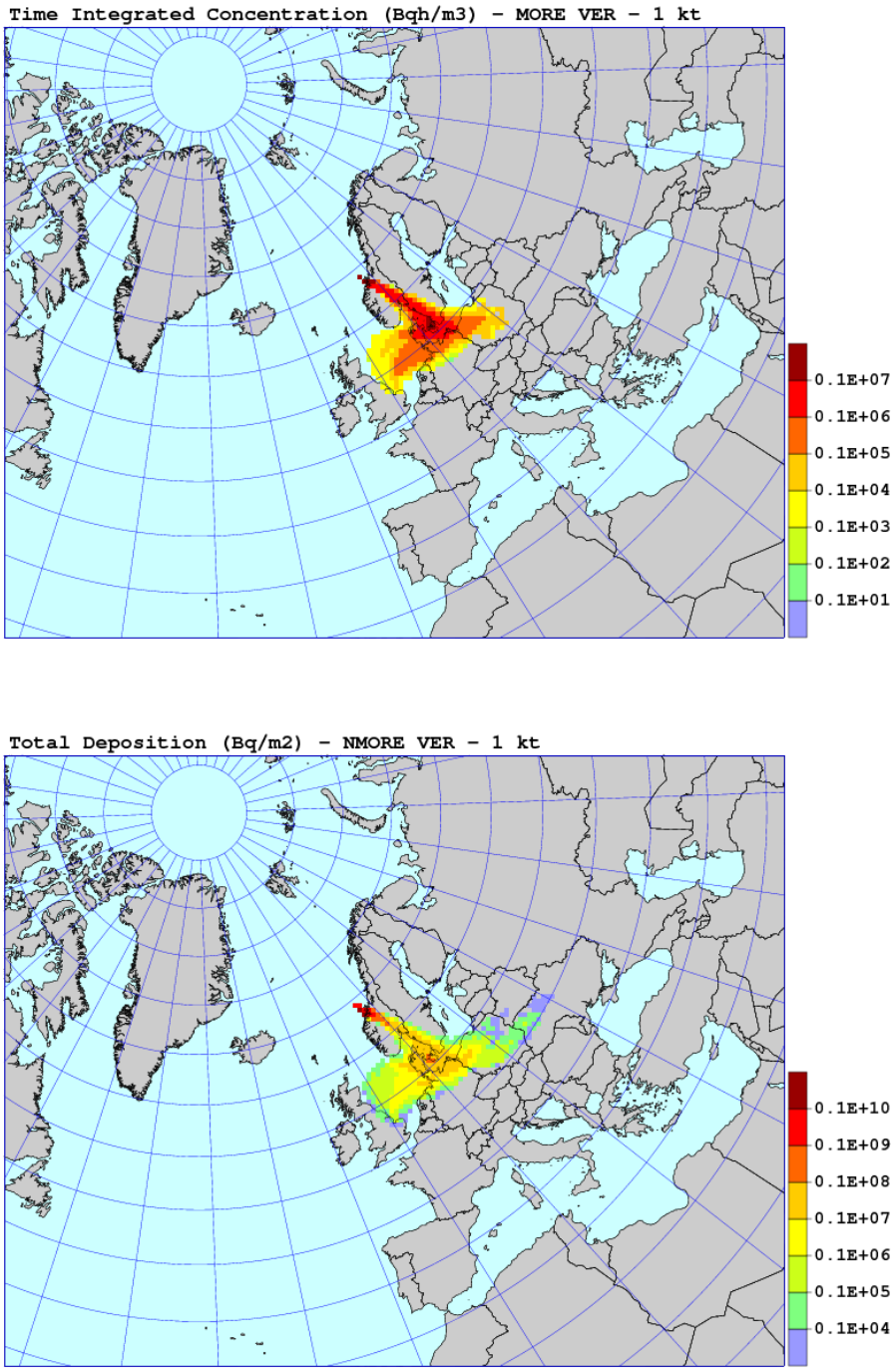

Figure 97: The results of the SNAP run with enhanced vertical diffusion for 1 kt nuclear explosion, 48 hours after the detonation. Time integrated concentrations in Bq h m^{-3} above and total deposition in Bq m^{-3} in the bottom.

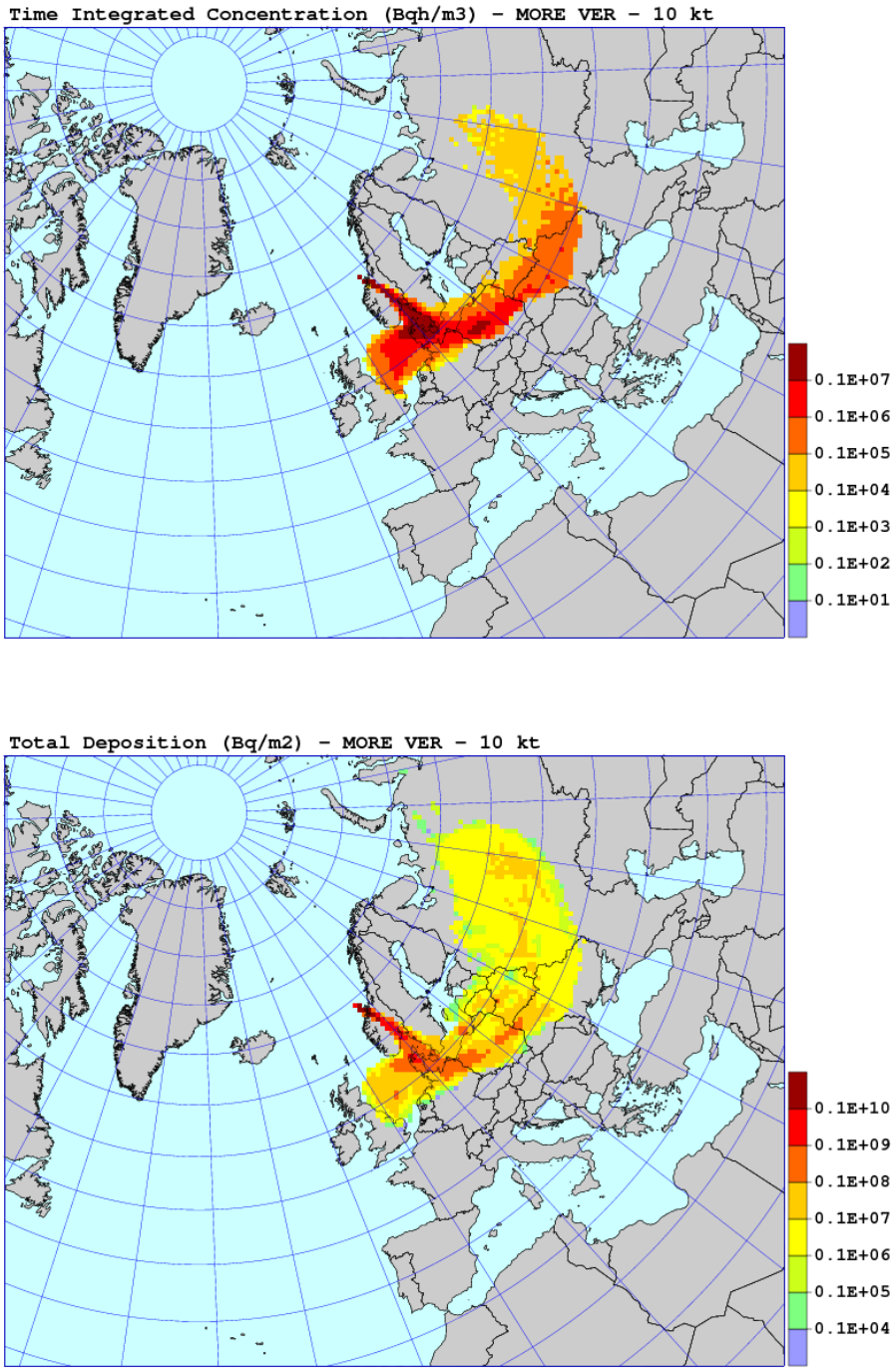

Figure 98: The results of the SNAP run with enhanced vertical diffusion for 10 kt nuclear explosion, 48 hours after the detonation. Time integrated concentrations in Bq h m^{-3} above and total deposition in Bq m^{-3} in the bottom.

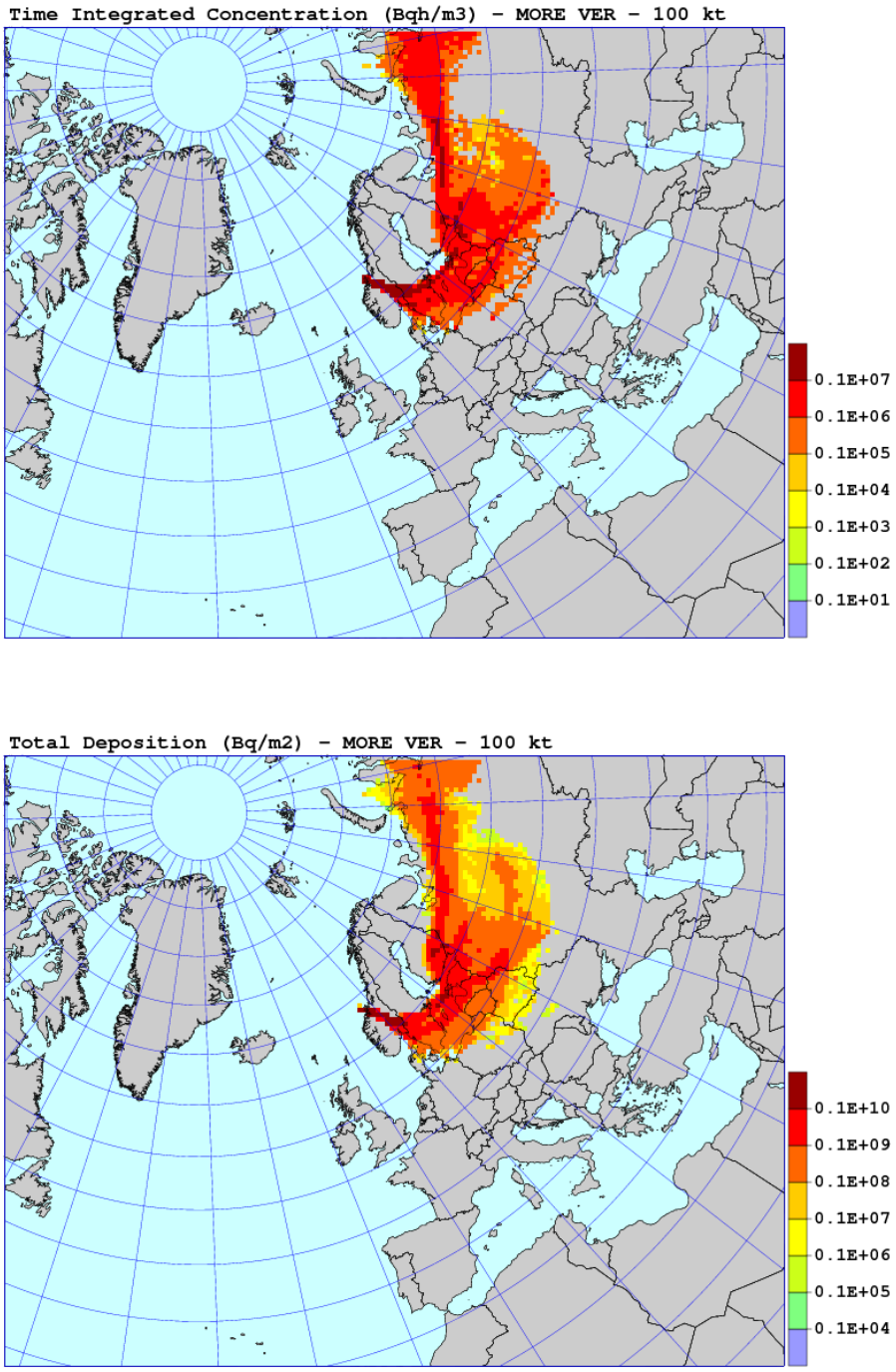

Figure 99: The results of the SNAP run with enhanced vertical diffusion for 100 kt nuclear explosion, 48 hours after the detonation. Time integrated concentrations in Bq h m^{-3} above and total deposition in Bq m^{-3} in the bottom.

6.7. Sensitivity to total diffusion

Sensitivity to total diffusion was tested in the model run without both horisontal and vertical diffusion. The maps of time integrated concentration and total deposition for 1 kt, 10 kt and 100 kt explosion are shown in Fig. 100, 101 and 102, respectively. There are large differences between these maps and corresponding maps from the standard run. In the run without horisonatal and vertical diffusion at the same time, the plume is very narrow and the values in the centre of it high. This especially applies to the maps of time integrated concentrations, for all selected explosive yields.

Time integrated concentrations and deposition in the model grid cell where the city of Oslo is located are shown in Table 53 for the model run without horisontal and vertical diffusion, 48 hours after the detonation. Except for deposition from 1 kt explosion, all values of time integrated concentration and deposition are higher in the sensitivity run than in the standard run.

Table 53: Time integrated concentrations and deposition, 48 hours after the start of release, in the model grid cell where the city of Oslo is located. Results of the model run without both horisontal and vertical diffusion.

Explosive yield (kt	Time integrated concentration (Bq h m^{-3})	Total deposition (Bq m^{-2})
1 kt	0.58E+06	0.31E+07
10 kt	0.25E+07	0.64E+09
100 kt	0.67E+07	0.18E+10

Sensitivity measures for the run without horisontal and vertical diffusion are shown in Table 54. These measures are relatively high, higher than corresponding measures for the runs without horisontal and without vertical diffusion separately.

Table 54: Sensitivity measures as defined in Eqs. (29) - (32), for the run without both horisontal and vertical diffusion.

Explosive yield	SDF	SCF	SDG	SCG
1 kt	204.5	481.9	-65.1	-19.3
10 kt	196.9	253.1	27.1	48.4
100 kt	172.8	396.7	47.0	145.3

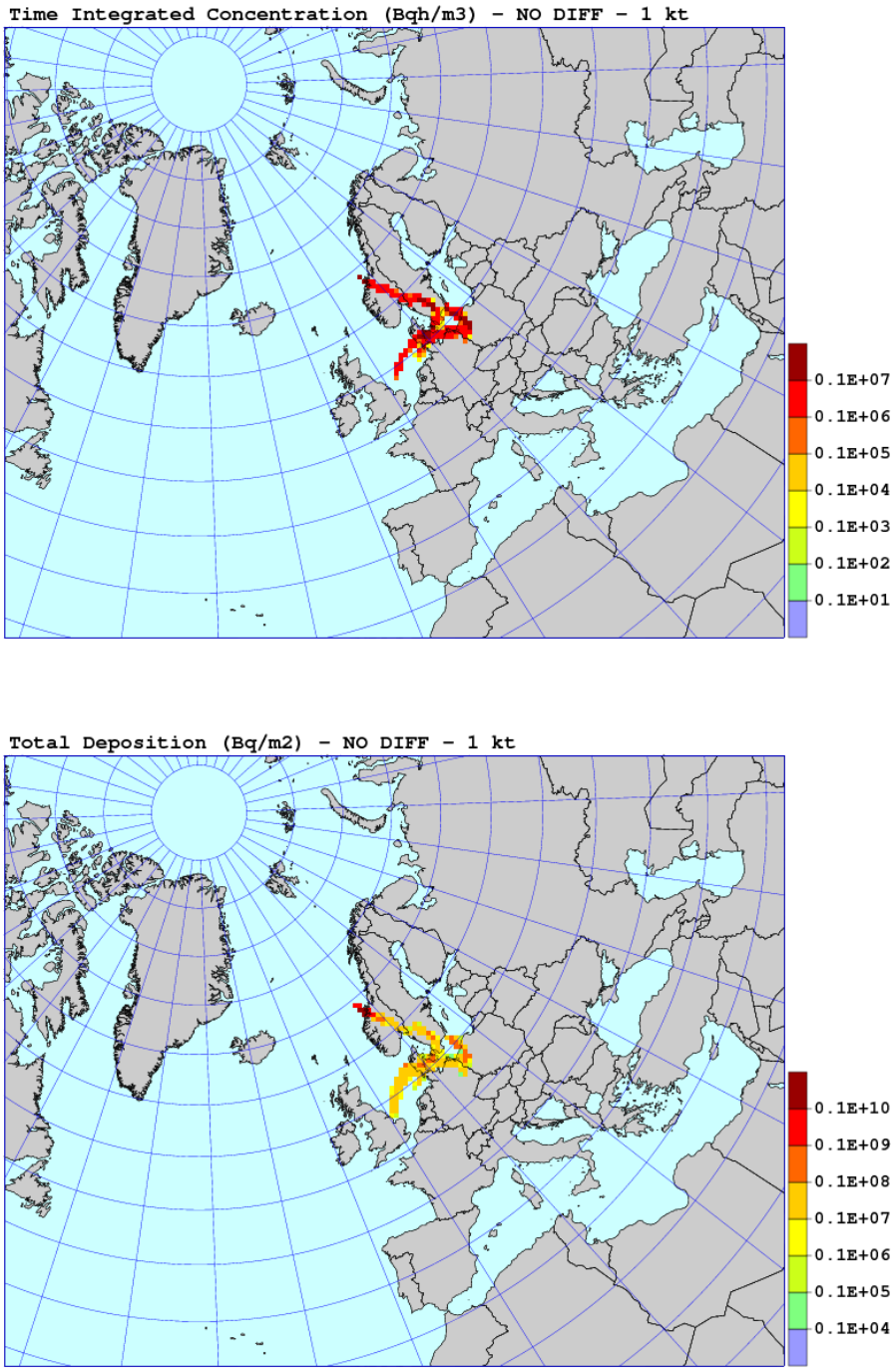

Figure 100: The results of the SNAP run without horisontal and vertical diffusion for 1 kt nuclear explosion, 48 hours after the detonation. Time integrated concentrations in Bq h m^{-3} above and total deposition in Bq m^{-3} in the bottom.

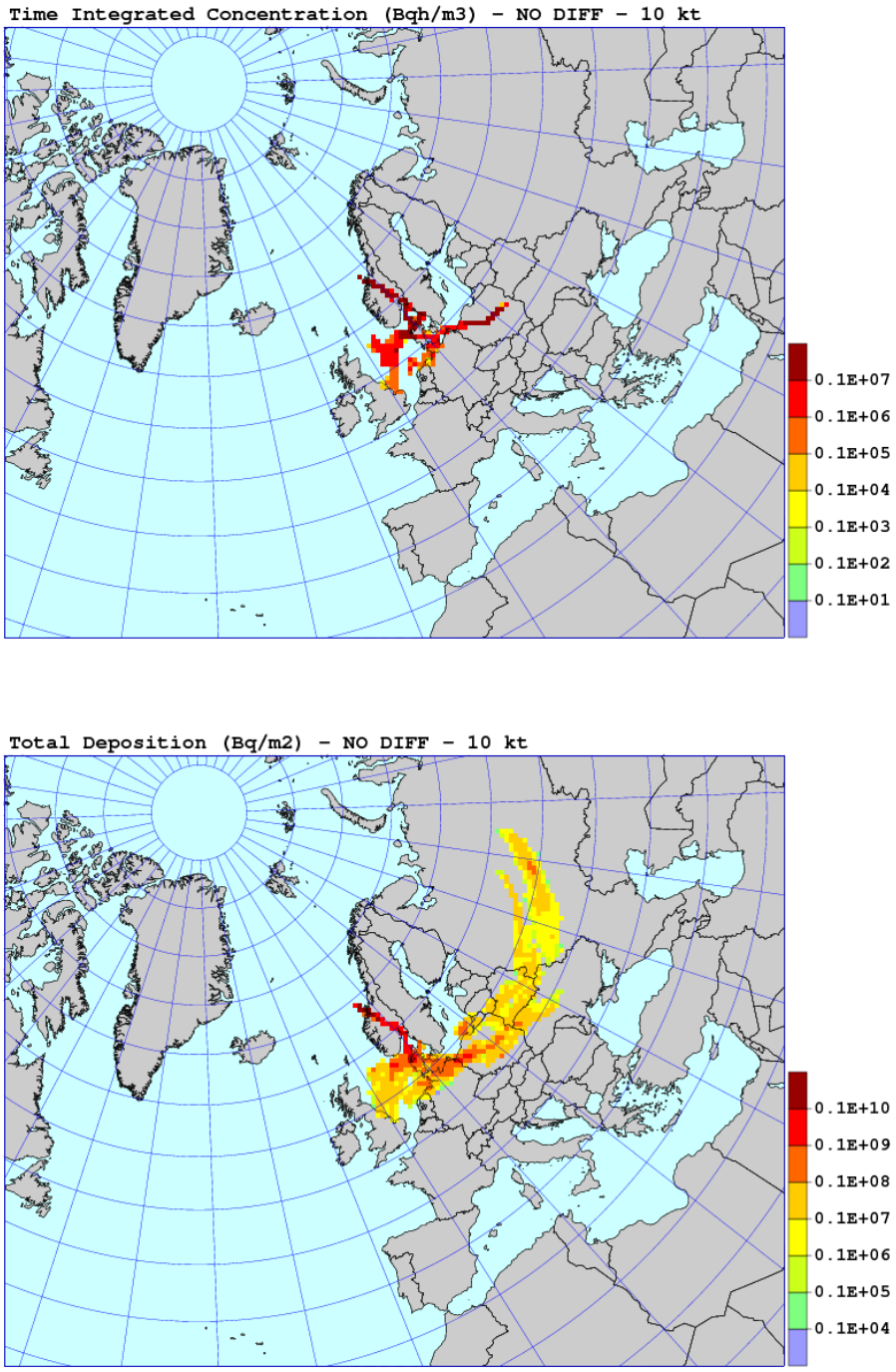

Figure 101: The results of the SNAP run without horisontal and vertical diffusion for 10 kt nuclear explosion, 48 hours after the detonation. Time integrated concentrations in Bq h m^{-3} above and total deposition in Bq m^{-3} in the bottom.

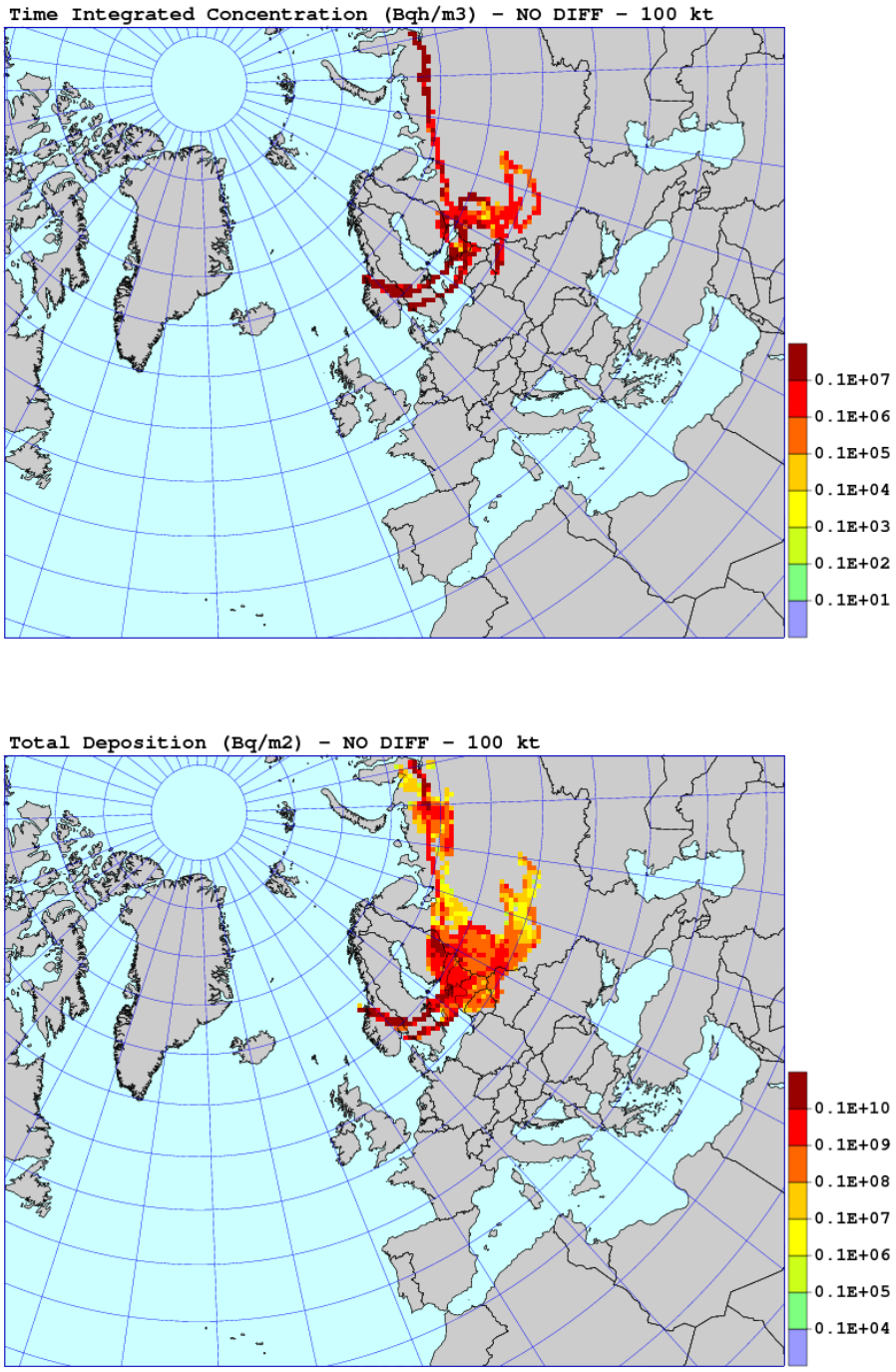

Figure 102: The results of the SNAP run without horisontal and vertical diffusion for 100 kt nuclear explosion, 48 hours after the detonation. Time integrated concentrations in Bq h m^{-3} above and total deposition in Bq m^{-3} in the bottom.

6.8. Sensitivity to the number of model particles

Also in the case of nuclear explosion, the number of model particles decides about the accuracy of the approximation of the model equations. The accuracy of the model results increases with the number of model particles and it should be as large as possible for simulating nuclear explosion. In the standard model run, the number of model particles was set to 200 000. In the sensitivity tests we have tried the following numbers of model particles: 20 000, 50 000, 400 000 and 800 000.

The results of sensitivity runs with different number of the model particles are shown in Fig. (103) - (114), for all selected explosive yields. For 1 kt explosion, differences between standard runs and test runs are small for arbitrary number of model particles. This is true, both for time integrated concentration and deposition. Only for model run with the smallest number of model particles - 20 000 the differences are slightly more visible. Compared to 1 kt explosion, the differences between the standard run and test run are slightly larger for 10 kt explosion. However, this mainly applies to model runs with 20 000 particles and 50 000 particles, both for time integrated concentration and deposition. For the test runs with 400 000 and 800 000 model particles, the differences are very small again. In case of 100 kt explosion, small differences can be noticed for the model runs with minimum number of model particles - 20 000 and maximum number of model particles - 800 000. These differences are mostly visible in the fields of time integrated concentration for the run with 20 000 model particles and in both fields for the run with 800 000 model particles.

The results of the SNAP runs, as time integrated concentrations and deposition, for different numbers of model particles are summarised in Table 55 in the model grid square where the city of Oslo is located. The results are shown 48 hours after the detonation. For the model test runs with the number of model particles larger than standard, the differences between the results are small, both for time integrated concentration and deposition. The differences between time integrated concentration and deposition in the standard run and in the all test runs are also relatively small for 1 kt explosion. The same applies to 10 kt explosion, but only for time integrated concentration. The largest differences between the standard run and test runs can be noticed for 100 kt explosion and the model run with the number of model particles reduced to 20 000, both for time integrated concentration and deposition.

Sensitivity measures as defined in Eq. (29) - (32), for the SNAP runs with different number of model particles and for selected explosive yields are given in Table 56. For global measures (SDF and SCF) there is a clear declining tendency with the number of model particles, which agrees well with the expectations. The largest values can be noticed for the runs with the lowest number of model particles - 20 000, for all tested explosive yields. In general, the sensitivity measures for the number of model particles are lower than for other sensitivity tests.

Table 55: Time integrated concentrations and deposition, 48 hours after the detonation, in the model grid cell where the city of Oslo is located. Results of the model runs with different number of model particles (N), for all selected explosive yields. Values for the standard run are highlighted. Units for time integrated concentration: Bq h m^{-3} and for deposition: Bq m^{-2}.

N	1 kt	10 kt	100 kt
Time integrated concentration			
20 0000	0.70E+06	0.16E+07	0.41E+07
50 0000	0.73E+06	0.17E+07	0.21E+07
200 000	**0.72E+06**	**0.17E+07**	**0.27E+07**
400 000	0.74E+06	0.17E+07	0.27E+07
800 000	0.72E+06	0.17E+07	0.27E+07
Deposition			
20 0000	0.93E+07	0.46E+09	0.18E+10
50 0000	0.93E+07	0.40E+09	0.12E+10
200 000	**0.88E+07**	**0.50E+09**	**0.12E+10**
400 000	0.90E+07	0.41E+09	0.11E+10
800 000	0.89E+07	0.50E+09	0.12E+10

Table 56: Sensitivity measures as defined in Eq. (29) - (32), for the SNAP runs with different number of model particles (N) and for selected explosive yields.

N	SDF	SCF	SDG	SCG
1 kt yield				
20 000	11.6	23.1	5.0	-2.6
50 000	5.3	16.6	5.9	1.4
400 000	5.5	9.4	1.5	2.3
800 000	4.7	8.0	0.8	0.6
10 kt yield				
20 000	173.0	46.8	-8.6	-7.3
50 000	13.4	27.3	-19.8	-1.1
400 000	10.1	14.2	-19.4	-0.1
800 000	9.4	13.5	-19.4	0.3
100 kt yield				
20 000	55.5	80.9	47.2	51.3
50 000	24.8	53.2	-6.1	-22.7
400 000	19.2	25.2	-8.1	1.2
800 000	19.3	29.8	-4.4	-1.0

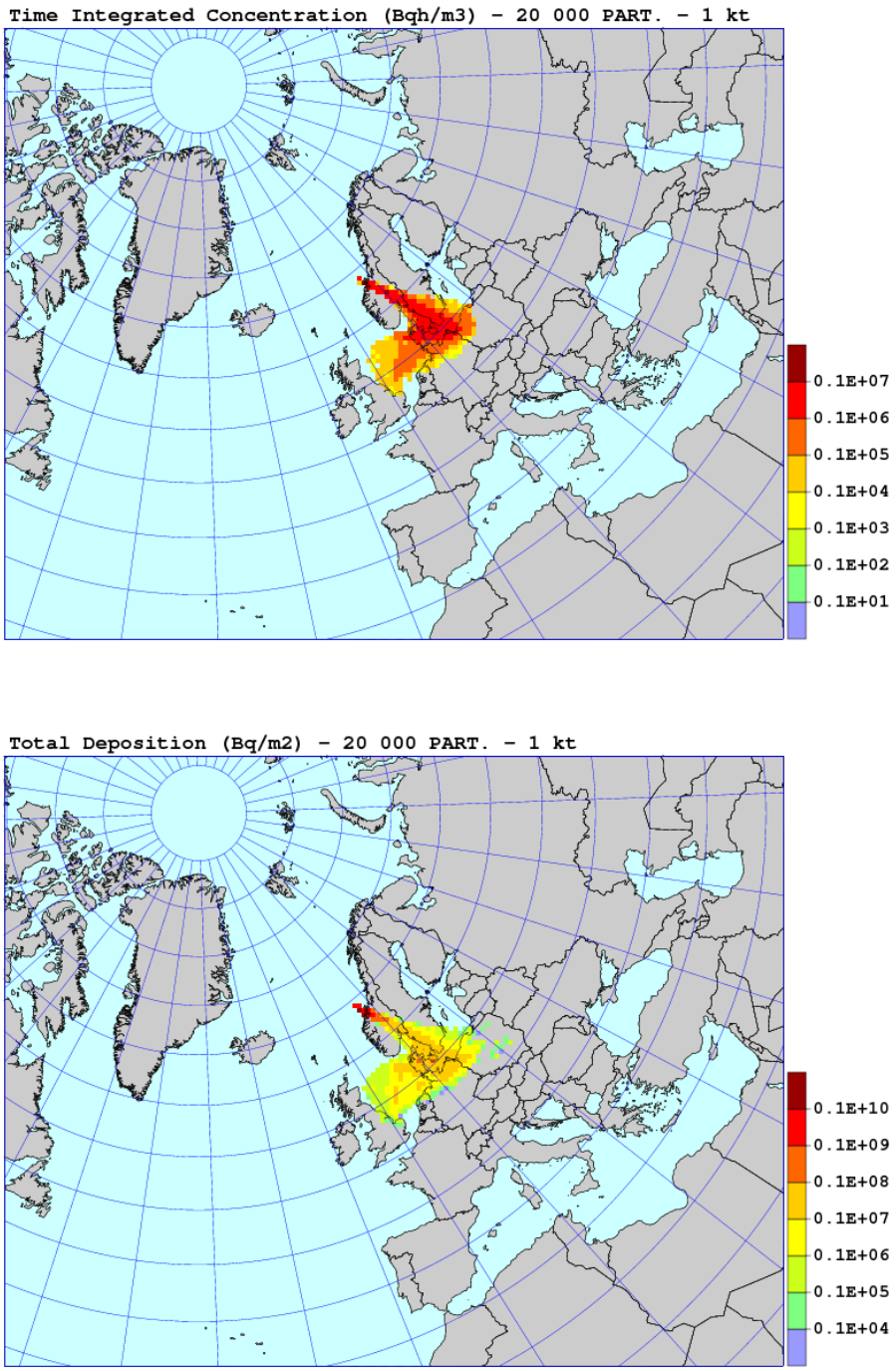

Figure 103: The results of the sensitivity run with 20 000 model particles. Maps of time integrated concentrations and total deposition for 1 kt nuclear explosion.

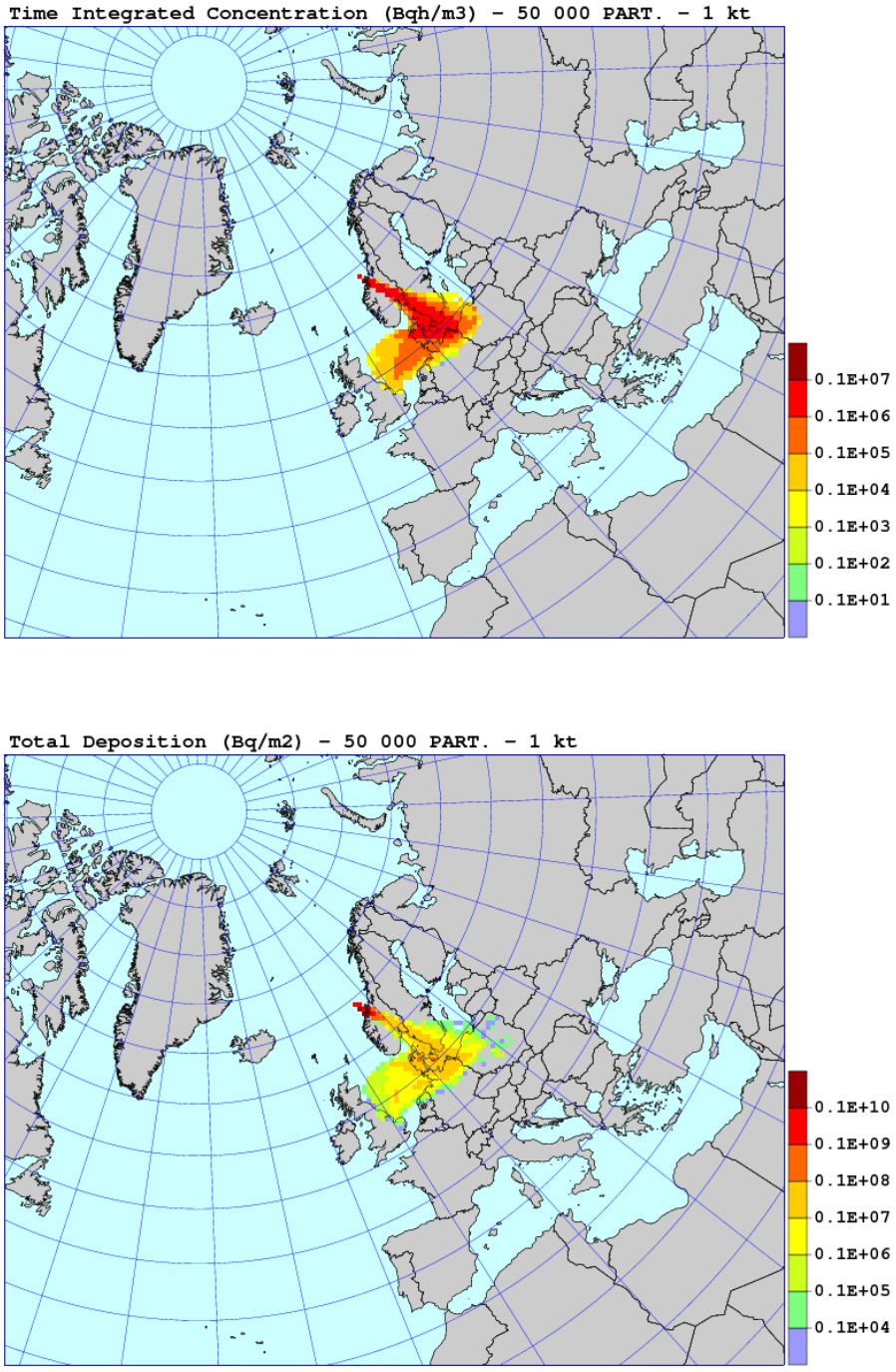

Figure 104: The results of the sensitivity run with 50 000 model particles. Maps of time integrated concentrations and total deposition for 1 kt nuclear explosion.

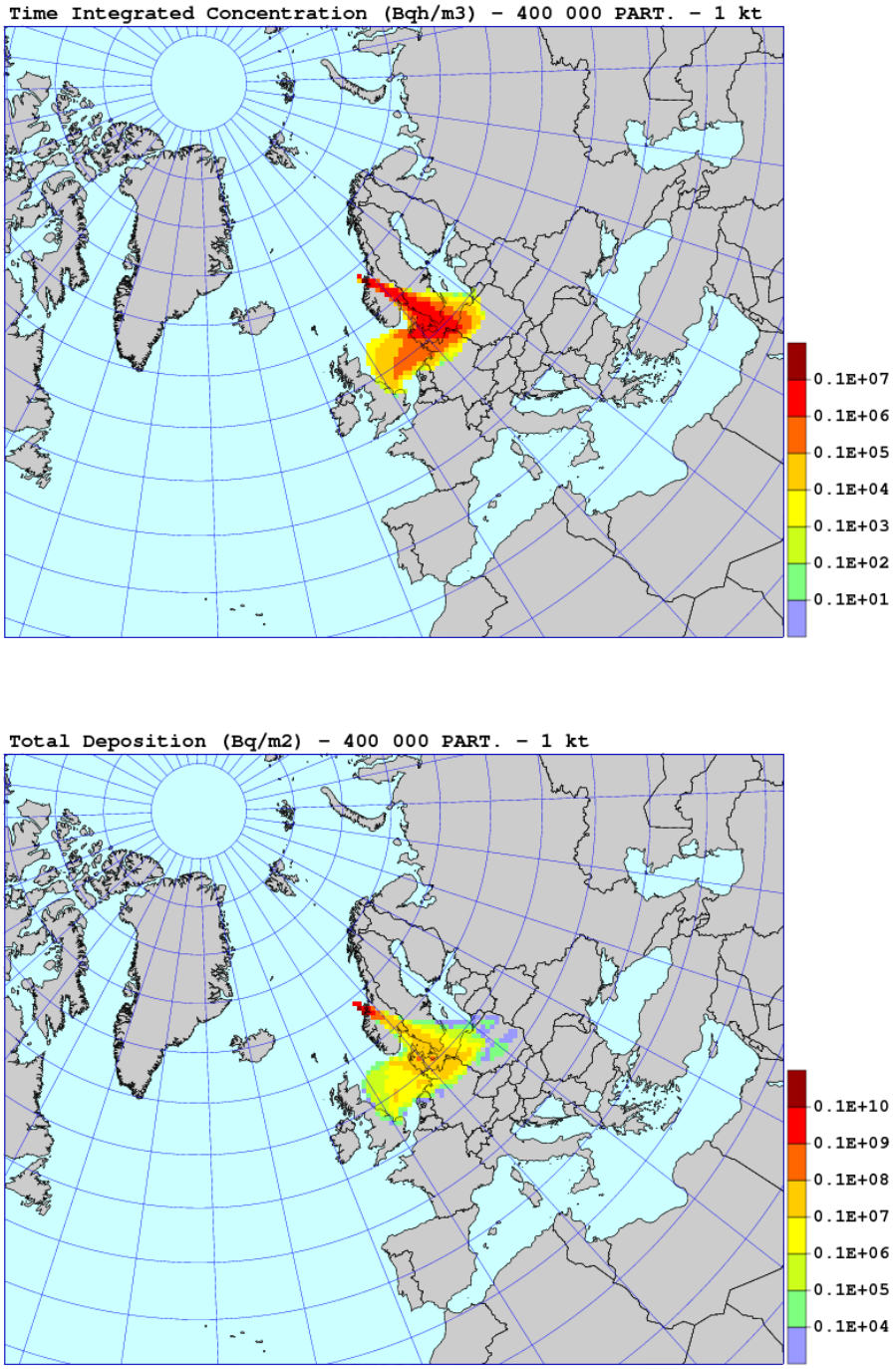

Figure 105: The results of the sensitivity run with 400 000 model particles. Maps of time integrated concentrations and total deposition for 1 kt nuclear explosion.

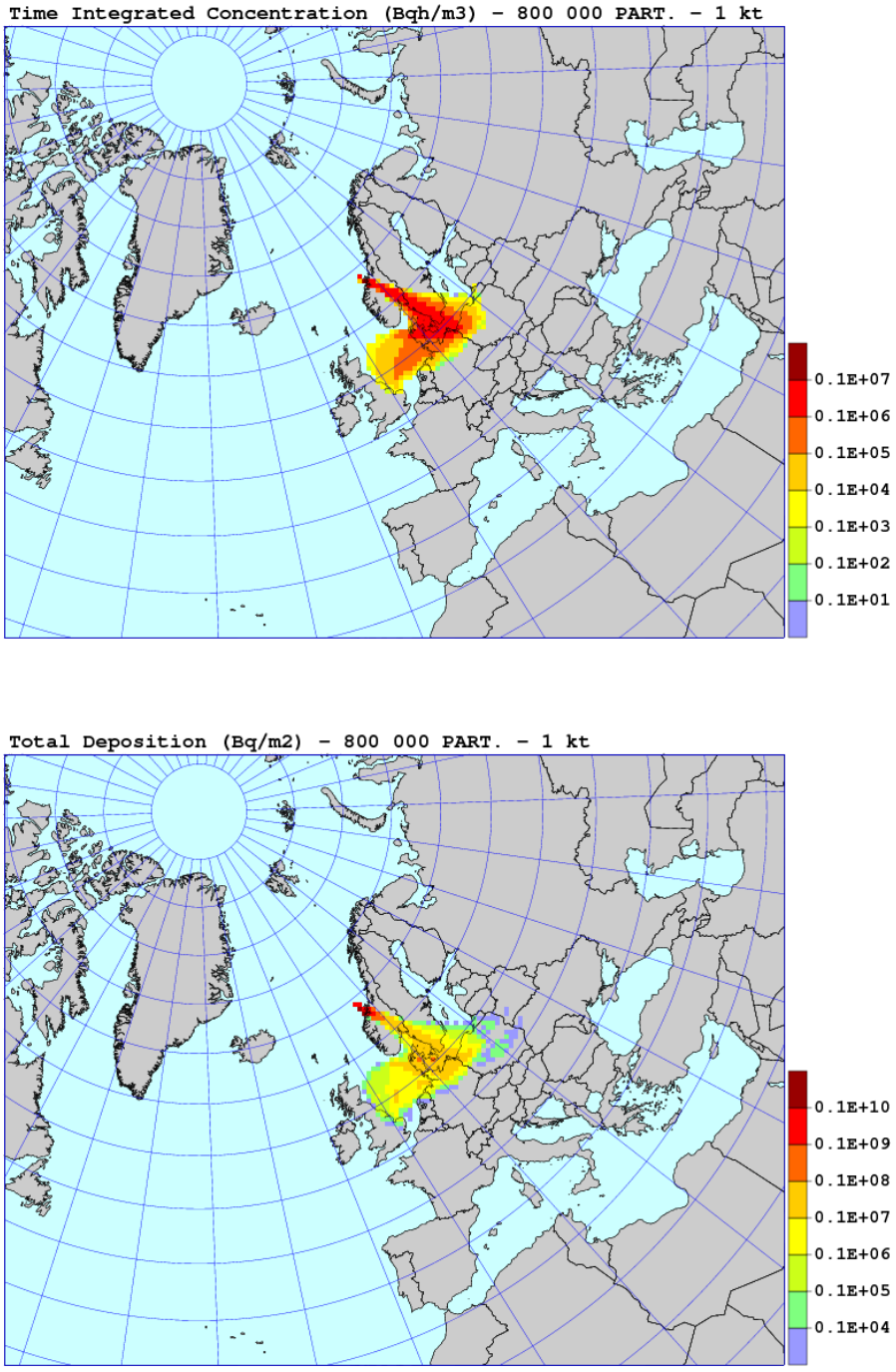

Figure 106: The results of the sensitivity run with 800 000 model particles. Maps of time integrated concentrations and total deposition for 1 kt nuclear explosion.

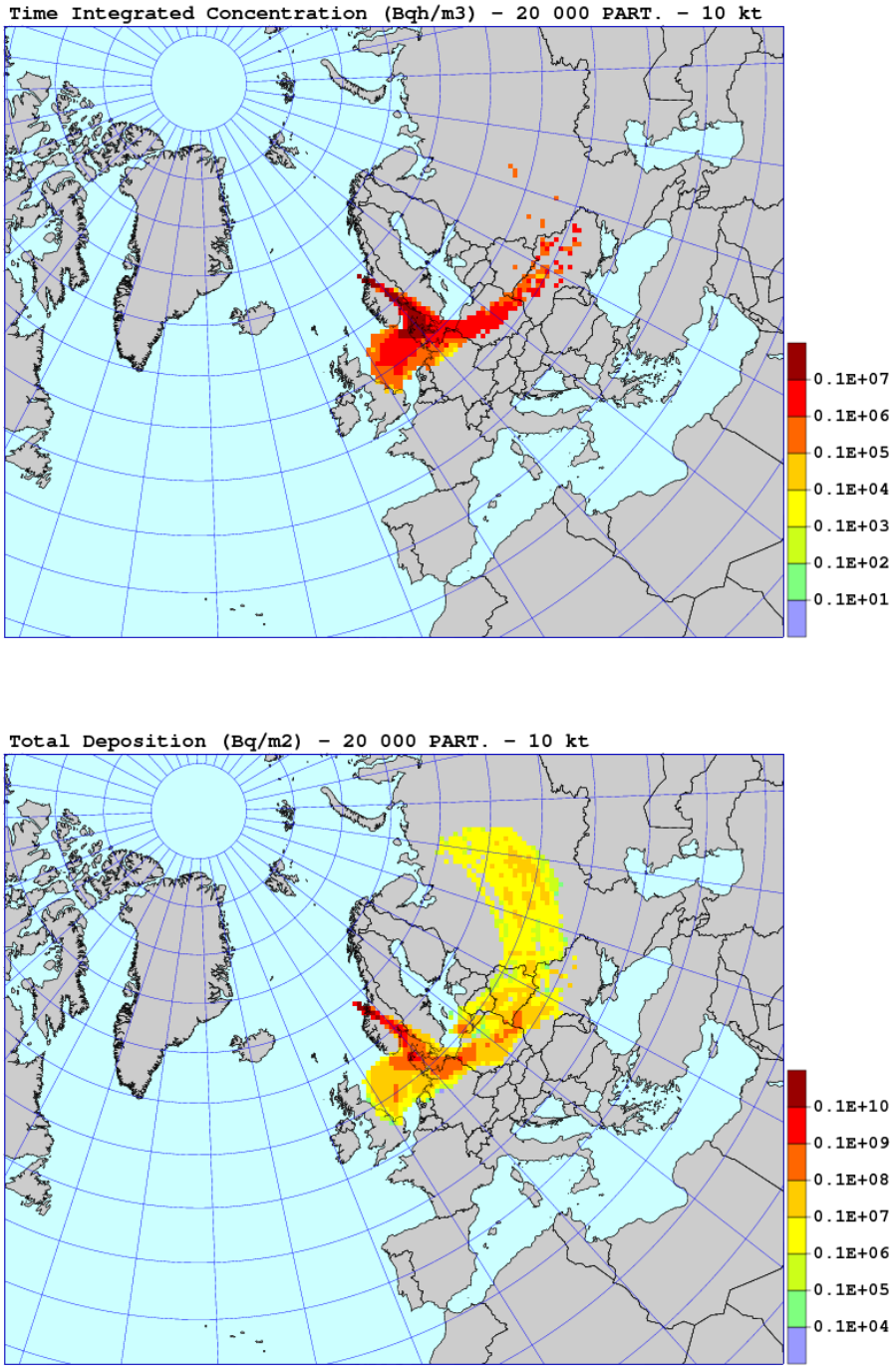

Figure 107: The results of the sensitivity run with 20 000 model particles. Maps of time integrated concentrations and total deposition for 10 kt nuclear explosion.

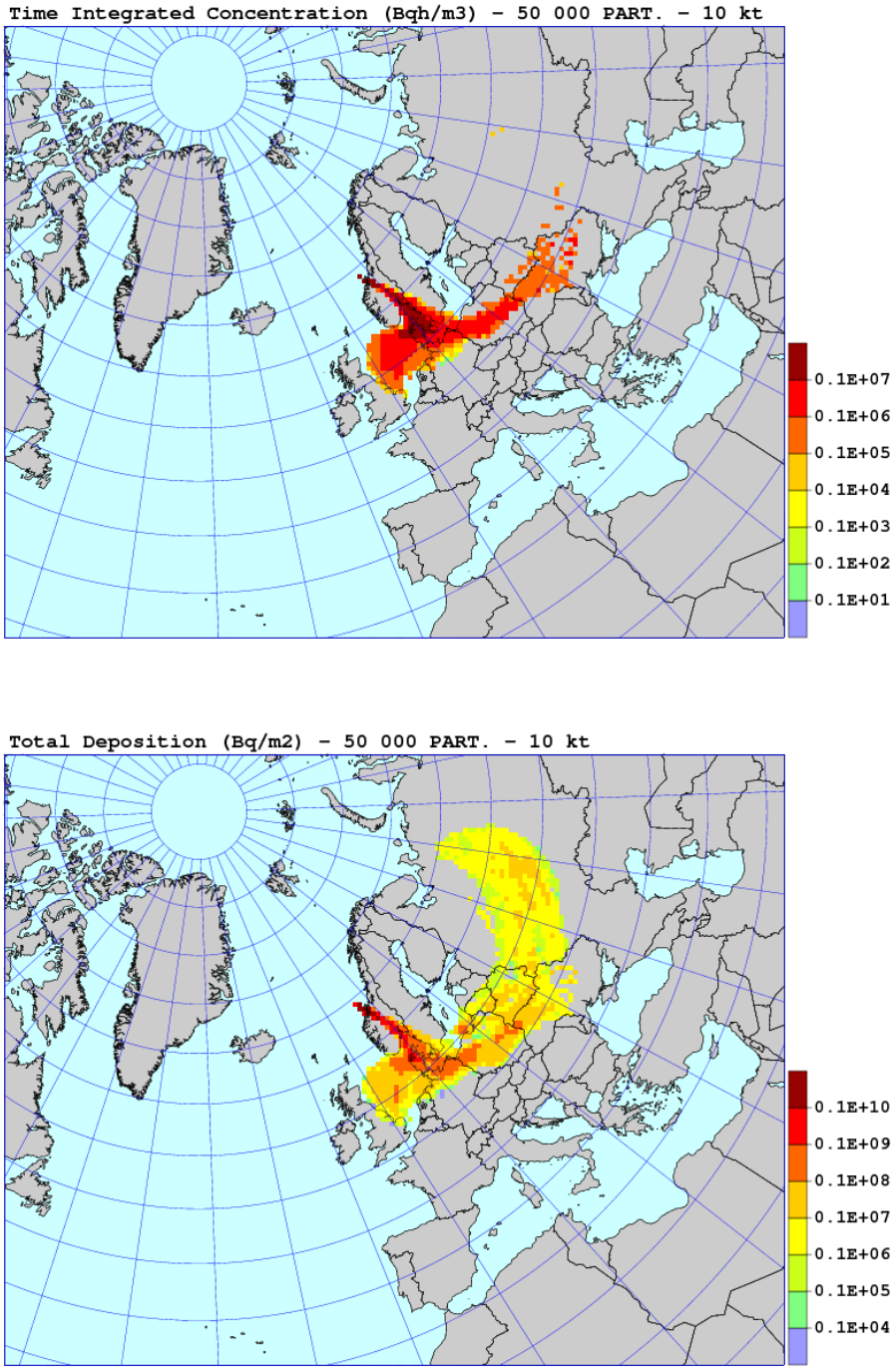

Figure 108: The results of the sensitivity run with 50 000 model particles. Maps of time integrated concentrations and total deposition for 10 kt nuclear explosion.

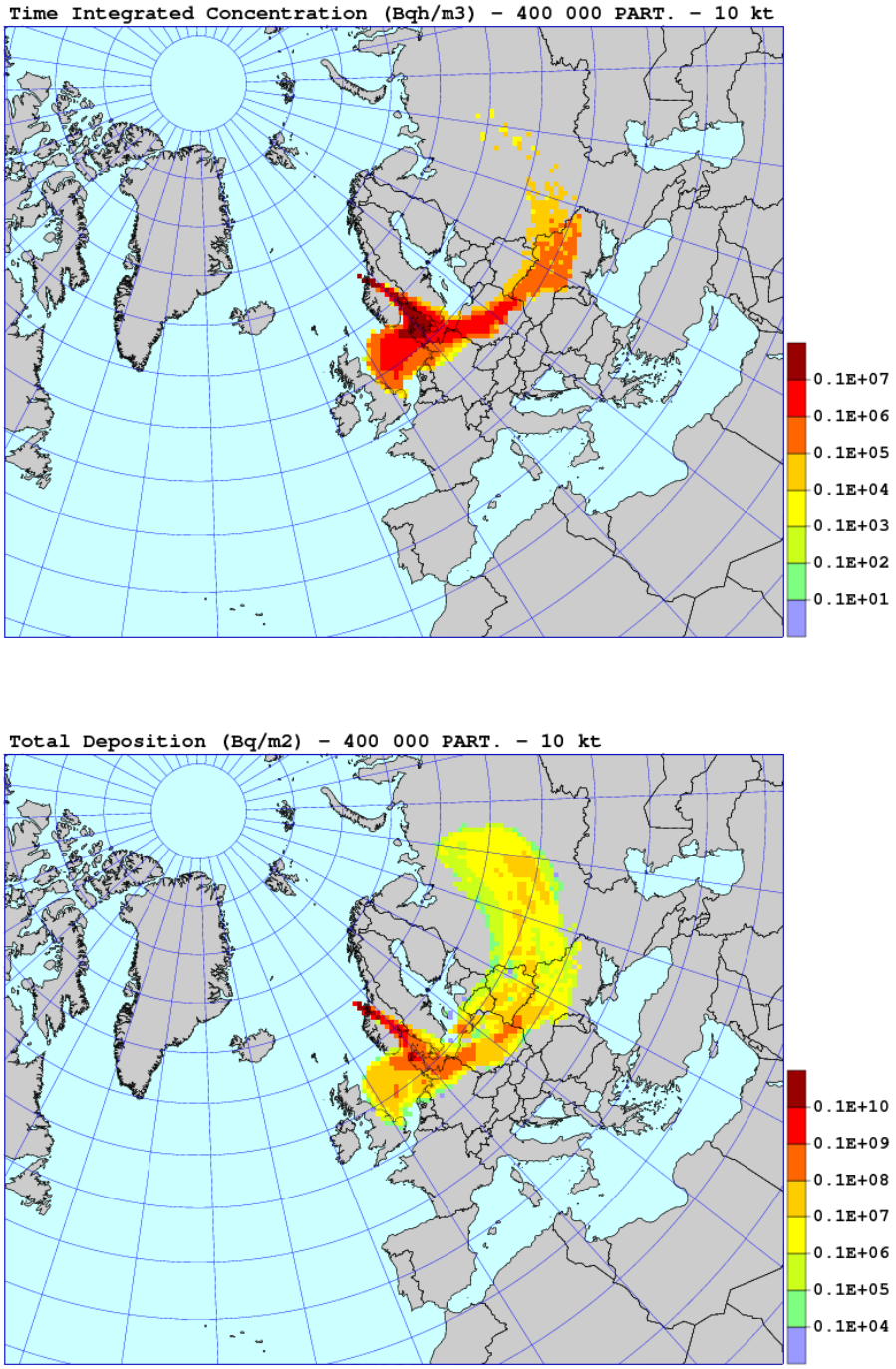

Figure 109: The results of the sensitivity run with 400 000 model particles. Maps of time integrated concentrations and total deposition for 10 kt nuclear explosion.

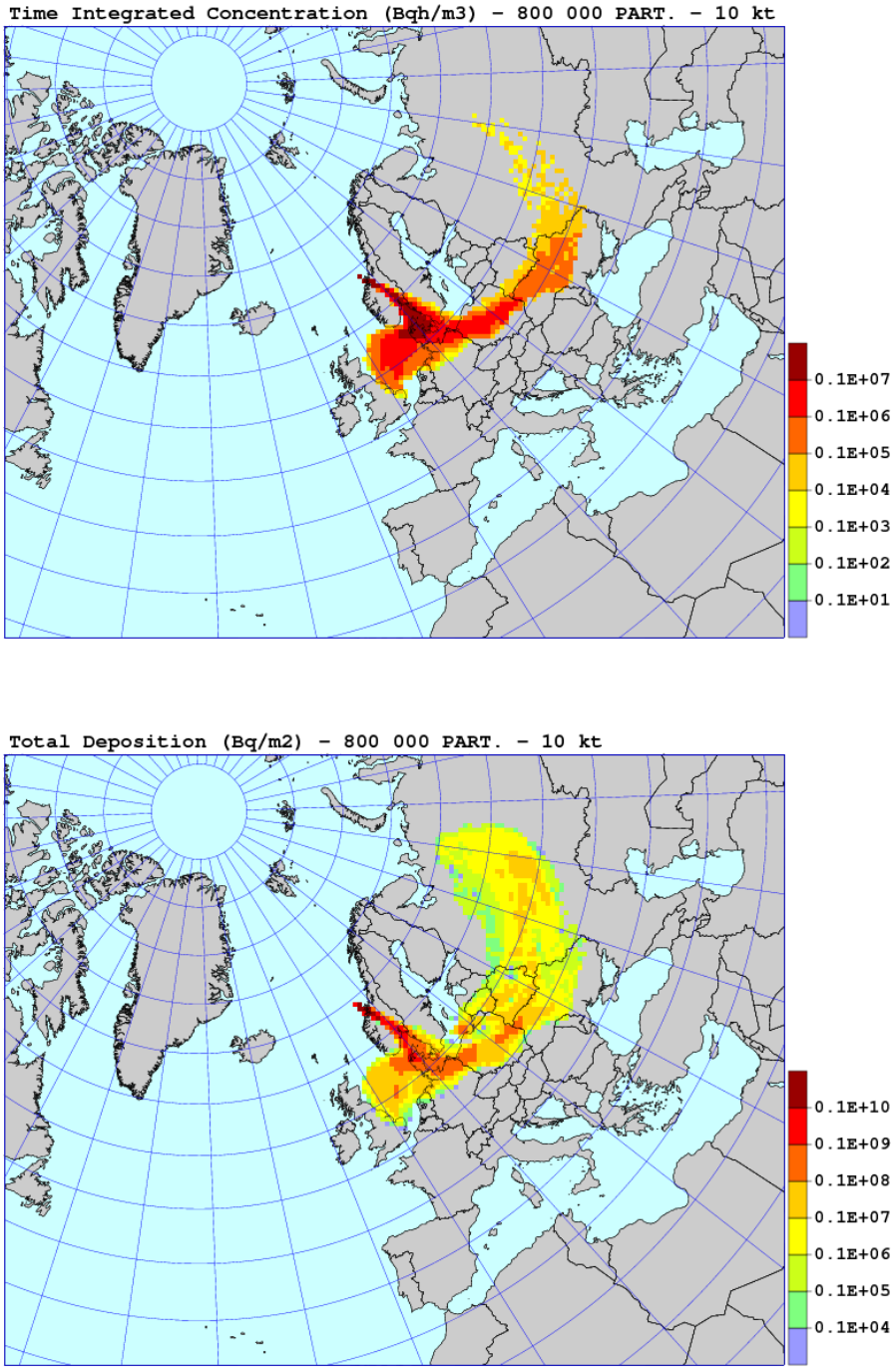

Figure 110: The results of the sensitivity run with 800 000 model particles. Maps of time integrated concentrations and total deposition for 10 kt nuclear explosion.

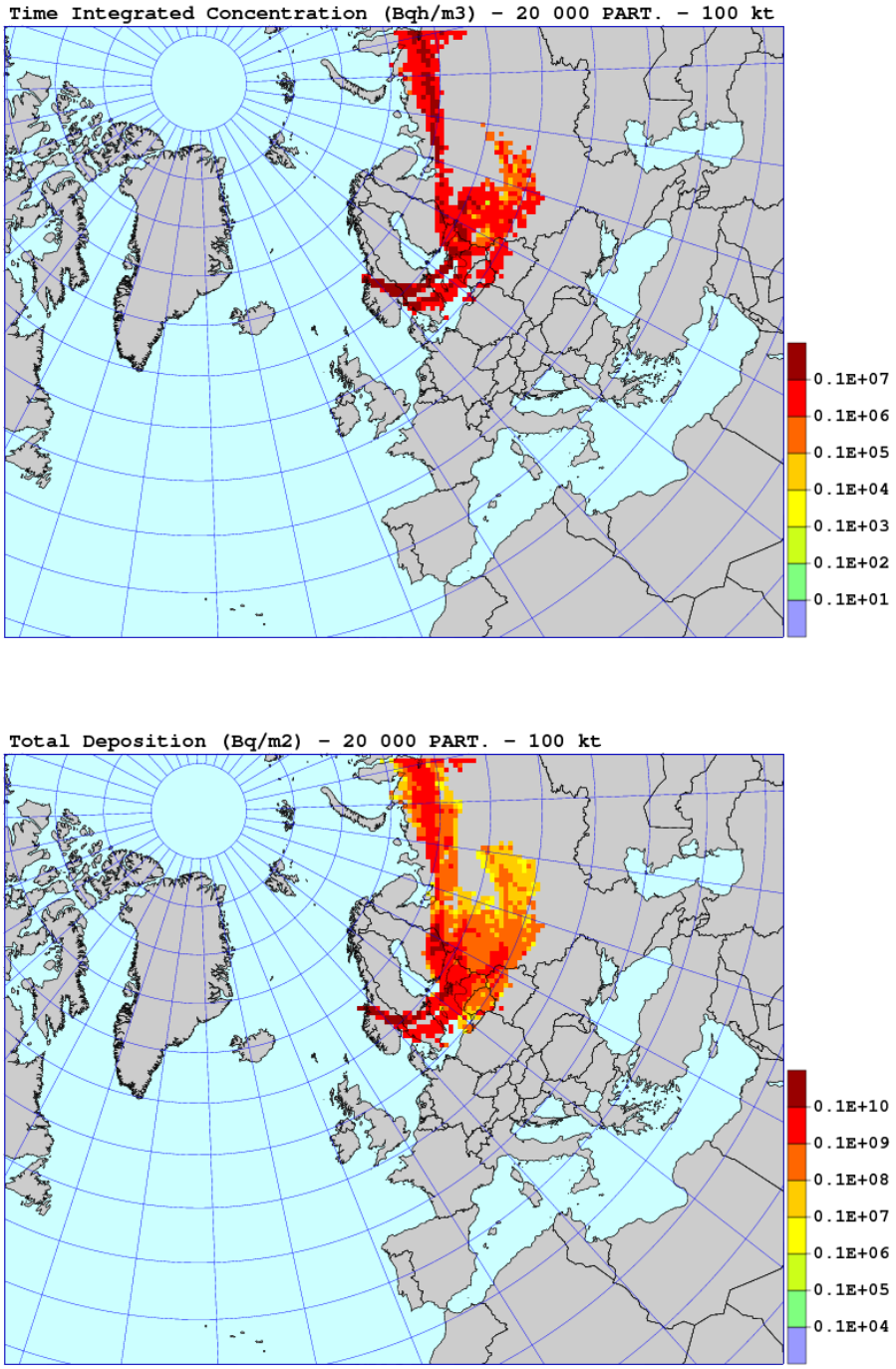

Figure 111: The results of the sensitivity run with 20 000 model particles. Maps of time integrated concentrations and total deposition for 100 kt nuclear explosion.

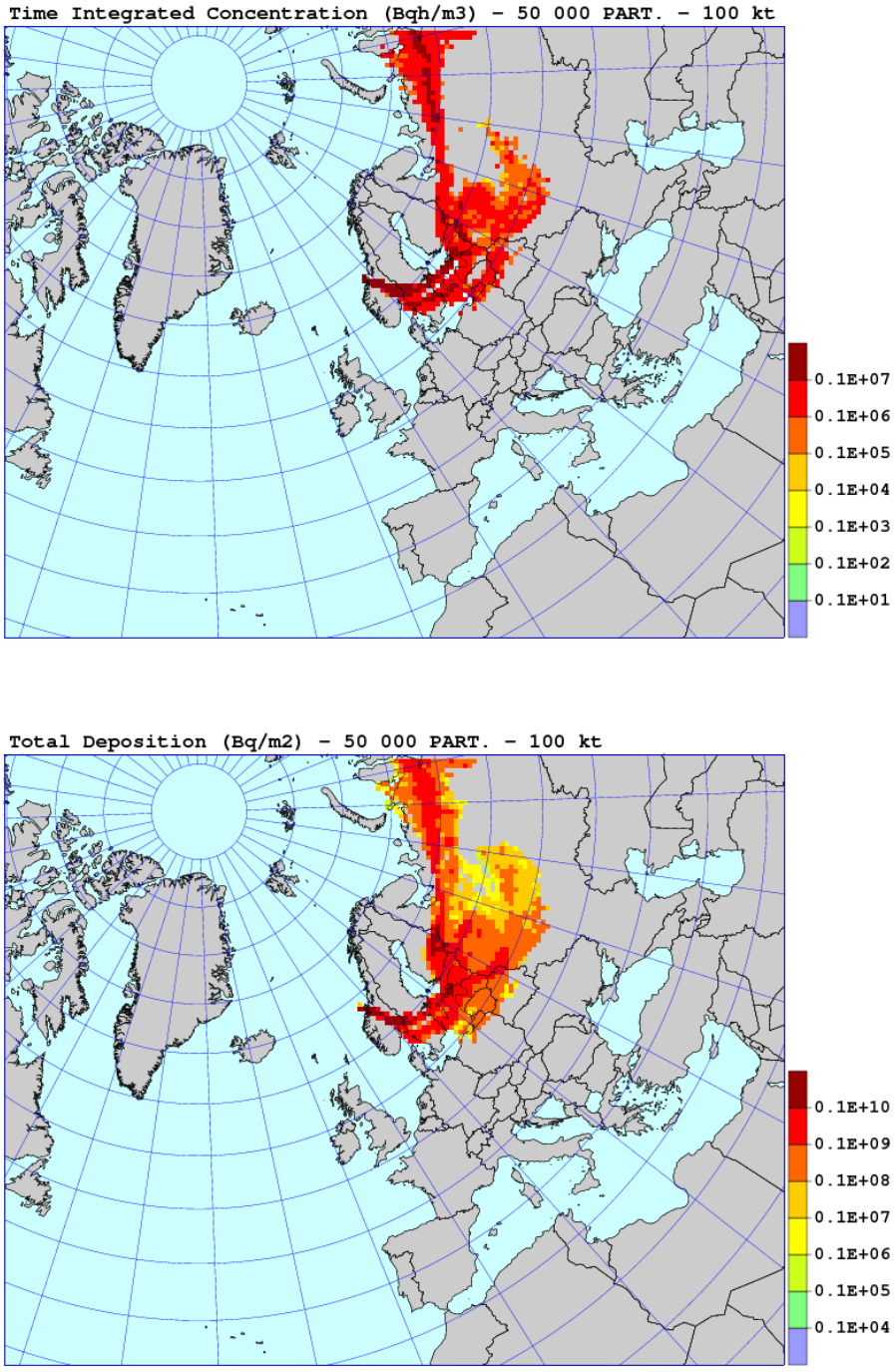

Figure 112: The results of the sensitivity run with 50 000 model particles. Maps of time integrated concentrations and total deposition for 100 kt nuclear explosion.

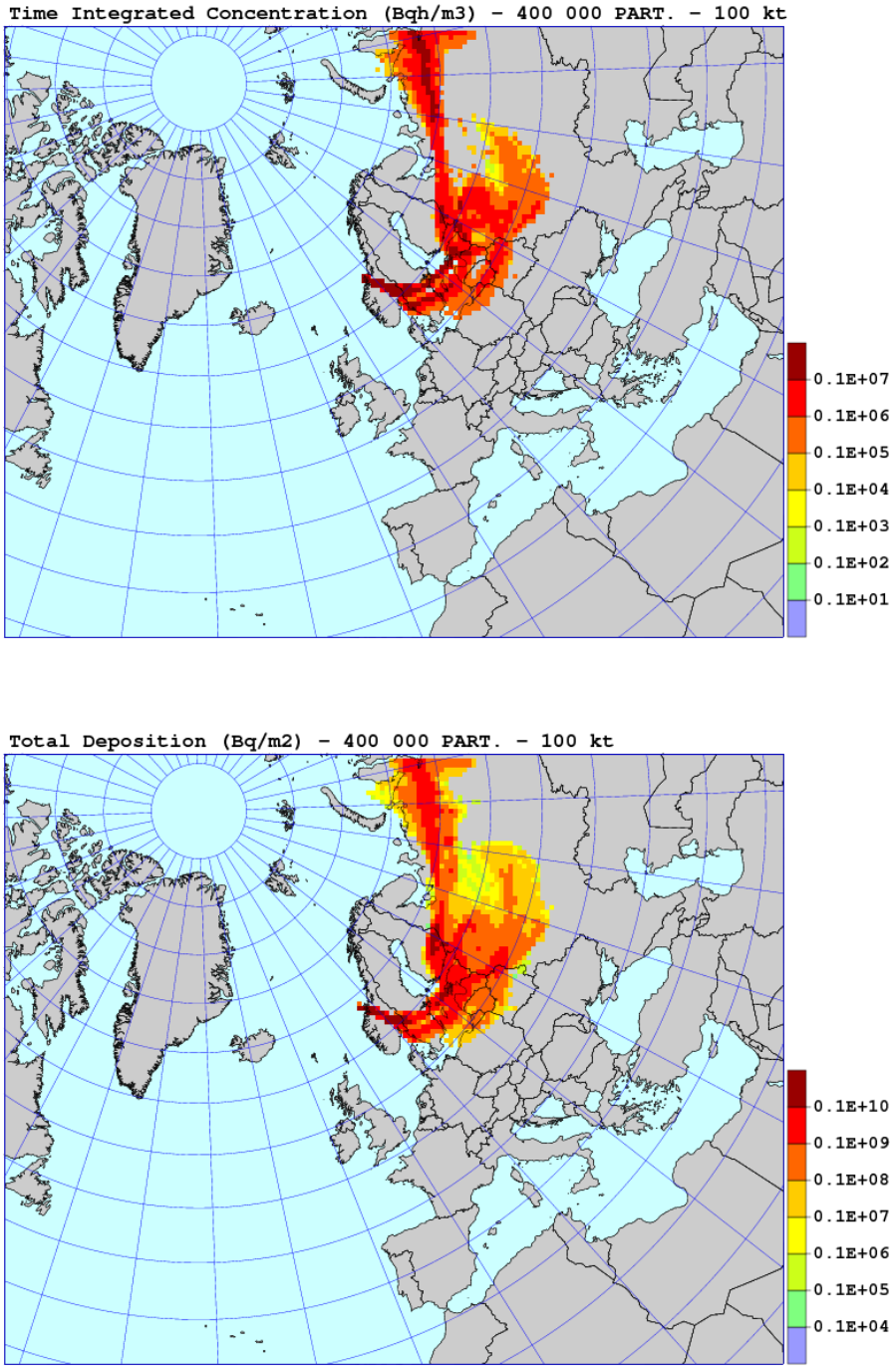

Figure 113: The results of the sensitivity run with 400 000 model particles. Maps of time integrated concentrations and total deposition for 100 kt nuclear explosion.

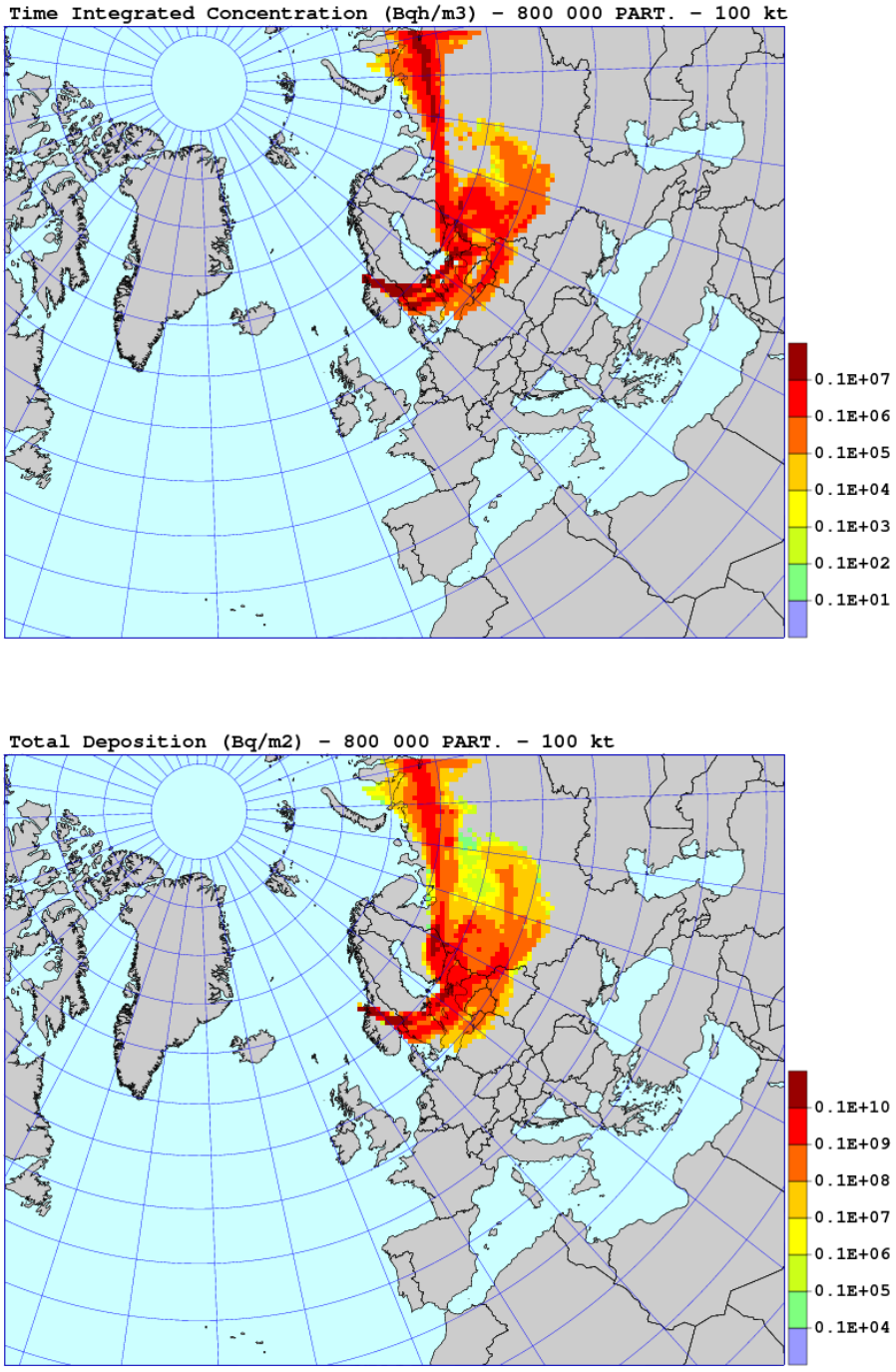

Figure 114: The results of the sensitivity run with 800 000 model particles. Maps of time integrated concentrations and total deposition for 100 kt nuclear explosion.

6.9. Sensitivity ranking for nuclear explosion

Sensitivity ranking for nuclear explosion was based on the comparison of sensitivity measures, as well as on the comparison of the maps with time integrated concentration and deposition, in relation to the standard run. The sensitivity measures for selected test runs are given in Table 57 for 1 kt, 10 kt and 100 kt explosions. The most interesting in these Tables are the global sensitivity measures: SDF - for total deposition and SCF - for time integrated concentration.

The model sensitivity of calculated total deposition to different processes varies slightly for different explosive yields, but a relatively clear general pattern for all explosive yields can be found. The sensitivity ranking for total deposition is the following: 1) wet deposition, 2) gravitational settling and 3) diffusion and especially vertical diffusion. The model sensitivity to the number of model particles used in the simulation is relatively very low with only slightly higher sensitivity in case of the lowest number of model particles used - 20 000.

The model sensitivity of calculated time integrated concentration to different processes also varies for different explosive yields, more than in the case of total deposition. However, also for time integrated concentration, a general pattern for all explosive yields can be seen. The calculated time integrated concentration is the most sensitive to 1) diffusion and slightly less to 2) gravitational settling and 3) wet deposition. Sensitivity to dry deposition is much lower, as well as sensitivity to the number of model particles used.

Sensitivity of the SNAP model was also estimated by comparing the maps of total deposition and time integrated concentration for the standard run and the test runs. Also in this comparison a general pattern can be found for all explosive yields. The visual comparison of total deposition and time integrated concentration indicates that the SNAP model is the most sensitive to vertical diffusion, quite sensitive to gravitational settling and wet deposition and its sensitivity to dry deposition is slightly lower. However, for larger explosive yields, model sensitivity to gravitational is much larger than for any other process. The reason is in very high altitude, above the troposphere, of many model particles in the initial distribution after explosion. For these very high located particles, gravitational settling is the only mechanism bringing them down.

If we take into account both, data in Tables **??**, **??**, **??** and the results of visual inspection of the maps, the model sensitivity ranking for application to nuclear explosion is the following:

1. Gravitational settling
2. Vertical diffusion
3. Wet deposition
4. Dry deposition
5. Number of model particles used

However, it should be mentioned that the number of model particles cannot be too low and already with 20 000 model particles used, the results are visibly different from the standard run with 200 000 model particles.

Table 57: Comparison of sensitivity measures for nuclear explosion for different sensitivity tests.

Run	SDF	SCF	SDG	SCG
1 kt explosion				
No dry dep.	289.3	15.3	-100.0	4.3
No gravity	421.0	557.4	84.2	163.9
On gravity	206.5	73.7	212.6	26.5
No wet dep.	468.3	225.3	125.4	89.3
No hor. diff.	158.7	30.7	3.4	1.0
More hor. diff.	191.9	16.9	-5.0	-4.5
No ver. diff.	56.6	317.0	-62.1	-45.8
More ver. diff.	42.7	118.7	11.5	-11.6
No diffusion	204.5	481.9	-65.1	-19.3
20 000 part.	11.6	23.1	5.0	-2.6
50 000 part.	5.3	16.6	5.9	1.4
400 000 part.	5.5	9.4	1.5	2.3
800 000 part.	4.7	8.0	0.8	0.6
10 kt explosion				
No dry dep.	173.4	29.2	-100.0	3.1
No gravity	480.9	246.1	-99.9	-97.6
On gravity	126.9	55.5	-25.4	-1.6
No wet dep.	952.7	369.7	160.6	150.8
No hor. diff.	151.0	18.8	2.6	1.8
More hor. diff.	372.1	26.3	-26.0	-4.1
No ver. diff.	188.4	216.3	22.4	43.1
More ver. diff.	163.1	159.6	-35.1	23.1
No diffusion	196.9	253.1	27.1	48.4
20 000 part.	173.0	46.8	-8.6	-7.3
50 000 part.	13.4	27.3	-19.8	-1.1
400 000 part.	10.1	14.2	-19.4	-0.1
800 000 part.	9.4	13.5	-19.4	0.3
100 kt explosion				
No dry dep.	120.4	22.1	-100.0	0.0
No gravity	477.1	209.4	-100.0	-100.0
On gravity	214.7	188.7	9.7	36.5
No wet dep.	399.9	97.1	26.2	48.9
No hor. diff.	37.2	35.4	-6.3	1.7
More hor. diff.	82.4	37.3	-16.3	-19.5
No ver. diff.	162.4	356.4	11.7	27.7
More ver. diff.	49.1	75.5	-6.9	-24.7
No diffusion	172.8	396.7	47.0	145.3
20 000 part.	55.5	80.9	47.2	51.3
50 000 part.	24.8	53.2	-6.1	-22.7
400 000 part.	19.2	25.2	-8.1	1.2
800 000 part.	19.3	29.8	-4.4	-1.0

7. Conclusions

The new version of the SNAP model for remote applications from NRPA has been developed and can be applied for simulating dispersion of radioactive debris from nuclear accident and to simulate movement of the radioactive cloud from nuclear explosion. In addition, SNAP model can be used for calculating three-dimensional trajectories from arbitrary point in the model domain. This new version has been tested on selected cases and it was also a subject of sensitivity analysis. The following conclusions can be drown from the development of the new SNAP version for remote applications from NRPA, sensitivity analysis and operational tests of the model.

- The meteorological input for the current SNAP model has been significantly improved by using meteorological input data from the operational HIRLAM model with 12 km resolution and increased grid dimension in horisontal (864×699 nodes) and in vertical (60 layers).

- In the latest SNAP version parameterisation of both, wet and dry deposition processes has been improved as well as, parameterization of vertical diffusion and gravitational settling. Also, the radioactive decay algorithm has been implemented for dry and wet deposition fields.

- The parameterisation of the source term has been improved and made more general for ARGOS applications by implementing flexible vertical and time profile options. In case of nuclear explosion, two initial shapes were tested: cylinder and mushroom, but as agreed with NRPA based on the test results, only cylinder shape will be used in remote applications.

- The list of SNAP output has been extended for remote applications from NRPA. At present, it includes: instantaneous and time integrated concentrations, wet, dry and total (wet+dry) deposition and trajectory points. The temporal resolution for output data is flexible and can be specified in the ARGOS system.

- The new model version has been tested for different source terms for nuclear accidents and nuclear explosions and for different meteorological conditions. All these tests were performed remotely from NRPA. and were successful. However, still more different operational tests are necessary, before the new SNAP model version becomes fully operational in remote applications from NRPA.

- Concerning trajectories, the model has been tested for different meteorological situations and for all of them there was no problem with calculating three-dimensional trajectories starting from the prescribed locations. It was interesting to notice a significant vertical movements of the trajectories. Some of them stating at the ground level ended up at 3000-4000m. However, the opposite case could have been noticed more frequently, e.g. start at 1500 m and the end at 10 m.

- The model sensitivity to different processes, as well as the number of model particles used, has been an important part of this study. The sensitivity tests have been performed separately for nuclear accident and for nuclear explosion. Sensitivity ranking was based on the comparison of sensitivity measures, as well as on the comparison of the maps with time integrated concentration and deposition, in relation to the standard run.

- The sensitivity ranking for nuclear accident is similar for Cs-137 and I-131. The model is most sensitive to wet deposition then diffusion and dry deposition. For Xe-133, the model is most sensitive to vertical diffusion and then to radioactive decay and horisontal diffusion. The sensitivity to the number of model particles used is relatively low for all radionuclides.

- The model sensitivity ranking for application to nuclear explosion is the following: 1) gravitational settling, 2) vertical diffusion, 3) wet deposition, 4) dry deposition, 5) number of model particles used. However, it should be mentioned that the number of model particles cannot be too low and 90% reduction of the standard number of model particles gives the results visibly different from the standard run.

- In general, sensitivity tests indicate that improvement of the paramerization of wet deposition and vertical diffusion is the number one priority for the SNAP model, followed by the improvements in parameterization of gravitational settling and dry deposition. However, it should be mentioned that for nuclear explosion with high explosive yield (100 kt and above), parameterization of gravitational settling velocity is definitely the most important.

- The new version of the SNAP model is ready and is runs well at met.no. However, more joint operational tests involving NRPA and met.no are necessary to make remote SNAP application fully operational.

References

[1] Baklanov A. and J. H. Sørensen (2001) Parameterization of radionuclide deposition in atmospheric long-range transport modeling. Physics of the Chemistry of the Earth (B) 26(10), 787-799.

[2] Barrett K. and E. Berge (1996) Transboundary Air Pollution in Europe. Part 1 and Part 2. EMEP/MSC-W Status Report 1/96. Norwegian Meteorological Institute, Oslo, Norway.

[3] Bartnicki, J. and J. Saltbones (1996) Severe Nuclear Accident Program (SNAP) - A real time dispersion model. In: Development and Application of Computer Techniques to Environmental Studies VI. (P. Zannetti and C.A. Brebbia, eds.), pp. 17-26. Computational Mechanics Publications, Southampton, Boston.

[4] Bartnicki, J. and J. Saltbones (1997) Analysis of Atmospheric Transport and Deposition of Radioactive Material Released During a Potential Accident at Kola Nuclear Power Plant. Research Report No. 43, ISSN 0332-9879. Norwegian Meteorological Institute, Oslo, Norway.

[5] Bartnicki J., Salbu B., Saltbones J., Foss A. and O. Ch. Lind (2001) Gravitational settling of particles in dispersion model simulations using the Chernobyl Accident as a test case. DNMI Research Report No. 131. Norwegian Meteorological Institute, Oslo, Norway.

[6] Bartnicki J., B. Salbu, J. Saltbones, A. Foss and O. Ch. Lind (2003) Long-range transport of large particles in case of nuclear accident or explosion. Preprints of 26th NATO/CCMS International Technical Meeting on Air Pollution Modelling and its Application, 26-30 May 2003. Istanbul Technical University, Istanbul, Turkey, pp. 53-60.

[7] Bartnicki, J., Salbu B., Saltbones J. and A. Foss (2005) Analysis of Atmospheric Transport and Deposition of Radioactive Material Released During a Potential Accident at Kola Nuclear Power Plant. Research Report No. 10, ISSN 1503-8025. Norwegian Meteorological Institute, Oslo, Norway.

[8] Bartnicki J., B. Salbu, J. Saltbones, A. Foss and O. C. Lind (2006) Long-range transport and deposition of radioactive particles from potential accidents at Kola Nuclear Power Plant. Proceedings of 1st Joint Emergency Preparedness and Response/Robotic and Remote Systems Topical Meeting. February 11-16, 2006 Salt Lake City, Utah, USA

[9] Bartnicki J. and J. Saltbones (2008) Atmospheric dispersion of radioactive debris released in case of nuclear explosions using the Norwegiain SNAP model. Proceedings of The 12th International Conference on Harmonization within Atmospheric Dispersion Modelling for Regulatory Purposes HARMO12. 6-10 October 2008 - Cavtat, Croatia. pp. 111-115.

[10] Bartnicki, J., Haakenstad H. and O. Hov (2010) Volcano version of the SNAP model. Research Report No. 15, ISSN 0332-9879. Norwegian Meteorological Institute, Oslo, Norway.

[11] Crandall W.K., Molenkamp C.R., Wiliams A.L., Fulk M.M., Lange R. and J.B. Knox (1973) An investigating of scavenging of radioactivity from nuclear debris clouds: research in progress. lavrence Livermore National Laboratory, california, USA, Report UCRL-51328.

[12] Csanady G.T. (1973) Turbulent Diffusion in the Environment. Reidel, Dordrecht, Holland.

[13] Directions (1994). Directions for Actions in a Nuclear Weapons Explosion, Publications of the Ministry of the Interior, Department for Rescue Services, Series A:48.(in Finnish: Toiminta ydinräjähdystilanteessa Sisäasianministeriö, pelastusosaston julkaisu, Sarja A:84).

[14] EMEP web-site (2010) http://www.emep.int/

[15] ENSEMBLE web-site (2010) http://ensemble.jrc.ec.europa.eu/

[16] Galmarini, S., Bianconi, R., Klug, W., Mikkelsen, T., Addis, R., Andronopoulos, S., Astrup, P., Baklanov, A., Bartnicki, J., Bartzis, J.C., Bellasio, R., Bompay, F., Buckley, R., Bouzom, M., Champion, H., D'Amours, R., Davakis, E., Eleveld, H., Geertsema, G.T., Glaab, H., Kollax, M., Ilvonen, M., Manning, A., Pechinger, U., Persson, C., Polreich, E., Potemski, S., Prodanova, M., Saltbones, J., Slaper, H., Sofiev, M.A., Syrakov, D., Sørensen, J.H., Van der Auwera, L., Valkama, I., Zelazny, R., 2004a. Ensemble dispersion forecasting, part 1: concept, approach and indicators. Atmos. Environ. 38 (28): 4607-4617.

[17] Galmarini S., Bianconi R., Klug W., Mikkelsen T., Addis R., Andronopoulos S., Astrup P., Baklanov A., Bartnicki J., Bartzis J. C., Bellasio S., Bompay F., Buckley R., Bouzom M., Champion H., D'amours R., Davakis E., Eleveld H., Geertsema G. T., Glaab H., Kollax M., Ilvonen M., Manning A., Pechinger U., Persson C., Polreich E., Potempski S., Prodanova M., Saltbones J., Slaper H., Sofiev M. A., Syrakov D., Sørensen J. H., Van der Auvera L., Vaikama I. and R. Zelazny (2004) Can the confidence in long range atmospheric transport models be increased? The Pan-European experience on ENSEMBLE. Radiation Protection Dosimetry, 109 (1-2), pp. 19-24.

[18] Haga P.E. (1991) Hvordan influerer nedbørprocesser tids- og romskala pålangtransport av svoveldioksyd og partiklataert sulfat? (in Norwegian). Thesis, Oslo University.

[19] Maryon R.H., Smith J.B., Convay B.J., and D.M Godard (1991) The United Kingdom Nuclear Accident Model. Prog. Nucl. Energy, 26:85-104.

[20] Maryon R.H., J. Saltbones, D.B. Ryall, J. Bartnicki, H.A. Jakobsen and E. Berge (1996) An intercomparison of three long range dispersion models developed for the UK Meteorological Office, DNMI and EMEP. UK Met Office DoE Report DOE/RAS/96.011.

[21] Maryon R.H. and D. B. Ryall (1996) Developments of the UK nuclear accident response model (NAME). Department of Environment, UK Met Office Turbulence and Diffusion Note 234. UK Meteorological Office, Bracknell, United Kingdom.

[22] Persson Ch., Robertson L. and Thaning L. (2000) Model Simulation of Air and Ground Contamination Associated with Nuclear Weapons. An Emergency Preparedness Model. SMHI report No 95. Swedish Meteorological and Hydrological Institute. Norrkoping, Sweden.

[23] Pettersen S. (1956) Weather Analysis and Forecasting. McGraw-Hill, New York.

[24] RAFF (1999) Properties of nuclear fule particles and release of radionuclides from carier matrix. RAFF final report. A research programme carried out with the financial support from the Commision of EC - DG XII. Contract No. FICCT960007.

[25] Rao K.S. (2005) Uncertainty analysis in atmospheric dispersion modeling. Pure appl. geophys. 162, 1893-1917.

[26] Richardson D. (2010) Changes to the operational forecasting system. ECMWF Newsletter No.122, Winter 2009/2010.

[27] Robertson L. and J. Langner (1998) An Eulerian Limited-Area atmospheric transport model. Journal of Applied Meteorology, 38: 190-210.

[28] Ryall D.B. and Maryon R.H. (1996) The NAME2 dispersion model: a scientific overview. UK Meteorological Office. MetO(Apr) Turbulence and Diffusion note 217b.

[29] Ryall D.B. and Maryon R.H. (1998) Validation of thr UK Mte. Office's NAME model against the ETEX dataset. Atmospheric Environment 32(24): 4265-4276.

[30] Saltbones J.(1995) Real-time dispersion model calculations as part of NORMEM-WP19. Safety Science 20, 51-59.

[31] Saltbones J. and A. Foss (1994) Real-time dispersion model calculations of radioactive pollutants at DNMI. Part of Norwegian preparedness against nuclear accidents. Preprints of the XIX Nordic Meteorologists Meeting, June 1994, Kristiansand, Norway.

[32] Saltbones J., Foss A. and J. Bartnicki (1995) Severe Nuclear Accident Program. Technical Description. Research Report No. 15. Norwegian Meteorological Institute. Oslo, Norway.

[33] Saltbones J., Foss A. and J. Bartnicki (1995) Severe Nuclear Accident Program (SNAP) - A real time dispersion model. In: Proceedings of Oslo Conference on International Aspects of Emergency management and Environmental Technology. (K.H. Drager ed.), pp. 177-184.

[34] Saltbones J., Foss A. and J. Bartnicki (1995) ETEX - the European Tracer Experiment - DNMI's participation in an international program for evaluation of real time dispersion models. In: Proceedings of Oslo Conference on International Aspects of Emergency management and Environmental Technology. (K.H. Drager ed.), pp. 129-138.

[35] Saltbones J., Foss A. and J. Bartnicki (1996) A real time dispersion model for severe nuclear accidents tested in the European Tracer Experiment. Systems Analysis Modelling Simulation 25, 263-279.

[36] Saltbones J. and J. Bartnicki (1997) Atmospheric transport of radioactive material from potential accident in Kola nuclear power plant (in Norwegian). Naturen 4, 178-188.

[37] Saltbones J., Foss A. and J. Bartnicki (1998) Norwegian Meteorological Institute's Real-Time Dispersion Model SNAP (Severe Nuclear Accident Program). Runs for ETEX and ATMES II Experiments with Different Meteorological Input. Atmospheric Environment 32(24), 4277-4283.

[38] Saltbones J., Foss A. and J. Bartnicki (2000) Threat to Norway from potential accidents at the Kola nuclear power plant. Climatological trajectory analysis and episode studies. Atmospheric Environment 34, 407-418.

[39] Saltbones J., Foss A. and J. Bartnicki (2002) Intercomparison of real time dispersion model results, supporting decision making in case of nuclear accident and focusing on quantification of uncertainty. In; Eighth International Conference on Harmonisation Within Atmospheric Dispersion Modelling for Regulatory Purpose. Sofia, Bulgaria, 14-17 October 2002. E. Batcharova and D. Syrakow (Eds.), pp.92-96.

[40] Saltbones J., Bartnicki J. and A. Foss (2003) Handling of Fallout Processes from Nuclear Explosions in Severe Nuclear Accident Program - SNAP. Research Report No. 157. Norwegian Meteorological Institute. Oslo, Norway.

[41] Sandu I, F. Bompay and S. Stefan S. (2003) Validation of atmospheric dispersion models using ETEX data. International Journal of Environment and Pollution 19(4): 367-389.

[42] Savijärvi H.(1990) Fast radiation parameterization schemes for mesoscale and short-range forecast models. J. Appl. Meteor., 29, 437-447.

[43] Seinfeld J.H. (1986) Atmospheric Chemistry and Physics of Air Pollution. John Wile & Sons. New York. 738 pp.

[44] Venkatram A. and J. Pleim (1999) Atmospheric Environment, 33, 3075-3076.

[45] Undén, P., Rontu, L., Järvinen, H., Lynch, P., Calvo, J., Cats, G., Cuaxart, J., Eerola, K., Fortelius, C., Garcia-Moya, J.A., Jones, C., Lenderlink, G., McDonald, A., McGrath, R., Navascues, B., Nielsen, N.W., Ødegaard, V., Rodriguez,E., Rummukainen, M., Rööm, R., Sattler, K., Sass, B.H., Savijärvi, H., Schreur, B.W., Sigg, R., The, H. and Tijm,A. (2002) HIRLAM-5 Scientific Documentation, HIRLAM-5 Project. Available from SMHI, S-601767 Norrköping, Sweden.

A. List of Isotopes used in Remote Simulations from NRPA

In this Appendix we show the list of isotopes included in the input file `isotope-list.txt` used for remote SNAP runs from NRPA. Altogether there are 382 isotopes which can be used in remote applications of SNAP from NRPA. Identification number of each isotope is given in the first column and name of the isotope in the second coulmn. There can be three forms of the isotope specified by one digit number: 0-noble gas, 1-gas and 2-aerosol. This information is included in the third column. The radioactive decay constant is given in column four with the unit s^{-1}.

Identification number	Name	Type	Decay constant
1	H - 3	0	0.178E-08
2	Na- 24	2	0.128E-04
3	Ar- 41	0	0.105E-03
4	Co- 58	2	0.113E-06
5	Co- 60	2	0.416E-08
6	Zn- 72	2	0.414E-05
7	Ga- 72	2	0.137E-04
8	Ga- 73	2	0.395E-04
9	Ge- 75	2	0.140E-03
10	Ge- 77m	2	0.128E-01
11	Ge- 77	2	0.170E-04
12	Ge- 78	2	0.133E-03
13	As- 77	2	0.496E-05
14	As- 78	2	0.127E-03
15	Se- 79	2	0.338E-12
16	Se- 81m	2	0.202E-03
17	Se- 81	2	0.625E-03
18	Se- 83m	2	0.990E-02
19	Se- 83	2	0.513E-03
20	Br- 82m	2	0.189E-02
21	Br- 82	2	0.544E-05
22	Br- 83	2	0.802E-04
23	Br- 84m	2	0.193E-02
24	Br- 84	2	0.363E-03
25	Kr- 83m	0	0.104E-03
26	Kr- 85m	0	0.438E-04
27	Kr- 85	0	0.203E-08
28	Kr- 87	0	0.152E-03
29	Kr- 88	0	0.686E-04
30	Kr- 89	0	0.364E-02
31	Rb- 86m	2	0.114E-01
32	Rb- 86	2	0.430E-06
33	Rb- 87	2	0.470E-18
34	Rb- 88	2	0.642E-03
35	Rb- 89	2	0.760E-03
36	Sr- 89	2	0.154E-06
37	Sr- 90	2	0.787E-09
38	Sr- 91	2	0.203E-04
39	Sr- 92	2	0.711E-04
40	Y - 90m	2	0.604E-04

Identification number	Name	Type	Decay rate
41	Y - 90	2	0.301E-05
42	Y - 91m	2	0.232E-03
43	Y - 91	2	0.137E-06
44	Y - 92	2	0.545E-04
45	Y - 93	2	0.189E-04
46	Y - 94	2	0.608E-03
47	Y - 95	2	0.110E-02
48	Zr- 93	2	0.231E-13
49	Zr- 95	2	0.123E-06
50	Zr- 97	2	0.115E-04
51	Nb- 94m	2	0.185E-02
52	Nb- 94	2	0.110E-11
53	Nb- 95m	2	0.222E-05
54	Nb- 95	2	0.228E-06
55	Nb- 96	2	0.823E-05
56	Nb- 97m	2	0.128E-01
57	Nb- 97	2	0.157E-03
58	Nb- 98	2	0.227E-03
59	Mo- 99	2	0.289E-05
60	Mo-101	2	0.791E-03
61	Mo-102	2	0.104E-02
62	Tc- 99m	2	0.320E-04
63	Tc- 99	2	0.103E-12
64	Tc-101	2	0.814E-03
65	Tc-102m	2	0.269E-02
66	Tc-102	2	0.131E+00
67	Tc-104	2	0.642E-03
68	Ru-103	2	0.203E-06
69	Ru-105	2	0.434E-04
70	Ru-106	2	0.219E-07
71	Rh-103m	2	0.206E-03
72	Rh-105m	2	0.182E-01
73	Rh-105	2	0.542E-05
74	Rh-106m	2	0.883E-04
75	Rh-106	2	0.232E-01
76	Rh-107	2	0.532E-03
77	Pd-107m	2	0.325E-01
78	Pd-107	2	0.338E-14
79	Pd-109	2	0.143E-04
80	Pd-111m	2	0.350E-04

Identification number	Name	Type	Decay rate
81	Pd-111	2	0.525E-03
82	Pd-112	2	0.958E-05
83	Ag-109m	2	0.175E-01
84	Ag-110m	2	0.297E-07
85	Ag-111m	2	0.937E-02
86	Ag-111	2	0.107E-05
87	Ag-112	2	0.615E-04
88	Ag-113m	2	0.105E-01
89	Ag-113	2	0.363E-04
90	Ag-115m	2	0.408E-01
91	Ag-115	2	0.550E-03
92	Cd-111m	2	0.237E-03
93	Cd-113m	2	0.151E-08
94	Cd-113	2	0.244E-23
95	Cd-115m	2	0.180E-06
96	Cd-115	2	0.360E-05
97	Cd-117m	2	0.566E-04
98	Cd-117	2	0.741E-04
99	Cd-118	2	0.230E-03
100	In-113m	2	0.116E-03
101	In-115m	2	0.428E-04
102	In-115	2	0.431E-23
103	In-116m	2	0.213E-03
104	In-116	2	0.488E-01
105	In-117m	2	0.993E-04
106	In-117	2	0.263E-03
107	In-118m	2	0.263E-02
108	In-118	2	0.139E+00
109	In-119m	2	0.642E-03
110	In-119	2	0.462E-02
111	Sn-117m	2	0.573E-06
112	Sn-119m	2	0.328E-07
113	Sn-121m	2	0.440E-09
114	Sn-121	2	0.718E-05
115	Sn-123m	2	0.289E-03
116	Sn-123	2	0.622E-07
117	Sn-125	2	0.831E-06
118	Sn-126	2	0.220E-12
119	Sn-127	2	0.908E-04
120	Sn-128	2	0.196E-03

Identification number	Name	Type	Decay rate
121	Sn-130	2	0.312E-02
122	Sb-124m	2	0.569E-03
123	Sb-124	2	0.133E-06
124	Sb-125	2	0.805E-08
125	Sb-126m	2	0.608E-03
126	Sb-126	2	0.647E-06
127	Sb-127	2	0.211E-05
128	Sb-128m	2	0.111E-02
129	Sb-128	2	0.214E-04
130	Sb-129	2	0.444E-04
131	Sb-130m	2	0.175E-02
132	Sb-130	2	0.312E-03
133	Sb-131	2	0.502E-03
134	Te-125m	2	0.138E-06
135	Te-127m	2	0.736E-07
136	Te-127	2	0.205E-04
137	Te-129m	2	0.240E-06
138	Te-129	2	0.165E-03
139	Te-131m	2	0.642E-05
140	Te-131	2	0.462E-03
141	Te-132	2	0.247E-05
142	Te-133m	2	0.209E-03
143	Te-133	2	0.924E-03
144	Te-134	2	0.275E-03
145	I -129	1	0.138E-14
146	I -130m	1	0.130E-02
147	I -130	1	0.155E-04
148	I -131	1	0.994E-06
149	I -132	1	0.836E-04
150	I -133m	1	0.770E-01
151	I -133	1	0.921E-05
152	I -134m	1	0.321E-02
153	I -134	1	0.222E-03
154	I -135	1	0.288E-04
155	Xe-129m	0	0.100E-05
156	Xe-131m	0	0.680E-06
157	Xe-133m	0	0.355E-05
158	Xe-133	0	0.152E-05
159	Xe-134m	0	0.239E+01
160	Xe-135m	0	0.743E-03

Identification number	Name	Type	Decay rate
161	Xe-135	0	0.210E-04
162	Xe-137	0	0.296E-02
163	Xe-138	0	0.815E-03
164	Cs-134m	2	0.664E-04
165	Cs-134	2	0.107E-07
166	Cs-135m	2	0.218E-03
167	Cs-135	2	0.956E-14
168	Cs-136	2	0.617E-06
169	Cs-137	2	0.729E-09
170	Cs-138	2	0.359E-03
171	Ba-135m	2	0.671E-05
172	Ba-137m	2	0.453E-02
173	Ba-139	2	0.139E-03
174	Ba-140	2	0.627E-06
175	La-140	2	0.456E-05
176	La-141	2	0.498E-04
177	La-142	2	0.125E-03
178	La-143	2	0.825E-03
179	Ce-141	2	0.243E-06
180	Ce-142	2	0.440E-24
181	Ce-143	2	0.584E-05
182	Ce-144	2	0.282E-07
183	Ce-146	2	0.814E-03
184	Pr-142m	2	0.791E-03
185	Pr-142	2	0.101E-04
186	Pr-143	2	0.591E-06
187	Pr-144m	2	0.161E-02
188	Pr-144	2	0.669E-03
189	Pr-145	2	0.322E-04
190	Pr-146	2	0.477E-03
191	Pr-147	2	0.963E-03
192	Nd-144	2	0.105E-22
193	Nd-147	2	0.730E-06
194	Nd-149	2	0.111E-03
195	Nd-151	2	0.932E-03
196	Nd-152	2	0.101E-02
197	Pm-147	2	0.838E-08
198	Pm-148m	2	0.194E-06
199	Pm-148	2	0.149E-05
200	Pm-149	2	0.363E-05

Identification number	Name	Type	Decay rate
201	Pm-150	2	0.718E-04
202	Pm-151	2	0.678E-05
203	Pm-152m	2	0.642E-03
204	Pm-152	2	0.282E-02
205	Sm-147	2	0.205E-18
206	Sm-148	2	0.275E-23
207	Sm-149	2	0.220E-23
208	Sm-151	2	0.236E-09
209	Sm-153	2	0.414E-05
210	Sm-155	2	0.520E-03
211	Sm-156	2	0.205E-04
212	Eu-154	2	0.256E-08
213	Eu-155	2	0.458E-08
214	Eu-156	2	0.528E-06
215	Eu-157	2	0.127E-04
216	Eu-158	2	0.252E-03
217	Eu-159	2	0.638E-03
218	Gd-159	2	0.104E-04
219	Gd-162	2	0.116E-02
220	Tb-160	2	0.111E-06
221	Tb-161	2	0.116E-05
222	Tb-162m	2	0.863E-04
223	Tb-162	2	0.155E-02
224	Tb-163	2	0.592E-03
225	Dy-165	2	0.819E-04
226	Hg-206	2	0.144E-02
227	Tl-206	2	0.276E-02
228	Tl-207	2	0.241E-02
229	Tl-208	2	0.373E-02
230	Tl-209	2	0.525E-02
231	Tl-210	2	0.889E-02
232	Pb-207m	2	0.866E+00
233	Pb-209	2	0.583E-04
234	Pb-210	2	0.105E-08
235	Pb-211	2	0.320E-03
236	Pb-212	2	0.181E-04
237	Pb-213	2	0.116E-02
238	Pb-214	2	0.431E-03
239	Bi-209	2	0.110E-25
240	Bi-210	2	0.160E-05

Identification number	Name	Type	Decay rate
241	Bi-211	2	0.537E-02
242	Bi-212	2	0.191E-03
243	Bi-213	2	0.246E-03
244	Bi-214	2	0.586E-03
245	Bi-215	2	0.165E-02
246	Po-210	2	0.580E-07
247	Po-211	2	0.133E+01
248	Po-212	2	0.228E+07
249	Po-213	2	0.165E+06
250	Po-214	2	0.423E+04
251	Po-215	2	0.389E+03
252	Po-216	2	0.462E+01
253	Po-217	2	0.693E-01
254	Po-218	2	0.379E-02
255	At-215	2	0.693E+04
256	At-216	2	0.231E+04
257	At-217	2	0.217E+02
258	At-218	2	0.347E+00
259	At-219	2	0.128E-01
260	Rn-218	2	0.198E+02
261	Rn-219	2	0.173E+00
262	Rn-220	2	0.126E-01
263	Rn-221	2	0.462E-03
264	Rn-222	2	0.210E-05
265	Rn-223	2	0.269E-03
266	Fr-221	2	0.241E-02
267	Fr-222	2	0.781E-03
268	Fr-223	2	0.525E-03
269	Ra-222	2	0.182E-01
270	Ra-223	0	0.702E-06
271	Ra-224	0	0.220E-05
272	Ra-225	0	0.542E-06
273	Ra-226	0	0.137E-10
274	Ra-227	0	0.280E-03
275	Ra-228	0	0.328E-08
276	Ra-229	0	0.693E+12
277	Ac-225	2	0.802E-06
278	Ac-226	2	0.664E-05
279	Ac-227	2	0.102E-08
280	Ac-228	2	0.314E-04

Identification number	Name	Type	Decay rate
281	Ac-229	2	0.175E-03
282	Th-226	2	0.374E-03
283	Th-227	2	0.441E-06
284	Th-228	2	0.115E-07
285	Th-229	2	0.299E-11
286	Th-230	2	0.275E-12
287	Th-231	2	0.755E-05
288	Th-232	2	0.156E-17
289	Th-233	2	0.520E-03
290	Th-234	2	0.333E-06
291	Pa-230	2	0.453E-06
292	Pa-231	2	0.676E-12
293	Pa-232	2	0.612E-05
294	Pa-233	2	0.297E-06
295	Pa-234m	2	0.987E-02
296	Pa-234	2	0.285E-04
297	U -230	2	0.386E-06
298	U -231	2	0.187E-05
299	U -232	2	0.305E-09
300	U -233	2	0.136E-12
301	U -234	2	0.889E-13
302	U -235	2	0.309E-16
303	U -236	2	0.919E-15
304	U -237	2	0.119E-05
305	U -238	2	0.487E-17
306	U -239	2	0.492E-03
307	U -240	2	0.134E-04
308	Np-235	2	0.196E-07
309	Np-236m	2	0.170E-15
310	Np-236	2	0.875E-05
311	Np-237	2	0.103E-13
312	Np-238	2	0.382E-05
313	Np-239	2	0.341E-05
314	Np-240m	2	0.158E-02
315	Np-240	2	0.183E-03
316	Pu-235	2	0.444E-03
317	Pu-236	2	0.771E-08
318	Pu-237	2	0.176E-06
319	Pu-238	2	0.255E-09
320	Pu-239	2	0.900E-12

Identification number	Name	Type	Decay rate
321	Pu-240	2	0.334E-11
322	Pu-241	2	0.166E-08
323	Pu-242	2	0.580E-13
324	Pu-243	2	0.387E-04
325	Pu-244	2	0.275E-15
326	Pu-245	2	0.193E-04
327	Am-240	2	0.378E-05
328	Am-241	2	0.480E-10
329	Am-242	2	0.495E+02
330	Am-242m	2	0.145E-09
331	Am-242	2	0.120E-04
332	Am-243	2	0.276E-11
333	Am-244m	2	0.444E-03
334	Am-244	2	0.191E-04
335	Am-245	2	0.917E-04
336	Cm-241	2	0.229E-06
337	Cm-242	2	0.492E-07
338	Cm-243	2	0.686E-09
339	Cm-244	2	0.125E-08
340	Cm-245	2	0.236E-11
341	Cm-246	2	0.399E-11
342	Cm-247	2	0.137E-14
343	Cm-248	2	0.467E-13
344	Cm-249	2	0.181E-03
345	Cm-250	2	0.318E-11
346	Bk-249	2	0.255E-07
347	Bk-250	2	0.598E-04
348	Cf-249	2	0.610E-10
349	Cf-250	2	0.169E-08
350	Cf-251	2	0.275E-10
351	Cf-252	2	0.829E-08
352	Cf-253	2	0.456E-06
353	Cf-254	2	0.133E-06
354	Es-253	2	0.392E-06
355	Es-254m	2	0.491E-05
356	Es-254	2	0.291E-07
357	Es-255	2	0.209E-06
358	C - 11	0	0.567E-03
359	N - 13	0	0.116E-02
360	O - 15	0	0.567E-02

Identification number	Name	Type	Decay rate
361	F - 18	0	0.115E-03
545	I -129e	1	0.138E-14
645	I -129o	1	0.138E-14
745	I -129a	1	0.138E-14
547	I -130e	1	0.155E-04
647	I -130o	1	0.155E-04
747	I -130a	1	0.155E-04
548	I -131e	1	0.994E-06
648	I -131o	1	0.994E-06
748	I -131a	1	0.994E-06
549	I -132e	1	0.836E-04
649	I -132o	1	0.836E-04
749	I -132a	1	0.836E-04
551	I -133e	1	0.921E-05
651	I -133o	1	0.921E-05
751	I -133a	1	0.921E-05
553	I -134e	1	0.222E-03
653	I -134o	1	0.222E-03
753	I -134a	1	0.222E-03
554	I -135e	1	0.288E-04
654	I -135o	1	0.288E-04
754	I -135a	1	0.288E-04